DISSERTATION

submitted to the

Combined Faculties for the Natural Sciences and for Mathematics

of the Ruperto-Carola University of Heidelberg, Germany

for the degree of

Doctor of Natural Sciences

presented by

M. Sc. Franziska Hentzschel

Born in Berlin

Oral examination: June 30th, 2017

THE RNAI-COMPETENT MALARIA PARASITE: A NOVEL STRATEGY TO KNOCK DOWN *PLASMODIUM* GENES VIA NON-CANONICAL RNAI

Referees: Prof. Dr. Michael Lanzer

Prof. Dr. Dirk Grimm

Für Mama

Abstract

Malaria, caused by apicomplexan parasites of the *Plasmodium* species, is one of the deadliest infectious diseases worldwide. Despite the urgent need to identify new drug targets and vaccine candidates, a large proportion of the *Plasmodium* genes are uncharacterized, as tools to study gene function are limited. In many eukaryotes, genes can be silenced via RNA interference (RNAi) using artificial short hairpin RNAs (shRNAs). However, *Plasmodium* parasites lack the machinery required for RNAi. In this study, I therefore engineered a non-canonical RNAi machinery into the rodent parasite *Plasmodium berghei* (*P. berghei*).

To this end, I exploited a non-canonical RNAi pathway which requires only a single protein, Argonaute 2 (Ago2), and a specifically designed shRNA, a so-called AgoshRNA, for gene silencing. I generated a *P. berghei* line constitutively expressing Ago2, named *Pb*Ago2, and demonstrated that this parasite can complete its life cycle through the mammalian and insect host, despite exhibiting a reduced growth in blood and mosquito stages. Expression of AgoshRNAs targeting the mRNA of the green fluorescent protein GFP (constitutively expressed by *Pb*Ago2) induced a potent knockdown of GFP both in blood and in non-erythrocytic stages. As different AgoshRNAs mediated gene silencing to various levels, target gene expression could be fine-tuned. AgoshRNA-mediated gene knockdown was also possible for endogenous genes, and the knockdown of a non-essential gene phenocopied the full knockout. Additionally, the expression of a blood-stage-essential gene was reduced using RNAi. The analysis of the transcriptome of *Pb*Ago2 by RNA sequencing suggested a possible interaction between Ago2 and a *Plasmodium* mRNA storage protein as a putative reason for the growth impairment. To further increase the potential applications of the RNAi-competent parasite, Ago2 expression was restricted to the liver stage using a stage-specific promoter. This transgenic line behavee indistinguishable from wild type and the expression of an AgoshRNA targeting GFP silenced fluorescence exclusively in late liver stages.

In summary, *Pb*Ago2 is a potent tool to modulate gene expression without the need to alter the genetic locus. In contrast to existing tools, *Pb*Ago2 provides the option to target genes exclusively in a single life cycle stage, to multiplex different AgoshRNAs enabling the simultaneous knockdown of multiple genes, or to screen for phenotypes using a library of AgoshRNAs. This novel, RNAi-competent parasite line opens a wealth of new options to annotate genes in *Plasmodium*.

Zusammenfassung

Malaria, verursacht von *Plasmodium*-Parasiten, ist eine der tödlichsten Infektionskrankheiten weltweit. Die Funktion vieler *Plasmodium*-Gene ist unbekannt, obwohl dieses Wissen für die Entwicklung neuer Medikamente und Impfstoffe unabdingbar ist. Ein Grund dafür ist, dass nur wenige Technologien eine gezielte Manipulation der Genexpression ermöglichen. In vielen Eukaryoten nutzt man RNA-Interferenz (RNAi) zur Unterdrückung der Genexpression mittels kurzer RNA-Moleküle (short hairpin RNAs, shRNAs). *Plasmodium*-Parasiten haben diesen RNAi Mechanismus jedoch nicht. In der vorliegenden Arbeit wurde RNAi deshalb in den murinen Erreger *Plasmodium berghei* (*P. berghei*) eingeführt.

Dazu habe ich einen alternativen RNAi-Mechanismus genutzt, in dem das Protein Argonaute 2 (Ago2) und eine spezielle shRNA, eine sogenannte AgoshRNA, ausreichend sind, um Genexpression zu inhibieren. Die in dieser Arbeit entwickelte *P. berghei*-Linie *Pb*Ago2, die Ago2 sowie das grün fluoreszierende Protein GFP konstitutiv exprimiert, durchlief trotz eines Wachstumsdefekts in Blut- und Mosquitostadien den Lebenszyklus vollständig. Die Expression von AgoshRNAs gegen die mRNA von GFP reduzierte die Fluoreszenz von Parasiten in allen Stadien und unterschiedliche AgoshRNAs modulierten die Stärke dieser Genrepression. Auch endogene Gene konnten mittels RNAi inhibiert werden, und die Inhibition eines nicht-essentiellen Gens hatte den gleichen Phänotyp wie die vollständige Abschaltung des Gens. Die Analyse des Transkriptoms von *Pb*Ago2 mittels RNA-Sequenzierung deutet darauf hin, dass Ago2 mit einem *Plasmodium* mRNA-Speicherprotein interagieren könnte und so möglicherweise den Wachstumsdefekt verursacht. Um die Anwendungsmöglichkeiten des RNAi-kompetenten Parasiten zu erweitern, wurde in einer zweiten transgenen Linie Ago2 spezifisch in Leberstadien exprimiert. Diese Linie hat keinen Wachstumsdefekt und ermöglichte es, GFP Expression ausschließlich in Leberstadien zu inhibieren.

Zusammengefasst bietet der *Pb*Ago2-Parasit eine vielseitige Technologie, um Gene in *Plasmodium* zu regulieren ohne dafür den genetischen Lokus zu modifizieren. Im Gegensatz zu aktuellen Technologien ermöglicht es *Pb*Ago2, ein Gen nur in einem spezifischen Stadium des Lebenszyklus zu inhibieren, mehrere Gene parallel durch Expression mehrerer AgoshRNAs zu regulieren, oder Screenings durchzuführen. Dieser neuartige RNAi-kompetente Parasit eröffnet somit neue Möglichkeiten, Genfunktionen in *Plasmodium* zu erforschen.

Contents

List of Figures

List of Tables

Acronyms and Symbols

µg	Microgram
µl	Microliter
µM	Micromolar
5-FC	5-Fluorocytosine
α	Anti- (target for sh/AgoshRNAs)
AAV	Adeno-associated virus
ACT	Artemisinin combination therapy
Ago	Argonaute
AgoshRNA, AgoshR	Ago2-associated shRNA
AID	Auxin-inducible degron
Amp	Ampicillin
ANOVA	Analysis of variance
ApoH	Apolipoprotein H
APS	Ammonium persulfate
aTc	Anhydrotetracycline
bp	Base pair
BSA	Bovine serum albumin
C	Celsius
Cas9	CRISPR-associated protein 9
cDNA	Complementary DNA
CITH	Homolog of worm CAR-I and fly Trailer Hitch
CMV	Cytomegalovirus
CRISPR	Clustered regulatory interspaced short palindromic repeats
d	Day
d. p. i.	Days post-infection
DD	Destabilization domain
DDD	*E. coli* DHFR destabilization domain
ddH_2O	Double-distilled water
DDX6	DEAD-box helicase 6
DGCR8	DiGeorge syndrome critical region gene 8
DHFR	Dihydrofolate reductase
DMEM	Dulbecco's Modified Eagle Medium
DMSO	Dimethyl sulfoxide
DNA	Deoxyribonucleic acid
dNTP	Deoxynucleoside triphosphate
DOZI	Development of zygote inhibited
DSB	Double-strand break
dsDNA	Double-stranded DNA
dsRNA	Double-stranded RNA
DTT	Dithiothreitol
E. coli	*Escherichia coli*
e. g.	*Exempli gratia*
ECL	Enhanced chemiluminescence

ECM	Experimental cerebral malaria
EDTA	Ethylenediaminetetraacetic acid
EEF	Extra-erythrocytic form
EF-1α	Elongation factor 1-alpha
EXP1	Exported protein 1
FBS	Fetal bovine serum
FKBP	FK506-binding protein
FLP	Flippase
FOV	Fields of view
FRB	FKBP12-rapamycin-associated protein
frt	FLP recognition sites
g	Gram
GAP	Genetically attenuated parasites
GFP	Green fluorescent protein
GlcN	Glucosamine
GlcN-6P	Glucosamine-6-phosphate
glmS	Glucosamine-6-phosphate synthase
GOI	Gene of interest
gRNA	Guide RNA
GW182	Glycine-tryptophane-rich protein
h	Hours
HA	Hemagglutinin
hAgo2	Human Ago2
Hb	Hemoglobin
HEK	Human embryonic kidney cells
HSP70	Heat-shock protein 70
HuH7	Human hepatoma cells
i. e.	*id est*
i. v.	Intravenous
i. p.	Intraperitoneal
IF	Immunofluorescence
IgG, IgM	Immunoglobulin G, M
iRBC	Infected red blood cell
K/X	Ketamine/Xylazine
kb	Kilo base
kDa	Kilo Dalton
L	Liter
L.	*Leishmania*
LB	Lysogeny broth
LISP2	Liver-specific protein 2
M	Molar
mA	MilliAmpere
MCS	Multiple cloning site
MEF	Mouse embryonic fibroblasts
MEM-NEAA	Minimum essential medium non-essential amino acids
min	Minutes
miRNA, miR	MicroRNA
ml	Milliliter

Mm	Mus musculus
mM	Millimolar
mm	Millimeter
mRNA	Messenger RNA
MSP1	Merozoite surface protein 1
Neg Sel	Negative selection
ng	Nanogram
NLS	Nuclear localization signal
NMRI	Naval Medical Research Institute
ns	Not significant
nt	Nucleotide
O/N	Over night
*Os*TIR1	*Oryzae sativa* transport inhibitor response 1
P-bodies	Processing bodies
p.	Page
P. berghei, *Pb*	*Plasmodium berghei*
P. falciparum, *Pf*	*Plasmodium falciparum*
PBS	Phosphate-buffered saline
PCR	Polymerase chain reaction
PEI	Polyethylenimine
*Pf*EMP1	*P. falciparum* erythrocyte membrane protein 1
PlasmoGEM	*Plasmodium* Genetic Modification Project
PMO	Phosphorodiamidate morpholino oligomers
PPLP2	*Plasmodium* perforin-like protein 2
Pre-miRNA	Precursor miRNA
Pri-miRNA	Primary miRNA
PV	Parasitophorous vacuole
PVM	Parasitophorous vacuole membrane
qRT-PCR	Quantitative reverse transcription PCR
RBC	Red blood cell
RIPA	Radioimmunoprecipitation assay buffer
RISC	RNA-induced silencing complex
RNA	Ribonucleic acid
RNAi	RNA interference
RNA-Seq	RNA sequencing
RPKM	Reads per kilobase per million mapped reads
RT	Room temperature or reverse transcriptase (context-dependent)
s	Seconds
SCF complex	Skp1, Cullin1, F box protein ubiquitin ligase complex
Scr	scrambled
SD	Standard deviation
SDS	Sodium dodecyl sulfate
SDS-PAGE	SDS polyacrylamide gel electrophoresis
SEM	Standard error of the mean
shRNA, shR	Short hairpin RNA
SIL6	Silent intergenic locus on chromosome 6
siRNA	Short interfering RNA

snoRNA	Small nucleolar RNA
snRNA	Small nuclear RNA
SOB	Super optimal broth
SOC	Super optimal broth with Catabolite repression
Spz	Sporozoite
T. brucei	*Trypanosoma brucei*
T. cruzii	*Trypanosoma cruzii*
T. gondii, *Tg*	*Toxoplasma gondii*
TAE	Tris/Acetic acid/EDTA buffer
TBS (-T)	Tris-buffered saline (with Tween-20)
Tet	Tetracycline
TetO	Tet operator
TetR	Tet repressor
Tfb	Transformation buffer
TGS	Tris/Glycine/SDS
TRAD	Transcriptional transactivator domain
TRAP	Thrombospondin-related anonymous protein
TRBP	Tar RNA binding protein
tRNA	Transfer RNA
UIS4	Upregulated in infectious sporozoites 4
UTR	Untranslated region
V	Volt
v	Volume
w	Weight
WB	Western blot
WT	Wild type
XPO5	Exportin 5
yFCU	Yeast cytosine deaminase and uridyl phosphoribosyl transferase fusion protein
ZFN	Zinc-finger nuclease

Introduction

1

1.1 MALARIA, A DEADLY DISEASE

"I was still hesitating whether these elements were parasites, when on November 6th, 1880, on examining the pigmented spherical bodies mentioned above, I observed […] moveable filaments or flagella, whose extremely rapid and varied movements left no doubt as to their nature."[1]

~ Charles Louis Alphonse Laveran (1845-1922)

Malaria, caused by parasites of the *Plasmodium* genus, continues to be a devastating disease. In 2015, an estimated 214 million people worldwide were infected with malaria, and about 438,000 people died due to the infection[3]. Years of intense research have yielded potent anti-malarial drugs such as the artemisinin combination therapy (ACT), which is now the recommended therapy for *Plasmodium* infection[4], and even resulted in the development of a vaccine against malaria, RTS,S5. However, the rapid rise of drug resistance in malaria parasites remains problematic, and there are already first studies reporting ACT-resistant parasites[6–8]. The RTS,S vaccine, on the other hand, has a relatively low efficacy ranging from 25 % to 55 %, which further decreases over time[5,9]. Therefore, the use of insecticide-treated bed nets is still the most effective method to prevent morbidity and mortality caused by malaria[3].

Malaria comes from the Italian term mala aria, bad air, and refers to the initial assumption that the disease is transmitted by the air of swampy regions[2].

There are more than 200 *Plasmodium* species known, all of which have a vertebrate host (mammals, birds or reptiles) and an invertebrate host (mosquitoes). Five *Plasmodium* species, *Plasmodium falciparum* (*P. falciparum*), *P. vivax*, *P. malariae*, *P. ovale* and *P. knowlesi*, are known to infect humans. All of them are transmitted by biting mosquitoes of the *Anopheles* genus. With the exception of *P. knowlesi*, which is zoonotic, there are no animal reservoirs of *Plasmodium*, making the eradication of malaria, in theory, feasible. However, more basic research is required to understand the biology of the parasites, in turn enabling the identification of new drug targets and vaccine candidates.

The name Anopheles comes from the Greek αν, an, ("not"), and όφελος, óphelos, ("benefit"), and translates to "useless"[10].

Rodent-infecting malaria species, such as *P. berghei, P. chabaudi* or *P. yoelii*, have proven to be of tremendous value for malaria research, as these species allow to study malaria infection in mouse models and to maintain the complete life cycle of *Plasmodium* under laboratory conditions. Many findings of rodent parasites, although not all, could later be validated in human *Plasmodium* species[11,12].

1.2 THE MALARIA LIFE CYCLE

This Section will give a general overview of the life cycle of *Plasmodium* parasites through the mammalian and mosquito host. A summary is depicted in in Figure 1.

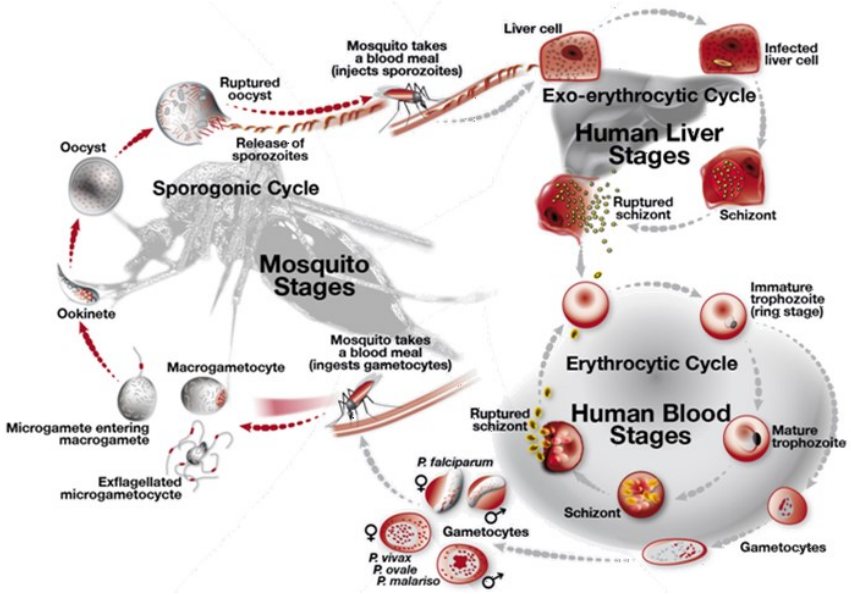

FIGURE 1: **Life cycle of human malaria parasites.** Sporozoites are transmitted into the skin of the mammalian host by the bite of an infected mosquito. After entering the bloodstream, they reach the liver where they establish an infection within hepatocytes. Liver stages mature into thousands of merozoites, which are released into the bloodstream to invade erythrocytes. Within the erythrocytes, parasites undergo multiple rounds of asexual replication, yielding more merozoites to invade more red blood cells. Occasionally, parasites differentiate into female and male gametocytes. When these are taken up by another mosquito bite, they will fertilize and develop into a motile ookinete. The ookinete then traverses the midgut and forms an oocyst just outside of the midgut wall. Within the oocyst, sporozoites develop (sporogeny), that upon rupture of the oocysts, are released into the hemolymph from where they invade the salivary glands. There, sporozoites await the transmission to the next mammalian host by another mosquito bite. Image modified from www.euvaccine.eu/vaccines-diseases/diseases-of-poverty/malaria.

1.2.1 ESTABLISHING AN INFECTION

Infection of the mammalian host begins with the bite of a *Plasmodium*-infected mosquito, through which so-called sporozoites are injected into the skin of the new host. These banana-shaped, motile parasite stages move through the skin in search of a blood vessel to invade. Only a third of the transmitted sporozoites actually penetrate a capillary[13] and are subsequently carried away with the bloodstream until they reach the liver. In the liver sinusoids, sporozoites interact with heparin sulfate proteoglycans (HSPGs)[14] as well as additional receptors. They then attach to the endothelium and penetrate it by traversing through either Kupffer cells or liver sinusoidal endothelial cells (LSECs)[15–17]. After transmigration of several hepatocytes, sporozoites establish a persistent infection within a hepatocyte[17,18]. The latter occurs by invagination of the hepatocyte membrane, forming a parasitophorous vacuole (PV) around the parasite that physically shields it from the host cytoplasm.

1.2.2 THE LIVER STAGE

Once inside the hepatocyte, sporozoites de-differentiate and develop into a so-called liver stage, or extra-erythrocytic form (EEF). The parasites scavenge nutrients from the host, such as apolipoprotein H (ApoH)[19] and phosphatidylcholine[20], to support their massive growth, and exploit host pathways such autophagy (reviewed by Graewe *et al*., 2011[21] and Kaushansky and Kappe, 2015[22]). Despite highly dynamic host-parasite interactions at this stage, liver stage infections are clinically silent and do not cause disease symptoms. This is partially due to the fact that, in general, the liver is an immune privileged organ[23]. Additionally, only a very low number of liver stages result from a single infection, and the parasites effectively hide within their PV. Nevertheless, the host mounts an innate immune response to hepatic infection[24]. Arresting parasite development at this stage of the life cycle, *e. g.* by disrupting a gene essential for liver stage development, elicits a robust and protective immune response. This liver-stage attenuation is the basis of all vaccine candidates that induce sterile protection in human clinical trials, such as radiation-attenuated sporozoites (RAS)[25,26], genetically attenuated parasites (GAP)[27] or sporozoite infection under drug cover[28] (reviewed *e. g.* by Bijker *et al*., 2015[29]).

Parasites complete their intrahepatic development with a massive proliferation, during which thousands of daughter cells, so-called merozoites, are formed in a single liver stage. For this enormous asexual replication, the parasite undergoes several rounds of DNA replication and nuclear division without a subsequent cytokinesis, yielding a large syncytium, the multinucleated schizont. Then, daughter cells are formed by invagination of the plasma membrane that separates the nuclei from each other, resulting in up to 30,000 individual merozoites[21]. After merozoite formation is completed, the parasitophorous vacuolar membrane (PVM) is dissociated, while the host cell membrane stays intact, triggering the death of the host cell[30,31].

From the infected hepatocytes, merosomes (membrane-enclosed vesicles containing thousands of merozoites) bud off into the bloodstream[30,32]. Through the circulation, they reach the pulmonary capillaries of the lung, where the merosomes rupture and the freed merozoites can infect the red blood cells (RBCs) surrounding them[33]. Invasion of RBCs occurs in a sequential manner (reviewed by Koch and Baum, 2016[34]). Parasites attach through one of several possible receptor-ligand interactions to the erythrocyte membrane and re-orient themselves such that their apical tips face the erythrocyte membrane. The subsequent release of the content of micronemes and rhoptries (specialized secretory organelles of apicomplexan parasites) causes the formation of a tight junction through which parasites pull themselves actively into the RBC. As in hepatocytes, the parasite surrounds itself with a PV to shield it from the host cytoplasm.

1.2.3 THE BLOOD STAGE

In the erythrocyte, the parasite initiates a cycle of asexual replication, leading to the formation of new merozoites. Initially, the merozoite establishes itself in the RBC as a ring stage, which grows substantially and develops into a trophozoite. The trophozoite undergoes schizogeny, yielding a schizont containing about 8 to 32 daughter merozoites. Upon rupture of the erythrocyte, the merozoites are released into the blood and invade new RBCs. This asexual replication step is the phase of infection causing the clinical symptoms of malaria, including recurrent fever and anemia resulting from the loss of erythrocytes.

Plasmodium parasites extensively remodel their erythrocyte surrounding (reviewed by Gilson *et al.*, 2017[35]). Through an export machinery named PTEX (*Plasmodium* translocon of exported proteins), parasites export a wide variety of their own proteins into the RBC cytoplasm[36]. Many of these proteins serve to modify the erythrocyte allowing the transport of virulence factors to the parasite surface. One of the most important virulence factors in *P. falciparum* is *P. falciparum* erythrocyte membrane protein 1 (*Pf*EMP1), which is exported to knob-like structures on the surface of the erythrocytes[37–39]. There, *Pf*EMP1 interacts with receptors on the blood vessel endothelium, causing the parasites to cytoadhere in the vessels and thus avoid clearance by the spleen[40]. *Pf*EMP1 is expressed in a mutually exclusive manner from a large multigene family called *var* genes, and antigenic variation by switching *var* gene expression is a major part of the immune evasion of *Plasmodium*[41–43]. The cytoadherence of parasites leads to the clotting of vessels, especially in the brain microvasculature, and an inflammatory response[44]. Both contribute to cerebral malaria, one of the most severe forms of malaria, which often results in coma and death[44]. Cerebral malaria is often modeled by infecting C57BL/6 mice with the *P. berghei* ANKA strain[45], although not all mechanisms seem to be conserved[11].

The validity of the experimental cerebral malaria (ECM) mouse model has been extensively debated in the past[11].

Most blood-stage parasites continue the cycle of asexual replication, formation of merozoites and invasion of new red blood cells. However, some parasites will develop into sexual stages, the female and male gametocytes of the parasite. Factors that trigger gametocyte formation remain unknown, but parasite-derived microvesicles have been proposed to play a role[46,47]. These gametocytes initially leave the blood stream and hide in the bone marrow from the immune system until they are fully matured[48,49]. Then, they return to the blood, from which they are eventually taken up by a mosquito during its blood meal.

1.2.4 THE MOSQUITO INFECTION

Once in the mosquito midgut, gametocytes sense the change in the environment, indicated by a drop in temperature from 37 °C to 20 °C, an increase in pH and the presence of the mosquito molecule xanthurenic acid[50].

Male gametocytes then undergo several rounds of mitosis to develop into eight male gametes. These gametes are flagellated and highly motile, and, in a process called exflagellation, they rupture the PVM and the erythrocyte membrane to search for female gametocytes (reviewed by Bennink *et al*., 2016[51]). In the mosquito midgut, male and female gametocytes mate and form a zygote, which further develops into an ookinete, another motile stage of the *Plasmodium* parasite.

The ookinete traverses the midgut wall of the mosquito to establish an infection just outside of the midgut at the basal lamina. There, the ookinete transforms into a so-called oocyst, encapsulating itself into a cyst wall (reviewed by Aly *et al*., 2009[52]). Within the cyst, the parasite replicates again, forming thousands of sporozoites. These are already motile within the oocyst[53], and upon maturation, rupture the cyst wall to enter the hemolymph of the mosquito. From there, they are passively transported to the salivary glands of the mosquito, which they subsequently invade[54]. In the salivary glands, sporozoites await their transmission to the next vertebrate host by a mosquito bite, completing the life cycle.

1.3 GENETIC TOOLS FOR *PLASMODIUM* RESEARCH

With such a complex life cycle involving various hosts and tissues, the malaria parasite is a difficult organism to study. To identify new drug targets and vaccine candidates to fight malaria, deciphering the function of individual parasite genes in the various parts of the life cycle is essential. In 2002, the genome sequence of *P. falciparum* was published, revealing around 5300 genes in this parasite, of which about 60 % have no homology to known genes in other organisms[55]. These "orphan" genes are attractive drug candidates as inhibitors might not cause unintended side effects in the host. However, the lack of homologs renders the identification of the biological role of these *Plasmodium*-unique genes difficult. Therefore, a whole plethora of genetic tools has been developed to study *Plasmodium* genes, allowing the manipulation of gene expression, with the aim to infer the biological function from the resulting phenotype (reviewed *e. g.* by de Koning-Ward *et al*., 2015[56] or Shaw *et al*., 2017[57]). This section will summarize currently available technologies and discuss their advantages and disadvantages.

1.3.1 GENE KNOCKOUT AND GENE EDITING

Gene knockout, meaning the disruption of a gene of interest (GOI) on the DNA level, has been used in *Plasmodium* parasites since the mid-90s, when the development of efficient transfection protocols enabled the introduction of exogenous DNA to *Plasmodium* blood stages[58–61]. Exogenous DNA that comprises regions homologous to a *Plasmodium* sequence can integrate into the parasite genome via homologous recombination[59,61]. The presence of a single

homologous sequence on a circular plasmid results in a single crossover event by which the entire exogenous DNA sequence is inserted into the genome at this locus. If a sequence is flanked by two homologous arms, it can insert via double crossover, thereby replacing the *Plasmodium* DNA between the homologous regions[62]. As integration events resulting from single crossover can revert to wild type, most genetic modifications are now performed using double cross-over strategies.

Traditionally, gene knockout is achieved by allelic replacement of the target gene with a selection cassette that confers drug resistance to transgenic parasites (Figure 2 A). Among the first genes disrupted by allelic replacement with a selection marker were the circumsporozoite protein in *P. berghei*[63] and the knob-associated histidine-rich protein in *P. falciparum*[64], followed by many more. It is now estimated that about 500 *Plasmodium* genes (almost 10 % of all genes) have been successfully disrupted using this strategy[56]. Recently, even a genome-wide knockout screen was performed in *P. berghei*, using integration vectors with very long homology arms that have a high integration frequency[65]. These vectors, produced during the *Plasmodium* Genetic Modification Project (*Plasmo*GEM)[66], all carry an individual barcode, which allows for the parallel transfection of multiple knockout vectors. The growth phenotype of the individual knockout is then assessed by next generation sequencing of the pool of transfectants. This way, the effect of each knockout of all roughly 5700 *P. berghei* genes on blood-stage growth is now characterized[65].

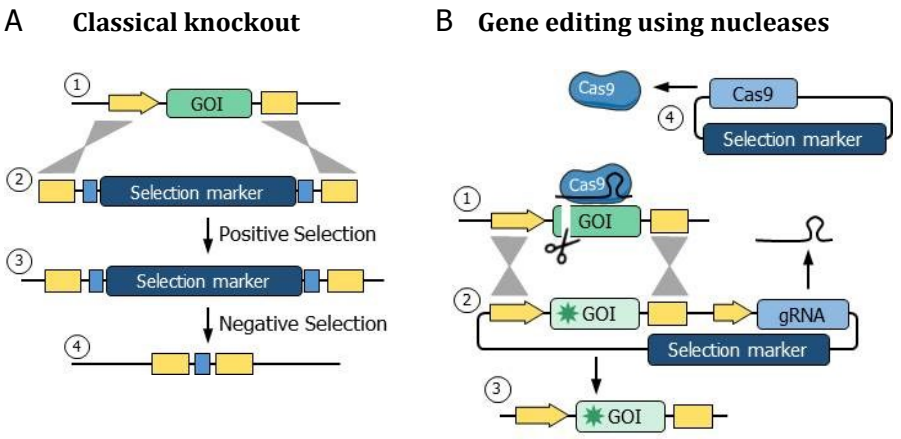

FIGURE 2: **Gene knockout and gene editing.** DNA segments in the *Plasmodium* genome can be replaced by exogenous DNA via double-crossover homologous recombination. (A) Conventional gene disruption relies on replacing the GOI ① with a drug-selectable marker ②. Drug selection (positive selection) yields parasites that have the selection marker integrated ③. If the selection marker also encodes y*FCU* and is flanked by homologous sequences, negative selection can select for marker-free parasites ④. (B) Nucleases such as Cas9, directed by gRNAs, sequence-specifically cleave the GOI ①. This cleavage event greatly increases the rate of homologous recombination, so that the GOI is efficiently replaced by a co-transfected repair template ②, yielding a marker-free, mutated GOI ③. This strategy requires the transfection of two plasmids, one encoding the repair template and the gRNA ② and the other encoding the Cas9 ④. This image has been created using elements from Servier Medical Art (www.servier.de)

The relatively low efficiency of homologous recombination especially in *P. falciparum* renders gene knockout very laborious. The introduction of a DNA double-strand break (DSB) at the target locus substantially increases the frequency of homology-directed recombination. Not surprisingly, this approach has been applied to *Plasmodium*. The first strategy to site-specifically cleave a gene in *Plasmodium* was the expression of zinc-finger nucleases (ZFN), artificial enzymes that can be engineered to target a specific locus on the DNA[67]. The parasite uses a repair template provided in parallel to restore the integrity of the genome. This repair is highly efficient, as the alternative repair pathway via non-homologous end-joining (NHEJ) is absent in *Plasmodium* species[68,69]. Thus, transgenic parasites can be obtained without the need to integrate a selectable marker, facilitating construct design and marker-free introductions of point mutations at the target site[68,70,71].

One major disadvantage of ZFNs is that proteins binding a specific target site are challenging and laborious to generate. Recently, a much simpler tool to achieve targeted DSBs has been introduced to *Plasmodium*: The CRISPR (clustered regulatory interspaced short palindromic repeats)-Cas9 (CRISPR-associated protein 9) system (Figure 2 B)[72,73]. In this system, a guide RNA (gRNA) targets the endonuclease Cas9 to the genomic locus of interest. Cas9 then cleaves the DNA at this locus, which is subsequently repaired by homologous recombination, provided a homologous template is present (reviewed *e. g.* by Wang *et al*., 2016[74]). Target specificity is solely determined by the sequence of the 20 nt-long gRNA, rendering CRISPR-Cas9 a versatile and easily adaptable system that even enables genomic-wide screens. Such a genome-wide CRISPR-Cas9-mediated knockout screen has already been successfully performed in *Toxoplasma gondii* (*T. gondii*), a close relative of *Plasmodium*[75]. CRISPR-Cas9-mediated genome editing in *P. falciparum* is highly efficient and easily adaptable to any desired target sequence, making it the current standard procedure for gene targeting. While it was also successfully applied to *P. yoelii*[76], there are no reports of its application in *P. berghei*.

Gene knockout and gene editing have been invaluable to study the biological role of individual genes. Recent advances in the efficiency of these technologies are expected to further extend this knowledge, especially for the 1900 genes (*P. berghei*) or 2075 genes (*P. falciparum*) that are currently annotated as having unknown functions (www.plasmodb.org, April 2017). However, all these systems have a major drawback in common: as transfection and gene editing occurs in the blood stages of *Plasmodium*, any genes that are essential for this stage cannot be targeted since their knockout is lethal to the parasite. Conditional systems permitting inducible gene knockout are thus necessary to study the function of blood-stage essential genes. These will be discussed in the next section.

1.3.2 CONDITIONAL GENE KNOCKOUT

One approach to control the timing of gene deletion is the use of recombinases. These proteins will excise DNA segments that are flanked by recombinase recognition sites from the genome. Two systems have been adapted for *Plasmodium*: the flippase FLP, which binds to FLP recognition sites (frt)[77], and the Cre protein that binds to loxP sites[78]. The frt or loxP sites are very short nucleotide sequences (about 30 bp long) and flanking a gene with these sequences (referred to as *flirting* or *floxing*) should not interfere with normal gene function. Upon expression of the corresponding recombinase, however, the gene flanked by the recognition sites is rapidly excised and removed from the genome. The deletion of the gene is entirely dependent on the expression of the recombinase, which thus must be tightly controlled.

Recombinase-mediated knockout

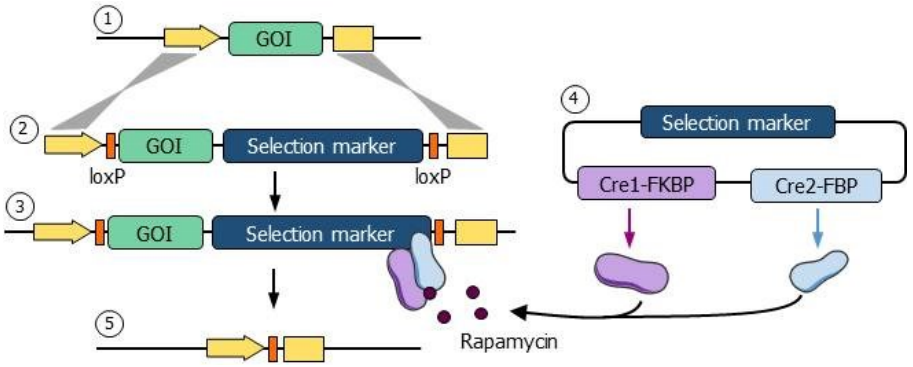

FIGURE 3: **Recombinase-mediated knockout.** Here, the regulatable DiCre System is depicted exemplarily. The GOI ① is replaced with a version of the GOI that is flanked by recombinase recognition sites (here loxP sites) ②. A selection marker is included to allow for the selection of double-crossover recombination events ③. In the resulting line, a plasmid is transfected which encodes the two fragments of the split Cre recombinase: Cre1-FKBP and Cre2-FBP ④. Upon addition of rapamycin, the two parts dimerize, and the active Cre recombinase mediates the recombination of the loxP sites, resulting in the deletion of the GOI ⑤. This image has been created using elements from Servier Medical Art (www.servier.de)

In *P. falciparum*, Cre recombinase has been shown to be more efficient than the FLP/frt system[79]. The expression of Cre can be controlled using a tetracycline (Tet) regulatable promoter (discussed in detail below). Thus, the knockout of a *floxed* GOI can be precisely timed by the addition of anhydrotetracycline (aTc) to the culture medium[79]. A more recent strategy, called the DiCre System, uses a split Cre protein in which one part is fused to a human FK506-binding protein 12 (FKBP12) and the other to the binding domain of the FKBP12-rapamycin-associated protein (FRB) (Figure 3)[80,81]. While the split Cre is inactive, addition of the small ligand rapamycin triggers heterodimerization and thus activation of Cre. Akin to the Tet-controlled Cre, this allows for a timed and inducible gene knockout, *e. g.* of the blood-stage essential apical membrane antigen 1 (AMA1)[82]. As recombinase-mediated gene excision is not 100 % efficient and single parasites can evade the gene deletion,

the DiCre system has been combined with a reporter gene whose expression is only turned on after recombination[81]. Reporter gene expression can thus be used to identify positive recombinants.

A major drawback of the recombinase-mediated gene knockout is that *flirting* or *floxing* large target genes can be very laborious, as it requires either cloning the whole gene or sequential transfection of integration constructs to insert both recognition sites. The use of a short synthetic intron carrying a loxP site (loxPint), which can be integrated close to the 5'end of the GOI, facilitates *floxing*[83]. However, although the loxPint has been used to ablate expression of several genes, it is unclear if this artificial intron is correctly spliced in all genetic contexts. Another disadvantage is the minor antimalarial activity of rapamycin (IC50: 2.7 μM)[82], and side effects of the treatment have to be considered. Additionally, the DiCre system is not applicable in mammalian hosts, due to immune-modulatory effects of rapamycin in mice[84].

In *P. berghei*, the expression of recombinases is thus not controlled by small ligands, but by exploiting stage-specific promoters[85,86]. In this manner, FLP has been expressed under the TRAP (thrombospondin-related anonymous protein) promoter or the UIS4 (upregulated in infectious sporozoites 4) promoter, to express FLP only in mosquito stages[85,87]. Genes flanked with frt sites are unaffected in blood stages, but excised upon transmission of the parasites to mosquitoes. Using this strategy, the blood-stage essential merozoite surface protein 1 (MSP1) was deleted in liver stages, which revealed that this protein is essential for the correct formation of merozoites in the intrahepatic development[85].

In summary, recombinases are useful tools to target genes for which a conventional knockout strategy is not possible. Due to the rapid gene deletion, there is no selection of evasion mutants as can happen during the long procedure of generating traditional knockouts. Conditional gene knockouts are "all-or-nothing", and do not allow for intermediate expression levels. Other systems have been developed to regulate and tune gene expression to investigate "dose-dependent" phenotypes and will be discussed in the following Section.

1.3.3 KNOCKDOWN OF GENE EXPRESSION

Expression of a GOI can be altered not only by removal, *i. e.* knockout, but also by modulating gene expression at the transcriptional, post-transcriptional or post-translational level. For all these steps, tools have been developed in *Plasmodium*. These knockdown strategies have in common that they are not 100 % efficient, which can be a disadvantage when low levels of gene expression are sufficient for gene function. On a positive note, knockdown strategies allow for the investigation of intermediate phenotypes.

Regulation of gene expression on a transcriptional level is achieved through modifying the promoter. In *P. berghei*, a "promoter swap", *i. e.* the replacement of the endogenous promoter by a different promoter, is a widely used method to alter the gene expression profile across the life cycle[88]. If the GOI is *e. g*. expressed across the life cycle, but essential in blood stages, the promoter of said gene can be exchanged with a blood-stage-specific promoter. This promoter swap should not affect blood stage development but ablate gene expression in other stages, resulting in loss-of-function phenotypes there. However, this method changes the overall expression pattern of the gene and is not inducible or reversible. It also does not permit to study essential genes in blood stages. Additionally, many promoters are leaky and at least weakly expressed in all life cycle stages, confounding phenotypic analysis[89,90].

Alternatively, the promoter of a GOI can be replaced by an inducible promoter. In both *P. berghei* and *P. falciparum*, the "Tet-OFF" system has been used (Figure 4 A)[91,92]. Here, the promoter of the GOI is replaced with a promoter containing tetracycline operator (TetO) sites. Transcriptional transactivator domains (TRAD) bind to these TetO sites and trigger expression of the gene. Upon addition of the tetracycline analog aTc, TRAD binds to aTc instead of the TetO. Thus, gene expression is silenced. In *P. falciparum*, this system can regulate gene expression from episomes, but not endogenous genes, likely due to low activation of transcription by the TRAD proteins[56,91]. In *P. berghei*, TRAD activity has been improved by using endogenous transactivator domains[92,93]. This improved Tet-OFF system was used to regulate the expression of various genes, including some that are essential for blood-stages[92,94], and could also downregulate a reporter gene in *in vitro* liver stages[92]. The dynamic range of the knockdown is somewhat limited, yielding knockdown efficiencies of around three to four-fold[94].

Several tools to mediate gene knockdown act on the mRNA of the GOI. In many eukaryotic organisms, RNA interference is the method of choice to silence genes by cleaving the mRNA (discussed in detail in Section 1.4). Unfortunately, *Plasmodium* parasites lack the required machinery, rendering this potent tool unavailable for malaria research[95]. One alternative that has been employed with limited success in *P. falciparum* are small chemical molecules that bind in an antisense manner to the RNA of interest and thereby inhibit translation (Figure 4 B). For example, synthetic peptide nucleic acids (PNAs), oligonucleotides with uncharged backbones, bind *in vivo* to complementary RNA and prevent translation[96–98]. Similarly, vivo morpholinos, which are phosphorodiamidate morpholino oligomers (PMOs) conjugated to octa-guanidinium dendrimers to improve cellular uptake, have been shown to inhibit splicing and translation by binding to the corresponding RNA[99]. PMOs can also be conjugated to peptides (PPMO), and these can be designed in such a way that they mimic the natural substrate of RNaseP, triggering target cleavage by the *Plasmodium* RNaseP[100,101]. These inhibitors have been shown to reduce gene expression by up to four-fold. However, as this requires very high

amounts of the inhibitors, off-target effects are frequently observed that confound the phenotypic analysis.

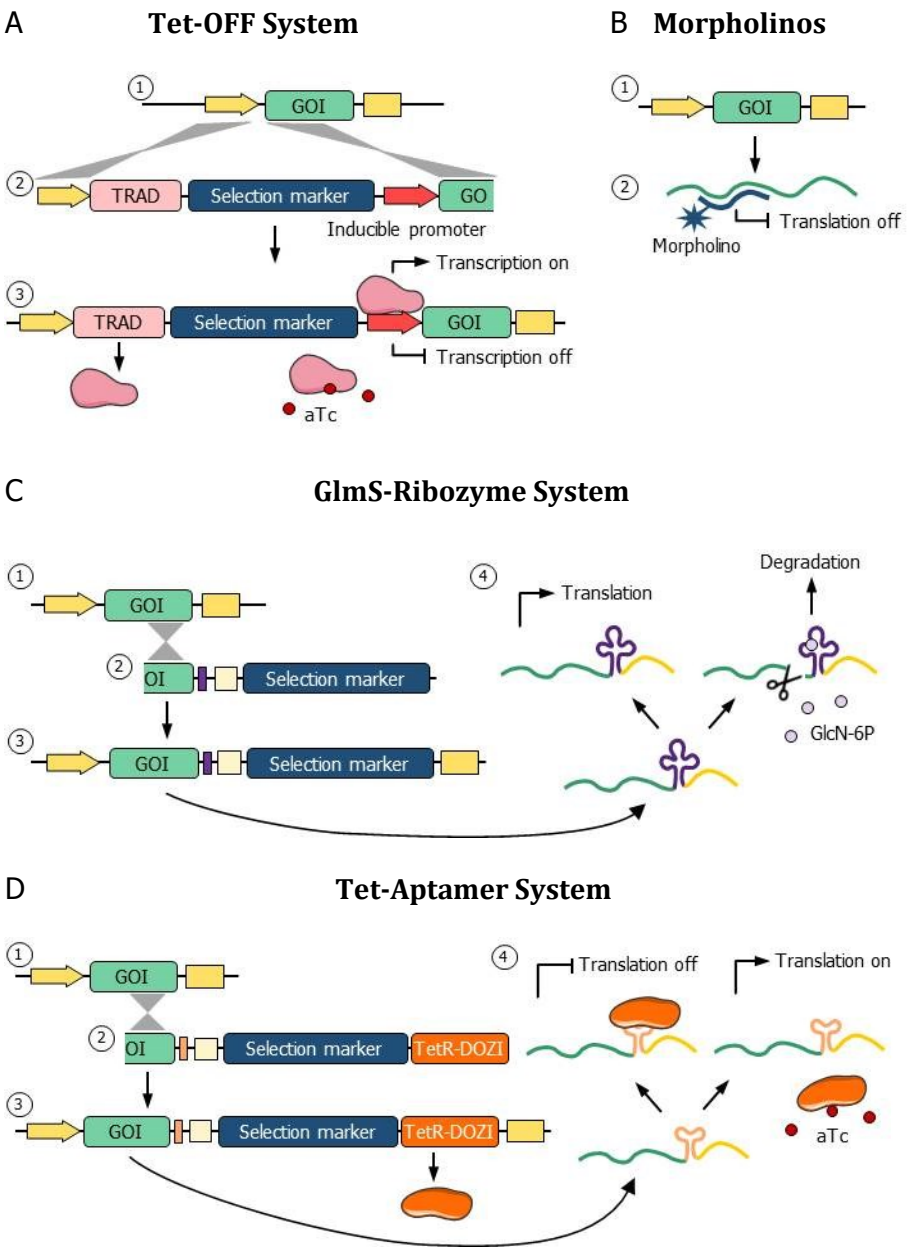

FIGURE 4: **Transcriptional and post-transcriptional repression.** (A) For the Tet-OFF-system, the promoter of the GOI ① is replaced by a cassette encoding TRAD, a selection marker, and an inducible promoter ②. TRAD is expressed and triggers the transcription of the GOI. Upon addition of aTc, TRAD is sequestered from the inducible promoter, and gene transcription is inhibited ③. (B) Morpholinos are synthetic RNA molecules binding to the mRNA of the GOI ② and preventing translation. The genetic locus is unaffected ①. (C) For the glmS-ribozyme system, the 3'UTR of the GOI ① is replaced with a ribozyme-containing UTR ② via single crossover ③. Upon addition of GlcN-6P, the ribozyme is activated and cleaves the mRNA, triggering degradation ④. (D) In the Tet-aptamer system, the 3'UTR of the GOI ① is modified by single crossover to include an aptamer sequence ②. At the same time, a gene encoding the TetR fused to DOZI is introduced ②. The TetR-DOZI is constitutively expressed ③ and prevents gene translation by binding to the aptameric sequence and initiating storage. Upon addition of aTc, the TetR-DOZI is sequestered, and the gene can be translated. This image has been created using elements from Servier Medical Art (www.servier.de)

Other strategies to regulate mRNAs act *in cis*, as regulatory elements are introduced to the mRNA itself by genetic modification. Widely used are self-cleaving ribozymes, such as the 5' cis-regulatory element in the glucosamine-6-phosphate synthase (glmS) gene of bacteria[102]. This glmS element can be placed in the 3'UTR of the GOI and, upon induction with glucosamine-6-phosphate (GlcN-6P), cleaves the mRNA, reducing its translation (Figure 4 C)[103]. Cleavage commonly results in a roughly three-fold reduction on the RNA level, which translates into an about 10-fold reduction of protein levels[103]. The introduction of the glmS element requires only a single 3' replacement strategy and does not interfere with normal protein expression, making it an attractive and easy tool for inducible gene knockdown. As GlcN-6P is toxic to *Plasmodium*, the precursor glucosamine (GlcN) is used to trigger knockdown and is converted in the parasite to GlcN-6P[57,103]. However, also GlcN affects parasite growth at higher concentrations[103]. Thus, when the level of knockdown that can be achieved with non-toxic GlcN concentrations is not sufficient to detect a phenotype, the use of the glmS system is limited. In *P. berghei*, only a single publication reports the successful application of the glmS system to regulate gene expression, and the knockdown was restricted to *in vitro* cultures[104].

Tet-responsive aptamers are an alternative to ribozymes. *In vitro* selection revealed small artificial RNA aptamers that bind to the Tet repressor (TetR)[105]. If such an aptamer is introduced close to the translation initiation site, the TetR binds the mRNA and prevents translation. Upon addition of aTc, the interaction is blocked, and protein expression is induced. This system is rapid, stable and reversible, yielding up to about five-fold knockdown[106]. It has recently been refined by coupling TetR to the DOZI (development of zygote inhibited) protein (Figure 4 D)[107]. This protein mediates storage of mRNA in processing bodies of the gametocyte until the parasite reaches the mosquito[108]. Binding of TetR-DOZI to the target mRNA thus inhibits its translation and targets it for storage, greatly improving the knockdown capacity to up to 300-fold for a luciferase reporter.

The tools discussed so far modify mRNA levels by either controlling transcription, inhibiting translation or degrading the mRNA. Another option to regulate gene expression is the direct modification of protein levels. Here, transcription and translation of the GOI are unaffected, but the protein is either degraded or mislocalized to prevent its function.

One of the most widely used strategies for post-translational regulation is the fusion of the protein of interest to a degron (Figure 5 A). Degrons are small protein domains that are structurally unstable and promote their own ubiquitination. Fusion of these to the protein of interest thus results in proteasomal degradation of the whole protein. This degradation can be prevented by small ligands which, when added to the medium, bind to the degron and stabilize it. Two degrons have been used in *Plasmodium*: the FKBP-based destabilization domain (DD), which is stabilized by the small ligand

Shield-1[109,110], and the *Escherichia coli* (*E. coli*) DHFR destabilizing domain (DDD), which is stabilized by trimethoprim[111]. The latter can only be applied in parasites expressing hDHFR, which mediates resistance against the antimalarial trimethoprim[111]. As it is a ligand-on system, meaning that the ligand has to be supplied to ensure protein stability, DD- or DDD-are especially well suited for the regulation of dominant negative genes[112] or auto-regulatory protein domains[113]. Yet, DD- or DDD-based knockdowns are restricted to proteins that tolerate tagging, and that are accessible to the proteasomal degradation system. The knockdown efficiency appears to depend on the gene context but is typically around four-fold for the DD system[114]. In some cases, stabilization by Shield-1 was insufficient to restore protein expression to its full extent[114], and in others, the knockdown was not strong enough to observe a phenotype[113]. Additionally, Shield-1 has slightly anti-malarial activity at high concentrations[114]. Only a single report exists that describes the application of the DD system in *P. berghei*, and only a moderate knockdown without corresponding phenotype was observed[115].

Another degron system that has been applied to both *P. falciparum*[116] and *P. berghei*[117] acts as ligand-off system: the auxin-inducible degron (AID) (Figure 5 B)[118]. Here, parasite lines are used that express an auxin-responsive F-box protein (transport inhibitor response 1 from the rice plant *Oryzae sativa* (*Os*TIR1)). This F-box protein interacts with the Plasmodium proteins to form the Skp1, Cullin1, F box protein ubiquitin ligase (SCF) complex. The GOI is fused to the AID domain. In the presence of auxin, OsTIR1 interacts with AID, recruits the SCF complex and ubiquitylates the protein, targeting it for degradation. This way, protein levels could be reduced by up to 30-fold[118]. However, high amounts of the inducer are needed to achieve this knockdown, and although auxin is not toxic to the parasite, this requirement limits the application in mice. In *P. berghei*, a knockdown was thus only realized in *in vitro* cultures[117]. As for the DD or DDD systems, the knockdown efficiency likely depends on the protein target.

Other strategies perturb protein function not by degradation, but by conditional aggregation or conditional mislocalization of the protein. The first has been realized by fusion of a protein to a conditional aggregation domain (CAD)[119]. CAD causes self-aggregation of the protein in the ER, which is reversible upon addition of the compound AP12998. This strategy is only applicable for secreted proteins and publications reporting its use are sparse. Recently, a conditional mislocalization system (knock sideways) has been adapted to *Plasmodium* (Figure 5 C)[120,121]. Here, the GOI is fused to an FKBP domain which, upon addition of rapamycin binds to an FRB domain that localizes differently, *e. g.* in the nucleus. As the GOI is thereby detargeted from its regular locus, *e. g.* the cytoplasm, it can no longer perform its function, essentially resulting in a loss-of-function phenotype. Successful inducible protein displacement has been demonstrated for *P. falciparum* blood stages *in vitro*[120] and for *P. berghei* blood stages and mosquito stages *in vivo*[121].

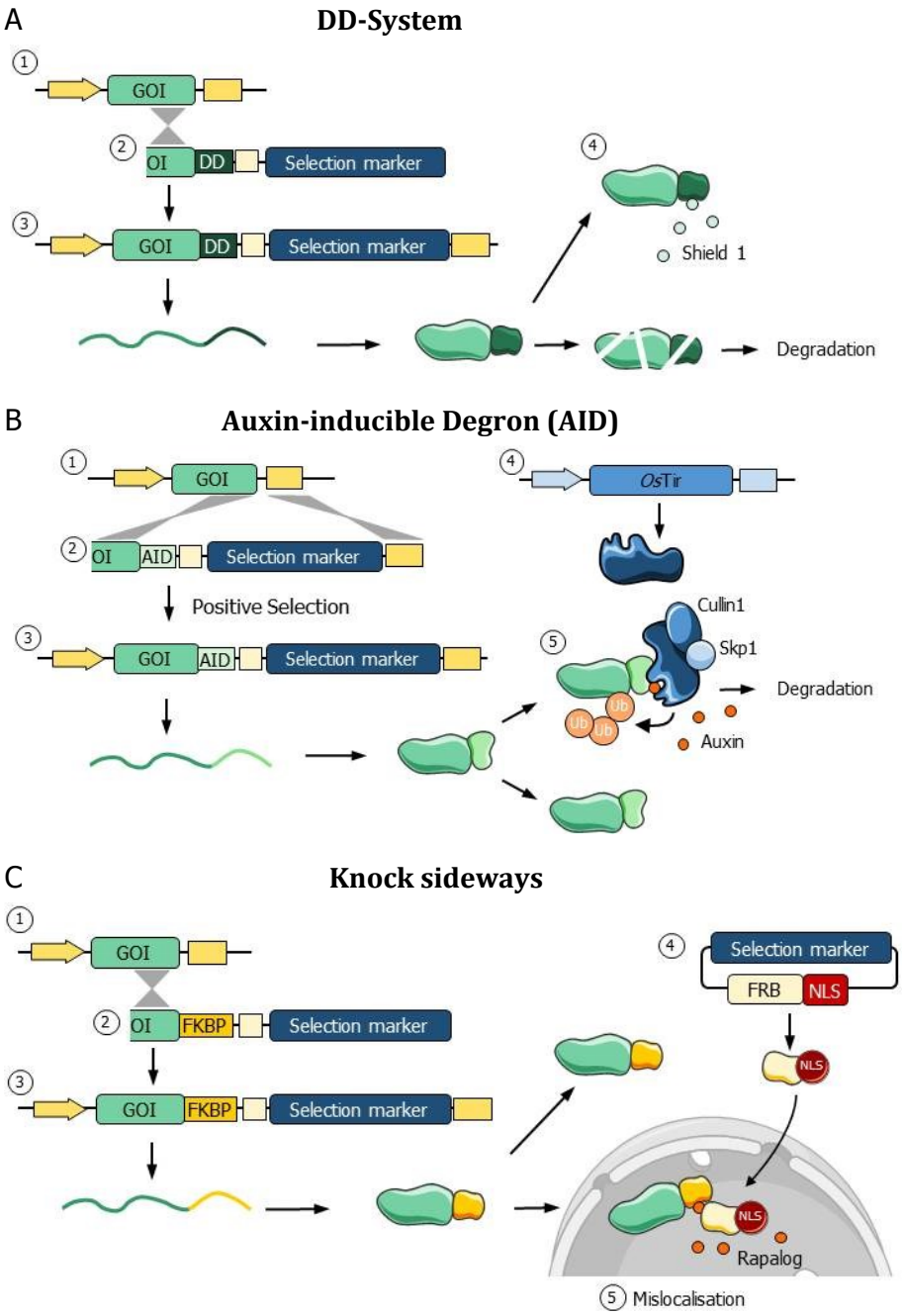

FIGURE 5: **Post-translational modification of protein activity.** (A) To control protein degradation, the GOI ① is tagged C-terminally with a degron domain (DD) using a single crossover strategy ②. From the modified locus ③ the gene is translated. The DD domain fused to the GOI will destabilize the protein, resulting in its degradation, unless the stabilizing molecule Shield-1 is present ④. (B) A similar strategy utilizes the auxin-inducible degron AID. Fusion of the GOI ① to AID by double crossover ② yields expression of a fusion protein ③. From a different locus, the *Os*Tir is expressed that forms the SCF complex with endogenous *Plasmodium* proteins ④. Upon addition of auxin, the SCF is recruited to the AID and ubiquitylates the protein (Ub), targeting it for degradation ⑤. (C) Knock sideways is a different approach in which the GOI ① is fused to an FKBP domain ②. The protein is expressed from its genomic locus ③ and exerts its function in the cytoplasm. In parallel, an FRB fused to an nuclear localization signal (NLS) is expressed ④. Upon addition of the rapamycin analogue rapalog, the FRB and the FKBP-domain dimerize, sequestering the protein from its regular localization into the nucleus. This image has been created using elements from Servier Medical Art (www.servier.de)

Despite many advances in recent years, the technologies available to study *Plasmodium* gene function are still limited, and several challenges remain unsolved. Tunability is one of these issues, as there are only limited options to modulate or fine-tune gene expression in order to observe intermediate phenotypes. Also, many genetic tools only act on the asexual blood stage of *P. falciparum*. Manipulation of *P. berghei* gene expression *in vivo*, especially in mosquito or liver stages, is still difficult. Finally, as most tools require the manipulation of the genetic locus of the GOI, which is often labor- and time-intensive, high-throughput screens remain out of reach.

1.4 RNA INTERFERENCE

"RNA interference has proven to be a quite reliable mechanism for turning genes off in a whole variety of different plants and animals."

~ Craig Cameron Mello (*1960)

RNA interference (RNAi) is a widespread mechanism to regulate gene expression posttranscriptionally. Almost all eukaryotes, including plants, animals, and protozoa such as trypanosomes use RNAi to control gene expression. RNAi is based on short RNA molecules, so-called microRNAs (miRNAs), which bind complementary target mRNA sequences and induce their cleavage, translational repression and/or degradation. In humans, more than 60 % of all protein-coding genes are predicted to be controlled by miRNAs[123], demonstrating the importance of RNAi. It is thus surprising that *Plasmodium* parasites have lost all components of the RNAi machinery[95]. This is particularly unfortunate for research, as RNAi can be easily exploited for targeted gene knockdown by introducing short hairpin RNAs (shRNAs) or short interfering RNAs (siRNAs). The following Sections will briefly delineate the mechanism of canonical RNAi in animals and introduce the various non-canonical RNAi pathways that have been described recently.

RNAi has been discovered for the first time in the nematode Caenorhabditis elegans*, with lin-4 being the first miRNA described*[122]

1.4.1 CANONICAL RNAI PATHWAY

RNAi in animals is executed by small RNA molecules, the miRNAs, which can be encoded by separate genes or within introns of protein-coding genes[124,125]. Their generation is a multistep process requiring several proteins (Figure 6, reviewed *e. g.* by Ha and Kim, 2014[126]). MiRNAs are transcribed by RNA polymerase II as primary (pri)-miRNAs and processed akin to protein-coding mRNAs by splicing, capping, and polyadenylation[127,128]. The typically over 1 kb long transcripts contain one or more hairpin structures[128], which are processed by an RNase III family enzyme called Drosha[129–132]. Drosha acts in conjunction with the protein DGCR8 (DiGeorge syndrome critical region gene 8), forming a complex called microprocessor[133–136]. The microprocessor cleaves the flanking sequences from the hairpin structures, yielding precursor (pre)-miRNAs. These are exported from the nucleus by Exportin 5 (XPO5)[137–139].

Once in the cytoplasm, pre-miRNAs are further processed by the endonuclease Dicer, which cleaves the loop of the hairpin structure and releases the mature miRNA duplex[141–144]. Dicer requires the association with another RNA binding protein. In humans, this is often the Tar RNA binding protein (TRBP), although the protein PACT can also associate with Dicer[145–148]. After Dicer/TRBP-mediated processing, the miRNA-duplex is loaded into a protein of the Argonaute (Ago) family, forming the RNA-induced silencing complex (RISC)[149–151]. Humans have four different Ago proteins (Ago1-4), which all participate in miRNA-mediated gene silencing, but only one, Ago2, has a catalytically active RNaseH domain and can cleave targeted mRNAs in a process called slicing[152–154]. Within RISC, one strand of the miRNA duplex, the so-called guide strand is selected, while the other, the star or passenger strand, is removed. Strand selection is mainly determined by the thermodynamic stability of the 5' terminus: the strand with the lesser stability is preferred as guide strand[155,156]. Removal occurs either by cleavage and degradation of the star strand (in the case of Ago2 and a perfect complementarity between the two strands of the duplex)[157–161] or by helicase-assisted unwinding (for non-slicing Ago proteins and if there are mismatches between the guide and star strand)[162–168]. While the guide strand is generally preferentially loaded into RISC, next generation sequencing showed that for almost all miRNAs, the passenger strand is infrequently selected as well[169].

PACT stands for protein activator of the interferon-induced protein kinase as it has first been implicated in the immune response to viral infections[140].

After one strand is removed, mature RISC then binds to the target mRNA based on its complementarity to the miRNA. Target selection is mainly determined by the nucleotides 2-8, which constitute the seed region of the miRNA[171–175]. Target mRNAs are then silenced depending on the extent of base pairing between miRNA and mRNA and the Ago protein within RISC (reviewed *e.g.* by Wilczynska and Bushell, 2014[176]). Ago2 cleaves the mRNA if there is perfect complementarity in the central region of the miRNA[177,178]. In animal cells, the base pairing between miRNA and mRNA is usually imperfect, which triggers translational repression through inhibition of translation initiation[179–186], followed by deadenylation and degradation of the mRNA. Both processes are mediated by effector proteins binding to Ago2, first and foremost the glycine-tryptophan-rich protein GW182[187–189]. GW182 binds to Ago2 and recruits additional effector proteins, such as the poly(A) binding protein PABP and the CCR4-NOT deadenylase complex[190–192]. Also, the DEAD-box RNA helicase DDX6/Rck-p54 is directly or indirectly recruited to Ago2 and essential for miRNA-mediated gene silencing, possibly also by recruiting the CCR4-NOT complex[193–196]. Decapping and removal of the poly(A) tail finally target the mRNA for rapid degradation. Both GW182 and DDX6/Rck-p54 target RISC to processing (P-) bodies, cytoplasmic foci of mRNA storage and degradation, although miRNA-mediated knockdown also occurs in the absence of P-bodies[187,193,197,198].

In humans, there are three different GW182 proteins: TNRC6 A, B and C

Only about 1 % of all Ago2 localizes to P-bodies, while the majority of miRNA-mediated silencing happens in the cytoplasm[170].

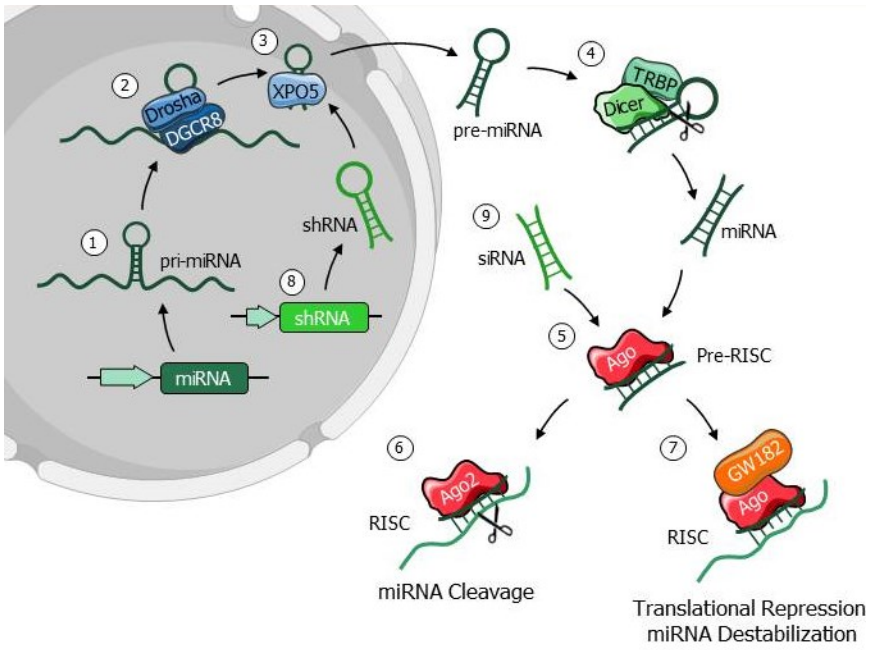

FIGURE 6: **The canonical RNAi pathway.** MiRNAs are transcribed in the nucleus as pri-miRNAs ①, which are processed by Drosha and DGCR8 to pre-miRNAs ②. XPO5 is then responsible for their translocation into the cytoplasm ③, where the pre-miRNAs are further processed by Dicer with the help of an RNA-binding protein such as TRBP ④. Then, the mature miRNA is incorporated into the pre-RISC complex by binding to an Ago protein ⑤. Note that loading of Ago likely involves additional proteins, and that the free miRNA is depicted here only for simplicity. One strand of the miRNA is selected as guide strand, yielding the mature RISC, while the other strand is degraded. The RISC then binds to its mRNA target complementary to the miRNA sequence. In the case of perfect complementarity and if RISC contains Ago2, Ago2 will slice the mRNA, resulting in its degradation ⑥. More commonly, however, miRNA binding is imperfect, and additional proteins such as the GW182 are recruited to RISC, mediating translational repression and mRNA destabilization ⑦. RNAi can be artificially induced by introducing either genetically encoded shRNAs ⑧ or short RNA duplexes (siRNAs) ⑨. This image has been created using elements from Servier Medical Art (www.servier.de)

The endogenous RNAi pathway can easily be exploited to artificially induce gene silencing[205] (Figure 6). For example, synthetic siRNAs, small RNA duplexes that can be introduced into cells *e. g.* by transfection, act directly as Ago2 substrate[199]. These siRNAs are typically designed to be perfectly complementary to the target mRNA and thereby induce target cleavage through the slicing activity of Ago2. In contrast, shRNAs are DNA-encoded small RNAs that upon transcription form a hairpin, which is subject to XPO5 export and Dicer processing before entering RISC[200]. As target specificity is solely determined by the 20-21 nt long sequence of the si- or shRNA, RNAi-mediated knockdown can be easily adapted to a target of choice, and genome-wide screening approaches using shRNA/siRNA libraries have yielded a plethora of new information about gene function in RNAi-competent organisms[201–203].

1.4.2 NON-CANONICAL RNAI PATHWAY

Besides the canonical RNAi-pathway, by which 99 % of all miRNAs are processed, various alternative, non-canonical mechanisms exist that generate

active RISCs[204,205] (Figure 7). Several different short RNA species have been reported to serve as Drosha-independent precursors for active miRNAs, including tRNAs or tRNA- like precursors[206–209], small nucleolar RNAs (snoRNAs)[210–212], or naturally occurring dsRNA transcripts that give rise to endo-siRNAs or endo-shRNAs[213–216]. A prominent class of non-canonical RNAi mediators are miRtrons, which are miRNAs derived from introns during splicing[217–220]. They bypass Drosha, as the small introns form hairpins which are further processed by the lariat-debranching enzyme to a pre-miRNA[217–219]. The pre-miRNAs then enter the canonical RNAi pathway by XPO5-mediated export and Dicer-processing prior to Ago2 loading. A subclass of miRtrons, so-called agotrons, not only circumvent Drosha- but also Dicer-mediated processing, and are directly loaded into Ago2. The biological function of these agotrons is however unclear[221].

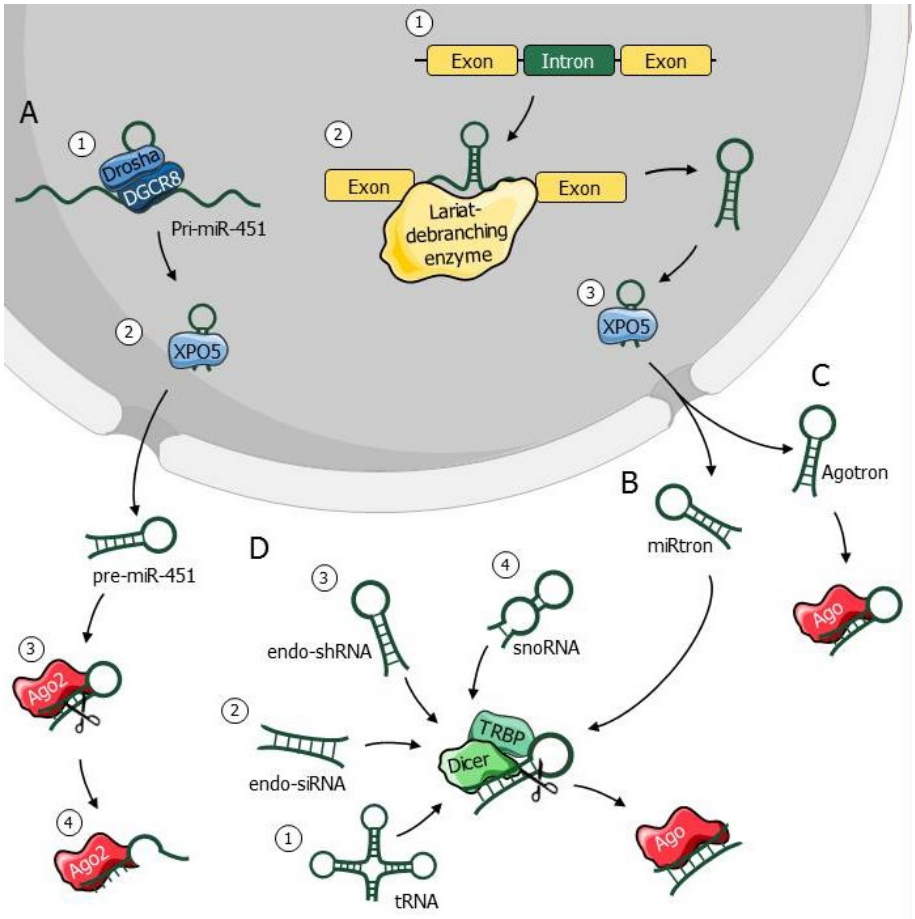

FIGURE 7: **Non-canonical processing of Ago-associated RNAs.** (A) MiR-451 is processed by Drosha and DGCR8 ① and exported by XPO5 ② akin to canonical miRNAs. Instead of Dicer processing, this miRNA is loaded directly into Ago2 ③. Cleavage of the passenger strand then activates RISC for target knockdown ⑤. (B, C) Introns ① can also serve as a substrate for Ago2 loading. They are processed by the lariat-debranching enzyme ② and exported into the cytoplasm ③. (B) MiRtrons are processed by Dicer and TRBP, following the canonical RNAi pathway. (C) Agotrons are directly loaded into Ago2, but their biological function is unclear. (D) Also, other small RNAs are processed by Dicer, including tRNAs ①, endo-siRNAs ②, endo-shRNAs ③ and snoRNAs ④. This image has been created using elements from Servier Medical Art (www.servier.de)

Other small RNAs are a substrate of Drosha, but bypass Dicer-mediated processing. A prime example is miR-451, which is an unconventional miRNA that is abundant in red blood cells and important for erythropoiesis[222–227]. Drosha-processing of the pri-miR-451 yields a very short hairpin with a stem length of only 17 nt, which is no longer recognized by Dicer as substrate[228–230]. Instead, it is directly incorporated into Ago2, which slices the 3' strand of the miRNA in its center, resulting in a 30 nt-long intermediate RNA. This precursor is then further trimmed at the 3' end by the Poly(A)-specific ribonuclease PARN, yielding the about 23 nt-long mature miR-451[231]. This trimming is, however, not essential for the function of miR-451[231].

As for the canonical RNAi pathway, also non-canonical pathways can be exploited for targeted gene silencing. This is exemplified by shRNAs that mimic the Dicer-independent miR-451, so-called AgoshRNAs[232,233]. These AgoshRNAs are characterized by shortened stems of 16-19 nt, a mismatch at the bottom of the stem and a small loop, all of which prevents the processing by Dicer[232–237]. Instead, they are directly bound by Ago2, which, similar to miR-451 processing, will cleave the 3' strand, yielding a roughly 30 nt long mature AgoshRNA[232,238]. AgoshRNAs tend to be less active than their shRNA counterparts[236] but they have other advantages. Because their biogenesis involves no passenger strand (which could participate in RNAi silencing[236]), AgoshRNAs are proposed to have reduced off-targeting effects. They also are less toxic to cells as their overexpression does not saturate the endogenous RNAi machinery[233,236], in contrast to conventional sh- or siRNAs[239]. Additionally, these AgoshRNAs rely solely on Ago2 and can thus also be used in cells that lack Dicer, such as monocytes[240].

1.5 *PLASMODIUM* AND RNAI

1.5.1 INTERACTION OF *PLASMODIUM* WITH HOST MIRNAS

Plasmodium interacts in many ways with its host during infection, and it is thus not surprising that this interaction also involves the hosts RNAi pathway. Investigation of the miRNAs of *Plasmodium*-infected RBCs showed that miR-451 is the predominant miRNA[241,242] and implied that it has both beneficial as well as inhibitory effects for the parasite. During blood-stage infection, infected red blood cells were reported to shed extracellular vesicles which parasites use for cell-to-cell communication[46,47]. Among other host and parasite proteins, these vesicles also contain functional Ago2-miR-451 complexes that are transferred to endothelial cells[243]. In these cells, miR-451 silences Caveolin-1 and Activating Transcription Factor 2. As silencing of these genes stimulate the expression of cellular receptors on the endothelial cells, it enhances the binding and sequestration of the infected RBC[243]. While miR-451 is favorable for parasite infection in this case, this effect seems to be reverted when miR-451 expression is greatly increased, *e. g.* in sickle cell disease[244]. Apparently, miR-

451, along with the miRNA let-7i, translocates to the parasite cytoplasm. There, it integrates into essential parasite mRNAs, which prevents translation by impairing ribosomal loading[245]. In normal blood cells, this effect is minor and does not impede parasite growth. In contrast, the increased miRNA levels in sickle cell disease significantly affect parasite growth, contributing to the known resistance of sickle cell erythrocytes to malaria infection[245,246]. However, trans-splicing of erythrocyte miRNAs into parasite mRNAs has not been reported previously, and independent validation of these data is still lacking.

Besides miR-451, other host miRNAs also affect *Plasmodium* growth. We and others have previously shown that *Plasmodium* liver stage infection alters the miRNA profile of the host[247,248]. In particular, miR-155 was significantly upregulated upon infection with wild type or genetically attenuated parasites (GAP). Importantly, ectopic upregulation of miR-155 using adeno-associated viral (AAV) vectors improved the experimental immunization of mice with GAPs by reducing the number of vaccinations needed for sterile protection. A differential miRNA profile was also observed between mice susceptible to ECM and those that are resistant[249,250]. Again, miR-155 was described as a key player and found to be upregulated in *P. berghei*-infected mice that are susceptible to cerebral malaria[250]. *Vice versa*, miR-155-deficient mice were less susceptible to cerebral malaria. A possible explanation is that miR-155 increases inflammation and aggravates blood-brain-barrier dysfunction. This example demonstrates that the same miRNA can have very different effects on *Plasmodium* infection depending on context and expression level. While it is clear that host miRNAs impact *Plasmodium* infection, there is less evidence for the presence of *Plasmodium*-endogenous miRNAs, as the following Section shows.

1.5.2 RNAi IN PROTOZOAN PARASITES

The discovery of RNAi and miRNAs as a universal strategy to regulate gene expression raised hopes that protozoan parasites would also be equipped with this machinery and that this could be exploited as a tool to study gene function. Indeed, the RNAi machinery was readily identified in the kinetoplast parasite *Trypanosoma brucei* (*T. brucei*)[251], the causative agent of sleeping sickness. With two Dicer-like homologs[252,253] and one Ago protein[254,255], *T. brucei* possesses proteins for the canonical RNAi pathway, and this has been exploited for genome-wide screens[201,256]. A subspecies of the kinetoplast *Leishmania*, *L. Vienna braziliensis*, is also capable of RNAi-mediated gene silencing[257]. In the evolution of kinetoplasts, however, the RNAi pathway has been lost twice: Both *T. cruzii* and the Old world *Leishmania* species lack functional RNAi[258,259]. In apicomplexans, only *T. gondii* has proteins of the RNAi machinery[260], and the existence of miRNAs has been shown[261262]. In line with this, several publications reported a downregulation of gene expression using dsRNA[261,263,264]. However, it seems to be difficult to reproduce these results, and

the existence of a canonical RNAi pathway is debated[265]. Consequently, RNAi is not a popular tool to study this parasite.

A few studies also report gene silencing in *Plasmodium* upon expression of dsRNA. The first work targeted the dihydroorotate dehydrogenase (DHODH) of *P. falciparum* using dsRNA, causing a growth defect[266]. In a second study, the *P. falciparum* cysteine proteases falcipain 1 and 2 were targeted by dsRNA, yielding a moderate growth defect along with enlarged food vacuoles[267]. Surprisingly, later gene disruption studies revealed that only falcipain 2 has an important role in blood stages, while the knockout of falcipain 1 had no phenotype in the erythrocyte development[268–270]. Two studies also report dsRNA-mediated gene silencing in *P. berghei*: in one, the *Plasmodium* berghepains were targeted by injecting corresponding siRNAs into infected mice[271], while in the second study, a downregulation of eukaryotic initiation factor 5A (eIF-5A) and Deoxyhypusine synthase (DHS) was observed upon transfection of *P. berghei* with shRNAs against these genes[272]. Both studies, however, determine mRNA and protein knockdown only semi-quantitatively.

Despite these promising first studies, several publications argue against the activity of dsRNA in *Plasmodium* via a canonical RNAi pathway. First and foremost, a study using bioinformatical as well as experimental methods demonstrated the absence of Ago- and Dicer-homologs in *Plasmodium* as well as the failure to downregulate gene expression with dsRNA delivered by various approaches[95]. Secondly, two studies that investigated miRNAs isolated from *P. falciparum*-infected red blood cells found only human miRNAs[241,242]. In conclusion, it is now commonly accepted that *Plasmodium* lacks an endogenous miRNA pathway. The initially reported effects of dsRNA on *Plasmodium* were thus either due to non-specific effects of dsRNA on parasite growth or to a non-canonical mechanism of gene silencing in *Plasmodium* that has yet to be elucidated. Therefore, it is not possible to study gene function in *Plasmodium* using canonical RNAi-mediated gene silencing. The aim of the present thesis was to overcome this bottleneck by introducing an artificial, non-canonical RNAi pathway into *P. berghei*.

2 Aim of the Thesis

For a long time, the absence of the RNAi machinery has been hampering gene annotation efforts in *Plasmodium*. While the canonical RNAi pathway is complex and involves the interplay of many different proteins, newly adapted non-canonical RNAi pathways are much simpler. This is best exemplified by AgoshRNAs, which rely only on Ago2 for processing and gene silencing. In this thesis, I aimed to test the hypothesis that expression of the protein Ago2 along with a target-specific AgoshRNA is sufficient to mediate gene silencing in *P. berghei*.

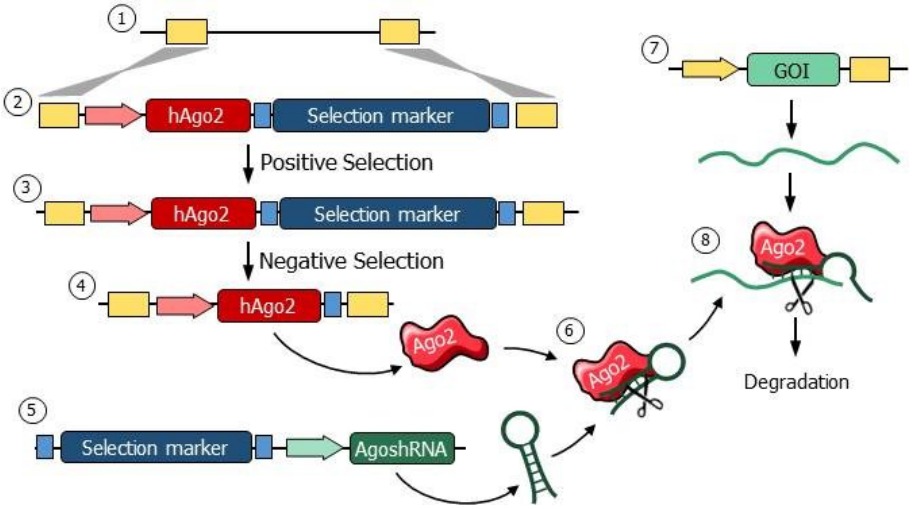

FIGURE 8: **Introduction of non-canonical RNAi into *Plasmodium*.** A cassette encoding Ago2 along with a selection marker ② is integrated into a silent intergenic locus ①. Positive ③ and negative selection ④ yield a marker-free transgenic line expressing Ago2. A second transfection introduces an expression cassette for an AgoshRNA against the GOI ⑤. The AgoshRNA is processed by Ago2 ⑥, and the minimal RISC can target the mRNA of a GOI⑦ for degradation ⑧. This image has been created using elements from Servier Medical Art (www.servier.de)

To this end, I planned to first stably integrate an Ago2 expression cassette into *P. berghei* and to then investigate whether Ago2 expression in the resulting line *Pb*Ago2 impacts parasite development. In parallel, I wanted to design and test Dicer-independent AgoshRNAs against a *proof-of-principle* target (GFP). These AgoshRNAs, when expressed in *Pb*Ago2, should reduce GFP levels significantly in blood stages, as well as in mosquito and liver stages. In case of promising results from the *proof-of-concept* study, I aimed to target endogenous GOI for AgoshRNA-mediated knockdown. If likewise successful, the RNAi-competent *P. berghei* could serve as a new tool to study gene function in the *Plasmodium* parasite (Figure 8).

Results

3

"The first principle is that you must not fool yourself, and you are the easiest person to fool."[273]

~ Richard Feynman (1918 – 1988)

3.1 *IN VITRO* TEST OF DICER-INDEPENDENT AGOSHRNAS

The introduction of a minimal, functional RNAi machinery in *Plasmodium* is based on two premises: First, the parasite needs to express the protein Ago2. Second, an AgoshRNA against the gene of interest is required, which can induce Dicer-independent knockdown of said target gene. As AgoshRNAs are a fairly recent development, their optimal structure was not yet determined at the beginning of this work, and only a few requirements were known that render them Dicer-independent. The first Section of the Results Chapter thus presents the optimization of AgoshRNA design, with the aim to identify potent AgoshRNAs that only need Ago2 for processing and target knockdown.

3.1.1 OPTIMIZATION OF THE AGOSHRNA DESIGN

As a *proof-of-principle* target for AgoshRNA-mediated knockdown in *Plasmodium* I selected GFP, which the parasite line *Pb*GFPcon expresses constitutively in all stages of the life cycle[274]. To be able to compare different AgoshRNA designs to conventional shRNAs, I first performed GFP knockdown experiments in cell culture. To this end, shRNAs and AgoshRNAs were cloned under the U6 promoter into an expression plasmid which also encodes mCherry as a marker for successful transfection. In parallel, I subcloned the GFP gene into a mammalian expression plasmid under the Cytomegalovirus (CMV) promoter. Human embryonic kidney (HEK) 293T cells were co-transfected with these two plasmids and, two days later, the median GFP fluorescence of mCherry-positive (*i. e.* transfected) cells was measured by flow cytometry. The knockdown efficiency of a given shRNA or AgoshRNA was calculated by normalizing the GFP median fluorescence of cells expressing this particular RNA to the GFP median fluorescence of cells transfected with an empty vector (mCherry-plasmid lacking the U6-expression cassette).

The testing of AgoshRNAs by flow cytometry was performed in part by Daria Krzikalla during her Master thesis.

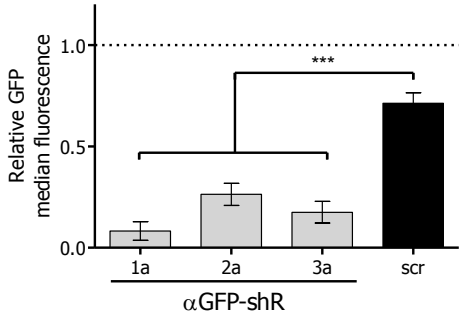

FIGURE 9: **GFP knockdown mediated by three different αGFP-shRNAs.** HEK293T cells were co-transfected with a GFP expression plasmid and one of three shRNAs targeting GFP (αGFP-shR1a to 3a). A scrambled shRNA (scr) served as positive control. Two days after transfection, GFP median fluorescence of mCherry-positive cells was measured by flow cytometry and normalized to that of cells transfected with an empty vector (indicated by the dashed line at 1). Shown is the mean +/- SEM of three independent experiments. Statistical analysis: One-way ANOVA followed by Dunnett's test. *** $p<0.001$.

In this way, I tested three different shRNAs that were designed using an online tool (siRNA wizard, www.invivogen.com/sirnawizard). A scrambled shRNA served as negative control. Out of the three tested shRNAs, αGFP-shR1a performed best and reduced GFP fluorescence to approximately 8 % (Figure 9). Interestingly, also the expression of the scrambled shRNA negatively affected the GFP fluorescence, reducing it to 71 % of the empty vector control. The presence of an active U6 promoter thus appears to influence the expression from a CMV promoter, potentially by competing for the same transcription factors.

AgoshRNAs have to meet certain structural requirements in order to be recognized by Ago2 directly and to mediate a potent knockdown independent of Dicer. In contrast to well-established shRNAs, there are no tools available yet to select the target sequence and to design functional AgoshRNAs. The first publication describing Dicer-independent AgoshRNAs listed three main design rules that should prevent recognition of the hairpin by Dicer and facilitate Ago2-mediated processing[232]:

1) With only 19 nt, the length of the target sequence is shorter than that of conventional shRNAs (20-21 nt).
2) The loop size is reduced from 7 nt to 3 nt.
3) The sense strand of the AgoshRNA is located at the 3' end, while shRNAs start with the sense strand at the 5' end.

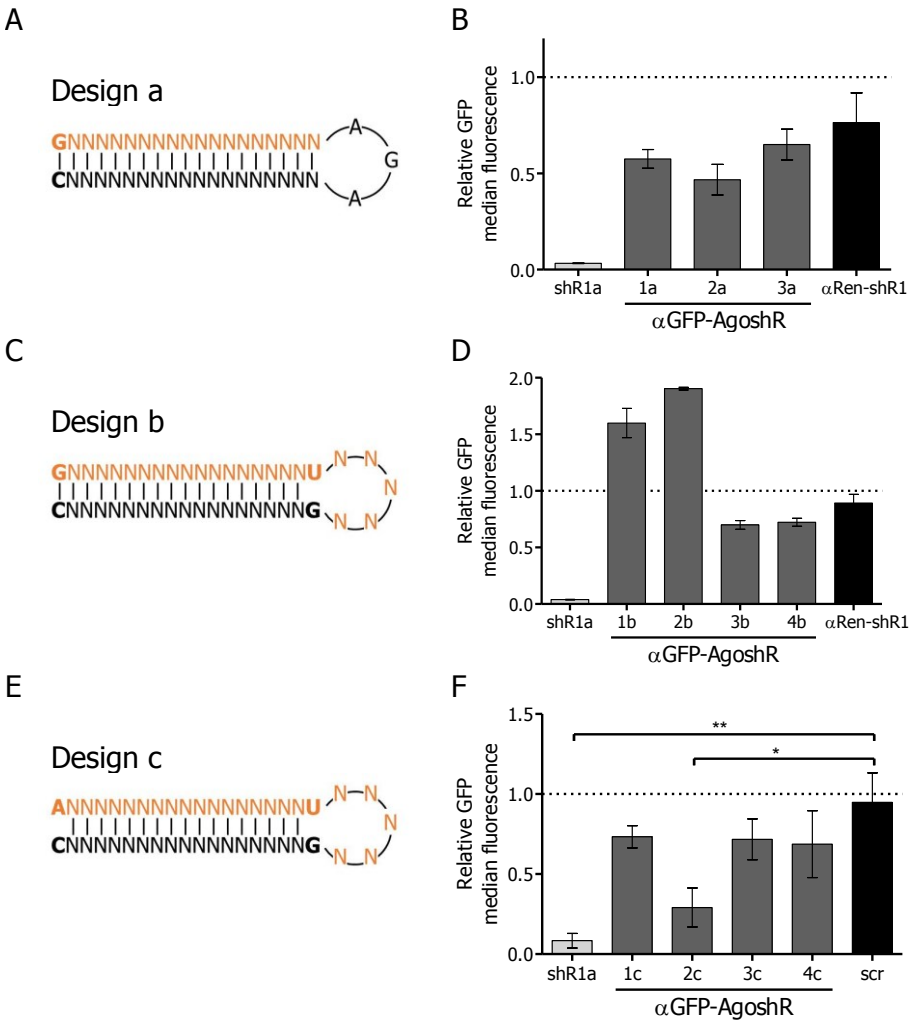

FIGURE 10: **Optimization of the AgoshRNA design**. (A), (C) and (E) depict the structure of the AgoshRNAs based on design rules a, b and c, respectively. The antisense strand that is complementary to the target mRNA sequence is indicated in orange. (B), (D) and (F) show the relative GFP fluorescence (measured by flow cytometry) of HEK293T cells co-transfected with a GFP-expression plasmid and one of three or four AgoshRNAs targeting GFP based on (B) design a, (C) design b or (F) design c. A previously validated shRNA, αGFP-shR1a, served as positive control, a non-targeting shRNA (αRen-shR1, (B) and (D)), or a scrambled AgoshRNA (scr, (F)) as a negative control. Shown is the median GFP fluorescence intensity normalized to control cells transfected with an empty vector (indicated by a dashed line at 1). (B) and (D) Mean +/- SD of a single experiment. (F) Mean +/- SEM of three independent experiments. Statistical analysis: One-way ANOVA followed by Dunnett's test. * $p<0.05$; ** $p<0.01$.

Based on these criteria, I designed a set of three different AgoshRNAs against GFP (αGFP-AgoshR1-3a, Figure 10 A). The knockdown efficiency of these three AgoshRNAs was assessed by flow cytometry of transfected HEK293T cells as described above. The αGFP-shR1a served as positive control, and a non-targeting shRNA against Renilla (αRen-shR1) served as negative control. While the αGFP-shR1a silenced GFP expression to about 3 % fluorescence intensity, the knockdown mediated by the AgoshRNAs was much less pronounced and not statistically significant different from that with the shR-αRen1. Thus, it was necessary to improve the AgoshRNA design.

As the U6 promoter used for expression of shRNAs requires a G or A as first nucleotide[275], target sequences ending on C were selected, so that the AgoshRNA antisense strand starts with a G.

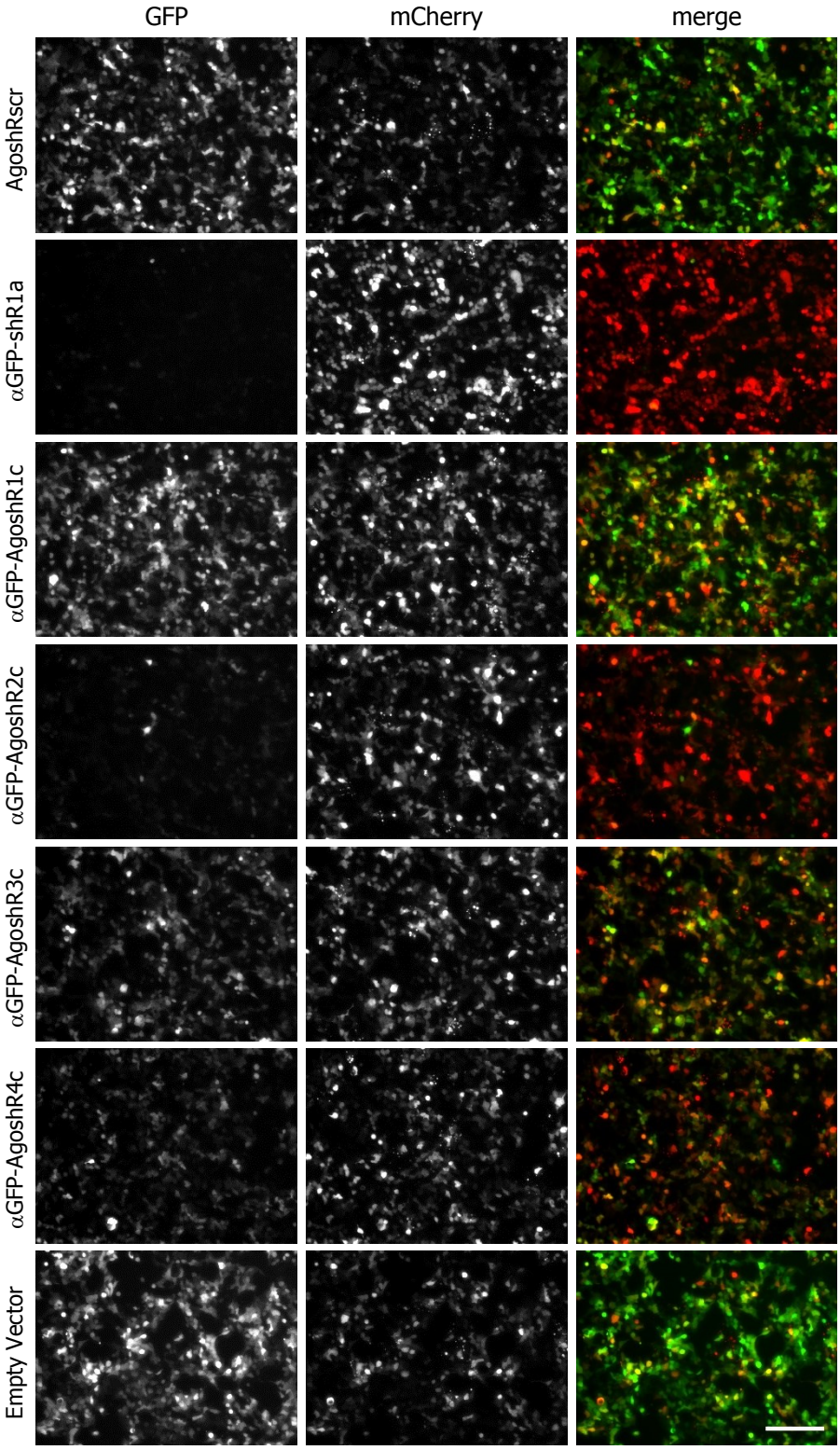

FIGURE 11: **Microscopy images of HEK293T cells co-transfected with GFP and sh- or AgoshRNAs.** HEK293T cells were co-transfected with a GFP-expression plasmid and a plasmid encoding mCherry and one of four αGFP-AgoshRNAs (αGFP-AgoshR1c to 4c). The previously validated αGFP-shR1a served as positive control, and a scrambled AgoshRNA (AgoshRscr) and an empty vector not encoding any short RNA as two negative controls. Cells were imaged two days after transfection. One representative image of three per condition is shown. Pictures were taken with identical settings with a wide-field fluorescence microscope and are all processed alike. The scale bar indicates 200 nm.

In the meantime, additional optimizations regarding the design of AgoshRNAs were published[234]. Taking these new data into account, I designed a second set of four different αGFP-AgoshRNAs with a loop length of 5 nt and a terminal G-U mismatch (αGFP-AgoshR1-4b, Figure 10 C). Additionally, target sequences were extended across the loop, to maximize base pairing of AgoshRNA and mRNA. However, flow cytometry of cells transfected with these AgoshRNAs again revealed no significant knockdown of GFP (Figure 10 D).

Based on personal communication with Ben Berkhout and newly published data[276], I again modified the AgoshRNA design to include an initial A-G mismatch (αGFP-AgoshR1-4c, Figure 10 E). As a more appropriate negative control, I replaced the non-targeting shRNA with a scrambled AgoshRNA (AgoshRscr). Of the four AgoshRNAs in this set, αGFP-AgoshR2c significantly reduced GFP fluorescence to about 29 % compared to AgoshRscr (Figure 10 F). Microscopical analysis of the cells further confirmed the reduction of GFP fluorescence (Figure 11).

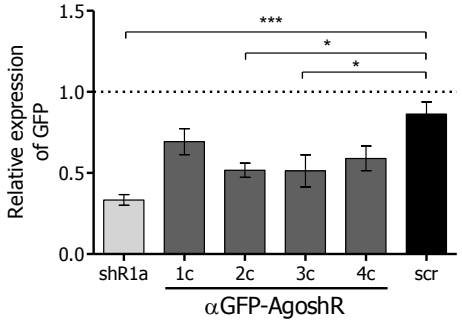

FIGURE 12: **GFP mRNA expression after expression of sh- or AgoshRNAs.** HEK293T cells were transfected with a GFP-expression plasmid and the shR1a (positive control) or one of the four αGFP-AgoshRNAs of set c. A scrambled AgoshRNA (scr) served as negative control. Two days post-transfection, RNA was isolated from the cells and GFP mRNA levels were determined by qRT-PCR. mCherry, which is also encoded on the sh-/AgoshRNA expression plasmids, served as a housekeeper to account for transfection variability. Results were normalized to cells transfected with an empty vector instead of an sh- or AgoshRNA-expression plasmid (indicated by the dashed line). Mean +/- SEM of three independent experiments. Statistical analysis: One-way ANOVA followed by Dunnett's test. * $p<0.05$; *** $p<0.001$.

To assess whether the decreased GFP fluorescence is due to mRNA cleavage by Ago2 or rather due to translational inhibition, I performed quantitative reverse-transcription PCR (qRT-PCR) on RNA isolated from transfected HEK293T cells. As expected, the level of GFP mRNA was significantly reduced to about 33 % in cells expressing the αGFP-shR1a. Importantly, also AgoshRNAs led to mRNA degradation, as seen by the approximately twofold reduction of GFP mRNA in cells co-transfected with αGFP-AgoshR2c or αGFP-AgoshR3c (Figure 12). The optimization of the AgoshRNA design thus yielded an αGFP-AgoshRNA that silences GFP in RNAi-competent cells by means of mRNA degradation.

3.1.2 KNOCKDOWN EFFICIENCY IN DICER-DEFICIENT CELLS

HEK293T cells possess all proteins required for RNAi. It is thus conceivable that αGFP-AgoshR2c is processed by Dicer and exerts the knock down via the conventional RNAi pathway, although the short stem of 18 nt should prevent recognition by Dicer. To evaluate if the AgoshRNAs of set c truly act independently of Dicer, they were tested in mouse embryonic fibroblast (MEF) cells lacking Dicer (Dicer$^{-/-}$ MEF)[278], along with the most potent shRNA αGFP-shR1a. As a control, the same experiment was performed in RNAi-competent MEF cells that still express Dicer. As MEF cells are hard to transfect, I employed recombinant AAVs that packaged GFP or sh/AgoshRNA expression vectors to transduce these cells, followed by flow cytometry to measure GFP fluorescence four days after transduction.

The vectors were packaged in AAV-DJ[277], a capsid that transduces MEF cells very efficiently.

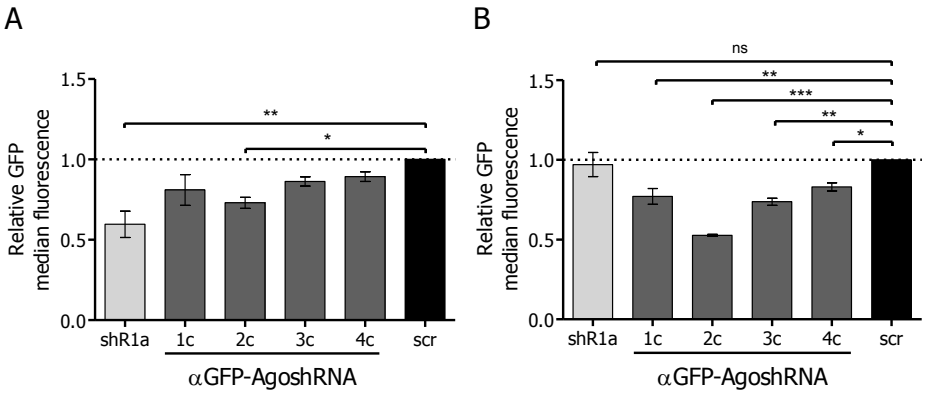

FIGURE 13: **GFP knockdown in Dicer-deficient cells.** (A) Wild type or (B) Dicer$^{-/-}$ MEF cells were co-transduced with AAVs encoding GFP and either the shR1a or one of the four αGFP-AgoshRNAs. A scrambled AgoshRNA (scr) served as negative control. Four days after transduction, GFP fluorescence of cells was analyzed via flow cytometry, and results were normalized to cells transduced with the scrambled AgoshRNA (dashed line). Mean +/- SEM of three independent experiments performed with independent AAV productions. Statistical analysis: One-way ANOVA followed by Dunnett's test. ns: not significant. * $p<0.05$; ** $p<0.01$; *** $p<0.001$.

In RNAi-competent MEF cells, I observed a GFP knockdown pattern comparable to that measured in HEK293T cells, albeit the absolute knockdown efficiencies were lower in the MEF cells. The αGFP-shR1a exerted the most potent knockdown to about 60 %, and out of the four AgoshRNAs, only αGFP-AgoshR2c significantly reduced GFP fluorescence to about 73 % (Figure 13 A). As expected, the αGFP-shR1a is not functional in MEF cells lacking Dicer. Importantly, in contrast to the shRNA, αGFP-AgoshR2c retains its knockdown capacity in Dicer$^{-/-}$ MEF cells, reducing the GFP fluorescence to about 53 % (Figure 13 B). Interestingly, also the other AgoshRNAs 1c, 3c, and 4c silence GFP in Dicer$^{-/-}$ MEFs (Figure 13 B). Possibly, AgoshRNAs are more potent in Dicer-deficient cells as they do not compete with endogenous miRNAs for Ago2, an observation that has been made before[235].

Presumably, Dicer$^{-/-}$ MEFs express miRNA genes to the same level as wild type MEFs. However, as Dicer does not further process the pre-miRNAs, they might be no substrate for Ago2.

Alltogether, the data support the successful generation of AgoshRNAs that act independently of Dicer. This is a first essential step towards the establishment of the non-canonical RNAi pathway in *P. berghei*. The following Section addresses the next important step, namely, the expression of Ago2 in *P. berghei*.

3.2 GENERATION OF *PB*AGO2

3.2.1 INTEGRATION OF AN AGO2-EXPRESSION CASSETTE

In order to generate a *P. berghei* line expressing Ago2 constitutively across the life cycle, it is necessary to integrate an Ago2-expression cassette into the genome. Previously, a silent intergenic locus on chromosome 6 (SIL6) has been published, along with vectors that can be used for integration of DNA sequences into this locus without affecting the expression of any endogenous neighboring genes of *P. berghei*[279]. Here, I used one of these published vectors to integrate the Ago2 cDNA into the GFP-positive *P. berghei* ANKA line *Pb*GFPcon. Figure 14 shows a schematic representation of the integration strategy.

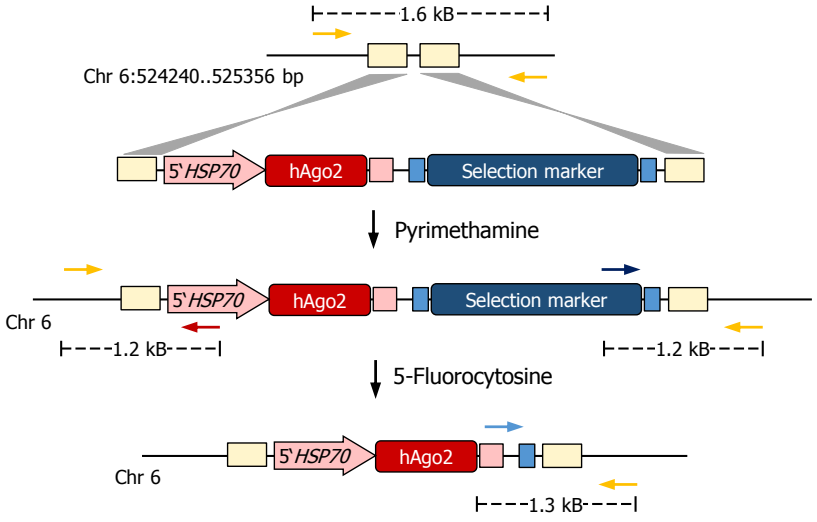

FIGURE 14: **Strategy to integrate Ago2 into the *Pb*GFPcon genome.** A 5'*HSP70*-promoter-driven human (h)Ago2 expression cassette (red) together with a selection marker (blue) for positive and negative selection (*hDHFR-yFCU*) is placed between two DNA segments that are homologous to a genomic sequence on chromosome 6 of *P. berghei* (yellow). After transfection, the vector integrates via double homologous crossover into the genome and parasites positive for this integration can be enriched by pyrimethamine drug pressure. As the resistance cassette is flanked by homologous sequences owing to a duplication of the 3'*DHFR-TS* UTR (light blue), parasites can remove the resistance cassette by recombination. Application of the prodrug 5-FC selects for this event, resulting in a marker-free insertion of the 5'*HSP70-hAgo2* expression cassette into the chromosome 6 of *P. berghei*. The arrows indicate the location of the primers used for diagnostic PCR to verify integration and recombination events (see also Figure 15 and Figure 16).

In short, the human Ago2 coding sequence fused to a FLAG- and an HA-tag was cloned into the vector pBAT-SIL6 behind the *Plasmodium HSP70* promoter, a strong and ubiquitously active promoter. Transfection of *Pb*GFPcon parasites with a linearized plasmid allowed for the integration of the Ago2 expression cassette as well as a drug-selectable marker (*hDHFR-yFCU*) via double homologous crossover into the SIL6. Parasites positive for integration were selected by administering pyrimethamine to the drinking water. A subsequent limiting dilution allowed the selection of a single clone that only carries the integration and was devoid of wild type parasites. As homologous regions flanked the drug-selectable marker, parasites could remove the cassette by recombination, and negative selection using 5-FC selected for variants that have done so. This recycling of the selectable marker is of particular importance for this project, as additional pyrimethamine selection is required when these parasites are transfected with AgoshRNA-expression vectors (see *e. g.* Section 3.3.) A final limiting dilution gave rise to a single clone of the parasite line *Pb*Ago2.

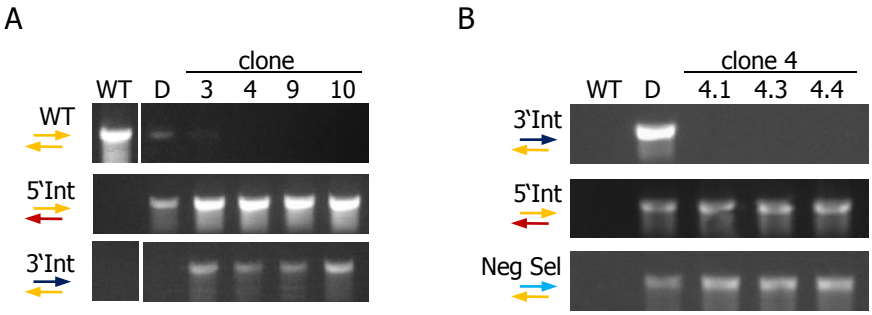

FIGURE 15: **Diagnostic PCR of *Pb*Ago2 clone 4.3.** (A) Genotyping of clones obtained after positive selection. After transfection with pBAT-SIL6-Ago2, parasites were put under positive selection pressure using pyrimethamine. Limiting dilution (intravenous injection of a single parasite per mouse) yielded four clones (3, 4, 9 and 10). DNA isolated from these was subject to diagnostic PCR using primers described in Figure 14, which demonstrated successful 3' and 5' integration of the vector as well as the absence of wild type in three out of four clones. (B) Genotyping of clones obtained after negative selection. *Pb*Ago2 clone 4 was injected into a donor mouse and subject to negative selection pressure with 5-FC. After limiting dilutions, three clones (4.1, 4.3 and 4.4) were obtained. Diagnostic PCR using primers described in Figure 14 confirmed the complete recycling of the selection marker (absence of 3' integration band and the presence of a band in neg sel PCR) as well as the continued presence of the 5' integration site. WT: wild type; 5'Int: 5' Integration; 3'Int: 3' Integration; Neg Sel; Locus obtained after negative selection. D: Donor used for limiting dilution.

During the generation of this line, all steps were verified by diagnostic PCR using different sets of primers binding outside of the integration site as well as within the vector (Figure 15, primer binding sites depicted in Figure 14). Parasites appeared within one to two weeks after transfection, and four clones were obtained after limiting dilution (Figure 15 A). From the clone *Pb*Ago2 4, the selection cassette was recycled by negative selection, and the resulting parasite population was subjected to another limiting dilution, yielding three marker-free clones (Figure 15 B). In this work, all further experiments were performed with clone *Pb*Ago2 4.3. In order to obtain two independent clones, the transfection and selection procedure was repeated a second time, yielding

the second clone *Pb*Ago2 3.2. Figure 16 shows the final diagnostic PCR of these two clones which confirmed correct integration of the vector, the recycling of the resistance marker and the absence of wild type in both clones. The next two Sections delineate the experiments that were performed to further characterize these two clones of *Pb*Ago2 regarding the expression of Ago2 and their growth behavior across the life cycle.

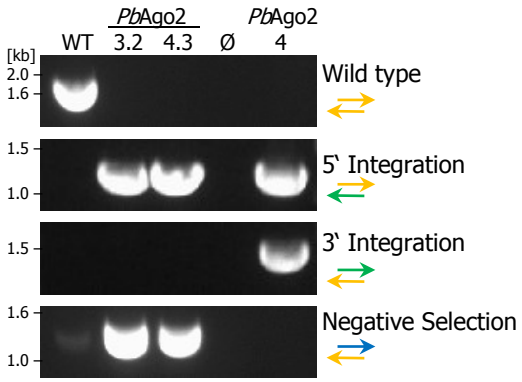

FIGURE 16: **Diagnostic PCR of the final clones *Pb*Ago2 3.2 and 4.3.** Genotyping of *Pb*GFPcon (wild type, WT) and two independently generated clones of *Pb*Ago2, clone 3.2 and clone 4.3. Primers used amplified the wild type locus, the 5' integration site, and the 3' integration site as well as the locus following recycling of the selection cassette (negative selection) and are indicated as arrows. Their respective binding site is depicted in Figure 14. WT: *Pb*GFPcon; Ø: no-template control; *Pb*Ago2 4: Clone prior to negative selection, served as a positive control for the 3' integration PCR.

3.2.2 EXPRESSION OF AGO2 ACROSS THE LIFE CYCLE

The promoter of *HSP70* is a strong promoter and ubiquitously active across all life cycle stages of *Plasmodium*[280]. I performed Western blotting of mixed blood stages of *Pb*GFPcon and *Pb*Ago2 to analyze if this promoter also drives Ago2 expression. Probing with an anti-Ago2 antibody revealed a band corresponding to the size of Ago2 in both *Pb*Ago2 clones, as well as in the positive control (cell lysate of HEK293T cells overexpressing Ago2) (Figure 17). Notably, this band is absent from the *Pb*GFPcon sample, even though the HSP70 loading control indicates that the amount of protein in this sample is comparable to the *Pb*Ago2 samples.

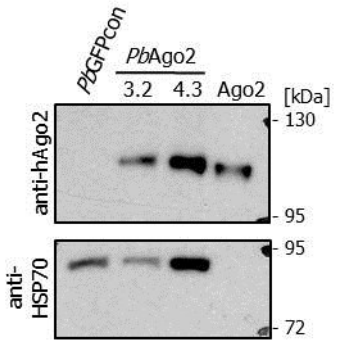

FIGURE 17: **Ago2 expression in mixed blood stages.** Western blots of protein lysates of *Pb*GFPcon or *Pb*Ago2 mixed blood stages were probed for Ago2 with an anti-hAgo2 antibody (upper blot). Lysate of HEK293T cells transfected with an Ago2 expression construct served as positive control. Probing with an anti-HSP70 antibody served as a loading control for the parasite samples (lower blot).

In addition to blood stages, I also analyzed expression of Ago2 in liver stages by immunofluorescence. To this end, I infected human hepatoma cells (HuH7 cells) with *Pb*GFPcon or *Pb*Ago2 sporozoites and fixed the developing liver stages 48 h later. Staining of the samples with an anti-FLAG antibody against the tagged hAgo2 verified expression of Ago2 in late liver stages of *Pb*Ago2 3.2 and 4.3, while no signal above background was detected in *Pb*GFPcon liver stages (Figure 18).

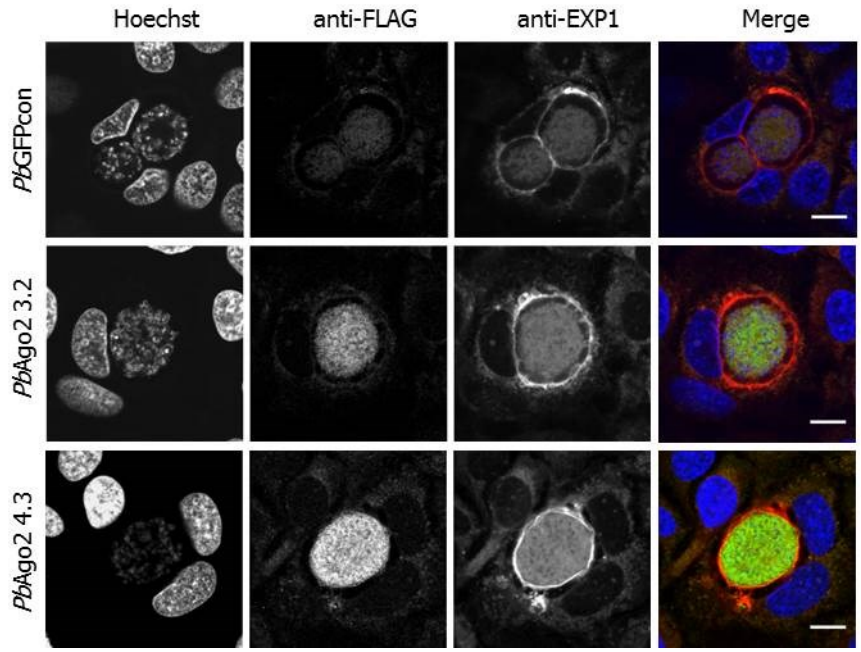

FIGURE 18: **Expression of Ago2 in liver stages.** Immunofluorescence staining of liver stages 48 h post-infection of HuH7 cells with either *Pb*GFPcon or *Pb*Ago2 sporozoites. Cells were incubated with Hoechst to stain the nuclei of parasites and host cells (first column), an antibody against the FLAG-tag of Ago2 (second column), and an antibody against the PVM protein exported protein 1 (EXP1) (third column). One representative image of ten per condition is shown. Pictures were taken with identical settings with a confocal microscope and are all processed alike. Scale bars indicate 10 µm.

3.2.3 CHARACTERIZATION OF *PB*AGO2

In eukaryotic cells, Ago2 is not only a key player in RNAi but has been implicated in a wide range of additional functions, including roles in transcriptional silencing or splicing[281]. For some functions, the interaction of Ago2 with a short non-coding RNA is required, while others rely on direct protein-protein interaction between Ago2 and additional partners. *Plasmodium* parasites encode a large variety of non-coding RNAs, whose functions remain mostly unknown[282]. Although *P. berghei* does not express miRNAs[95], it is conceivable that exogenously expressed Ago2 in this parasite interferes with the endogenous non-coding RNAs and thus may affect parasite development and growth. To evaluate any such unspecific effects, I assessed the life cycle progression of *Pb*Ago2 and compared it to the parental line *Pb*GFPcon.

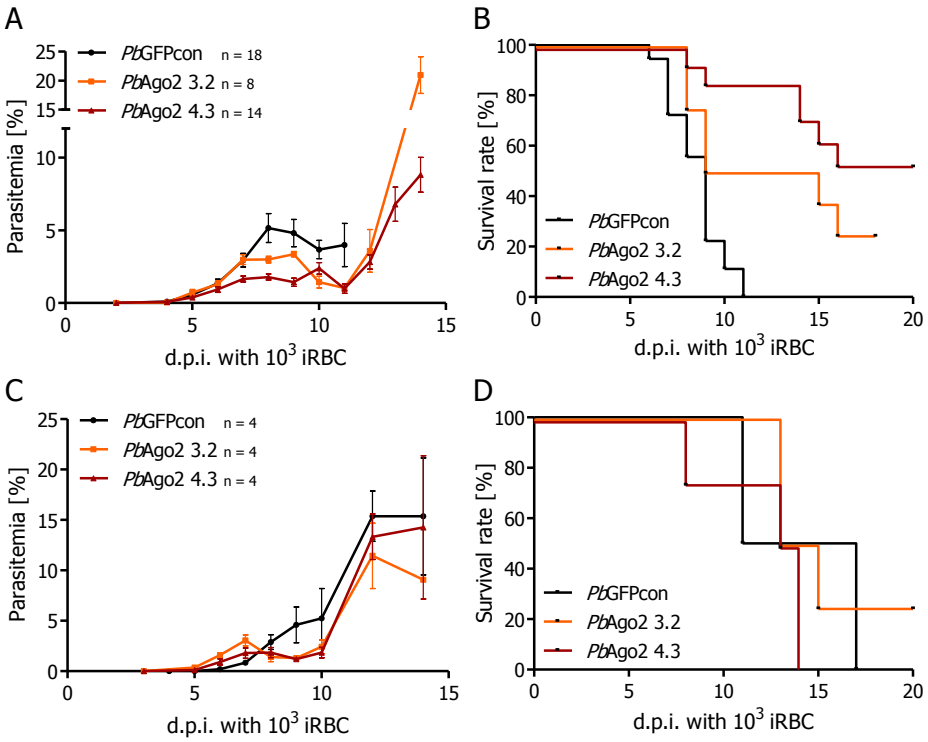

FIGURE 19: **Growth of *Pb*Ago2 blood stages**. (A, B) Inbred C57BL/6J mice or (C, D) outbred NMRI mice were intravenously infected with 1000 iRBC of either *Pb*GFPcon, *Pb*Ago2 3.2 or *Pb*Ago2 4.3. (A, C) Parasitemia was monitored from day 3 to day 14/15 post-infection via Giemsa-stained thin blood smears. The number of mice (n) for each group is indicated in the legend. Shown is the mean parasitemia +/-SEM. (B, D) Survival of the infected mice. Mice were observed until day 20 post-infection for signs of (B) experimental cerebral malaria or (B, D) severe disease symptoms and sacrificed accordingly. d.p.i: days post-infection.

In order to compare the growth rate of *Pb*Ago2 to *Pb*GFPcon, inbred C57BL/6J mice were intravenously injected with 1000 iRBCs, and parasitemia was determined by daily blood smears from day 3 to day 14/15 post-infection (Figure 19 A). The growth of *Pb*Ago2 during the first six days of infection was comparable to that of *Pb*GFPcon. The parasitemia of *Pb*GFPcon-infected mice then continued to increase until it reached a plateau at approximately 5 % on day 8 to 10. Around this time, these mice developed signs of ECM and

succumbed to the infection (Figure 19 B), as it is expected for *Pb*ANKA-infected C57BL/6 mice[283]. In contrast to wild type, *Pb*Ago2 parasites grew significantly slower, with a declining parasitemia on days 8 to 10 post infection followed by resurgence two weeks post-infection. The reduced growth rate was accompanied by an increased survival of *Pb*Ago2-infected mice, with only a subpopulation succumbing to the disease in the 20 days following infection.

To assess if this growth impairment is mouse strain specific or a general feature of *Pb*Ago2, I repeated the experiment in outbred NMRI mice (Figure 19 C, D). In this strain, the parasitemia of *Pb*GFPcon increased rather steadily over the course of infection, reaching a peak of 15 % at day 14 after infection. Early after infection, the parasitemia of *Pb*Ago2-infected mice was even higher than in the wild type-infected mice. However, as observed for the C57BL/6 mice, it then dropped on day 8 to 10 post-infection. This reduction is followed by another increase, reaching a peak parasitemia of 10 to 15 %. In contrast to C57BL/6 mice, NMRI mice do not develop cerebral symptoms but rather die due to hyperparasitemia and anemia. Interestingly, the survival of NMRI mice is not different between *Pb*GFPcon- and *Pb*Ago2-infected animals. In conclusion, while the expression of Ago2 affects the blood-stage growth rate, the differences of *Pb*Ago2 to *Pb*GFPcon are much less pronounced in NMRI mice than in C57BL/6 mice.

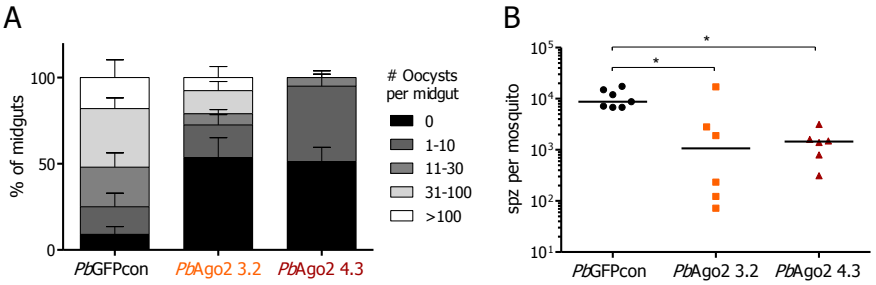

FIGURE 20: **Mosquito stage development.** Mosquitoes were infected by blood meal on parasite-infected mice. (A) Midguts were isolated 12 to 14 days after blood mean from 10 to 15 mosquitoes per cage, and the number of oocysts per midgut was scored by microscopic examination. Depicted is the percentage of midguts (+/-SEM) belonging to one of five groups: No oocysts, 1 to 10 oocysts, 11 to 30 oocysts, 31 to 100 oocysts, >100 oocysts per midgut. Data is the mean of four to five independent feedings per strain. (B) Salivary gland sporozoites were isolated 18 days post-feeding from at least 25 female mosquitoes per cage and counted. Depicted is the average number of sporozoites per female mosquito. Each dot represents an individual cage (independent feeding). Statistics: One-way ANOVA followed by Dunnett's test. * $p<0.05$.

Within oocysts, sporozoites develop, which are released into the hemolymph of the mosquito to invade the salivary glands. On day 18 after infectious blood meal, I dissected salivary glands from mosquitoes and determined the average number of sporozoites per mosquito. The infectivity of *Pb*Ago2-infected mosquitoes (on average 1500 to 3000 sporozoites per mosquito) was significantly lower than that of *Pb*GFPcon-infected mosquitoes (on average 10000 sporozoites per mosquito) (Figure 20 B). The reduced number of salivary gland sporozoites is likely a direct consequence of the lower infection rate of *Pb*Ago2- compared to *Pb*GFPcon-infected mosquitoes and does

not necessarily mean that *Pb*Ago2 forms fewer infectious sporozoites than the wild type. To conclude at which stages the development of *Pb*Ago2 in the mosquito is impaired, one could quantify the mosquito infection rate more precisely regarding oocyst numbers as well as midgut sporozoite numbers per mosquito. Nevertheless, for the purpose of this work a general estimation of mosquito infectivity of *Pb*Ago2 is sufficient.

Sporozoites are transmitted to the mammalian host by the bite of an infected mosquito and, after entering the blood-stream, they subsequently infect hepatocytes to undergo the first round of asexual replication. This liver stage development can be monitored *in vitro* by adding a defined amount of sporozoites to human hepatoma (HuH7) cells and detecting the number and size of liver stages at various time points post infection by immunofluorescence. In Figure 21 A and B, numbers and sizes of *Pb*Ago2 liver stages 48 h after infection are compared to those of *Pb*GFPcon. Interestingly, in contrast to blood stages and mosquito stages, the expression of Ago2 does not have a significant impact on liver stage development *in vitro*.

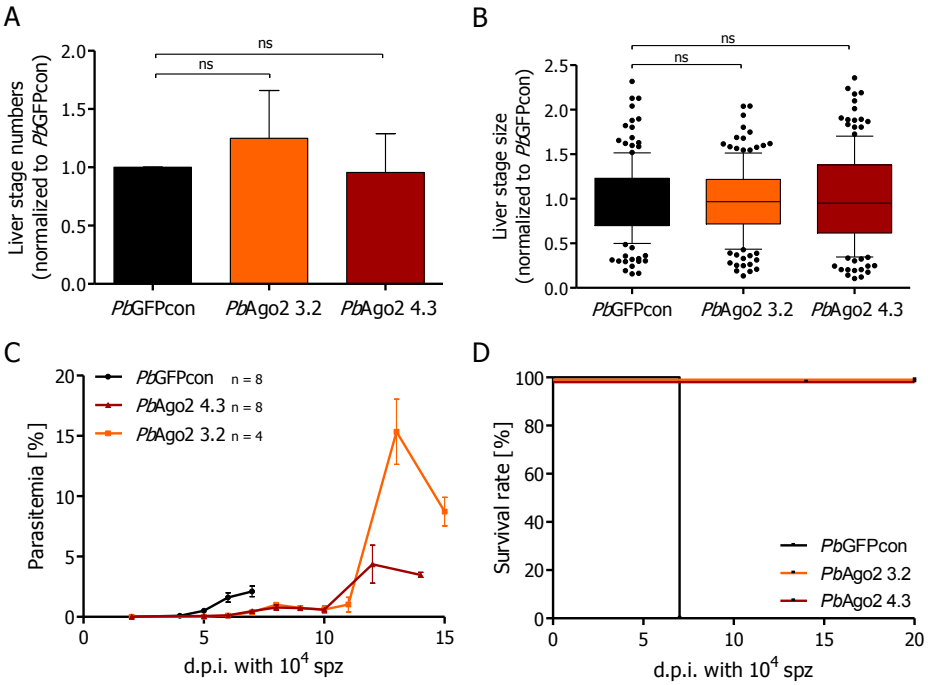

FIGURE 21: **Liver stage development *in vitro* and *in vivo*.** (A, B) HuH7 cells were infected with 10^4 sporozoites per well and incubated for 48 h prior to fixing and staining with an anti-HSP70 antibody. (A) Numbers of liver stages per well and (B) sizes of at least 50 randomly selected liver stages per experiment were determined by fluorescence microscopy and results were normalized to *Pb*GFPcon wild type liver stages analyzed in parallel. Shown is the merged data (A) as bar graph +/- SEM or (B) as whisker plots with 10-90 percentile of three independent experiments comprising 4-8 technical replicates each. Statistics: One-Way-ANOVA followed by Dunnett's test. ns: non-significant. (C, D) C57BL/6J mice were i. v. infected with 10^4 sporozoites. (C) Parasitemia was determined from daily blood smears from 3 to 14/15 days after infection. (D) Survival of mice. Mice were observed until day 20 post-infection for signs of ECM or severe disease and sacrificed accordingly.

To test if *Pb*Ago2 also completes liver stage development *in vivo*, I infected C57BL/6 mice i.v. with sporozoites and monitored parasitemia over the course of the infection. *Pb*Ago2-infected mice had a one day delay in prepatency when compared to *Pb*GFPcon-infected mice, and lower overall parasitemia (Figure 21 C). In concordance with the phenotype observed after iRBC inoculation, the survival of *Pb*Ago2-infected mice was increased, while *Pb*GFPcon-infected mice succumbed to ECM 7 days post-infection (Figure 21 D). Taking into account that the liver stage development is not impaired *in vitro*, the delay in prepatency and the reduced growth can most likely be attributed to the decreased growth rate in the blood stages. Importantly, despite a growth defect in blood and mosquito stages, *Pb*Ago2 can complete the whole life cycle.

3.3 KNOCKDOWN OF GFP IN BLOOD STAGES

The previous two Sections described the basic ingredients required for using the non-canonical RNAi machinery in *Plasmodium*: An AgoshRNA that targets GFP independently of Dicer, and a parasite line that expresses Ago2. The following Section summarizes how these two parts were subsequently combined to target GFP for Ago2-mediated downregulation in *P. berghei.*

3.3.1 KNOCKDOWN OF GFP IN *PB*AGO2

To begin to elucidate whether *Pb*Ago2 is indeed capable of executing RNAi, I selected the most potent AgoshRNA against GFP, αGFP-AgoshR2c and designed a vector to express this AgoshRNA in *Pb*Ago2. AgoshRscr was included as negative control. *P. berghei* blood stages are known to maintain circular plasmid DNA as episomes and amplify these along with the genomic DNA[60,285]. Transfection of plasmids as episomes instead of a stable integration of the DNA allows for a quick assessment of the effect of the specific AgoshRNA, without the need to select individual clones via limited dilution.

The mechanism by which Plasmodium *amplifies these episomes is still unknown, but there is apparently no need for a specific sequence to serve as origin of replication*[284]*.*

The first challenge was the identification of a promoter driving AgoshRNA expression in *P. berghei*. In contrast to protein-coding mRNAs, which are transcribed from a polymerase II promoter, many short non-coding RNAs are transcribed by polymerase III (Pol III)[286]. Only few Pol III-transcripts are well described in apicomplexan species, among these are spliceosomal RNAs such as the U6 snRNA[287]. With the introduction of the CRISPR/Cas9 technology to *Plasmodium* and *Toxoplasma* research, however, Pol III promoters were needed to transcribe the gRNAs that target the Cas9 protein to the DNA. Both for *P. falciparum* as well as for *T. gondii*, the expression of gRNAs has been achieved by using the 5' region of the spliceosomal U6 snRNA[288–290], however, no application of the *P. berghei* U6 promoter has been reported.

Based on homology to the *P. falciparum* U6 promoter, I chose 500 bp upstream of the *P. berghei* U6 snRNA gene to drive expression of AgoshRNAs. Additionally, I added a stretch of five adenosines at the 3' end of the AgoshRNA to serve as a termination signal for the polymerase III[286]. The vector that I designed for episomal expression consisted of three main components:

1) A pyrimethamine marker to permit selection for transfectants.
2) An mCherry fluorescence reporter driven by an *HSP70* promoter to distinguish between parasites carrying the episome and parasites that spontaneously became pyrimethamine resistant.
3) An expression cassette for the AgoshRNA.

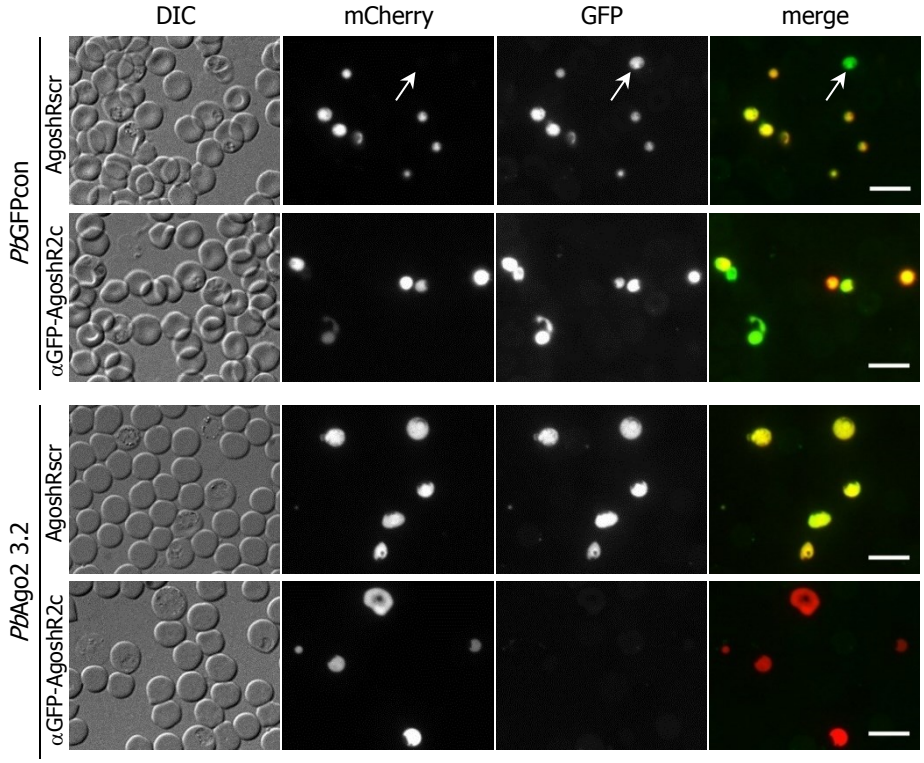

FIGURE 22: **GFP knockdown in blood stages.** *Pb*GFPcon or *Pb*Ago2 3.2 parasites were transfected with episomal vectors carrying mCherry and either αGFP-AgoshR2c or AgoshRscr. Upon appearance in the blood, parasites were imaged with a wide-field fluorescence microscope. Shown are representative images taken using the same settings. Only parasites that exhibited mCherry fluorescence were chosen for quantification of the GFP signal (Figure 23). The white arrows in the first row of images specify a parasite that does not carry the episome as indicated by a lack of mCherry fluorescence and which was thus excluded from the analysis. The scale bars indicate 10 μm.

Transfection of *Pb*Ago2 3.2, *Pb*Ago2 4.3 or *Pb*GFPcon parasites with such plasmids encoding either αGFP-AgoshR2c or AgoshRscr yielded pyrimethamine-resistant parasites in the usual time frame of one to three weeks. In almost all cases, 90-100 % of parasites were also mCherry-positive, indicating that they carry the episome (Figure 22). For quantification of the GFP fluorescence, only those parasites were considered that expressed mCherry, and parasites that lacked mCherry fluorescence were excluded from further analysis (an example is highlighted with an arrow in the upper lane of Figure

Transfection and imaging of the parasites in this Section were in part carried out together with the bachelor student Annika Binder during her lab rotation.

22). Parasite populations with less than 90 % mCherry-positive blood stages occurred in about 5 % of all transfections, suggesting that a subpopulation of parasites spontaneously acquired resistance to pyrimethamine and outgrew the parasites maintaining the episome. In this case, these parasites were discarded and the transfection was repeated.

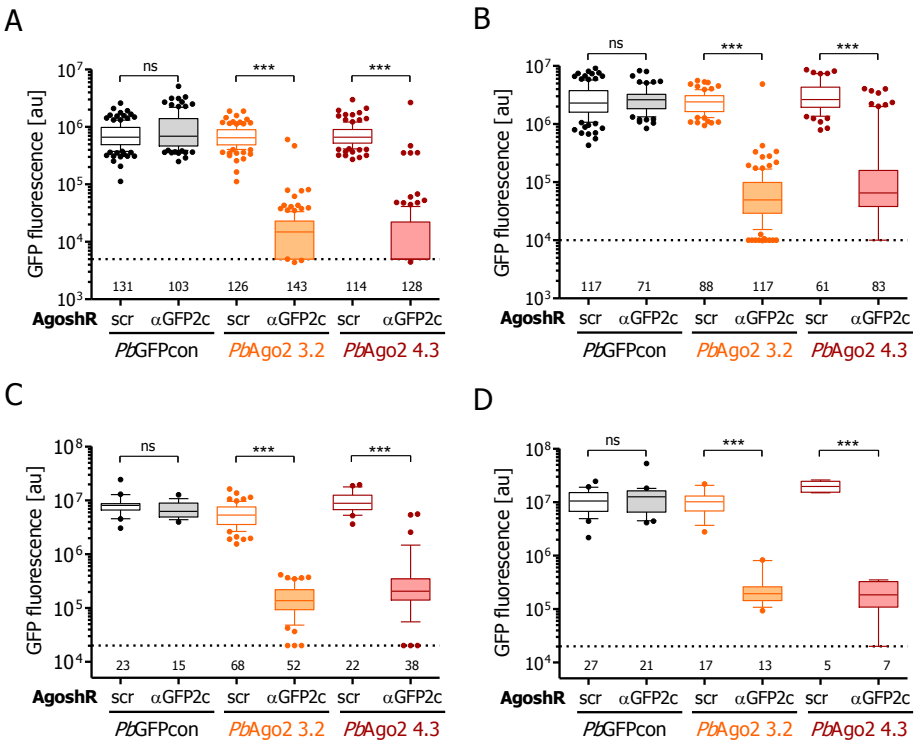

FIGURE 23: **Quantification of GFP fluorescence in blood stages.** *Pb*GFPcon, *Pb*Ago2 3.2 or *Pb*Ago2 4.3 were transfected with episomes encoding either AgoshRscr (scr) or the αGFP-AgoshR2c (αGFP2c) and selected with pyrimethamine drug pressure. After the appearance of pyrimethamine-resistant parasites, blood stages were imaged with a wide-field fluorescence microscope with constant settings across all samples. The integrated GFP fluorescence intensity of individual parasites was determined using the software ImageJ. Depicted is the integrated GFP fluorescence intensity for individual (A) ring stages, (B) early trophozoites, (C) late trophozoites and (D) gametocytes as whisker plots with 10-90 percentile. Data is merged from three independent experiments (based on independent transfections), and the number below each bar indicates the total number of individual parasites quantified. Statistics: Kruskal-Wallis-Test followed by Dunn's test. ns: not significant; *** $p<0.001$; au: arbitrary units.

While imaging the transfected parasites, I noted that the GFP fluorescence of *Pb*Ago2 parasites transfected with αGFP-AgoshR2c was greatly diminished compared to *Pb*GFPcon parasites or *Pb*Ago2 parasites transfected with AgoshRscr (Figure 22). Quantification of the GFP signal of individual parasites revealed that the GFP fluorescence of all *Pb*Ago2 blood stages (ring stages, early trophozoites, late trophozoites, and gametocytes) decreased significantly upon expression of αGFP-AgoshR2c as compared to AgoshRscr (Figure 23). Western blot analysis of schizont-enriched blood stages further supported a reduction of GFP on the protein level in *Pb*Ago2 upon expression of αGFP-AgoshR2 (Figure 24). Importantly, in *Pb*GFPcon parasites, αGFP-AgoshRNA did not alter GFP fluorescence or protein level (Figure 22-24). This observation further

corroborates that wild type *P. berghei* is devoid of any RNAi machinery and suggests that the detected reduction of GFP is indeed due to Ago2-mediated RNAi in *Pb*Ago2.

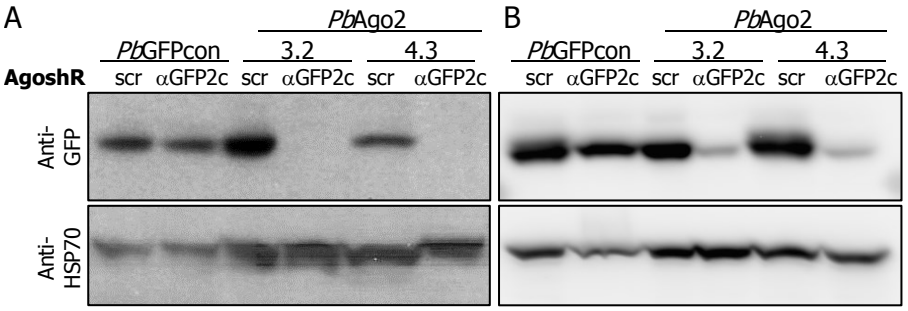

FIGURE 24: **GFP protein levels upon expression of αGFP-AgoshR2c.** Schizont-enriched protein samples of *Pb*GFPcon, *Pb*Ago2 3.2 or *Pb*Ago2 4.3 transfected with AgoshRscr or αGFP-AgoshR2c were analyzed by Western blotting. The blots were probed with an antibody against GFP or HSP70. (A) and (B) show representative blots from samples obtained from independent transfections (biological replicate). Each blot was done in technical duplicates.

It is notable that the αGFP-AgoshR2c-mediated knockdown of GFP is much more pronounced in *Pb*Ago2 (about 40-fold reduction of fluorescence in late trophozoites) than *in vitro* (about 2-fold reduction of GFP fluorescence) (compare Figure 10 F to Figure 23 C). Possible explanations for this will be discussed in detail in Chapter 4. The strength of the GFP knockdown prompted me to test also the other AgoshRNAs, which had shown only a limited effect against GFP *in vitro*, in *Pb*Ago2.

3.3.2 FINE-TUNING OF GFP EXPRESSION

To this end, I transfected *Pb*Ago2 3.2 with vectors encoding the other three αGFP-AgoshRNAs, namely αGFP-AgoshR1c, -AgoshR3c and -AgoshR4c, and performed the same microscopic analysis of blood stages as in the first experiment (see Section 3.3.1). Indeed, all AgoshRNAs were found to be active against GFP and significantly reduced the fluorescence of transgenic parasites. The extent of the knockdown varied between the individual AgoshRNAs, and ranged, for late trophozoites, from 5-fold (αGFP-AgoshR4c) to 13-fold reduction (αGFP-AgoshR3c) (Figure 25).

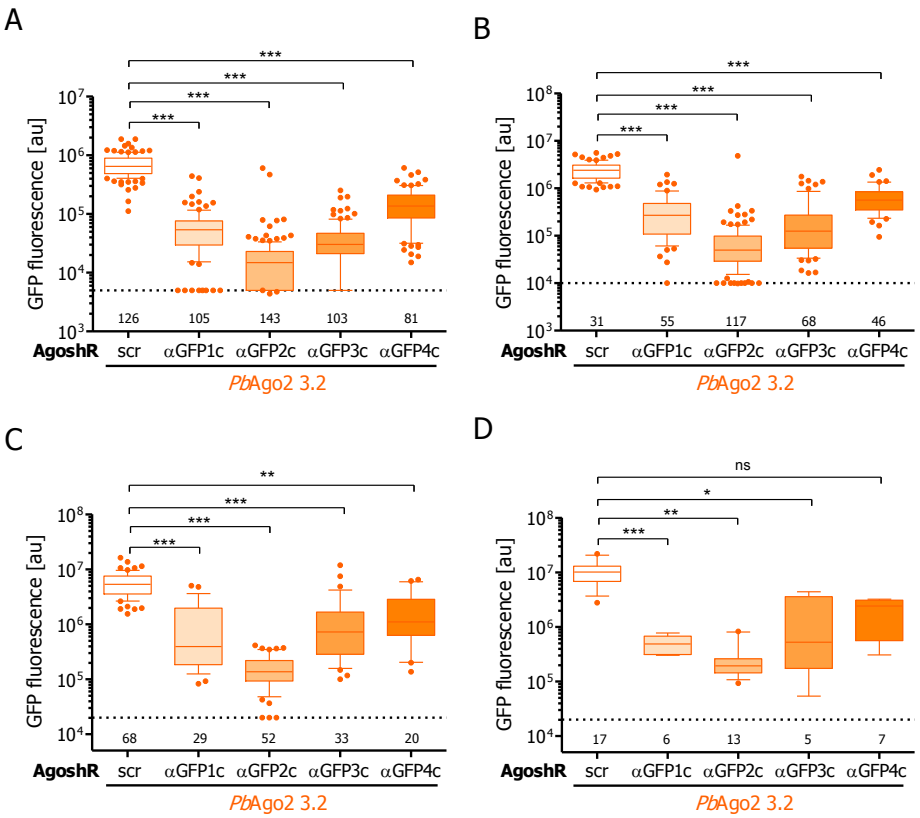

FIGURE 25: **Quantification of GFP fluorescence after expression of different AgoshRNAs.** *Pb*Ago2 3.2 was transfected with episomes encoding one of the αGFP-AgoshRNAs 1c, 3c or 4c. (αGFP1c, αGFP3c, or αGFP4c, respectively), and selected with pyrimethamine drug pressure. After the appearance of pyrimethamine-resistant parasites, blood stages were imaged with a wide-field fluorescence microscope with constant settings across all samples. The integrated GFP fluorescence intensity of individual parasites was determined using the software ImageJ. Depicted is the integrated GFP fluorescence intensity for individual (A) ring stages, (B) early trophozoites, (C) late trophozoites and (D) gametocytes as whisker plots with 10-90 percentile. Data is merged from two independent experiments (based on independent transfections), and the number below each bar indicates the total number of individual parasites quantified. Note that the data for *Pb*Ago2 3.2 transfected with AgoshRscr and AgoshR2c is taken from Figure 23 and plotted here again for comparison. Statistics: Kruskal-Wallis-Test followed by Dunn's test. ns: not significant; * $p<0.05$; ** $p<0.01$; *** $p<0.001$; au: arbitrary units.

A Western blot analysis of schizont-enriched blood stages yielded the same pattern, with αGFP-AgoshR2 inducing the strongest reduction of GFP, followed by the αGFP-AgoshR3c, AgoshR1c, and AgoshR4c, in this order (Figure 26). Interestingly, this observation parallels the results in Dicer-deficient MEF cells (see Section 3.1.2, Figure 13 B). This implies that the cell culture assays are a good indicator of the relative activity of individual AgoshRNAs against a given target, albeit they may not accurately predict the strength of the knockdown that can be observed *in vivo*.

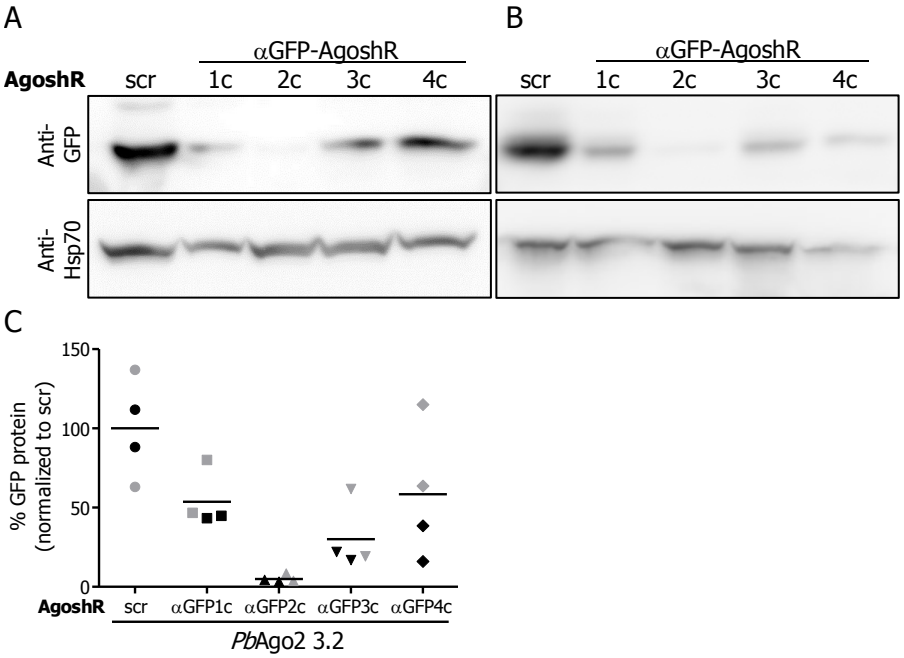

FIGURE 26: **GFP protein levels in *Pb*Ago2 expressing different αGFP-AgoshRNAs.** Schizont-enriched protein samples of *Pb*Ago2 3.2 transfected with AgoshRscr or one of the four αGFP-AgoshRNAs were analyzed by Western blotting. The blots were probed with an antibody against GFP or HSP70. (A) and (B) show representative blots from samples obtained from independent transfections (biological replicate). Each blot was done in technical duplicates. (C) Relative amount of GFP as compared to AgoshRscr-transfected samples. Protein amount was determined with ImageJ using the HSP70 band to normalize for input. Each dot represents an individual technical replicate and dots of the same shade (dark or light) belong to the same biological replicate. Note that while there is a high technical variation between blots, the overall trend is in line with previous quantifications of GFP fluorescence intensity (compare Figure 25).

3.4 KNOCKDOWN OF AN ENDOGENOUS TARGET IN BLOOD STAGES

Having confirmed that a knock down of GFP using AgoshRNAs is possible, the next step was to silence the expression of an endogenous gene. The target I chose for the first knockdown experiment was required to fulfill three main criteria:

1) It must not be essential for blood stage development, as it was not clear at this point whether RNAi-mediated knockdown would be possible for this group of genes.
2) The phenotype of the knockout of this gene should be published, to permit an assessment whether the knockdown phenocopies the knockout.
3) The phenotype should appear in blood stages, where episomally expressed AgoshRNAs would induce a knockdown, and should be easy to quantify.

Using these three criteria, I searched the literature and selected the gene encoding the *Plasmodium* perforin-like protein 2 (PPLP2), whose knockout has

been published both for *P. berghei* and *P. falciparum*[291,292]. This protein is important for the exflagellation of the male gametocytes, which occurs when gametocytes enter the mosquito midgut. The concurrent drop in temperature and increase of pH, as well as the presence of xanthurenic acid, induces a cascade of events in which the male gametocyte replicates its nucleus three times and forms eight flagellated gametes. These gametes then emerge from the red blood cell and actively search for a female gametocyte to fertilize[51]. Since PPLP2 is required for the lysis of the RBC membrane during the emergence of the gametes, the gametocytes are trapped within the erythrocyte if PPLP2 is missing. Instead of eight individual flagella, they form a single large "superflagellum" within the erythrocyte membrane, which can be easily distinguished under the microscope[291].

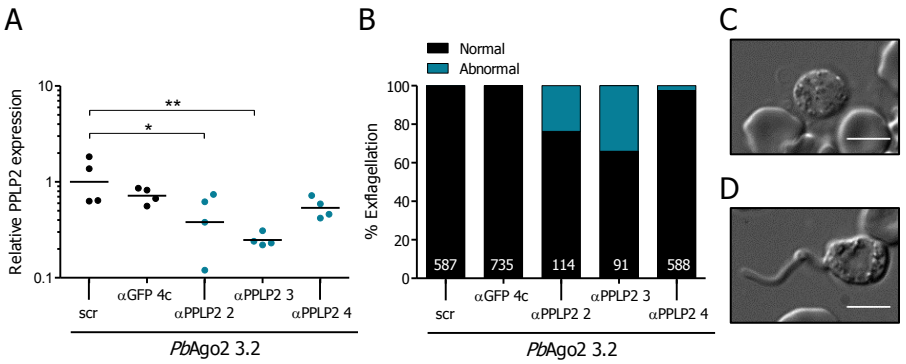

FIGURE 27: **Knockdown of PPLP2 phenocopies the *pplp2*(-) parasite.** *Pb*Ago2 3.2 parasites were transfected with AgoshRscr, αGFP-AgoshR4c (both black), or one of three αPPLP2-AgoshRNAs (2, 3 or 4, turquoise). To enrich for gametocytes, mice were pretreated with phenylhydrazine prior to i.v. infection with 10^6 iRBC. (A) Four days after infection, blood was collected and PPLP2 mRNA levels were determined by qRT-PCR. The gametocyte-specific gene PSOP1 (putative secreted ookinete protein, PBANKA_0619200) served as housekeeper[293]. Results were normalized to *Pb*Ago2 + AgoshRscr. Each dot represents parasites isolated from an individual mouse. Statistics: One-way-ANOVA followed by Dunnett's test. * $p<0.05$; ** $p<0.01$. (B) Exflagellation events were microscopically examined four days after infection and scored as either normal (black) with the formation of eight individual flagella or abnormal (turquoise) with the formation of a single large superflagellum. Numbers of individual exflagellations assessed are indicated at the bottom of the bars. (C) Representative picture of a normally exflagellating gametocyte. Note that the individual flagella are difficult to image due to their thin nature. The scale bar indicates 10 µm. (D) Representative picture of a gametocyte forming a superflagellum due to the lack of PPLP2. The scale bar indicates 10 µm.

To address whether an AgoshRNA-mediated knockdown of PPLP2 could phenocopy this effect, I designed four different AgoshRNAs against PPLP2 (αPPLP2-AgoshR1 to 4) based on the design rules outlined in section 3.1.1, and transfected these AgoshRNAs as episomes into *Pb*Ago2 3.2. Parasites positive for mCherry fluorescence appeared readily at one to two weeks after transfection. Surprisingly, sequencing of the four parasite lines revealed that the parasite line that should have been transfected with the αPPLP2-AgoshR1 episome instead carried the αGFP-AgoshR4c episome. It remains unclear at which point this mix-up occurred. Nevertheless, I included this line in all subsequent analyses as an additional non-targeting AgoshRNA. The other parasite lines obtained all carried the correct episome.

As PPLP2 is only expressed in gametocytes, I performed all experiments in conditions that promote gametocytogenesis. To this end, I pretreated mice prior to parasite infection with phenylhydrazine, a substance that induces reticulocytosis, which is known to foster the development of gametocytes[294]. Quantification of the PPLP2 mRNA by qRT-PCR of these gametocyte-enriched samples revealed a robust knockdown of PPLP2 for two out of three AgoshRNAs (αPPLP2-AgoshR2 and -AgoshR3), while PPLP2 mRNA levels remained unchanged in parasites expressing αGFP-AgoshR4c or αPPLP2-AgoshR4 (Figure 27 A). I then examined exflagellation of these transfected parasites. Parasites expressing AgoshRscr, αGFP-AgoshR4c or αPPLP2-AgoshR4, which all do not silence PPLP2, predominantly exflagellated normally by forming eight separate flagella (Figure 27 B, C). In contrast, a subpopulation of parasites that expressed αPPLP2-AgoshR2 or -AgoshR3 showed the previously described phenotype of a superflagellum (Figure 27 B, D). In conclusion, a knockdown of PPLP2 can induce the same phenotype as a full knockout[291,292].

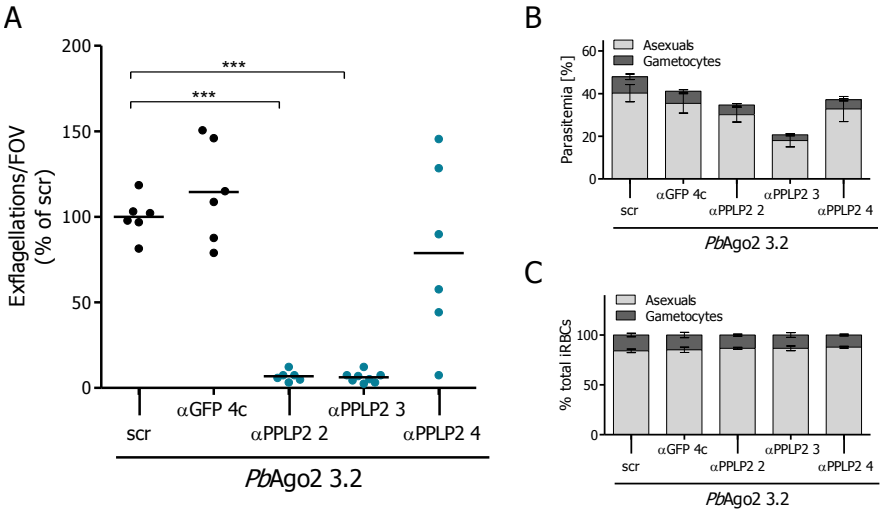

FIGURE 28: **PPLP2 knockdown is accompanied by a reduced exflagellation frequency.** (A) Four days prior to the analysis, phenylhydrazine-pretreated mice were i.v. infected with 2x10^6 iRBCs of *Pb*Ago2 3.2 carrying AgoshRscr, αGFP-AgoshR4c (both black), or one of three αPPLP2-AgoshRNAs (turquoise). A drop of tail blood was transferred to a glass slide, and exflagellation was induced with xanthurenic acid. Twelve min after induction, exflagellation events and field of views (FOV) were counted for 2.5 min. Shown are the exflagellation events per FOV normalized to the scr control quantified in parallel. Statistics: One-way ANOVA with Dunnett's multiple comparisons. *** $p<0.001$. (B) Absolute and (C) relative parasitemia and gametocytaemia of the mice were determined in parallel from Giemsa-stained thin blood smears.

While assessing the phenotype of the αPPLP2-AgoshRNAs, I noticed that parasites that expressed either αPPLP2-AgoshR2 or -AgoshR3 seemed to exflagellate less frequently than the others. I thus quantified the exflagellation rate in gametocyte-enriched parasite populations. Interestingly, there was a sharp and significant drop in the exflagellation rate of *Pb*Ago2 parasites expressing an active αPPLP2-AgoshRNA versus those expressing a scrambled AgoshRNA or the non-active αPPLP2-AgoshR3 (Figure 28 A). Although there was also a slight reduction of the overall parasitemia in these groups (Figure

28 B), its extent was not sufficient to explain the reduced exflagellation rate. PPLP2 inhibition did not influence the formation of gametocytes, as their in all iRBCs remained constant, irrespective of the AgoshRNA expressed (Figure 28 C). Additionally, the gametocytaemia of individual mice did not correlate with the exflagellation frequency (data not shown). The observation that a knockdown of PPLP2 reduces the rate of exflagellation contrasts the published phenotype of PPLP2-deficient *P. berghei* parasites, which presumably exflagellate at the same rate[291]. However, such a loss of exflagellation is reported for a PPLP2 knockout in *P. falciparum*[292].

3.5 STABLE INTEGRATION OF AGOSHRNAS

As demonstrated in the previous Sections, episomal AgoshRNA expression can lead to a potent knockdown of a target of interest in blood stages. However, episomes are no suitable tool for target knockdown in the mosquito stages, as the plasmids are not evenly distributed to daughter cells during asexual replication. Therefore, constant drug selection is required to retain the episome, which is not possible in the mosquito stages[285,295]. Hence, the episomal plasmid is lost during the asexual replication within the mosquito midgut. To study whether RNAi is also functional in non-erythrocytic stages of *Pb*Ago2, it is thus necessary to stably integrate the AgoshRNAs into the genome. This is the subject of the following Section.

3.5.1 INTEGRATION STRATEGY

Akin to the initial experiment in blood stages, GFP served as a *proof-of-principle* target for a knockdown in mosquito- and liver stages. Accordingly, I designed a construct to integrate the potent αGFP-AgoshR2c as well as the AgoshRscr as a negative control into the *Pb*Ago2 genome directly behind the Ago2 expression cassette. A scheme of the construct design and the integration strategy is depicted in Figure 29 A.

The integration vector was designed in such a way that the 3'UTR of Ago2 and the 3' region of SIL6 serve as homology regions for double homologous integration (Figure 29 A). In *Pb*Ago2, these two parts border the part of the selection marker that remained after recycling of the cassette by homologous recombination, *i. e.* the duplicate region of the 3'DHFR-TS site (see also Section 3.2.1, Figure 14). Inadvertently, this site was also present in the integration vector for the AgoshRNAs. Therefore, parasites could use the duplicate 3'*DHFR-TS* region as homology arm to integrate the selection marker only, without the 5'*Pb*U6-AgoshRNA cassette (depicted as red dashed lines in Figure 29). Consequently, the transfection of *Pb*Ago2 3.2 with this initial set of constructs resulted in a mixed population of parasites that either had the full selection marker and 5'*Pb*U6-AgoshRNA cassette incorporated into the genome or only integrated the resistance cassette. Still, a single clone of each line

*Pb*Ago2.αGFP2c and *Pb*Ago2.scr could be obtained after limiting dilution which had the 5'*Pb*U6-AgoshRNA cassette integrated as intended. Diagnostic PCR of the parental locus and the 3' integration site verified the absence of the *Pb*Ago2 parental line and of parasites with only the selection marker integrated (Figure 29 B, C).

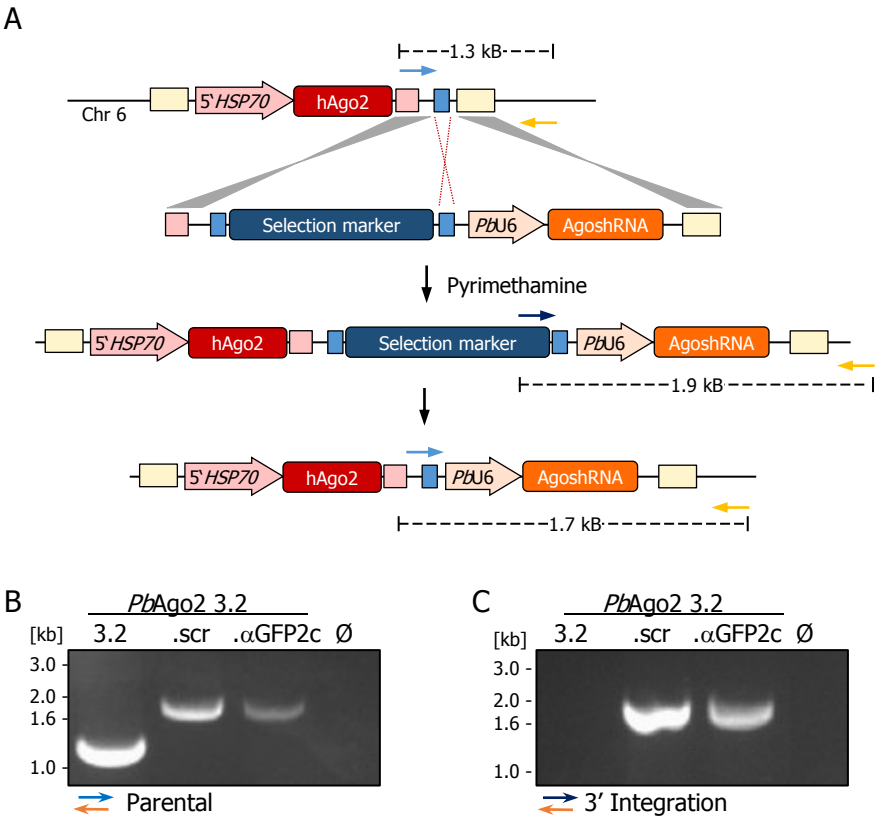

FIGURE 29: **Integration strategy and genotyping of *Pb*Ago2.scr and *Pb*Ago2.αGFP2c.** (A) Strategy to integrate the AgoshRNA under the 5'*Pb*U6 promoter (5'*Pb*U6-AgoshRNA) along with a selection marker for pyrimethamine resistance (*hDHFR-yFCU*) into the genome of *Pb*Ago2. The red dashed lines indicate an alternative 3' homology region that can lead to the insertion of the selection cassette only. (B, C) Diagnostic PCR of *Pb*Ago2.scr and *Pb*Ago2.αGFP2c clonal lines. *Pb*Ago2 3.2 (first lane) served as a control for the parental line. Ø: No-template control. Colored arrows indicate the respective primer pairs used for amplification in (A). (B) PCR amplifying the parental locus. Amplification of the parental locus yields a fragment of 1.3 kb which is visible for *Pb*Ago2 3.2, but absent in *Pb*Ago2.scr and *Pb*Ago2.αGFP2c. Note the larger amplicons in the lanes *Pb*Ago2.scr and *Pb*Ago2.αGFP2c. These indicate that a subpopulation of these lines has already removed the selection marker by homologous recombination (expected amplicon length for this event: 1.7 kb). (C) PCR amplifying the 3 'integration site, yielding an expected amplicon length of 1.9 kb. Note that in the case of an unwanted integration event of the selection cassette only, this PCR would result in a shorter amplicon of 1.4 kb, which is absent in both clonal lines.

3.5.2 GROWTH BEHAVIOR OF *PB*AGO2.SCR

Up to this point, it was still unclear what causes the growth impairment of *Pb*Ago2. A hypothesis was that in the absence of an AgoshRNA, Ago2 binds in an unspecific manner to endogenous non-coding RNAs, resulting in their dysregulation. An analogous growth impairment has been observed in *T. gondii* that constitutively express the Cas9 protein. Similar to Ago2, Cas9 requires a small RNA to function, and in the absence of a matching gRNA, the endonuclease might associate with endogenous small RNAs. A recent study has demonstrated that constitutive co-expression of a non-targeting decoy gRNA alleviated the growth defect induced by Cas9 expression in *T. gondii*[75]. I thus hypothesized that the expression of the AgoshRscr might have a similar effect and rescue the growth of *Pb*Ago2.

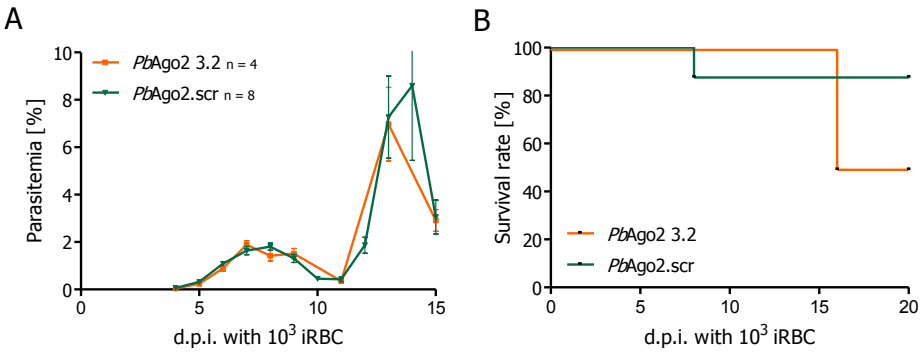

FIGURE 30: **Blood-stage growth of *Pb*Ago2.scr.** Inbred C57BL/6J mice were intravenously infected with 1000 iRBC of either *Pb*Ago2 3.2 or *Pb*Ago2.scr. (A) Parasitemia was monitored from day 3 to day 14 post-infection via Giemsa-stained thin blood smears. The number of mice (n) for each group is indicated in the legend. Shown is the mean parasitemia +/-SEM. (B) Survival of the infected mice. Mice were observed until day 20 post-infection for signs of ECM or severe disease symptoms and sacrificed accordingly. d.p.i: days post-infection.

To test this hypothesis, I infected C57BL/6J mice with 1000 iRBC of *Pb*Ago2 or *Pb*Ago2.scr and followed parasitemia and survival over 14 and 20 days, respectively (Figure 30). Both lines had a very comparable growth rate and survival of mice, which reflects the data observed in the previous experiments with *Pb*Ago2 (see Section 3.2.3, Figure 19). Vera Mitesser further analyzed these two lines during her master thesis. After feeding the two lines *Pb*Ago2.scr and *Pb*Ago2.αGFP2c to mosquitoes, she determined the mosquito infectivity of these lines by measuring oocyst prevalence and sporozoite numbers (Figure 31). Similar to the blood-stage growth, a decreased mosquito infectivity in the range of previously obtained data for *Pb*Ago2 became apparent (see Section 3.2.3, Figure 20). In conclusion, in contrast to observations for Cas9 expression in *T. gondii*, the expression of a scrambled AgoshRNA does not rescue the growth defect of *Pb*Ago2. The observation that Ago2 toxicity cannot be alleviated by the presence of an AgoshRNA indicates that the growth defect may not mediated by the RNA binding function of Ago2.

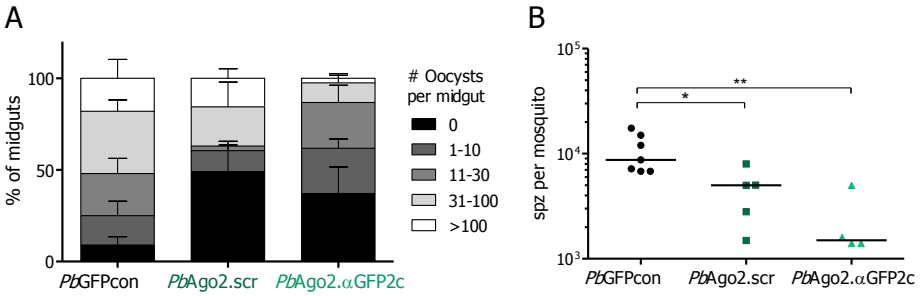

FIGURE 31: **Mosquito development of *Pb*Ago2.scr and *Pb*Ago2.αGFP2c.** Mosquitoes were infected by blood meal on parasite-infected mice. (A) Midguts were isolated 12 to 14 days after blood meal from 10 to 15 mosquitoes per cage, and the number of oocysts per midgut was scored by microscopic examination. Depicted is the percentage of midguts (+/-SEM) belonging to one of five groups: No oocysts, 1-10 oocysts, 11 to 30 oocysts, 31 to 100 oocysts, >100 oocysts per midgut. Data is the mean of four to five independent feedings per strain. (B) Salivary gland sporozoites were isolated 18 days after blood meal from at least 25 female mosquitoes per cage and counted. Depicted is the average number of salivary gland sporozoites per female mosquito. Each dot represents an individual cage (independent feeding). Note that data for the *Pb*GFPcon wild type is the same as in Figure 20, and presented here for comparison only.

3.5.3 KNOCKDOWN OF GFP ACROSS THE LIFE CYCLE

Importantly, the stable integration of AgoshRNAs into the genome of *Pb*Ago2 now allowed to assess whether Ago2-mediated RNAi is also possible in the other life cycle stages of the *PbAgo2* parasite line. First, however, I analyzed the GFP fluorescence of blood stages by microscopy and indeed observed that *Pb*Ago2.αGFP2c lacks any detectable GFP fluorescence (Figure 32 A). This finding was further confirmed by Vera Mitesser when she performed a Western blot of schizont-enriched *Pb*Ago2.scr and *Pb*Ago2.αGFP2c samples (Figure 32 B). Subsequently, Vera Mitesser and I both analyzed the non-erythrocytic stages of *Pb*Ago2.

The analysis of the GFP fluorescence of the lines Pb*Ago2.scr and* Pb*Ago2.αGFP2c were carried out in part by Vera Mitesser in the course of her master thesis.*

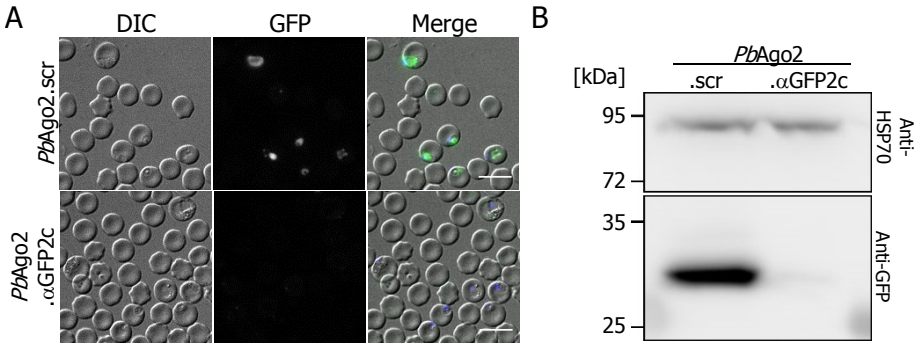

FIGURE 32: **Knock down of GFP in blood stages.** (A) Blood stage parasites of *Pb*Ago2.scr or *Pb*Ago2.αGFP2c were imaged with a fluorescence microscope with equal settings. Shown are the DIC and GFP channel, and in the merge additionally Hoechst-stained nuclei (blue) to indicate parasites. The scale bars indicate 10 µm. (B) Western blot analysis of schizont-enriched cultures of *Pb*Ago2.scr or *Pb*Ago2.αGFP2c. Blots were revealed with an anti-HSP70 antibody (upper blot) or an anti-GFP antibody (lower blot).

After feeding mosquitoes on *Pb*Ago2.scr or *Pb*Ago2.αGFP2c-infected mice, we imaged oocysts at day 13. Importantly, we measured a significant reduction of GFP fluorescence for *Pb*Ago2.αGFP2c compared to *Pb*Ago2.scr oocysts (Figure 33 A, B). We also imaged salivary gland sporozoites at day 18 and found that *Pb*Ago2.αGFP2c sporozoites were clearly less GFP-fluorescent than their *Pb*Ago2.scr counterpart (Figure 33 C, D). These findings confirm that both Ago2 and AgoshRNAs are active in the mosquito stages of *Pb*Ago2.

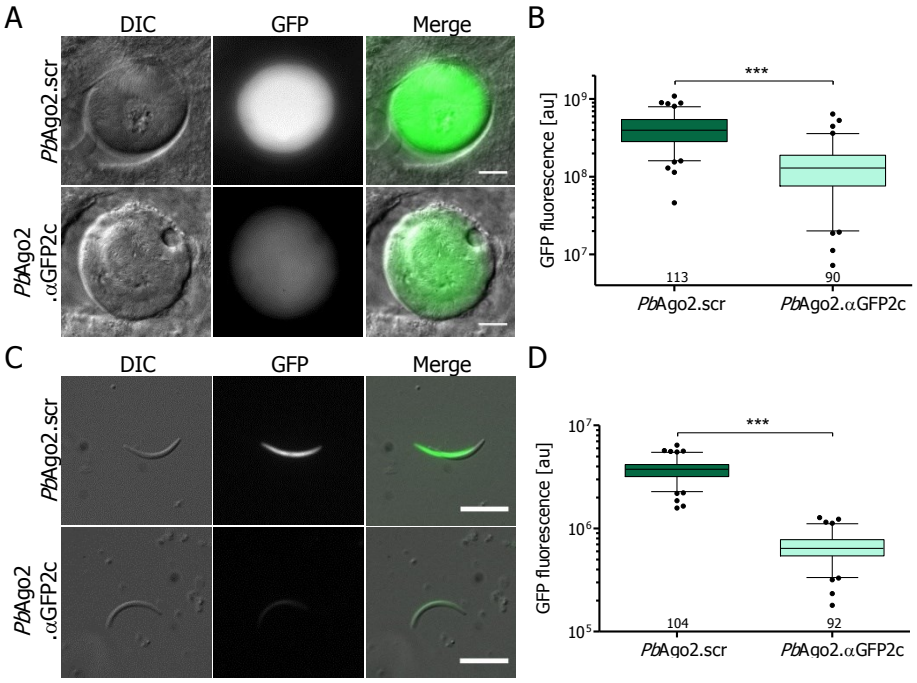

FIGURE 33: **Knock down of GFP in mosquito stages.** Mosquitoes were fed on *Pb*Ago2.scr- or *Pb*Ago2.αGFP2c-infected mice. (A) Midgut oocysts (day 13) and (C) salivary gland sporozoites (day 18) were imaged with a wide-field microscope. Shown are representative pictures of *Pb*Ago2.scr and *Pb*Ago2.αGFP2c. The scale bar indicates 10 µm. GFP fluorescence of (B) oocysts and (D) sporozoites was quantified using ImageJ. Depicted is the pooled data of three independent experiments (independent cages) as whiskers plot with 5-95 percentile. Numbers below the bars indicate the total number of individual parasites. Statistics: Student's T-test. *** $p<0.001$.

Finally, we also analyzed the GFP knockdown in liver stages. As imaging of the GFP fluorescence of live liver stages has proven to be difficult, we fixed sporozoite-infected liver stages with methanol after 48 h of intrahepatic development and stained them with an anti-GFP antibody as well as an antibody against HSP70 (Figure 34 A). We quantified the signal of the anti-GFP staining from microscopy images and again determined a marked downregulation of GFP in *Pb*Ago2.αGFP2c- versus *Pb*Ago2.scr-liver stages (Figure 34 B). In conclusion, the *Pb*Ago2 parasite strain is capable of RNAi-mediated target knockdown in all stages of the life cycle.

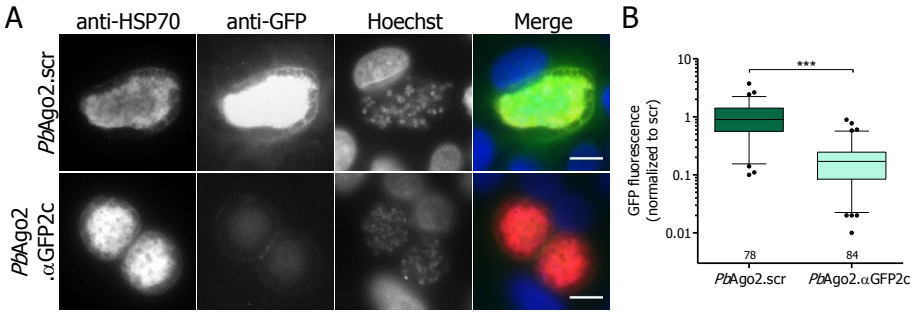

FIGURE 34: **Knock down of GFP in liver stages.** (A) Liver stages of *Pb*Ago2.scr and *Pb*Ago2.αGFP2c were fixed 48 h post-invasion and stained with an antibody against HSP70 (first column), an antibody against GFP (second column) and Hoechst to stain DNA (third column). Shown are representative images. All pictures were taken with a wide-field microscope with same settings and processed alike. The scale bars indicate 10 µm. (B) The GFP signal of liver stages after immunofluorescence staining was quantified using ImageJ, and normalized to the mean signal intensity of *Pb*Ago2.scr liver stages to control for different staining efficiencies. Shown is the pooled data of two independent experiments (independent cages). Numbers below the bars indicate the total number of individual parasites quantified. Statistics: Student's T-test. *** $p<0.001$.

3.6 KNOCKDOWN OF EXPORTED PROTEIN 1 (EXP1)

As shown in the previous Sections, expression of different AgoshRNAs in *Pb*Ago2 induce a target knockdown to various levels. This differential knockdown results in intermediate phenotypes, such as the partially reduced GFP fluorescence (see Section 3.3.2) or formation of a superflagellum in a part of the population when targeting PPLP2 (see Section 3.4). This observation prompted the hypothesis that *Pb*Ago2 might permit targeting of a blood-stage essential gene, as its partial knockdown might be compatible with parasite survival while still yielding a phenotype that allows to study gene function. To test this hypothesis, I chose the blood-stage essential gene exported protein 1 (EXP1) as a target. EXP1 is a dominant antigen in many immune responses and a major vaccine candidate[296]. This protein is located to the PVM of blood-stage as well as liver-stage parasites[297–299], and its function is not yet clearly identified. EXP1 has been refractory to gene deletion, but studies on truncated EXP1 have shown that in the liver, the C terminus of EXP1 is involved in the uptake of nutrients by directly interacting with the host cell factor ApoH1[19]. In blood-stages, EXP1 might act as glutathione transferase[300]. However, this current hypothesis is based on a single study applying computational gene analyses and requires further experimental validation.

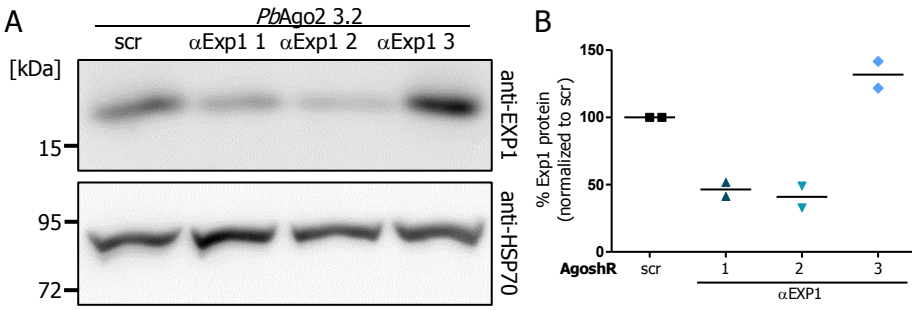

FIGURE 35: **EXP1-protein expression in *Pb*Ago2 parasites expressing αEXP1-AgoshRNAs.** (A) Schizont-enriched samples were analyzed by Western blotting probing for either EXP1 or HSP70 (as loading control). One representative blot of two technical replicates is shown. (B) Quantification of the Western blots. Band intensities were determined with ImageJ, and the EXP1 signal was normalized to the HSP70 signal. The *Pb*Ago2 3.2 + AgoshRscr sample served as control for normalization and was set to 100 %. Each dot represents the signal of an individual technical replicate.

To target this protein, I designed three different AgoshRNAs against EXP1 and transfected them episomally into *Pb*Ago2 3.2. Mice became blood-stage-positive one to two weeks after transfection. After confirming that all parasites retained the episome (indicated by mCherry fluorescence), I analyzed EXP1 protein expression of these parasites, as well as a *Pb*Ago2 + AgoshRscr control (Figure 35). A Western blot from a single protein preparation was performed in technical duplicates (Figure 35 A). Quantification of these blots indicated a reduction of EXP1 to about 40-50 % for the αEXP1-AgoshR1 and AgoshR2, while AgoshR3 did not change EXP1 expression levels (Figure 35 B). As Western blot is an inherently error-prone method to quantify protein levels, this observation needs to be verified by additional analysis of independent protein preparations.

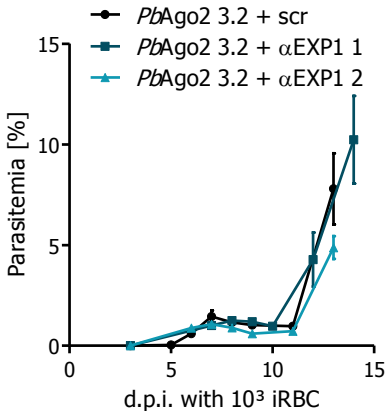

FIGURE 36: **Growth of *PbAgo2* 3.2 parasites expressing αEXP1-AgoshRNAs.** Female C57BL/6J mice (n=4) were intravenously injected with 10^3 iRBC of *Pb*Ago2 3.2 expressing either AgoshRscr or αEXP1 AgoshR1 or 2. Pyrimethamine was constantly supplied via the drinking water to retain the episome. Parasitemia was monitored from day 4 to day 14 post-infection by daily Giemsa-stained thin blood smears.

To assess whether the moderate knockdown of EXP1 influences parasite viability, I analyzed the blood-stage growth of *Pb*Ago2 3.2 parasites expressing αEXP1-AgoshR1 and 2, and compared that to parasites expressing AgoshRscr (Figure 36). After inoculation of 1000 iRBC into C57BL/6 mice, all three lines

grew comparably, recapitulating the growth phenotype of *Pb*Ago2 in the absence of any AgoshRNA. Thus, the expression of the αEXP1 AgoshRNAs does not affect the blood-stage growth rate.

A possible explanation for the relatively weak knockdown and the unaffected blood stage growth in parasites expressing αEXP1-AgoshRNAs could be that parasites with a spontaneous mutation in either the EXP1 locus or the AgoshRNA locus outgrew the population. Such a mutation could prevent the binding and efficient knockdown of EXP1 and thus be advantageous to the parasite. To exclude this possibility, I sequenced the EXP1 and the AgoshRNA locus in all *Pb*Ago2 lines, which revealed that no evasion mutations occurred which prevented the AgoshRNAs from binding (data not shown).

It thus remains thus unclear whether EXP1 was truly downregulated, and more quantitative measurements such as qRT-PCR should be used to unanimously determine successful knockdown. If these confirm a knockdown, further studies would be necessary to investigate whether there is a more subtle phenotype associated with the EXP1 knockdown.

3.7 OFF-TARGET ANALYSIS OF AGOSHRNAS VIA RNA-SEQ

The work so far has demonstrated that RNAi can be used in *Pb*Ago2 to knock down a gene of interest. To be broadly useful as a genetic tool, not only the efficiency of gene silencing is interesting, but also its specificity. Phenotypic analysis of a given target knockdown is confounded by side effects if the AgoshRNA also downregulates an unknown amount of other genes via so-called off-targeting. This is a concern for all technologies in which the target is determined by relatively short DNA or RNA sequences, such as shRNA-mediated knockdown in RNAi-competent organisms or CRISPR/Cas9-mediated gene editing[173,301]. For commonly used technologies, such as shRNA-mediated knockdown in human cells, tools exist that predict off-targets of a given shRNA sequence, allowing to experimentally test if these targets are indeed affected by the shRNA. However, such prediction tools do not yet exist for *Plasmodium*, in which RNAi is absent.

We therefore took a comprehensive and unbiased experimental approach to identify potential off-targets that are affected by AgoshRNA-mediated knockdown in *PbAgo2*. Specifically, we performed whole RNA sequencing (RNA-Seq) and quantified the entire transcriptome of *Pb*Ago2 expressing AgoshRscr, αGFP-AgoshR1c, αGFP-AgoshR2c or no AgoshRNA at all (as a reference). We also compared *Pb*Ago2 with the parental line *Pb*GFPcon as a second reference, hoping to be able to identify a reason for the growth impairment of *Pb*Ago2.

Sabine Fraschka performed the RNA-Seq work in the group of our collaboration partner Dr. Richard Bartfaí, Nijmegen, Netherlands.

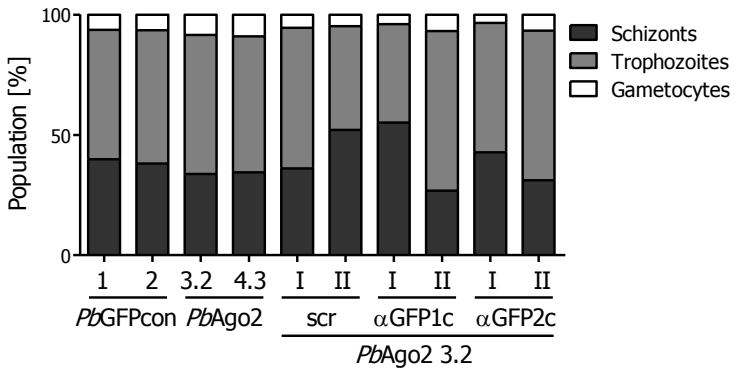

FIGURE 37: **Stage composition of RNA-Seq samples.** Mice with about 1-2 % parasitemia were bled and blood was cleared of leukocytes by column filtration. Parasites were then cultured for 18 h *in vitro* before analyzing stage compositions via Giemsa-stained thin blood smears. For each sample, at least 100 individual parasites were classified.

For RNA-Seq, a comparable sample preparation is critical to minimize intersample variation. As the various stages in the asexual replication cycle have very distinct transcriptional profiles[302], mixed blood-stage samples, in which the stage composition cannot be controlled, are not suitable for RNA-Seq. I thus synchronized the different samples by culturing blood stages overnight. As *P. berghei* schizonts are not able to egress *in vitro*, the prolonged culture will cause an enrichment of this stage and yield comparable stage distributions[303,304]. To ensure that samples were equivalent, I performed blood smears of all samples and quantified the stages present. Figure 37 depicts the percentage of schizonts, trophozoites, and gametocytes (no ring stages were observed) in all samples prepared for RNA-Seq. All samples (two biological replicates per sample) had a comparable composition with on average 39 % schizonts, 55 % trophozoites and 6 % gametocytes. RNA-Seq was subsequently performed by Sabine Fraschka, a PhD student in the laboratory of Richard Bartfaí, Nijmegen, the Netherlands.

We first compared *Pb*Ago2 to its parental line, *Pb*GFPcon, hoping to be able to identify differentially regulated transcripts that might explain the growth impairment of *Pb*Ago2. Indeed, when comparing the RPKM (reads per kilobase per million mapped reads) values for all transcripts between *Pb*Ago2 and *Pb*GFPcon, we identified a set of genes that were downregulated in *Pb*Ago2 as compared to *Pb*GFPcon. A closer analysis revealed that these genes all belong to a group which is translationally repressed in gametocytes through the association of their mRNA with the DOZI (development of zygote inhibited)/CITH (homolog of worm CAR-I and fly Trailer Hitch) complex[305]. In contrast, male gametocyte-specific genes[306], as well as female gametocyte-specific genes that are part of the DOZI/CITH complex, are not dysregulated (Figure 38). This finding is in line with the previous observation that the gametocytaemia was comparable in all RNA-Seq samples (Figure 37). Thus, the downregulation of a subset of gametocyte-specific genes in *Pb*Ago2 cannot be explained by an overall reduction in gametocytaemia. The data instead indicates that Ago2 interferes with DOZI/CITH-mediated mRNA storage in gametocytes, which will be further discussed in Chapter 4.

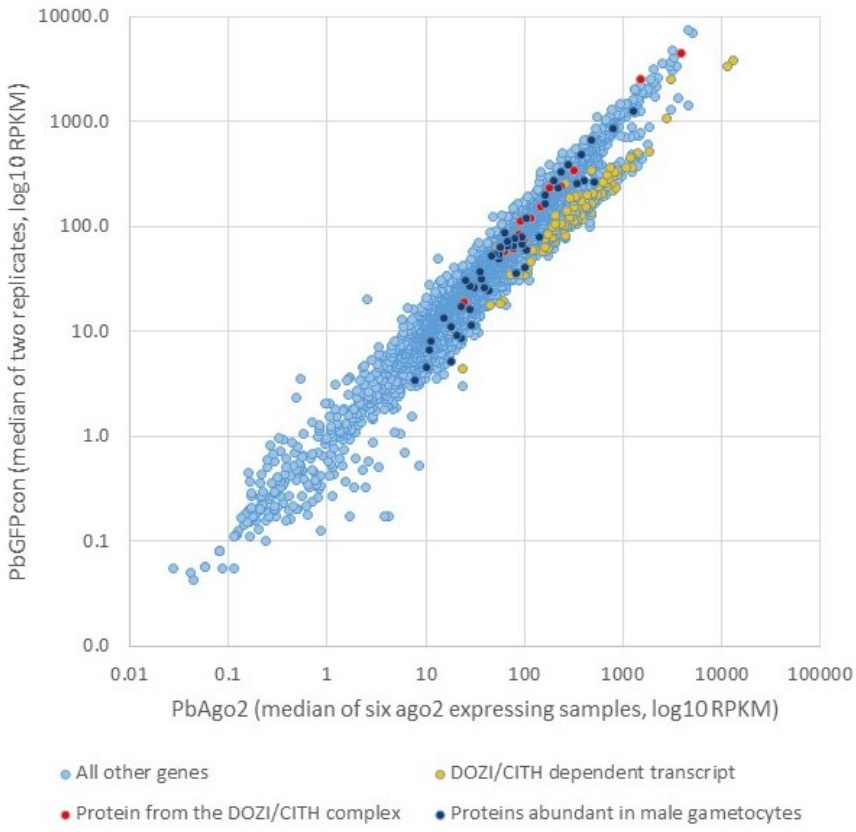

FIGURE 38: "**Ago2 expression results in the downregulation of DOZI/CITH dependent transcripts.** Scatter plot showing transcript levels (RPKM, log10) in *Pb*GFPcon (median of two biological replicates) in comparison to all *Pb*Ago2 samples (median of *Pb*Ago2, *Pb*Ago2 + scr, *Pb*Ago2 + αGFP2 with two replicates each). Fifty proteins previously reported to be abundant in male gametocytes are highlighted in dark blue[306]. Female gametocyte-specific proteins that are part of the DOZI/CITH complex are highlighted red[305]. Transcripts that are significantly downregulated both in DOZI and in CITH mutants[305] are marked with an orange dot." (Hentzschel *et al*., 2017, manuscript in preparation). The figure is provided by Sabine Fraschka, Radboud University, Nijmegen, The Netherlands.

We next compared gene expression in *Pb*Ago2 expressing αGFP-AgoshR1c or AgoshR2c against *Pb*Ago2 expressing the scrambled AgoshRNA (Figure 39 A, B). As expected, GFP was downregulated in both samples expressing an αGFP-AgoshRNA, most pronounced in *Pb*Ago2 expressing αGFP-AgoshR2c. Most other genes were unaffected by the expression of an αGFP-AgoshRNA, except a few, low-expressing, genes. These belong to multigene families, such as *bir* and *pir* genes, and the variation can most likely be largely attributed to intersample variation, rather than a specific effect of the AgoshRNA itself.

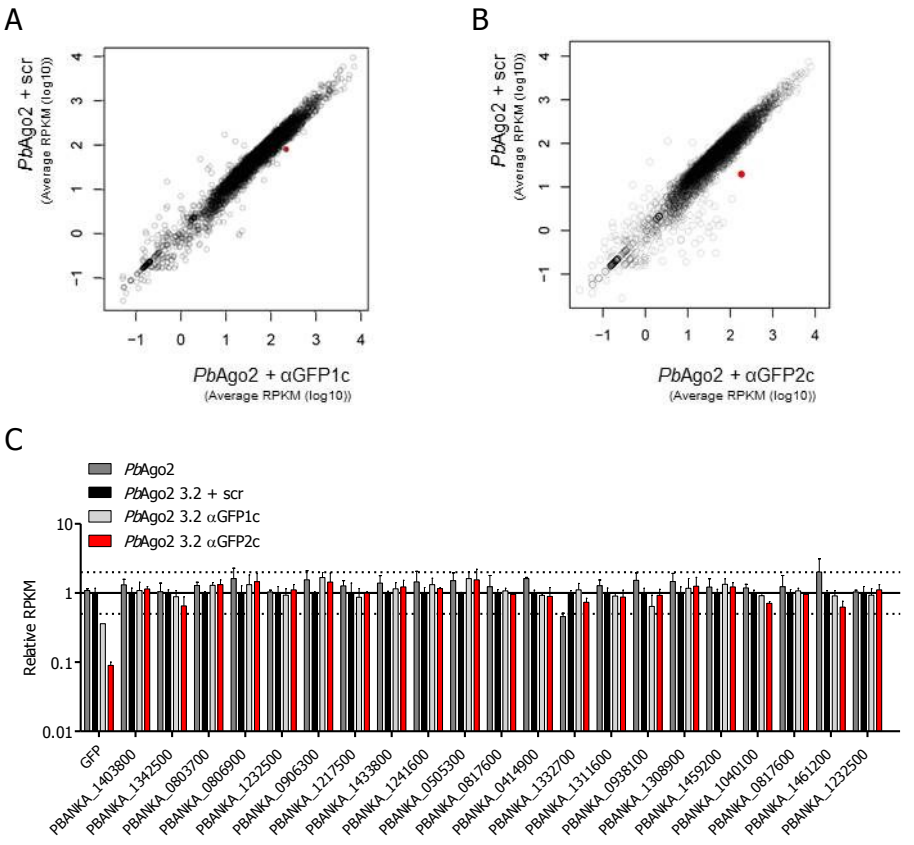

FIGURE 39: **Analysis of off-target effects from AgoshRNA expression in *Pb*Ago2.** (A, B) Scatter plots showing transcript levels of *Pb*Ago2 + scr compared to (A) *Pb*Ago2 + αGFP1c or (B) *Pb*Ago2 + αGFP2c. Shown is the log10 of the mean RPKM values of two biological replicates. In both blots, GFP is indicated in red. Both figures are provided by Sabine Fraschka, Radboud University, Nijmegen, The Netherlands. (C) Relative transcript levels of GFP and the top 21 genes with the highest sequence identity to AgoshRNA αGFP2c. Mean RPKM values of two biological replicates per sample were normalized to *Pb*Ago2 + scr (indicated by solid full line). The borders of two-fold changes (0.5 and 2) are indicated by dashed lines. Note that the data is depicted on a log scale.

To further identify potential AgoshRNA off-targets despite the absence of a prediction software, I reasoned that the sequence of an off-target of a given AgoshRNA would align to the AgoshRNA sequence. Thus, I identified the 21 *P. berghei* genes that had the highest sequence identity with the αGFP-AgoshR2c (11 or 10 nt), and, based on the RNA-Seq data, analyzed their relative transcript expression in *Pb*Ago2, *Pb*Ago2 + scr, *Pb*Ago + αGFP1c and *Pb*Ago2 + αGFP2c (Figure 39 C). Importantly, none of these genes were significantly deregulated upon expression of the αGFP-AgoshR2c, indicating that these genes are not off-targets. As sequence identity is not the only determinant of off-target activity, it will be important to further predict and study potential off-targets once respective software is available for *Plasmodium*. Until then, the present data indicate that AgoshRNA expression in *Pb*Ago2 causes no major off-targeting.

3.8 STAGE-SPECIFIC KNOCKDOWN

3.8.1 GENERATION OF *PB$_{LISP2}$*AGO2

So far I have established that constitutive, high-level expression of Ago2 in *P. berghei* is feasible and allows for AgoshRNA-mediated gene knockdown throughout the life cycle, albeit at the expense of parasite viability. For many applications, it would be desirable to further control the timing of the downregulation of the GOI. For example, a general knockout or knockdown might be difficult to achieve for blood-stage essential genes, whereas restricting the knockdown to the liver stage might yield valuable information about the function of this gene in this particular stage. Such approaches have, for instance, been employed to achieve the stage-specific expression of the FRT-recombinase, enabling the excision a GOI in late mosquito stages, yielding a target knockout in liver stages only[85]. However, this strategy results in a permanent loss of the gene, and parasites can no longer progress from the liver to blood stages.

One advantage of the Ago2-mediated knockdown strategy that was established here is that it opens up the possibility to control the timing of the knockdown by regulating Ago2 expression, *e. g.* by expressing it under a stage-specific promoter. As the expression of Ago2 is limited to a single stage only, the knockdown is restricted to this stage, and gene function should be unaffected in all other stages where Ago2 is not expressed. To test the feasibility of such a stage-specific knockdown, Vera Mitesser and I chose to express Ago2 under the promoter of the *LISP*2 (liver-specific protein 2) gene, which is expressed in late liver stages only[307].

To generate the parasite line *Pb$_{LISP2}$*Ago2, Vera Mitesser pursued a strategy similar to the one I had already used to produce the line *Pb*Ago2 but she replaced the *HSP70* 5'UTR with the 5'UTR of *LISP2* (Figure 40 A). After transfecting *Pb*GFPcon with the 5'*LISP2*-Ago2 construct and limiting dilution, she obtained a single clone *Pb$_{LISP2}$*Ago2 that was positive for integration. Further negative selection and another round of limiting dilutions yielded the final clone *Pb$_{LISP2}$*Ago2 1.1. Diagnostic PCR verified the correct insertion of the construct and the complete recycling of the selection marker (Figure 40 B-E).

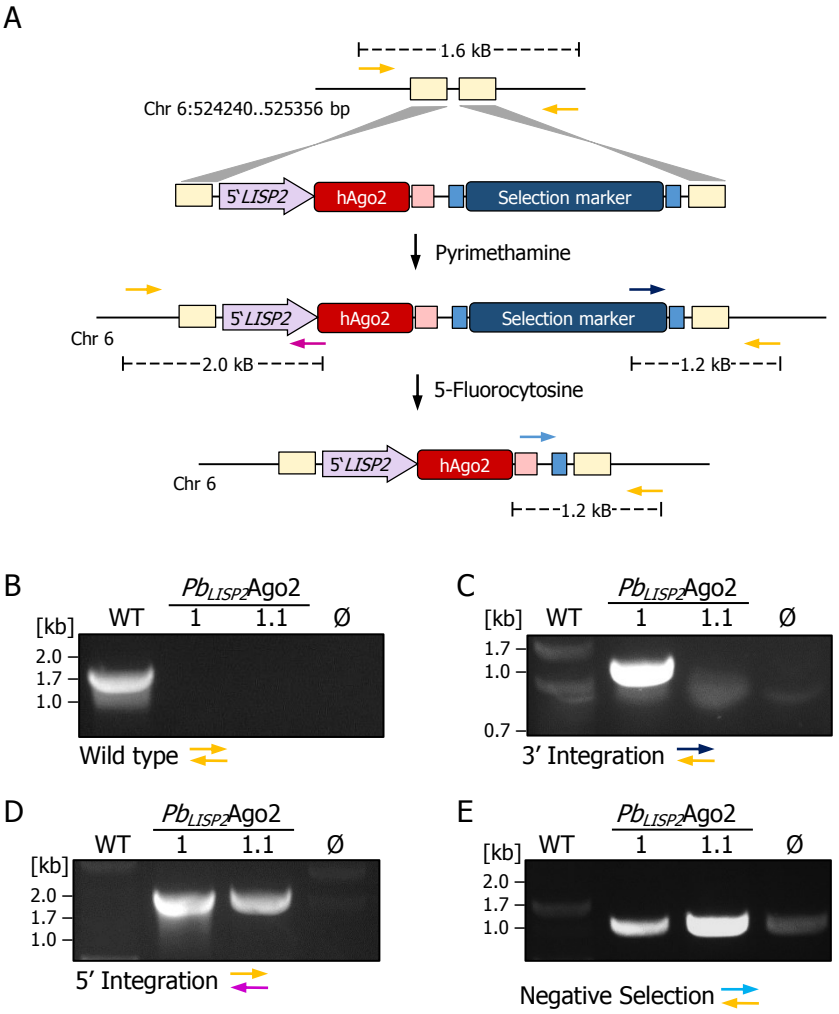

FIGURE 40: **Generation of *Pb*$_{LISP2}$Ago2.** (A) Scheme of the integration of a 5'*LISP2*-Ago2 expression construct into the SIL6. The integration strategy followed the same approach as for the *Pb*Ago2 line. (for details, see Figure 14). Proper integration of the construct into *Pb*GFPcon was confirmed by diagnostic PCR amplifying the (B) wild type locus, (C) 5' integration site, (D) 3' integration site, or (E) 3' integration site after negative selection. Colored arrows indicate the primers used for each diagnostic PCR as depicted in the scheme (A). *Pb*$_{LISP2}$Ago2 1 is a single clone obtained by limiting dilution after positive selection, which was subsequently negatively selected, yielding *Pb*$_{LISP2}$Ago2 1.1. WT: *Pb*GFPcon. Ø: No-template control.

Vera Mitesser also tested the expression of Ago2 in blood stages via Western blotting and in liver stages via immunofluorescence staining. As predicted from the activity of the *LISP2* promoter, no Ago2 could be detected in schizont-enriched blood stages (Figure 41 A), in contrast to a clear signal in the liver stages (Figure 41 B). *Pb*$_{LISP2}$Ago2 should thus allow the targeting of gene specifically at the liver stage.

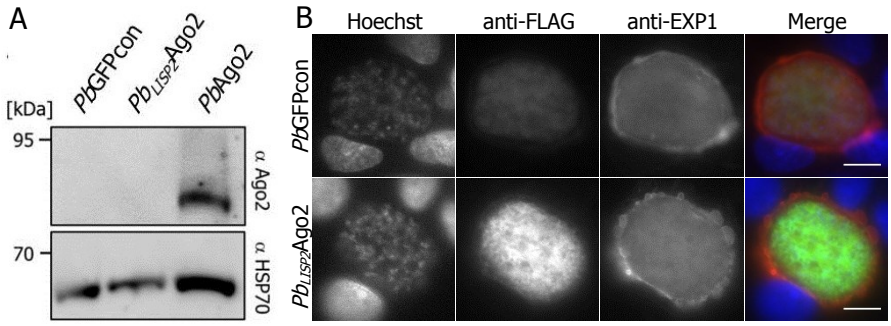

FIGURE 41: **Expression of Ago2 in *Pb*$_{LISP2}$Ago2.** (A) Western blotting analysis of schizont-enriched samples of *Pb*GFPcon, *Pb*$_{LISP2}$Ago2, and *Pb*Ago2. Western blots were probed with an antibody against hAgo2 (upper blot) or HSP70 (lower blot). (B) Immunofluorescence staining of liver stages 48 h after infection of HuH7 cells with either *Pb*GFPcon or *Pb*$_{LISP2}$Ago2. Liver stages were stained with Hoechst for DNA (first column), an antibody against the FLAG tag of Ago2 (second column) or an antibody against the PVM protein EXP1 (third column). One representative image of ten per condition is shown. Pictures were taken with same settings with a widefield fluorescence microscope and are all processed alike. The scale bars indicate 10 µm.

3.8.2 CHARACTERIZATION OF *PB*$_{LISP2}$AGO2

Constitutive expression of Ago2 in *P. berghei* has an adverse effect on blood-stage growth and mosquito infectivity, but apparently does not negatively impact liver stage development of the parasites (see Section 3.2.3). We thus hypothesized that limiting the expression of Ago2 to this particular stage of the life cycle would result in parasites whose growth is comparable to that of wild type parasites.

To test this, Vera Mitesser injected equal amounts of iRBC of *Pb*$_{LISP2}$Ago2 and *Pb*GFPcon into C57BL/6J mice and followed the blood stage growth (Figure 42 A, B). Indeed, she observed that both lines had a comparable growth, and both *Pb*GFPcon, as well as *Pb*$_{LISP2}$Ago2-infected mice, succumbed to ECM between 7 to 11 days post-infection. We also infected mosquitoes with *Pb*GFPcon- or *Pb*$_{LISP2}$Ago2 and assessed oocyst prevalence as well as sporozoite numbers. Importantly, we found that *Pb*$_{LISP2}$Ago2 infects mosquitoes at the same rate as *Pb*GFPcon, both in the midgut and in the salivary glands (Figure 42 C, D). When we subsequently infected HuH7 cells *in vitro* with sporozoites and quantified the number and size of liver stages 48 h post-infection, we detected no difference in liver stage infectivity or intrahepatic development between the two lines (Figure 42 E, F). Congruent with these findings, also the intravenous infection of C57BL/6 mice with sporozoites of either *Pb*GFPcon or *Pb*$_{LISP2}$Ago2 yielded comparable blood-stage growth and the majority of infected mice in both groups succumbed to ECM around seven days post-infection (Figure 42 G, H). In summary, liver-stage-restricted expression of Ago2 does not affect the growth of *P. berghei*.

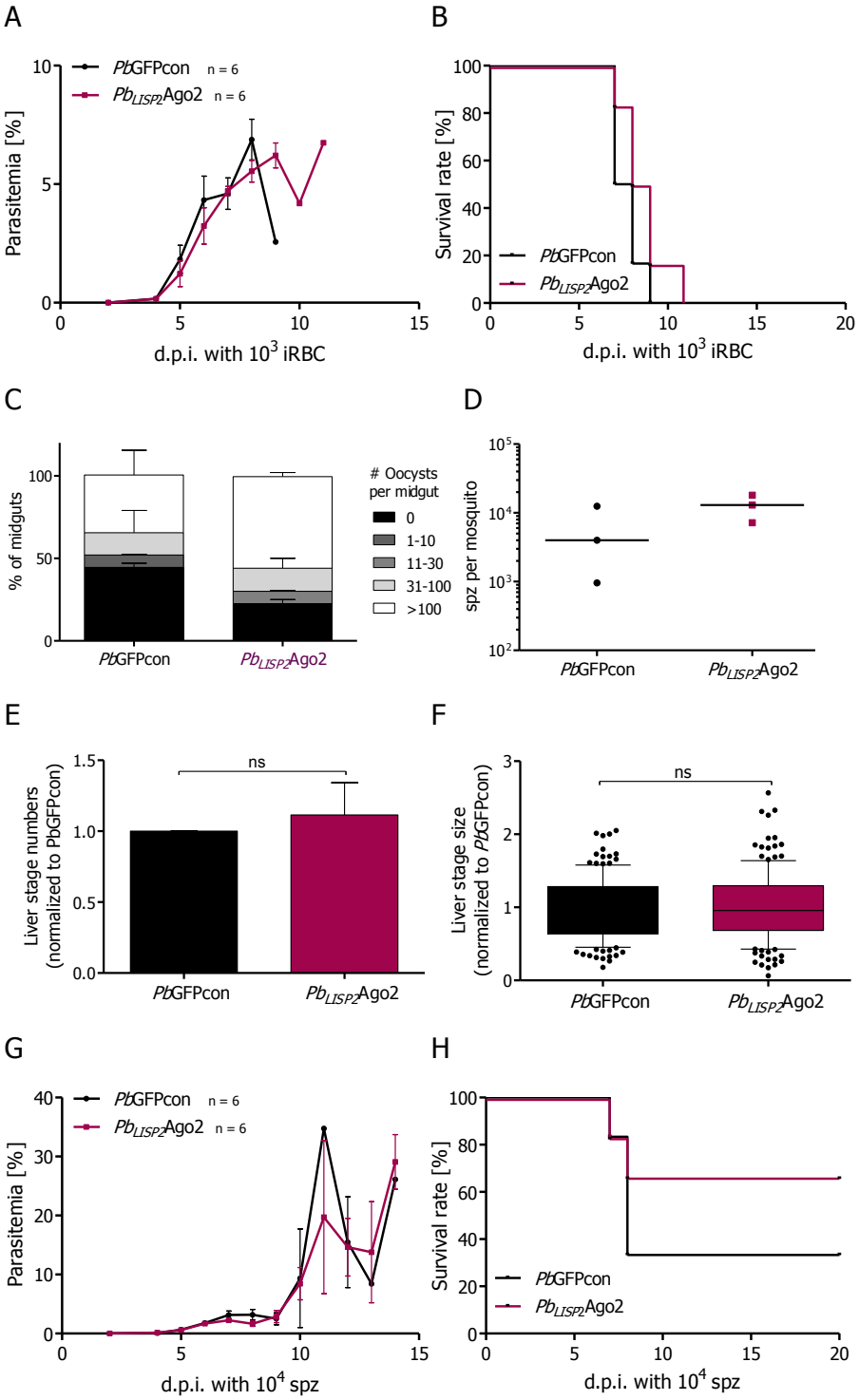

FIGURE 42: **Characterization of *Pb*$_{LISP2}$Ago2.** (A, B) Blood-stage growth. C57BL/6J mice were i.v. infected with 10^3 iRBC of *Pb*GFPcon or *Pb*$_{LISP2}$Ago2. (A) Parasitemia and (B) survival of mice were monitored over 14 and 20 days, respectively. (C, D) Mosquito infectivity. Mosquitoes were allowed to feed on *Pb*GFPcon- or *Pb*$_{LISP2}$Ago2-infected mice. (C) Oocyst numbers were scored in dissected midguts on day 10 to 14 post-infection. (D) Salivary gland sporozoite numbers were quantified at day 18 post feeding. (E, F) Liver stage development. HuH7 cells were infected with *Pb*GFPcon- or *Pb*$_{LISP2}$Ago2-sporozoites and liver stages were fixed 48 h post-invasion to determine (E) average numbers and (F) sizes of liver stages. Values are normalized to *Pb*GFPcon and result from three independent experiments. (G, H) Sporozoite-induced growth. C57BL/6J mice were i.v. infected with 10^3 spz of *Pb*GFPcon or *Pb*$_{LISP2}$Ago2. (G) Parasitemia and (H) survival of mice were monitored over 14 and 20 days, respectively.

3.8.3 INTEGRATION OF AGOSHRNAS INTO *PB*$_{LISP2}$AGO2

Restricting Ago2-expression to the liver should permit gene silencing in this stage only. As expression is unaffected in blood stages, this strategy would be of particular interest for blood-stage essential genes. To test the hypothesis that AgoshRNA expression in *Pb*$_{LISP2}$Ago2 silences gene expression only in the liver, we stably integrated expression cassettes for AgoshRscr (as a negative control) or AgoshR-αGFP2c into the genome. Thereby, any reduction of GFP levels across the life cycle, in particular in the liver stage, can be monitored using established assays.

Vera Mitesser generated the line Pb$_{LISP2}$*Ago2.scr, the others were produced by me.*

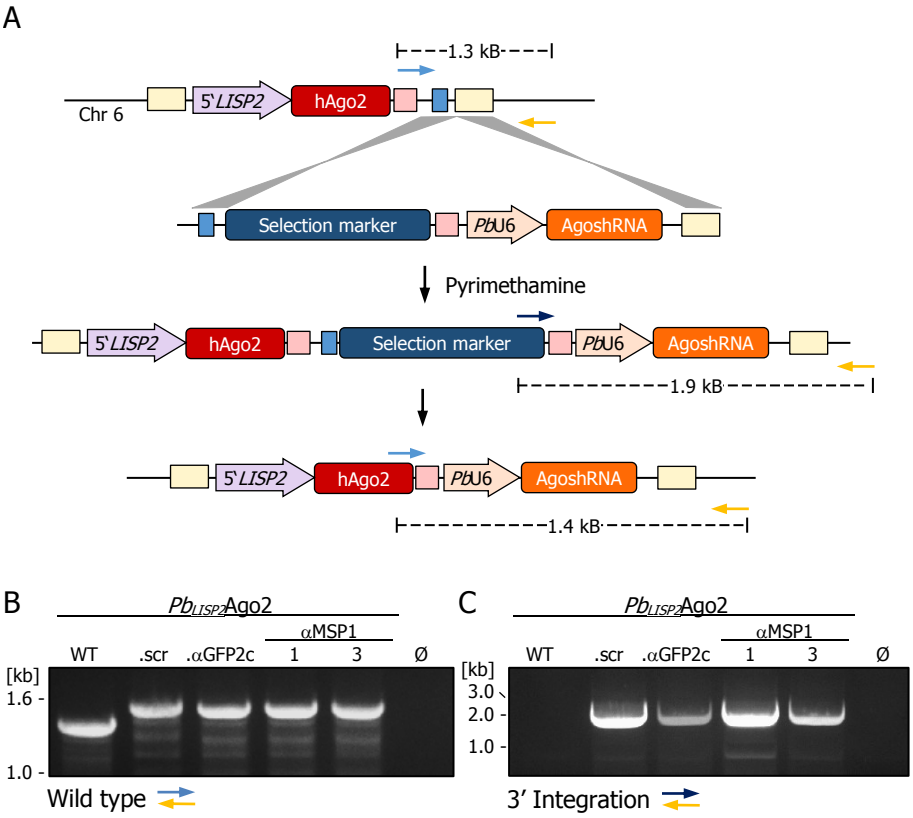

FIGURE 43: **Integration of AgoshRNAs in *Pb*$_{LISP2}$Ago2.** (A) Integration strategy. The strategy resembles the initial approach to integrate AgoshRNAs behind the Ago2 locus (depicted in Figure 29). Parasites use the 3' UTR of the selection cassette and the homology region of the SIL6 to integrate the selection marker along with the AgoshRNA cassette. Parasites can still recycle the selection marker, using the 3'UTR of the Ago2 cassette for recombination. (B, C) Diagnostic PCR of the clonal lines of *Pb*$_{LISP2}$Ago2.scr, *Pb*$_{LISP2}$Ago2.αGFP2c, *Pb*$_{LISP2}$Ago2.αMSP1 1, and *Pb*$_{LISP2}$Ago2.αMSP1 3. *Pb*$_{LISP2}$Ago2 (WT, first lane) served as a control for the parental line. Ø: No-template control. Colored arrows indicate the location of the respective primer pairs used for amplification in (A). (B) PCR amplifying the parental locus which yields the expected amplicon of 1.3 kb in the case of for *Pb*$_{LISP2}$Ago2. For the clones with the AgoshRNA integration, the higher amplicon of 1.4 kB indicates a subpopulation that has recycled the selection marker. (C) PCR amplifying the 3' integration site, yielding an expected amplicon length of 1.9 kb.

In parallel, we also aimed to integrate three AgoshRNAs targeting the cross-stage antigen merozoite surface protein 1 (MSP1). This protein is essential in blood stages, where it is required for the egress of the merozoites from the schizonts[308]. However, a conditional deletion of MSP1 in liver stages using the FLP/frt system demonstrated that MSP1 is additionally necessary for late liver stage development. Ablation of MSP1 in this stage results in aberrant merozoite formation, incomplete segmentation and an developmental arrest in the liver[85]. We intended to reproduce this phenotype by silencing MSP1 expression using AgoshRNAs.

As the initial vectors for integration of AgoshRNAs into *Pb*Ago2 were inefficient (see Section 3.5.1), Vera Mitesser improved the vector design. The new strategy, depicted in Figure 43 A, avoided the unwanted integration of the selection marker only, while still permitting its removal by negative selection. This strategy improved the efficiency of full integration, and we obtained transgenic parasites for all AgoshRNAs. Limiting dilution yielded single clones for *Pb*$_{LISP2}$Ago2.scr, *Pb*$_{LISP2}$Ago2.αGFP2c, *Pb*$_{LISP2}$Ago2.αMSP1 1 and *Pb*$_{LISP2}$Ago2.αMSP1 3 (Figure 43 B, C). No clones were obtained for *Pb*$_{LISP2}$Ago2.αMSP1 2. As the diagnostic PCR of the parental population revealed that a subpopulation had integrated the AgoshRNA cassette (data not shown), it is safe to assume that limiting dilution in a larger cohort of mice would also yield a single clone of this line. It is interesting to note that for all lines, a proportion of the parasites already underwent the recombination event that leads to recycling of the resistance cassette (evidenced by the higher band visible in the diagnostic PCR amplifying the wild type locus). Sequencing of the locus confirmed correct AgoshRNA integration for all lines.

3.8.4 KNOCKDOWN OF GFP IN *PB*$_{LISP2}$AGO2.αGFP2C

To test if *Pb*$_{LISP2}$Ago2 is indeed capable of mediating RNAi exclusively in liver stages, I compared the GFP expression of *Pb*$_{LISP2}$Ago2.αGFP2c to that to *Pb*$_{LISP2}$Ago2.scr. Even though the expression of Ago2 should be restricted to the late liver stage of *Pb*$_{LISP2}$Ago2, a leaky promoter might lead to Ago2 expression in other stages, which could induce RNAi-mediated GFP knockdown. Therefore, I analyzed the GFP fluorescence of *Pb*$_{LISP2}$Ago2.αGFP2c and *Pb*$_{LISP2}$Ago2.scr not only in liver stages, but across the whole life cycle. The following data is obtained from a single biological replicate and should thus be treated as preliminary data from a pilot experiment.

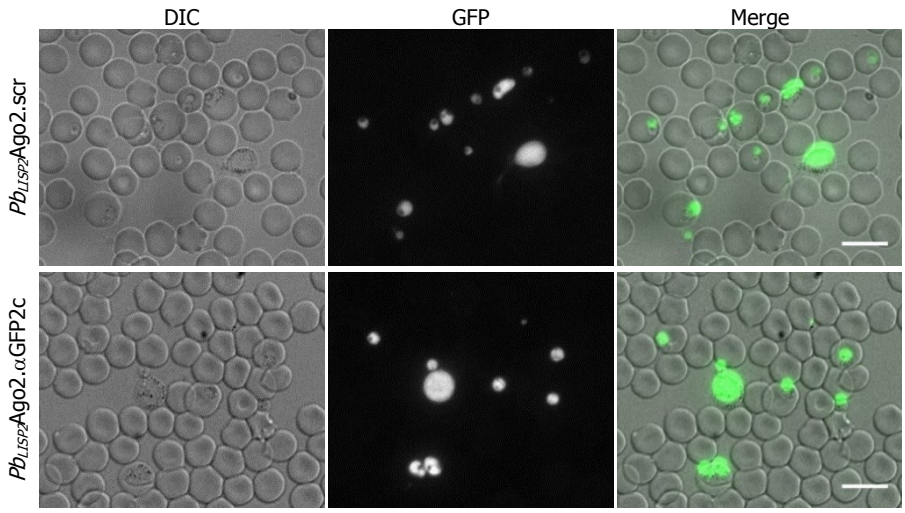

FIGURE 44: **GFP fluorescence of blood stages.** Blood stage parasites of *Pb*$_{LISP2}$Ago2.scr or *Pb*$_{LISP2}$Ago2.αGFP2c were imaged with a fluorescence microscope with equal settings. Images were processed alike. Shown are representative images of at least 10 per strain. The scale bars indicate 10 µm.

In blood stages, Ago2 levels were below the detection limit of a Western blot (see Figure 41) but very low amounts might be sufficient to mediate target knockdown. However, in mixed blood stages, there was no difference in GFP expression between *Pb*$_{LISP2}$Ago2.scr and *Pb*$_{LISP2}$Ago2.αGFP2c (Figure 45). Ring stages, early and late trophozoites and gametocytes showed comparable fluorescence intensity independent of the AgoshRNA expressed, indicating no RNAi activity. When transmitting both lines to mosquitoes and imaging oocysts 13 days later, I found that also in this life cycle stage, the GFP expression is not affected by the expression of the αGFP-AgoshR2c (Figure 45 A, B).

Interestingly, when imaging salivary gland sporozoites at day 17 after infectious blood meal, I found a small, but significant reduction of GFP in *Pb*$_{LISP2}$Ago2.αGFP2c (Figure 45 C, D). This is a unexpected finding, considering that the *LISP2* promoter should not be active at that stage[307,309]. Compared to the fully RNAi-competent *Pb*Ago2.αGFP2c, the RNAi activity of *Pb*$_{LISP2}$Ago2 is, however, minor. While GFP was reduced to about 17 % in the fully RNAi-competent *Pb*Ago2.αGFP2c (Figure 33 C, D), the knockdown in *Pb*$_{LISP2}$Ago2.αGFP2c is much weaker, with a remaining 85 % of GFP fluorescence. In order to exclude the possibility that the detected difference in GFP fluorescence is due to technical variations, the experiment should be repeated with an independent set of sporozoites.

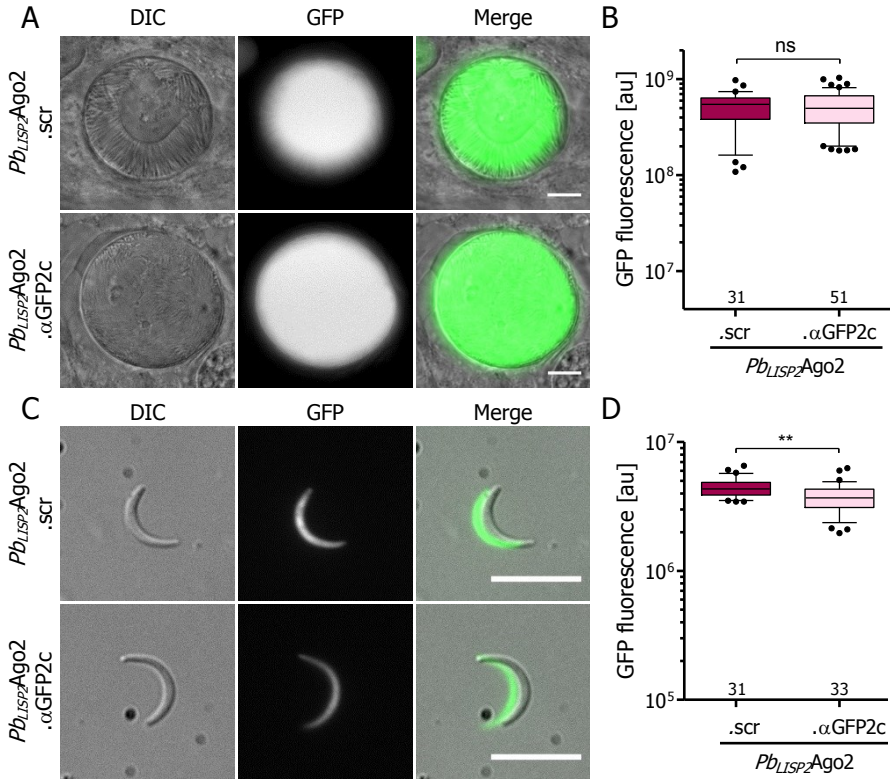

FIGURE 45: **Knockdown of GFP in *Pb*$_{LISP2}$Ago2.** Mosquitoes were fed on *Pb*$_{LISP2}$Ago2.scr- or *Pb*$_{LISP2}$Ago2.αGFP2c-infected mice. (A) Midgut oocysts (day 13 post feeding) and (C) salivary gland sporozoites (day 17 post feeding) were imaged with a wide-field microscope. Shown are representative pictures of *Pb*$_{LISP2}$Ago2.scr and *Pb*$_{LISP2}$Ago2.αGFP2c. The scale bar indicates 10 µm. The GFP fluorescence of (B) oocysts and (D) sporozoites was quantified using ImageJ and is here depicted as whiskers plot with 10-90 percentile. The numbers below the bars indicate the total number of individual parasites quantified. Statistics: Student's T-test. ns: not significant; *** $p<0.001$. Note that these data are obtained from a single experiment only, and need to be validated in biological replicates.

To assess a possible GFP knockdown in liver stages, HuH7 cells were infected with sporozoites of *Pb*$_{LISP2}$Ago2.scr or *Pb*$_{LISP2}$Ago2.αGFP2c. The *LISP2* promoter is reported to be active in late liver stages from around 36 h to 65 h post-infection, with a peak at 48 h[310]. In order to evaluate whether a potential knockdown of GFP may differ during intrahepatic development, *Pb*$_{LISP2}$Ago2 liver stages were thus fixed at 24 h, 48 h and 65 h post-infection. After immunofluorescence staining, the GFP signal of individual *Pb*$_{LISP2}$Ago2.αGFP2c was quantified and normalized to that of *Pb*$_{LISP2}$Ago2.scr (Figure 46).

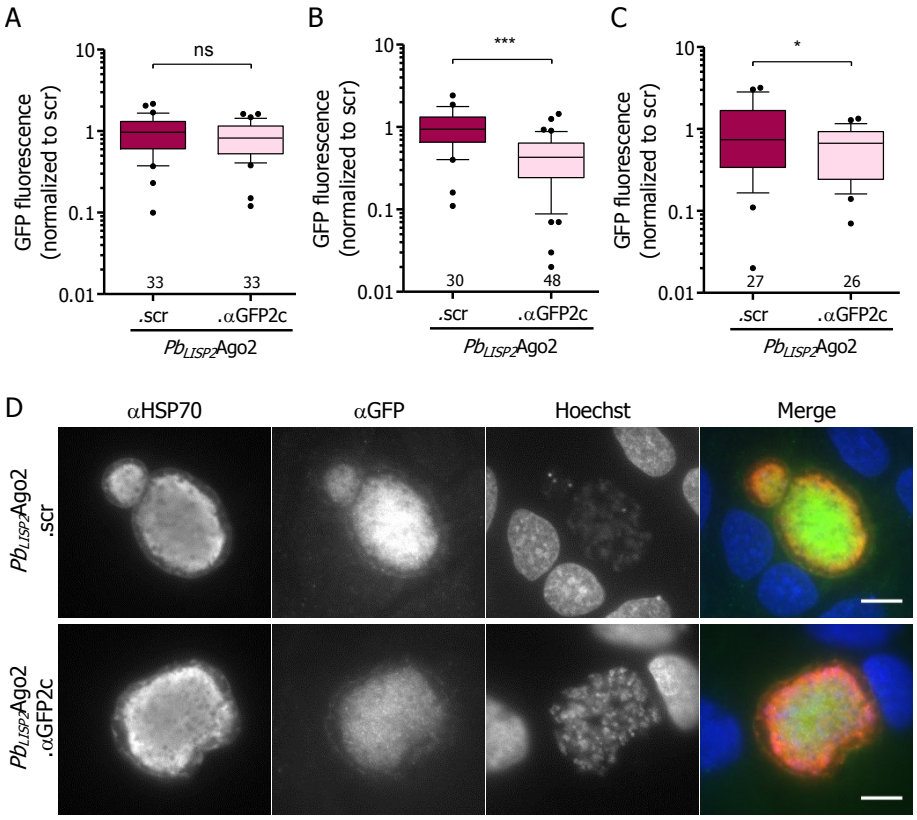

FIGURE 46: **Knockdown of GFP in liver stages of *Pb*$_{LISP}$Ago2.** Liver stages of *Pb*$_{LISP2}$Ago2.scr and *Pb*$_{LISP2}$Ago2.αGFP2c were fixed at various time points post-invasion and stained with antibodies against HSP70 and GFP. The GFP signal of immunostained liver stages at (A) 24 h, (B) 48 h, and (C) 65 h post-infection was quantified using ImageJ, and normalized to the mean signal intensity of *Pb*Ago2.scr liver stages to control for different staining efficiencies. The number below the bars indicate the total number of individual parasites quantified. Statistics: Student's T-test. *** $p<0.001$; * $p<0.05$. Note that these data are obtained from a single experiment only, and need to be validated in biological replicates. (D) Representative images of a liver stage at 48 h post-infection. All pictures were taken with a wide-field microscope with same settings and processed alike. The scale bars indicate 10 µm.

At an early time point, 24 h post-infection, the GFP fluorescence did not differ between the two transgenic lines, indicating no activity of Ago2 (Figure 45 A). In contrast, at a later time point (48 h post-infection), the GFP signal of *Pb*$_{LISP2}$Ago2.αGFP2c parasites dropped significantly compared to parasites expressing the scrambled AgoshRNA (Figure 45 B). The GFP fluorescence of *Pb*$_{LISP2}$Ago2.αGFP2c is still reduced 65 h post-infection, albeit to a lesser extent (Figure 45 C). Importantly, the observed knockdown pattern coincided with the reported expression pattern of the LISP2 promoter, peaking at 48 h post-infection[310]. In conclusion, the data of the pilot experiment supports that *Pb*$_{LISP2}$Ago2 is capable of eliciting a stage-specific knockdown in late liver stages. It will be interesting to see if such a knockdown also holds true for the endogenous gene MSP1.

Discussion

4

"When you study science, and especially these realms of the biology [...], what's clear is that every time you find out something, that brings up ten new questions, and half of those are better questions than you started with."[311]

~ Robert Sapolsky (born 1957)

4.1 *Pb*AGO2 AS A TOOL TO STUDY GENE FUNCTION

Despite years of research, Malaria continues to be a devastating infectious disease. *Plasmodium* parasites, belonging to the phylum Apicomplexa, are evolutionarily very distant from humans, and thus encode a great variety of genes that have no homologs in humans or other non-apicomplexan organisms. These "orphan" genes, about 60 % of all *Plasmodium* genes[55], are promising drug targets, as specific inhibitors of their encoded proteins should not cause unintended side effects in humans. On the downside, the lack of homology to known genes renders the functional annotation of these orphan genes difficult, although such a characterization is of utmost importance to develop efficient drugs. To overcome this obstacle, a variety of different genetic tools have been developed to study gene function in *Plasmodium*. As summarized in , all of these technologies have different advantages and disadvantages.

For genes that are not essential for blood-stage development, deletion by a classical gene knockout[62] is still the most straightforward approach to assess the gene function. In *P. falciparum*, the efficiency has been greatly increased with the use of CRISPR/Cas9 technology[73,72]. Recombinases that are either inducible[79,82] or stage-specifically expressed[85] permit a temporarily controlled knockout. However, gene knockouts are limited to genes that are not essential for blood stages, and the complete ablation of gene expression prevents the investigation of intermediate phenotypes. To study blood-stage essential genes, several inducible systems have been established, among them the regulation of gene expression by the Tet-OFF system in *P. berghei*[92], the inducible degradation of mRNA by the glmS-ribozyme[103] or the degradation of proteins by fusion to a destabilization domain[110,111,117]. These systems all require the addition of a small molecule to regulate gene expression, which is prone to causing unwanted side effects. Also, success seems to be gene-dependent. In particular, degron-mediated protein degradation can only be used for proteins that tolerate C-terminal tagging. While varying the amounts of inducer allows, in principle, for tunability, the dynamic range is limited[57]. Most importantly, however, these technologies are mainly restricted to *P. falciparum* or *P. berghei* blood stages.

TABLE 1: ADVANTAGES AND DISADVANTAGES OF DIFFERENT GENETIC TOOLS.

Technology	Advantages	Limitations
Gene knockout by double crossover	• Full depletion of the GOI, no residual protein • With PlasmoGEM vectors quite efficient in *P. berghei* • In *P. falciparum*, efficiency can be improved by using CRISPR/Cas9 technology	• Laborious in *P. falciparum* • Only for genes not essential for blood-stages • Not tunable, not inducible • Constitutive/long-term expression of Cas9 impedes with parasite growth
Recombinase-mediated gene knockout	• Full depletion of the GOI, no residual protein • Stage-specific knockout in *P. berghei* by controlling the expression of the recombinase • DiCre system is inducible	• Requires the modificaton of the GOI at the 3' and 5' UTR, which can be laborious • The DiCre system is not available for *P. berghei* • Not tunable
Tet-controlled gene expression	• Inducible knockdown of gene expression • Requires only the modification of the 5'UTR of the GOI • Reversible, tunable to some extent by varying the amount of the inducer	• No full knockout, residual protein left • Limited to *P. berghei* blood stages, only one report for liver stages • Addition of the inducer might have unwanted side-effects
glmS-System	• Rapid and inducible degradation of mRNA • Requires only the modification of the 3'UTR of the GOI • Reversible, tunable to some extent by varying the amount of the inducer	• Limited to *P.falciparum* blood stages • Success is gene dependent • Limited dynamic range, residual protein might confound phenotypic analysis • Glc-6P is toxic in high concentrations
Degron-mediated protein degradation	• AID for *P. berghei*, DD or DDD system for *P. falciparum* • Rapid, inducible degradation of protein • Requires only the modification of the 3'UTR of the GOI • Reversible, tunable to some extent by adding various amounts of the stabilizer	• Limited to blood stages • Success is gene-dependent and only possible for proteins that tolerate C-terminal tagging • Limited dynamic range, residual protein might confound phenotypic analysis • Addition of the stabilizer might have unwanted side-effects
***Pb*Ago2**	• Gene knockdown does not require a genetic modification of the locus of the GOI • Does not require the addition of a small molecule • Gene knockdown in the complete life cycle or stage-specific • Different AgoshRNAs allow tuning of gene expression • Multiplexing of AgoshRNAs could be used to target several genes in parallel • Potentially allows high-throughput screens	• Efficiency of AgoshRNAs cannot yet be predicted before testing • Dynamic range of the knockdown is gene-dependent, residual protein might confound phenotypic analysis • Potential for off-targets • Ago2 influences *Plasmodium* mosquito development • Not yet available for *P. falciparum*

In this work, I successfully developed a new genetic tool by engineering RNAi into the rodent malaria parasite *P. berghei.* This novel technology for the first time permits a knockdown of genes throughout the whole life cycle of *Plasmodium*, as demonstrated by the efficient silencing of GFP in all stages of *Pb*Ago2.αGFP2c (see Section 3.5.3). In contrast to almost all technologies that are currently available, AgoshRNA-mediated gene silencing does not require the modification of the genetic locus of the GOI, a task that is often fairly laborious due to the high AT-content of the *Plasmodium* genome[312]. Instead, the transfection of AgoshRNA expression vectors, either for episomal expression or stable integration, is sufficient to target a GOI, greatly facilitating the application of the technology. The present work indicates a high efficiency of AgoshRNA-mediated knockdown, as 80 % of all tested AgoshRNAs yielded a significant reduction of target gene expression. As demonstrated in Section 3.3.2 for GFP, the level of gene knockdown can be tuned using different AgoshRNAs. Additionally, the timing of gene silencing is flexible and can be readily modulated by controlling the expression of Ago2. As *proof-of-principle*, I developed in this work the parasite line Pb_{LISP2}Ago2, which permitted to restrict the silencing of GFP expression to late liver stages (see Section 3.8).

The unique ability to modulate gene expression in a specific stage only, in combination with the facile application of the technology, distinguishes *Pb*Ago2 from all currently available genetic tools for *Plasmodium*. In addition, AgoshRNA-mediated knockdown can be easily adapted to a variety of different purposes as discussed below, rendering it a very versatile genetic tool.

The most straightforward application of *Pb*Ago2 is the knockdown of a single target gene by expressing an corresponding AgoshRNA (Figure 47 B). The efficiency of the AgoshRNA-mediated knockdown of a GOI depends on several factors. In the initial cell culture screen in this work, it became apparent that AgoshRNAs tend to be less efficient than shRNAs (2-fold knockdown versus around 10-fold knockdown in HEK293T cells, see Figure 10). Also others report that AgoshRNAs are less effective than matching shRNAs with the same sequence[236]. This observation may reflect a lack of knowledge regarding the optimal structural requirements for Dicer-independent AgoshRNA processing. Alternatively, Ago2-dependent processing of AgoshRNAs might be inherently less efficient than the canonical processing of miRNAs or shRNAs, which in turn limits the strength of the gene silencing. While the reduced activity of AgoshRNAs may seem disadvantageous for gene silencing, it is compensated by the observation that the potency of AgoshRNAs is increased in the absence of Dicer and endogenous miRNAs (see Figure 13)[235]. Indeed, AgoshRNAs were more efficient in *Plasmodium* than *in vitro*. While only one out of four αGFP-AgoshRNAs diminished GFP fluorescence in RNAi-competent cells, and only by about 50 %, all four AgoshRNAs significantly reduced GFP fluorescence in *P. berghei* blood stages by 5- to 40-fold (see Figure 25).

The discrepancy of the knockdown efficiency in RNAi-competent cells versus *Plasmodium* could be explained by competition between AgoshRNAs and endogenous miRNAs for Ago2 processing. As a result, in the absence of miRNAs, AgoshRNA-mediated gene silencing is more efficient. It has also been suggested that in RNAi-competent cells, AgoshRNAs are alternatively loaded into Dicer and thereby sequestered from Ago2[235]. In addition, Ago2, as well as the AgoshRNAs, were expressed from different promoters in cell culture and in *Plasmodium*, yielding distinct expression levels of these factors which complicate a direct comparison of the two systems.

The target gene itself also influences the efficiency of the knockdown. While I could achieve a potent knockdown of GFP and of PPLP2 (see Sections 3.3 and 3.4), the expression of EXP1 could only be reduced by roughly 50 % (see Section 3.6). According to published and our own RNA-Seq data, the expression of EXP1 is about 10- to 100-fold higher than that of PPLP2 and the *EF-1α*-promoter driven GFP[313]. Thus, it seems that in *Pb*Ago2, highly expressed targets are more difficult to silence. While it appears intuitive that RNAi efficiency decreases with higher target mRNA concentrations, several studies report the opposite. Experimental findings suggest that siRNA-mediated silencing of a GOI is more efficient in cells expressing a high amount of the target than in cells that express relatively low amounts of target mRNA[314,315]. This observation is further supported by a recent model suggesting that RNAi becomes more efficient with increasing target concentration due to more efficient loading of Ago2, and only very high target mRNA levels will reduce the strength of the gene silencing[316]. Yet, is important to note that these observations are based on siRNA-mediated silencing. In the case of AgoshRNA-mediated gene silencing, the rate-limiting step might not be the release of the cleaved target (as has been suggested for siRNA-mediated knockdown[316]), but the cleavage and processing of the AgoshRNA itself. It is tempting to speculate that in case of the EXP1 silencing, the RNAi machinery of *Pb*Ago2 might have already reached a point of saturation. Also other factors should be considered, such as target mRNA turnover, which negatively correlates with RNAi efficiency[317].

Depending on the targeted GOI, its expression strength and mRNA turnover, it will be necessary to screen several AgoshRNAs to find one that mediates efficient knockdown. In this respect, AgoshRNA-mediated RNAi in *Pb*Ago2 is comparable to canonical RNAi in other cells. As the efficiency of a given shRNA cannot be predicted, also fully RNAi-competent cells require the screening of several shRNAs in order to identify one that is sufficiently potent[318]. The benefit of implementing well-established technology into *Plasmodium* is that the knowledge gathered in years of RNAi research can now be easily transferred to *Pb*Ago2, to further improve the power and breadth of this tool. For conventional RNAi, a variety of software exists to design shRNAs and to predict off-targets *in silico*[318]. It would be of great assistance if such tools were developed for AgoshRNA-mediated knockdown as well and likewise in a freely accessible manner. Such a program would not only facilitate the targeting

of a GOI but also permit to *in silico* predict off-targets and test them experimentally.

Despite the current absence of such a software tool, eight out of ten AgoshRNAs that I designed manually significantly reduced target expression in this study, albeit to varying extents. It is thus safe to conclude that AgoshRNA-mediated gene knockdown can be efficient in *Pb*Ago2, and that the chances of identifying robust AgoshRNAs are high. Based on the experience gathered throughout this work, I recommend to directly test three to four different AgoshRNAs against a GOI in *Plasmodium* (since pre-screens *in vitro* might not be fully predictive, see above), and consider it likely that at least one of them silences the gene efficiently.

For this purpose, the results of this work suggest that there are at least two possibilities. One is to express AgoshRNAs in *Pb*Ago2 from episomal vectors, which provides a rapid way of screening several AgoshRNAs in parallel. Alternatively, for a more comprehensive phenotypic analysis, stable integration of the AgoshRNA expression cassette is recommended to avoid heterogeneous populations that arise from parasites carrying different plasmid copy numbers. Additionally, especially for targets whose silencing affects parasite growth, parasites that have spontaneously acquired pyrimethamine resistance are likely to outgrow the population that carries the episome. Last but not least, stable integration of AgoshRNAs allows to address the phenotype of the knockdown across all stages of the life cycle.

The minimal RNAi machinery also allows, for the first time, a targeted gene silencing exclusively in a single life cycle stage by controlling the expression of Ago2 (Figure 47 A). In this work, we have already demonstrated with the line Pb_{LISP2}Ago2 that it is possible to restrict the expression of Ago2 to late liver stages. Consequently, expression of a GFP-specific AgoshRNA in this line silenced GFP expression in late liver stages only (see Figure 46). The only other technology that enables a stage-specific modulation of gene expression is a recombinase-mediated gene knockout in which FLP is expressed under a stage-specific promoter. In contrast to Pb_{LISP2}Ago2, where all parasites express Ago2 in the liver stage and thus gene expression is silenced to the same extent in the whole population, the liver-stage-specific FLP/frt system yields a somewhat heterogenous population, as around 10 % of the parasites do not excise the GOI as intended[319].

Intriguingly, the GFP knockdown induced by the αGFP-AgoshR2c in 48 h liver stages of Pb_{LISP2}Ago2 was weaker than the one of *Pb*Ago2 (50 % versus 20 % remaining GFP fluorescence). These two lines differ only in the promoter driving Ago2. While – to my knowledge – no publications exist that directly compare the *LISP2* promoter to the *HSP70* promoter, their relative strength can be indirectly inferred. The *LISP2* promoter is reported to be about 3-fold more active in late liver stages than the *EF-1α* promoter[307], while the *HSP70*

promoter is 10-fold stronger than the *EF-1α* promoter[280]. Taken together, this implies that the *HSP70* promoter is approximately 3-fold stronger than the *LISP2* promoter. Notably, this difference in promoter activity correlates reasonably well with the about 2.5-fold higher knockdown efficiency in *Pb*Ago2 versus Pb_{LISP2}Ago2. This suggests that in the liver stage, the level of Ago2 protein is the limiting factor for gene knockdown in *Plasmodium*. This is highly reminiscent of mammalian cells where it has also been reported that Ago2 expression limits RNAi efficiency, and that exogenous overexpression of Ago2 improves RNAi-mediated knockdown *in vitro* and *in vivo*[320].

These results suggest that the liver-stage-restricted knockdown could be enhanced by using a stronger, but still liver-stage-specific promoter. An elegant strategy that would allow rapid, liver-stage-exclusive expression of Ago2 would be the use of the regulatory sequences of UIS4. UIS4 is transcribed in sporozoites, but remains translationally repressed by the Pumilio protein Puf2[321]. Upon initiation of the liver stage development, the repression is relieved and high levels of UIS4 protein are detected from early (5 h) to late (48 h) liver stages[322]. It has been suggested, albeit not experimentally validated, that a short, 8-nt-long motif in the open reading frame of UIS4 serves as Puf2-binding signal[321]. If this holds true, the expression of Ago2 under the UIS4 promoter along with the integration of this putative Puf2-binding site into the mRNA sequence should allow for a rapid expression of Ago2, and thus gene silencing, only in liver stages.

A stage-specific knockdown is of course not only limited to late liver stages. Using different promoters, one could generate new lines that exhibit a specific pattern of Ago2 expression in one or several *Plasmodium* stages. For example, driving Ago2 by the promoter of the *TRAP* gene, which is active in mosquito stages, could be used to silence genes specifically in sporozoites and early liver stages. As the integration into SIL6 using the published vectors[279] proved to be facile, such a tool box encompassing a variety of different *Pb*Ago2 lines should be easy to generate.

Gene knockdown is readily achieved in *Pb*Ago2 and merely requires the expression of a short RNA molecule. Therefore, the parallel silencing of multiple genes should be achievable by co-expressing several AgoshRNAs (Figure 47 C). Such a multiplexed gene silencing could help to dissect complex pathways in which several proteins have redundant functions. It was shown, for example, that the gametocyte-specific proteins P25 and P28 are individually dispensable, but the double knockout has a severe developmental arrest at the ookinete/oocyst stage[323]. Moreover, for targets that are difficult to silence with a single AgoshRNA, the expression of multiple different AgoshRNAs could be an alternative to improve the knockdown.

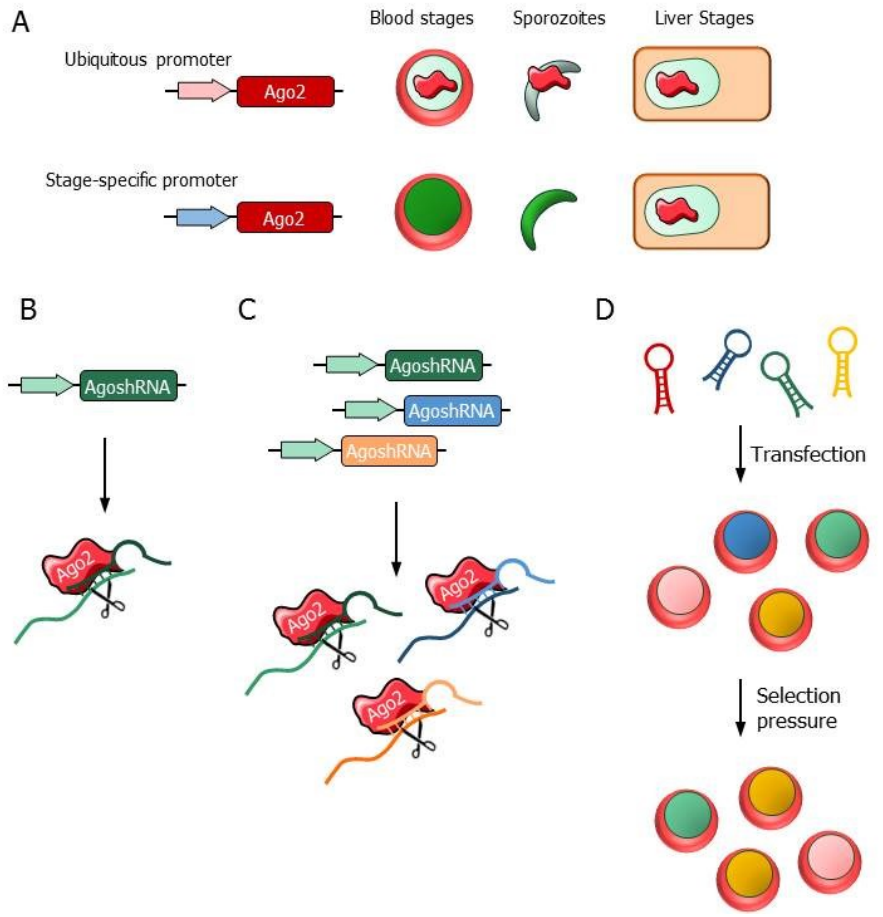

FIGURE 47: ***Pb*Ago2 as a tool to study gene function**. (A) If Ago2 is expressed from a ubiquitous promoter, the target gene can be silenced across the whole life cycle, as indicated here by a reduced green fluorescence. Stage-specific expression of Ago2 is predicted to yield a stage-specific gene silencing (here exemplified in the liver). (B) A single AgoshRNA can be expressed from an episome or a stably integrated cassette in *Pb*Ago2 and induce target gene silencing. Different AgoshRNAs allow fine-tuning of gene expression. (C) Expression of multiple AgoshRNAs within one parasite should allow the silencing of multiple target genes in parallel. (D) A library of AgoshRNA expression vectors could be transfected into *Pb*Ago2 to perform an RNAi screen. The pool of transfectants, each with a different gene silenced, can then be put under a selection pressure of interest. AgoshRNAs that are lost from the pool after selection likely silence a gene the parasite needs to survive the selection.

Instead of having to perform sequential genetic modifications, *e.g.* gene knockouts on multiple genes, several expression cassettes encoding multiple AgoshRNAs could be introduced into *Pb*Ago2 in a single step. As the repeated use of the *Pb*U6 promoter sequence could lead to unwanted recombination events, it would be helpful to identify further Pol III promoters in *Plasmodium* to drive the expression of additional AgoshRNAs. Multiplexing also requires that Ago2 is not saturated by the expression of a single AgoshRNA and that the concurrent expression of multiple AgoshRNAs does not compromise their knockdown potency. If Ago2 is already saturated by a single AgoshRNA expressed from the *Pb*U6 promoter (as it appears to be the case in Pb_{LISP2}Ago2 liver stages, see above), a higher expression of Ago2 is required for efficient multiplexing. Still, multiplexed RNAi-mediated gene knockdown has been successfully employed before in mammalian cells, *e. g.* to simultaneously target

two subunits of a protein[324]. Considering that no other genetic tools for *Plasmodium* allow simultaneous targeting of several genes at once, AgoshRNA multiplexing in *Pb*Ago2 is clearly an attractive option to explore in the future.

Finally, the fact that gene targeting is determined solely by a short nucleotide sequence might ultimately enable another technology that has so far been inapplicable in *Plasmodium*: RNAi screens (Figure 47 D). This requires the generation of a library of AgoshRNAs which covers a gene family of interest or even the whole genome. This library would need to be transfected as a pool into *Pb*Ago2. By comparing the AgoshRNAs present in the parasite population before and after applying a selection pressure (*e.g.* cycling through the mosquito), genes that are important for this selection can be identified, as AgoshRNAs targeting these genes should be lost in the process. Next generation sequencing (NGS) would be the easiest way to quantify the AgoshRNAs in the parasite population, as the sequence of the AgoshRNA itself could serve as a barcode. Akin to what has been done in the genome-wide knockout screen of the PlasmoGEM project[65], NGS could also be used to directly determine relative growth rates of AgoshRNA-expressing parasites. Genome-wide RNAi screens have already provided a wealth of new information about gene function in a variety of *in vitro* or *in vivo* settings[325]. Of course, both the multiplexing of AgoshRNAs and RNAi screens could be combined with stage-specific expression of Ago2, rendering the current tool box even more flexible and powerful.

4.2 ALTERNATIVE GENE SILENCING STRATEGIES IN *PB*AGO2

One of the main advantages of *Pb*Ago2 is that the knockdown of a target gene does not require the modification of the target locus. Yet, in rare cases it could happen that no efficient AgoshRNA against a GOI can be found. If the gene locus is amenable to genetic modification, in this situation the introduction of the targeting sequence of already established AgoshRNAs into the 3'UTR of the GOI could be an option. One could, for example, chose the targeting sequences of the αGFP-AgoshRNAs that have been thoroughly characterized in this work and introduce them via homologous recombination into the 3'UTR of the GOI within the *Pb*Ago2 line. An introduction of about 20 nt target sequence is not expected to affect the expression of the GOI, akin to loxP sites (34 bp long), whose introduction into UTRs also does not interfere with gene expression[83]. Using the established αGFP-AgoshRNAs, the GOI should then be efficiently silenced to degrees comparable to what has been observed for the GFP silencing (5- to 40-fold in trophozoites, see Figure 25). If experiments show that the AgoshRNAs are less effective in the current *Pb*GFPcon-based line as they can bind to two targets, GFP and the GOI, it might help to generate a GFP-free *Pb*Ago2 line in a different background. Alternatively, artificial AgoshRNAs that have no other target in *Pb*Ago2 could be established. Designing and testing

several sequences might yield a set of AgoshRNAs with known gene silencing efficiencies, which could additionally facilitate the fine-tuning of a GOI.

It would also be interesting to explore alternative strategies besides the expression of AgoshRNAs to induce RNAi. Importantly, Ago2 uses not only DNA-encoded AgoshRNAs to mediate RNAi but also siRNAs, which could be introduced to target cells as RNA molecules. It was shown previously that *Plasmodium* takes up DNA from preloaded erythrocytes and was suggested that erythrocyte miR-451 translocates into the parasite[326,327]. It is thus conceivable that *Plasmodium* can take up AgoshRNAs or siRNAs from RBCs that were preloaded *e g.* by RNA transfection. Such a strategy would be more suitable for *in vitro* culture due to the easy accessibility of RBCs under these conditions, and thus might be particularly relevant if AgoshRNA-mediated knockdown is to be introduced to *P. falciparum*. Given the difficulties to transfect *P. falciparum*, using preloaded erythrocytes would be an interesting alternative for the introduction of the regulatory RNA to the parasite, albeit any resulting knockdown is likely to be transient due to the rapid replication of *Plasmodium*.

Finally, the direct transfection of siRNAs into liver stages of *Pb*Ago2 would facilitate the targeting of liver-stage genes. Currently, no technologies are available to directly transfect sporozoites or liver stages. Furthermore, own preliminary experiments indicate that preloading hepatocytes with AgoshRNAs prior to *P. berghei* infection is not sufficient to transfer the RNA to the parasite (data not shown). It could be helpful to study in detail the mechanisms how *Plasmodium* blood stages spontaneously take up nucleic acids from the erythrocyte[326], as this would provide a strategy that could potentially be employed in the liver stage, too. Although it might be a difficult task to achieve, if successful, this would be greatly benefit future research on *Plasmodium* liver stages, as it would provide a rapid means to screen different siRNA target sequences without the need to generate an individual parasite line for each and to cycle it through the mosquito.

4.3 IMPAIRMENT OF *PB*AGO2 IN THE MOSQUITO STAGE

Curiously, the analysis of *Pb*Ago2 revealed that the expression of Ago2 impairs the parasite life cycle progression. In the blood, *Pb*Ago2 grew moderately slower than *Pb*GFPcon, and infected mice did not develop ECM. The development of ECM is in itself a quite variable outcome, and it is sensitive to small perturbations of parasite development and mouse environment. Within the same *P. berghei* species, only the strain ANKA causes ECM while the related strain NK65 does not induce cerebral symptoms[328]. Even within *Pb*ANKA, different clones vary in their ability to trigger ECM[329]. In fact, parasitemia progression and survival of *Pb*Ago2-infected mice closely resemble that of *Pb*NK65-infected mice. While *Pb*Ago2 might thus not be the best tool to

investigate the specific disease model of ECM, the blood-stage growth behavior should not hamper the study of other *Plasmodium*-specific biology. Already using a different mouse strain, *e. g.* NMRI mice, can alleviate the differences between *Pb*GFPcon and *Pb*Ago2 blood stage growth (see Figure 19).

A second and stronger phenotype that was initially unexpected is the reduced mosquito infectivity of *Pb*Ago2. Due to an about 10-fold drop in sporozoite numbers, working with mosquito stages of *Pb*Ago2 is fairly laborious, and the dynamic range to observe any further decrease of mosquito infectivity or sporozoite development caused by the knockdown of a GOI is diminished. We performed RNA-Seq comparing *Pb*GFPcon to *Pb*Ago2 and found that a group of genes that are known to be translationally repressed by the DOZI/CITH complex in gametocytes is downregulated in *Pb*Ago2 (see Section 3.7). The DOZI/CITH complex prevents translation of associated mRNAs and instead stores them in P-bodies[108,305]. Once gametocytes reach the mosquito environment, the repression is released, and the mRNAs are rapidly transcribed into protein, allowing for a quick transformation of the gametocytes into the subsequent life cycle stages. It has been described previously that a knockout of either DOZI or CITH results not in the premature translation of these mRNAs but in their degradation[108,305]. DOZI-deficient parasites are therefore not able to progress beyond the gametocyte stages, and do not infect mosquitoes[108].

The downregulation of this particular group of genes in *Pb*Ago2 indicates that the ectopic Ago2 expression may interfere with DOZI-mediated mRNA storage. Indeed, it was reported that Ago2 interacts with the human homolog of DOZI, DDX6 (Dead-box helicase 6, also called Rck/p54)[193]. DOZI is a remarkably well-conserved protein and shares 67 % amino acid identity and 90 % similarity with its human homolog (www.uniprot.org/align) (Figure 48). It is thus tempting to speculate that the human Ago2 expressed in *Pb*Ago2 binds to the *Plasmodium* DOZI protein, thereby inhibiting its function. This hypothesis provides an explanation why Ago2 expression in *P. berghei* adversely affects mosquito infectivity despite the formation of equal gametocyte numbers.

While it has been shown that Ago2 interacts with DDX6[193], it remains unclear if this interaction is direct or if mediator proteins are required. Indeed, a recent publication provides evidence that the interaction of DDX6 with Ago2 is mediated by the scaffold protein Pat1b[330]. Notably, the same study reports that the DDX6 residues R346, K352, and K353, which form a positively charged patch on the surface of the protein, are required for Pat1b interaction. Mutation of these residues not only prevented the DDX6 interaction with Pat1b but also ablated Ago2 recruitment and delocalized DDX6 from P-bodies. Interestingly, this patch is conserved in *Plasmodium* DOZI (Figure 48), yet a BLAST search revealed no homolog of Pat1b in *Plasmodium*. It thus remains to be investigated if a distant homolog of Pat1b in *Plasmodium* or another scaffold protein is required to mediate the Ago2-DOZI interaction, or if it is in fact a direct binding.

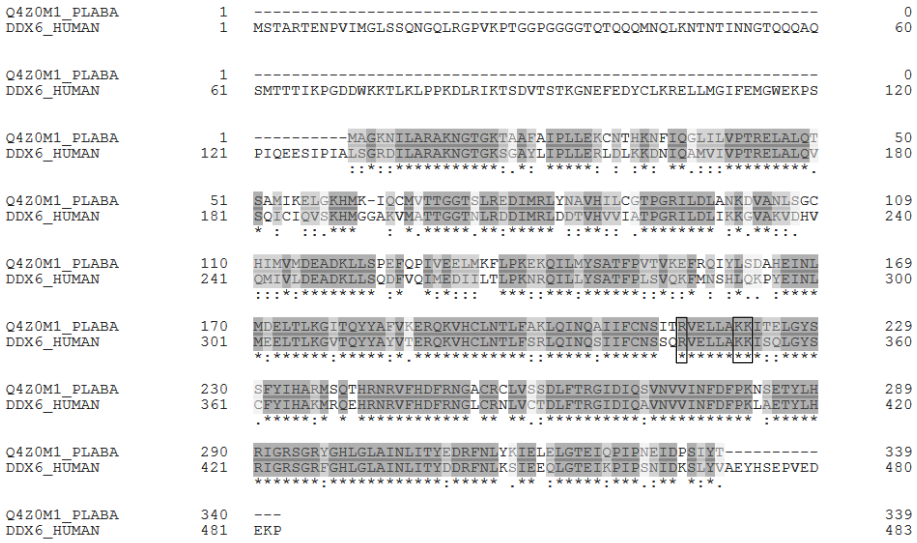

FIGURE 48: **Alignment of *P. berghei* DOZI with the human homolog DDX6.** Uniprot/Clustal Omega alignment of the *P. berghei* ANKA DOZI protein sequence (upper line, UniProt ID Q4Z0M1_PLABA) to the human DDX6 protein (lower row, UniProt ID DDX6_HUMAN). Identical amino acids are indicated by a star and a dark gray shading; similar amino acids are specified by a colon (:) and a light gray shading (strong similarity) or by a dot (.) and light font (weak similarity). Black boxes indicate the conserved residues responsible for Pat1 binding of human DDX6. The alignment was performed using www.uniprot.org/align.

So far, the interaction between hAgo2 and DOZI remains speculative and requires further validation by colocalization studies or immunoprecipitation experiments. If such experiments indeed implicate a DOZI-Ago2 interaction, it would open up possibilities to interfere with this interaction and thereby alleviate the growth defect. Interestingly, the interaction of Ago2 with DDX6 in human cells is required for miRNA-mediated, but not for shRNA-mediated gene silencing[193]. Thus, the slicing activity of Ago2 is independent of DDX6, and it is likely that the Ago2-DDX6/DOZI interaction can be disrupted without affecting AgoshRNA-mediated gene silencing. It would first be necessary to precisely identify the proteins involved in the Ago2-DOZI interaction and to map which Ago2 residues mediate the binding. Mutation of these residues should then hinder protein-protein interaction, preventing Ago2 from interfering with DOZI function and eventually alleviating the negative impact of Ago2 on mosquito infectivity.

4.4 RECONSTITUTION OF RNAI IN OTHER PARASITES

The effective engineering of the RNAi machinery in *P. berghei* in this work demonstrates that the concept of artificially introducing gene regulatory systems is a promising strategy to develop new genetic tools. A similar approach was successful in *Saccharomyces cerevisiae* (*S. cerevis*iae), where the expression of Dicer, TRBP, and Ago2 are sufficient to introduce the canonical RNAi pathway and to enable shRNA-mediated gene regulation[331]. Attempts to

likewise introduce the canonical RNAi machinery to *P. falciparum* remained unsuccessful so far, due to problems to express these large proteins and to introduce siRNAs into the parasite (personal communication with Oliver Billker, Sanger Institute, and Jake Baum, Imperial College, both from London, UK).

Importantly, the strategy followed in this study is much simpler, requiring the expression of only a single protein instead of three. Therefore, it would be tempting to extend the strategy of AgoshRNA-mediated knockdown to other RNAi-negative organisms, first and foremost the deadliest of the human malaria parasites, *P. falciparum*. In collaboration with Dr. Jude Przyborski and Matthias Diehl at the Philips University in Marburg, Germany, I attempted to generate *P. falciparum* expressing Ago2 from a stably maintained episome. However, two independent transfectants failed to generate parasites that express Ago2 along with a control AgoshRNA (data not shown). Ago2 expression may thus be detrimental to *P. falciparum*, potentially because DOZI-mediated repression may also play a role in asexual *P. falciparum* blood stages[332]. Fusing Ago2 to a degron in order to be able to induce its expression could help to elucidate any negative effect of Ago2 expression on *P. falciparum*. Such a combination with other genetic tools would provide the added advantage that AgoshRNA-mediated knockdown would become inducible, which would enhance the flexibility of the system. However, if Ago2 expression is truly incompatible with parasite development, further efforts have to be made to alleviate the growth defect, *e. g.* by disrupting the potential Ago2-DOZI interaction (in case this interaction can be confirmed as the reason for the growth impairment).

It would also be interesting to introduce this minimal RNAi machinery into other RNAi-negative parasites such as *L. major*, *L. donovani* or *T. cruzii*. Such an approach would open up new possibilities to study gene function in these important pathogens, similar to what was discussed for *Plasmodium* parasites (Section 4). Also in the apicomplexan parasite *T. gondii*, AgoshRNA-mediated knockdown could be a promising approach to enable genomewide RNAi screens. In this particular parasite, the presence of an endogenous Ago (*Tg*Ago1) protein might, however, interfere with this strategy. *Tg*Ago1 is phylogenetically very distant from its human paralog[260]. Although it lacks the catalytical residues described to be required for RNA cleavage (Asp-Asp-His[281]), *Tg*Ago1 was shown to have weak slicing activity when provided with a perfectly matched sequence, likely by using a non-canonical catalytical triad[333]. *Tg*Ago1 associates with a variety of proteins known to be part of the RISC, and putative miRNAs have been identified in *T. gondii*[260]. These were suggested to mediate gene silencing by translational repression but direct experimental evidence is still missing. Curiously, a knockout of *Tg*Ago1 did not yield a detectable phenotype compared to the wild type line[333], and the importance of miRNA mediated gene silencing in *T. gondii* remains to be further elucidated. The known features of *Tg*Ago1, in particular its poor homology to hAgo2 and the weak slicing activity, suggest that this enzyme will not process AgoshRNAs,

and that exogenous expression of hAgo2 is required for establishing the non-canonical RNAi pathway in *T. gondii*. Additionally, it remains to be studied if the expression of the human Ago2 protein interferes with the putative miRNAs expressed by *T. gondii*[260]. In this parasite, exogenous expression of Ago2 might thus not only be a potential new tool but could provide novel insights into the role of Ago proteins and miRNAs in this parasite.

Yet another option would be to exploit other mechanisms to regulate gene function, *e. g.* dCas9-mediated transcriptional inhibition. It has been shown that a catalytically inactive Cas9 protein (dead Cas9, dCas9) can still bind in a gRNA-dependent manner to a target gene[334–336]. However, as the catalytic residues are mutated in the dCas9, the target DNA is not cleaved. Instead, dCas9 poses a steric hindrance for the RNA polymerase and thereby inhibits transcription[334]. This effect can be even enhanced by fusing Cas9 to inhibitory protein domains such as the Krüppel-associated box (KRAB) that silence gene expression[335]. Alternatively, dCas9 can be fused to activator domains in order to boost expression of an endogenous gene[335,337,338], or, as another example, to fluorescent proteins as a means to label and track DNA[339]. Considering that CRISPR/Cas9 is functional in *Plasmodium*[72,73], it is tempting to speculate that the dCas9 system would function as well. This strategy would require the constant expression of a dCas9 protein, which raises concerns about toxicity, such as has been observed for Cas9-expression in *T. gondii*[75]. Preliminary experiments indeed showed that the constitutive expression of Cas9 or dCas9 in *P. berghei* completely abolished the mosquito passage of the parasite (data not shown). However, more detailed studies are required to pinpoint at which stage the block occurs and to unravel options to circumvent this defect.

4.5 CONCLUSION

Plasmodium parasites are the causative agents of one of the deadliest infectious diseases, malaria. As drug resistance is spreading and vaccination efforts are of limited success, basic research is of utmost importance to identify new targets for combatting the parasite. In this work, I reconstituted a non-canonical RNAi pathway in the rodent model organism *P. berghei*, thereby developing a new tool that allows for the targeted manipulation of gene expression in order to study gene function. As a major advance over all existing comparable technologies, *Pb*Ago2 enables the silencing of gene expression not only in blood stages but also in mosquito and liver stages. Due to the simplicity of the system, requiring only a single protein and a single RNA molecule, the tool is versatile and can be easily adapted to specific purposes, *e. g.* by restricting Ago2 expression, and thus gene silencing, to a single life cycle stage. I envision that this new technology will largely facilitate research on this important parasite and will thereby, eventually, contribute to ongoing world-wide efforts to fight, and ideally to ultimately eradicate, malaria disease.

Materials and Methods

5

5.1 MATERIALS

"The human animal differs from the lesser primates in his passion for lists."

~ H. Allen Smith (1907 – 1976)

5.1.1 LABORATORY EQUIPMENT

All equipment used in this work is listed in Table 2.

TABLE 2: **Laboratory equipment**

Equipment	Name	Company
Agarose gel electrophoresis	Gel caster	Bio-Rad (Hercules, CA, USA)
	Gel Doc XR	Bio-Rad (Hercules, CA, USA)
	Microwave oven	Sharp Electronics (Hamburg, Germany)
	Mini-SUB® cell GT/Sub-Cell® GT DNA electro-phoresis system	Bio-Rad (Hercules, CA, USA)
	UV transilluminator UST-30M-8E	Biostep GmbH (Burkhardtsdorf, Germany)
Balances	KERN EG200-2NM	Kern&Sohn GmbH (Bailingen, Germany)
	Analytical balance Pioneer	Ohaus (Nanickon, Switzerland)
	Precision balance	Mettler (Toledo, Switzerland)
Centrifuges	Allegra X-12R centrifuge	Beckman Coulter (Brea, CA, USA)
	Avanti J-26 XP centrifuge	Beckman Coulter (Brea, CA, USA)
	Megafuge 1.0R	Heraeus Instruments (Hanau, Germany)
	Microcentrifuge 5415 D	Eppendorf (Hamburg, Germany)
	Microcentrifuge 5415 R	Eppendorf (Hamburg, Germany)

Equipment	Name	Company
Electroporation devices	AMAXA Nucleofector II electroporator	Lonza (Cologne, Germany)
	Gene Pulser XcellTM	Bio-Rad (Hercules, CA, USA)
Flow cytometer	Cytomics FC500MPL analyzer	Beckman Coulter (Brea, CA, USA)
Heating blocks	DB1010	Alpha Laboratories (Hampshire, UK)
	ThermoCell Mixing Block MB-102	Bioer (Hangzhou, China)
	Thermomixer comfort	Eppendorf (Hamburg, Germany)
Incubators	Bacterial incubator Heraeus Function Line	Heraeus/Thermo Fisher Scientific (Waltham, MA, USA)
	Hera cell 150 incubator	Heraeus/Thermo Fisher Scientific (Waltham, MA, USA)
	Hera cell incubator	Heraeus/Thermo Fisher Scientific (Waltham, MA, USA)
	Shaking Incubator Multitron	INFORS HT (Basel, Switzerland)
Microscope	Confocal microscope TCS SP5	Leica (Wetzlar, Germany)
	Fluorescence microscope Axiovert 200M	Carl Zeiss (Oberkochen, Germany)
	Inverted fluorescence microscope IX-81	Olympus (Hamburg, Germany)
	Inverted microscope CKX-41	Olympus (Hamburg, Germany)
	Light microscope Axiostar Plus	Carl Zeiss (Oberkochen, Germany)
	Light microscope Axiovert 25	Carl Zeiss (Oberkochen, Germany)
	Light microscope Axiskop 40	Carl Zeiss (Oberkochen, Germany)
	Stereomicroscope Sterni 2000-C	Carl Zeiss (Oberkochen, Germany)
Pipets	accu-jet® pro	BRAND (Wertheim, Germany)
	Fisherbrand™ Finnpipette™ (5 - 50 µl, 10 – 100 µl)	Thermo Fisher Scientific (Waltham, MA, USA)

Equipment	Name	Company
Pipets	Pipetman (2-20 µl, 20-100 µl, 100-1000 µl)	Gilson, Inc. (Middleton, WI, USA)
	Pipetus®	Hirschman Laborgeräte (Eberstadt, Germany)
	Research multichannel (10 – 100 µl)	Eppendorf (Hamburg, Germany)
	Research plus multichannel (0.5 – 10 µl)	Eppendorf (Hamburg, Germany)
	Research plus pipettes (0.1-2 µl, 0.5-10 µl, 2-20 µl, 20-100 µl, 100-1000 µl)	Eppendorf (Hamburg, Germany)
Shaker and rotation devices	Shaker DOS-10L	neoLab (Heidelberg, Germany)
	Shaker DRS-12	neoLab (Heidelberg, Germany)
	Tube Rotator	VWR (Radnor, PA, USA)
Spectro-photometer	NanoDrop 2000 UV-Vis Spectrophotometer	Thermo Fisher Scientific (Waltham, MA, USA)
	NanoVue Spectrophotometer	GE Healthcare (Munich, Germany)
Storage	Freezer -20 °C	Liebherr (Bulle, Switzerland)
	Fridge	Liebherr (Bulle, Switzerland)
	Herafreeze Top -80 °C	Heraeus/Thermo Fisher Scientific (Waltham, MA, USA)
	Liquid nitrogen tank Cryosystem 4000 series	Panasonic (Kadoma, Japan)
	Liquid nitrogen tank MVE XC 34/18	MTG (Bruckberg, Germany)
Thermal cyclers	ABI 7500 Real-Time PCR System	Life Technologies (Paisley, UK)
	StepOnePlus Real-Time PCR System	Applied Biosystems/Thermo Fisher Scientific (Waltham, MA, USA)
	FlexCycler	analytikjena (Jena, Germany)
	Mastercycler® pro	Eppendorf (Hamburg, Germany)
Western blot equipment	Film developing cassettes	Dr. Goos-Suprema GmbH (Heidelberg, Germany)
	ChemoCam (ECL Imager)	INTAS Science Imaging Instruments (Göttingen, Germany)

Equipment	Name	Company
Western blot equipment	Mini-PROTEAN® comb 15-well	Bio-Rad (Hercules, CA, USA)
	Mini-PROTEAN® short plates	Bio-Rad (Hercules, CA, USA)
	Mini-PROTEAN® spacer plate (1 mm)	Bio-Rad (Hercules, CA, USA)
	Mini-PROTEAN® tetra cell casting module	Bio-Rad (Hercules, CA, USA)
	Mini-PROTEAN® tetra vertical electrophoresis cell	Bio-Rad (Hercules, CA, USA)
	PowerPac Power Supply	Bio-Rad (Hercules, CA, USA)
	Trans-Blot® SD Semi-Dry Electrophoretic Transfer Cell	Bio-Rad (Hercules, CA, USA)
	X-OMAT 2000 processor	KODAK (Rochester, NY, USA)
Other	CountessTM Automated Cell Counter	Invitrogen/Life Technologies (Paisley, UK)
	Haemocytometer (Neubaur)	Labotec Labor-Technik (Göttingen, Germany)
	Magnetic stirrer Heidolph MR3001	NeoLab Migge (Heidelberg, Germany)
	Micropistill for 1.5 ml tubes, conical	NeoLab Migge (Heidelberg, Germany)
	Mosquito cages	BioQuip Products (Rancho Dominguez, CA, USA)
	MSH basic – magnetic stirrer with steel heating plate	IKA Laboratory Equipment (Staufen, Germany)
	pH meter PB-11	Sartorius (Göttingen, Germany)
	Qubit® fluorometer	Invitrogen/Live Technologies (Paisley, UK)
	Sterile workbench HeraSafe®	Heraeus/Thermo Fisher Scientific (Waltham, MA, USA)
	Ultrasonic bath	BANDELIN (Berlin, Germany)
	Vortex Genie 2	Scientific Industries Roth (Karlsruhe, Germany)
	Water bath 1003	GFL (Burgwedel, Germany)
	Water bath TW12	Julabo Labortechnik (Seelbach, Germany)

5.1.2 LABORATORY MATERIAL

All consumables are listed in Table 3.

TABLE 3: **Consumables**

Name	Description	Company
Cell culture flasks	Cellstar® 75/175 cm^2	Greiner Bio-One (Frickenhausen, Germany)
Cell culture flasks	Nunclon delta surface 25 cm^2	Thermo Fisher Scientific (Waltham, MA, USA)
Cell culture plates	6 / 12 / 24 / 96 well	Greiner Bio-One (Frickenhausen, Germany) Nunc (Roskilde, Denmark)
Cryogenic vials	Cryo.S™, with screw cap, 2 ml	Greiner Bio-One (Frickenhausen, Germany)
Electroporation Cuvettes	25 x 1 mm gap	Peqlab (Erlangen, Germany)
Filter tips	Biosphere® 10/20/100/200/1000 µl	Sarstedt (Nuembrecht, Germany)
	FT 10 E 1µl	Greiner Bio-One (Frickenhausen, Germany)
Inoculation loops	1 µl	VWR (Darmstadt, Germany)
Insulin syringe	BD Micro-Fine™ U-100, 29G	Becton Dickingson, (Franklin Lakes, NJ, USA)
Lab-Tek chamber slides	8 well, with cover, Permanox	Thermo Fisher Scientific (Waltham, MA, USA)
Microscopic cover glasses	18 x 18 mm, 24 x 50 mm	Marienfeld (Lauda-Königshofen, Germany)
Microscopic slides	Frosted ends, 76 x 25 x 1 mm	Marienfeld (Lauda-Königshofen, Germany)
Needles	BD Microlance™ 3, 20G, 23G, 27G	Becton Dickingson, (Franklin Lakes, NJ, USA)
Nitrocellulose membrane	PROTAN®	Whatman (Maidstone, UK)
Parafilm M		Bernis, WI, USA
Pasteur pipettes	Plastic (Pastette)	Alpha Laboratories Limited (Hampshire, UK)
	Glas, 150 mm, 230 mm	Corning Incorporated, (Corning, NJ, USA)

Name	Description	Company
PCR tubes	0.2 ml, 8-strip	STARLAB (Hamburg, Germany)
Petri dishes	10 cm	Greiner Bio-One (Frickenhausen, Germany)
Pipette tips	200/1000 µl	Sarstedt (Nuembrecht, Germany)
	10 µl	Kisker Biotech (Steinfurt, Germany)
Precision wipes	Kimtech Science precision wipes	Kimberly-Clark (Ontario, Canada)
qPCR seals	Optical clear	Peqlab biotechnology (Erlangen, Germany)
qRT-PCR plate	Thermofast 96 well PCR detection plate	Thermo Fisher Scientific (Waltham, MA, USA)
Reaction tubes	0.5/1/2 ml	Sarstedt (Nuembrecht, Germany)
Serological pipettes	5/10/25 ml	Greiner Bio-One (Frickenhausen, Germany)
Syringes	BD Discardit™ 2/5/10 ml	Becton Dickingson, (Franklin Lakes, NJ, USA)
	BD Plastipak™ U-100, 1 ml	Becton Dickingson, (Franklin Lakes, NJ, USA)
Tubes	15/50 ml	Greiner Bio-One (Frickenhausen, Germany) Becton Dickingson, (Franklin Lakes, NJ, USA)
Whatman paper	3 mm	Whatman (Maidstone, UK)
X-ray films	Amersham Hyperfilm™ ECL	GE Healthcare (Munich, Germany)

5.1.3 *PLASMODIUM*, MICE, MOSQUITOES, BACTERIA AND CELLS

All *Plasmodium* strains, mouse strains and mosquito strains used in this study can be found in Table 4, Table 5, and Table 6, respectively. *E. coli* strains and cell lines are listed in Table 7 and Table 8, respectively.

TABLE 4: ***Plasmodium* strains**

***P. berghei* line**	**Description**	**Source**
*Pb*GFPcon	*P. berghei* ANKA strain that constitutively expresses GFP under the *Pb*ef1α 5' UTR	Franke-Fayard *et al.*, (2004)[274]

TABLE 5: **Mouse strains**

Mouse strain	**Description**	**Source**
C57BL/6J	Inbred	Janvier Labs (France)
Naval Medical Research Institute (NMRI)	Outbred	Janvier Labs (France)

TABLE 6: **Mosquito strains**

Mosquito line	**Source**
Anopheles stephensi	NIJ Nijmegen, Netherlands

TABLE 7: **Bacterial strains**

Bacterial strain	**Description**	**Source**
E. coli MAX Efficiency DH5α™	Chemically competent	Life Technologies (Paisley, UK)
E. coli MegaX DH10B™ T1^{R}	Electro-competent	Life Technologies (Paisley, UK)

TABLE 8: **Cell lines**

Cell line	**Description**	**Source**
HEK293T	Human embryonic kidney	DuBridge et al. (1987)
HuH7	Human hepatocellular carcinoma	Nakabayashi et al. (1982)
MEF (1c1)	Mouse embryonic fibroblasts	Glasmacher *et al.* (2010)[278]
Dicer$^{-/-}$ MEF (2G4)	Mouse embryonic fibroblasts, Dicer-deficient	Kind gift from Vigo Heissmeyer (Helmholtz-Zentrum Munich, Germany)

5.1.4 REAGENTS

Chemicals

All chemicals and reagents were bought in the highest purity available and are listed in Table 9.

TABLE 9: **Chemicals and reagents**

Product	Company
Acetic acid	Sigma-Aldrich (Munich, Germany)
Agarose	Biozym Scientific (Hessisch Oldendorf, Germany)
Albumin fraction V (BSA)	Carl Roth (Karlsruhe, Germany)
Alsever's solution	Sigma-Aldrich (Munich, Germany)
Ammonium persulfate (APS)	Grüssing GmbH (Filsum, Germany)
Ampicillin	Carl Roth (Karlsruhe, Germany)
40% Acryl/bisacrylamide	Carl Roth (Karlsruhe, Germany)
Aqua braun (ddH_2O)	B. Braun AG (Melsungen, Germany)
Bacto™ agar	BD (Franklin Lakes, NJ, USA)
Bacto™ tryptone	BD (Franklin Lakes, NJ, USA)
Bacto™ yeast extract	BD (Franklin Lakes, NJ, USA)
Bepanthen® eye and nose cream	Bayer AG (Leverkusen, Germany)
Bromophenol blue	Waldeck GmbH (Münster, Germany)
Calcium chloride ($CaCl_2$)	Carl Roth (Karlsruhe, Germany)
Chloroform	Sigma-Aldrich (Munich, Germany)
CF-11 Cellulose powder	Thermo Fisher Scientific (Waltham, MA, USA)
Deoxynucleoside triphosphate (dNTP)	NEB (Frankfurt am Main, Germany)
Dimethyl sulfoxide (DMSO)	Grüssing GmbH (Filsum, Germany)
Dimethyl sulfoxide (DMSO) for PCR	Thermo Fisher Scientific (Waltham, MA, USA)
Dodecylsulfate-Na-salt pellets (SDS)	SERVA Electrophoresis GmbH (Heidelberg, Germany)
Dithiothreitol (DTT)	AppliChem (Darmstadt, Germany)
Ethanol	Sigma-Aldrich (Munich, Germany)
Ethidium bromide	Carl Roth (Karlsruhe, Germany)
Ethylenediaminetetraacetic acid (EDTA)	Sigma-Aldrich (Munich, Germany)
5-Fluorocytosine	Sigma-Aldrich (Munich, Germany)
Gentamycin	Life Technologies (Paisley, UK)
Giemsa stock solution	Roth (Karlsruhe, Germany)
Glass beads	Sigma-Aldrich (Munich, Germany)

Product	Company
Glucose	Merk (Darmstadt, Germany)
Glycerol	Life Technologies (Paisley, UK) Carl Roth (Karlsruhe, Germany)
Heparin	Ratiopharm (Ulm, Germany)
Hoechst 33342	Invitrogen (Eugene, OR, USA)
Hydrochloric acid (HCl), 1 M	Sigma-Aldrich (Munich, Germany)
Immersol™ 518F	Carl Zeiss (Oberkochen, Germany)
Immersion oil, refractory index 1.482	Waldeck (Münster, Germany)
Isopropanol	Sigma-Aldrich (Munich, Germany)
Ketamine 10 %	Bremer Pharma GmbH (Warburg, Germany)
6x Loading dye	NEB (Frankfurt am Main, Germany)
Magnesium chloride ($MgCl_2$)	AppliChem (Darmstadt, Germany)
Magnesium sulfate ($MgSO_4$)	Merck (Darmstadt, Germany)
Methanol	Sigma-Aldrich (Munich, Germany)
Milk powder	Carl Roth (Karlsruhe, Germany)
MOPS ($C_7H_{15}NO_4S$)	Carl Roth (Karlsruhe, Germany)
Nuclease-free water	Qiagen (Hilden, Germany)
Nycodenz powder	Axis-Shield (Dundee, Scotland)
Para-aminobenzoic acid	Sigma-Aldrich (Munich, Germany)
Ponceau S solution	Sigma-Aldrich (Munich, Germany)
Potassium acetate (KAc)	AppliChem (Darmstadt, Germany)
Potassium chloride (KCl)	AppliChem (Darmstadt, Germany)
Potassium dihydrogen phosphate (KH_2PO_4)	AppliChem (Darmstadt, Germany)
Protease inhibitor cocktail	Roche (Basel, Switzerland)
Pyrimethamine	Sigma-Aldrich (Munich, Germany)
RLT buffer	Qiagen (Hilden, Germany)
QIAzol lysis reagent	Qiagen (Hilden, Germany)
Sucrose	AppliChem (Darmstadt, Germany)
Saponin	Sigma-Aldrich (Munich, Germany)
Sodium acetate (NaAc)	Grüssing (Filsum, Germany)
Sodium bicarbonate ($NaHCO_3$)	Merck (Darmstadt, Germany)
Sodium carbonate (Na_2CO_3)	Merck (Darmstadt, Germany)
Sodium chloride (NaCl)	Sigma-Aldrich (Munich, Germany)
Sodium fluoride (NaF)	Sigma-Aldrich (Munich, Germany)
Sodium hydroxide (NaOH)	Sigma-Aldrich (Munich, Germany)
TE buffer	Life Technologies (Paisley, UK)
TEMED (UltraPure™)	Life Technologies (Paisley, UK)

Product	Company
Tris/Glycine/SDS (TGS) buffer (10x)	BioRad (Hercules, USA)
Tris	Roth (Karlsruhe, Germany)
Tris-HCl	Roth (Karlsruhe, Germany)
Triton X-100	Merck (Darmstadt, Germany)
Tween™20	Roth (Karlsruhe, Germany)
Xylazine (Xylariem®)	Ecuphar GmbH (Greifswald, Germany)
β-mercaptoethanol	Roth (Karlsruhe, Germany)

Cell culture reagents

Media and supplements used in cell culture are listed in Table 10; transfection reagents can be found in Table 11.

TABLE 10: **Media and supplements for cell culture**

Component	Company	Category Number
Dulbecco's Modified Eagle Medium (DMEM), high glucose, GlutaMAX™	Life Technologies (Paisley, UK)	61965-026
Dulbecco's phosphate-buffered saline (1x PBS)	Life Technologies (Paisley, UK)	14190-094
Fetal bovine serum (FBS)	Sigma-Aldrich (Munich, Germany)	F7524
Fetal calf serum, US Origin (FCS-US)	Life Technologies (Paisley, UK)	16000-044
Minimum Essential Medium Non-Essential Amino Acids (MEM-NEAA, 100x)	Life Technologies (Paisley, UK)	11140-035
Penicillin-Streptomycin	Life Technologies (Paisley, UK)	15140-122
RPMI-1640	Life Technologies (Paisley, UK)	52400-025
Trypsin-EDTA (0.25 %), phenol-red	Life Technologies (Paisley, UK)	25200-056

TABLE 11: **Transfection reagents**

Component	Company	Category Number
Lipofectamine 2000	Life Technologies (Paisley, UK)	11668-019
Polyethylenimine (PEI)	Polysciences (Warrington, PA, USA)	23966

Standard markers

Standard markers listed in Table 12 were always loaded next to DNA or protein samples to allow size discrimination of the bands.

TABLE 12: **Standard markers**

Name	Company
1 kb plus ladder	Life Technologies GmbH (Paisley, UK)
100 bp ladder	Life Technologies GmbH (Paisley, UK)
PageRuler™ Plus Prestained Protein ladder	Thermo Fisher Scientific (Waltham, MA, USA)

Antibodies

All primary and secondary antibodies used for Western blotting or immunofluorescence staining are listed in Table 13 and Table 14, respectively. Details of their application can be found in the respective methods section (see p. 118 for Western blots and p. 125 for immunofluorescence).

TABLE 13: **Primary antibodies**

WB: Western blot
IF: Immuno-fluorescence

Antibody	**Application**	**Source**	**Category Number**
Mouse-anti-FLAG	IF	Sigma-Aldrich (Munich, Germany)	F1804-1MG
Mouse-anti-GFP	WB	eBioscience Inc. (San Diego, CA, USA)	14-6674-82
Mouse-anti-HA	WB	Santa Cruz Biotechnology (Heidelberg, Germany)	sc-7392
Mouse-anti-HSP70	WB IF	Tsuji *et al.*, 1994 [340]	-
Rabbit-anti-GFP	IF	Thermo Fisher Scientific (Waltham, MA, USA)	PA146326 A-11122
rat-anti-Ago2	WB	Sigma-Aldrich (Munich, Germany), Clone 11A9	MABE253
Rat-anti-EXP1	IF	Sá E Cunha *et al.*, 2017[19]	-
Mouse-anti-EXP1	WB	Sá E Cunha *et al.*, 2017[19]	-

TABLE 14: **Secondary antibodies**

Antibody	**Application**	**Source**	**Category Number**
Alexa Fluor ® 488 anti-mouse IgG	IF	Life Technologies (Paisley, UK)	A11029
Alexa Fluor ® 488 anti-rabbit IgG	IF	Life Technologies (Paisley, UK)	A11034
Alexa Fluor ® 546 anti-mouse IgG	IF	Life Technologies (Paisley, UK)	A11003
Alexa Fluor ® 546 anti-rat IgG	IF	Life Technologies (Paisley, UK)	A11081
ECL™ Rat IgG, HRP-linked whole antibody (from goat)	WB	GE-Healthcare (Chalfont St. Giles, UK)	NA935V
Peroxidase-AffiniPure Goat Anti-Mouse IgG + IgM	WB	Jackson Immuno-Research (West Grove, PA, USA)	115-035-068

Enzymes

All enzymes that were used in this work are listed in Table 15.

TABLE 15: **Enzymes**

Enzyme	Company	Category Number
Antarctic Phosphatase	NEB (Frankfurt am Main, Germany)	M0289S
*Bpi*I (*Bbs*I)	Thermo Fisher Scientific (Waltham, MA, USA)	ER1011
Gibson Assembly ® Master Mix	NEB (Frankfurt am Main, Germany)	E2611S
OneTaq® 2x Master Mix with standard buffer	NEB (Frankfurt am Main, Germany)	M0486S
Phusion Hot Start II DNA polymerase	Thermo Fisher Scientific (Waltham, MA, USA)	F-549L
Power SYBR® Green PCR Master Mix	Applied Biosystems (CA, USA)	4367659
Restriction enzymes (except for *Bbs*I)	NEB (Frankfurt am Main, Germany)	-
RNaseA	Qiagen (Hilden, Germany)	19101
T4 DNA ligase	NEB (Frankfurt am Main, Germany)	M0202L

Kits

Unless mentioned otherwise, kits listed in Table 16 were always used according to the instructions of the manufacturer.

TABLE 16: **Commercial Kits**

Kit	Company
Amaxa Human T cell Nucleofector Kit	Lonza (Cologne, Germany)
DNA Clean & Concentrator TM-5	Zymo Research (Irvine, CA, USA)
DNeasy Blood & Tissue Kit	QIAGEN (Hilden, Germany)
miRNeasy Mini Kit	QIAGEN (Hilden, Germany)
NucleoBond® Xtra Maxi	Macherey-Nagel GmbH (Duren, Germany)
PureYield™ Plasmid Midiprep Kit	Promega (Madison, WI, USA)
Qbit® protein assay kit	Thermo Fisher Scientific (Waltham, MA, USA)
QIAquick gel extraction kit	QIAGEN (Hilden, Germany)
Tetro cDNA Synthesis Kit	Bioline (London, UK)
Western lightning PLUS-ECL	PerkinElmer (Waltham, MA, USA)

5.1.5 BUFFERS AND SOLUTIONS

The composition of all buffers and solutions used in this work is listed in Table 17.

TABLE 17: **Composition of buffers**

Buffer	**Composition**	
Blocking buffer (Immunofluorescence)	5 % (v/v)	FBS in 1x PBS
Blocking buffer (Western blot)	5 % (w/v)	Milk powder in 1x TBS-T
DMEM complete	10 % (v/v) 1 % (v/v)	FBS Penicillin-Streptomycin in DMEM GlutaMAX™
Giemsa staining solution	10 %	Giemsa stock solution in dH_2O
Ketamine/Xylazine (K/X)	35.1 % 5.3 %	Ketamine Xylazine diluted in 1x PBS

Buffer	Composition	
Lysogeny broth (LB) medium	1 % (w/v) 0.5 % (w/v) 1 % (w/v)	Tryptone Yeast extract NaCl in ddH_2O
LB-Amp agar	1.5 % (w/v) 100 µg/ml	Agar Ampicillin in LB medium
LB-Amp medium	50 µg/ml	Ampicillin in LB medium
Nycodenz stock solution	5 mM 3 µM 0.3 mM 276 g/L	Tris KCl EDTA Nycodenz in ddH_2O, pH 7.5 autoclaved and stored in the dark at 4 °C
55 % Nycodenz/PBS	55 % (v/v)	Nycodenz stock solution in 1x PBS
P1 resuspension buffer	50 mM 10 mM 100 µg/ml	Tris-HCl EDTA RNaseA in ddH_2O, pH 8
P2 lysis buffer	200 mM 1 % (w/v)	NaOH SDS in ddH_2O
P3 neutralization buffer	2.8 M	KAc in ddH_2O, pH 5.1
Pyrimethamine drinking water	1x ~5 % (v/v)	Pyrimethamine stock solution HCl (1 M) to adjust pH in tap water, pH 3-5
Pyrimethamine stock solution (100x)	7 mg/ml	Pyrimethamine in DMSO

Buffer	Composition	
RIPA buffer	50 mM	Tris
	150 mM	NaCl
	5 mM	EDTA
	50 mM	NaF
	0.5%	Sodium deoxycholate
	0.1 %	SDS
	1 %	Triton X-100
		in H_2O, pH 7.5
		Add directly before use:
	2 mM	DTT
	1x	Protease inhibitor cocktail
SDS sample buffer (2x)	2 mM	EDTA
	100 mM	Tris-HCl
	4 % (w/v)	SDS
	20 % (v/v)	Glycerol
	10 % (v/v)	β-mercaptoethanol
	0.02 % (w/v)	Bromophenol blue
		in ddH_2O, pH 7.5
SDS sample buffer (6x)	6 mM	EDTA
	300 mM	Tris-HCl
	12 % (w/v)	SDS
	60 % (v/v)	Glycerol
	30 % (v/v)	β-mercaptoethanol
	0.06 % (w/v)	Bromophenol blue
		in ddH_2O, pH 7.5
SDS-PAGE Running gel buffer	1.5 M	Tris
	0.4 % (w/v)	SDS
		in ddH_2O, pH 8.8
SDS-PAGE Stacking gel buffer	500 mM	Tris
	0.4 % (w/v)	SDS
		in ddH_2O, pH 6.8
SOB medium	2 % (w/v)	Tryptone
	0.5 % (w/v)	Yeast extract
	0.05 % (w/v)	NaCl
	2.5 mM	KCl
	10 mM	$MgCl_2$ (autoclaved)
	10 mM	$MgSO_4$ (autoclaved)
		in ddH_2O
SOC medium	20 mM	Glucose (sterile-filtrated)
		in SOB medium

Buffer	Composition	
TAE buffer (50x)	2 M 50 mM 5.71 % (v/v)	Tris EDTA Acetic acid in ddH_2O, pH 8.3
TBS (10x)	250 mM 1.25 M	Tris NaCl in ddH_2O, pH 7.5
TBS-T (1x)	0.05 % (v/v)	Tween™20 in 1x TBS
TFBI	30.6 mM 80 mM 100 mM 16 mM 13.2 % (v/v)	KAc $MgCl_2$ KCl $CaCl_2$ Glycerol in ddH_2O, pH 5.8
TFBII	4.8 mM 76 mM 10 mM 13.2 % (v/v)	MOPS $CaCl_2$ KCl Glycerol in ddH_2O, pH 8.0
Transfection medium	20 % (v/v) 2 % (v/v)	FCS-US Gentamycin in RPMI-1640
Transfer buffer	20 %	methanol in 1x TGS
Washing buffer (Immunofluorescence)	1 % (v/v)	FBS in 1x PBS

5.1.6 DNA

Oligonucleotides

TABLE 18 shows the sequence of all oligonucleotides used in this work. Overhangs are depicted in small letters. Restriction sites used for cloning, overhangs created by oligo-annealing or homology arms for Gibson cloning are indicated in orange. If additional restriction sites were introduced to the oligonucleotide, they are labeled in bold. Sense strands of sh- or AgoshRNAs are marked in blue in the forward oligonucleotide. All oligonucleotides were ordered at Sigma-Aldrich (Munich, Germany) or Integrated DNA Technologies (Leuven, Belgium).

Table 18: **Oligonucleotides**

ID	Name	Sequence (5' → 3')
P1	*Xho*I-GFP-mut3 F	gtcgcctcgagATGCGTAAAGGAGAAGAACTTTTC
P2	*Nhe*I-GFP-mut3 R	gactagctagcTTATTTGTATAGTTCATCCATGCC
P3	*Xba*I-Stuffer-*Blp*I F	ctagaGAATTCAGATCTACTAGTGTTAACATGGGA TCTGGATCTGGTGGTGGTGGAACCGGTgc
P4	*Xba*I-Stuffer-*Blp*I R	ttagcACCGGTTCCACCACCACCAGATCCAGATCCC ATGTTAACACTAGTAGATCTGAATTCt
P5	*Nde*I-*Pac*I-*Asc*I-*BamH*I (MCS) F	tatgATGTACGAGACG**GGCGCGCC**ATGCATGC**TT AATTAA**CGTCTCAAGTGAg
P6	*Nde*I-*Pac*I-*Asc*I-*BamH*I (MCS) R	gatccTCACTTGAGACG**TTAATTAA**GCATGCAT**G GCGCGCC**CGTCTCGTACATca
P7	*Nde*I-FLAG-Ago2 F	gtcgccatatgATGGACTACAAGGACGACG
P8	*BamH*I-Ago2 R	agactaggatccTCAGGCGAAGTACATGGTCC
P9	5'*LISP2* Gibson F	gagaattcagatctactagtgttGCATTATCGTCAAAAGT G
P10	5'*LISP2* Gibson R	tcgtcgtccttgtagtccatcatatgtcccatatttaaatTTTTTA TGTGTAAAAAAGTAAAATGATT
P11	*Xma*I-*Bbs*I-*Pb*U6 F	cactcgacccgggGCAATGGT**CTTCAG**T**GAAGAC**T CAATAATATTGTATAACTCGAAGTATGC
P12	*Xho*I-*Pb*U6-R	cgatgctcgagCACACACCTATATATCGAGAAC
P13	Gibson GFP to mCherry F	tatcccaataaattacaattacaattatttaaatatgg**ccatgg**g acatATGGTGAGCAAGGGCG

ID	Name	Sequence (5' → 3')
P14	Gibson GFP to mCherry R	tccttaaacgggcttgcacacctttta**gctagc**cgcggTTACTTGTACAGCTCGTCCATG
P15	*NgoMV*I-*BamH*I stuffer F	ccggcAGACAACCATTACCTGTCCACACAATCTGCCCg
P16	*NgoMV*I-*BamH*I stuffer R	gatccGGGCAGATTGTGTGGACAGGTAATGGTTGTCTg
P17	*Bcl*I-3'*Pb*DHFS F	atgcgatgatcaCTAGCTAAAAGGTGTGCAAGC
P18	*Xho*I-3'*Pb*DHFS R	atgcgactcgagGGATATCATATTTGTAATGATGC
P19	5'*HSP*70 seq	CACTATTTTGCCATAAGCAC
P20	3'*Pb*DHFS-FPGS seq	AATCCTTAAACGGGCTTGC
P21	HA-Ago2-rev seq	AATCGGGCACGTCATAAGG
P22	SIL6R rev seq	GTGCCTGAATTATAGTGCA
P23	*Pb*U6 to *Bbs*I seq	ACATAGCATGCCGAATGC
P24	αGFP AgoshR 1a F	caccGTGTCTTGTAGTTCCCGTCAGAGACGGGAACTACAAGACAC
P25	αGFP AgoshR 1a R	aaaaGTGTCTTGTAGTTCCCGTCTCTGACGGGAACTACAAGACAC
P26	αGFP AgoshR 2a F	caccGTTAACTTTGATTCCATTCAGAGAATGGAATCAAAGTTAAC
P27	αGFP AgoshR 2a R	aaaaGTTAACTTTGATTCCATTCTCTGAATGGAATCAAAGTTAAC
P28	αGFP AgoshR 3a F	caccGTTGAACGCTTCCATCTTCAGAGAAGATGGAAGCGTTCAAC
P29	αGFP AgoshR 3a R	aaaaGTTGAACGCTTCCATCTTCTCTGAAGATGGAAGCGTTCAAC
P30	αGFP AgoshR 4a F	caccGTTGCATCACCTTCACCCTAGAAGGGTGAAGGTGATGCAAC
P31	αGFP AgoshR 4a R	aaaaGTTGCATCACCTTCACCCTTCTAGGGTGAAGGTGATGCAAC
P32	αRen shR 1 F	caccGCAACGCAAACGCATGATCACTCAAGAGGTGATCATGCGTTTGCGTTGC

ID	Name	Sequence (5' → 3')
P33	αRen shR 1 R	aaaaGCAACGCAAACGCATGATCACCTCTTGAGTGATCATGCGTTTGCGTTGC
P34	αGFP shR 1a F	caccGGGTGAAGGTGATGCAACATATCAAGAGTATGTTGCATCACCTTCACCC
P35	αGFP shR 1a R	aaaaGGGTGAAGGTGATGCAACATACTCTTGATATGTTGCATCACCTTCACCC
P36	αGFP shR 2a F	caccGGCCAACACTTGTCACTACTTTCAAGAGAAGTAGTGACAAGTGTTGGCC
P37	αGFP shR 2a R	aaaaGGCCAACACTTGTCACTACTTCTCTTGAAAGTAGTGACAAGTGTTGGCC
P38	αGFP shR 3a F	caccGAAGATGGAAGCGTTCAACTATCAAGAGTAGTTGAACGCTTCCATCTTC
P39	αGFP shR 3a R	aaaaGAAGATGGAAGCGTTCAACTACTCTTGATAGTTGAACGCTTCCATCTTC
P40	αGFP AgoshR 1b F	caccGTTGCATCACCTTCACCCTCTCCAGGGGTGAAGGTGATGCAAC
P41	αGFP AgoshR 1b R	aaaaGTTGCATCACCTTCACCCCTGGAGAGGGTGAAGGTGATGCAAC
P42	αGFP AgoshR 2b F	caccGCTAGTTGAACGCTTCCATCTTCAGTGGAAGCGTTCAACTAGC
P43	αGFP AgoshR 2b R	aaaaGCTAGTTGAACGCTTCCACTGAAGATGGAAGCGTTCAACTAGC
P44	αGFP AgoshR 3b F	caccAACAAGAATTGGGACAACTCCAGTGGTTGTCCCAATTCTTGTT
P45	αGFP AgoshR 3b R	aaaaAACAAGAATTGGGACAACCACTGGAGTTGTCCCAATTCTTGTT
P46	αGFP AgoshR 4b F	caccAACTCAAGAAGGACCATGTGGTCTGCATGGTCCTTCTTGAGTT
P47	αGFP AgoshR 4b R	aaaaAACTCAAGAAGGACCATGCAGACCACATGGTCCTTCTTGAGTT
P48	αGFP AgoshR 1c F	caccATTGCATCACCTTCACCCTCTCCAGGGGTGAAGGTGATGCAAC
P49	αGFP AgoshR 1c R	aaaaGTTGCATCACCTTCACCCCTGGAGAGGGTGAAGGTGATGCAAT
P50	αGFP AgoshR 2c F	caccACTAGTTGAACGCTTCCATCTTCAGTGGAAGCGTTCAACTAGC
P51	αGFP AgoshR 2c R	aaaaGCTAGTTGAACGCTTCCACTGAAGATGGAAGCGTTCAACTAGT

ID	Name	Sequence (5' → 3')
P52	αGFP AgoshR 3c F	caccAACAAGAATTGGGACAACTCCAGTGGTTGTCCCAATTCTTGTC
P53	αGFP AgoshR 3c R	aaaaGACAAGAATTGGGACAACCACTGGAGTTGTCCCAATTCTTGTT
P54	αGFP AgoshR 4c F	caccAACTCAAGAAGGACCATGTGGTCTGCATGGTCCTTCTTGAGTC
P55	αGFP AgoshR 4c R	aaaaGACTCAAGAAGGACCATGCAGACCACATGGTCCTTCTTGAGTT
P56	AgoshR scr F	caccAGACTCTCGTGTCCATAATCTTCAGTTATGGACACGAGAGTCC
P57	AgoshR scr R	aaaaGGACTCTCGTGTCCATAACTGAAGATTATGGACACGAGAGTCT
P58	*PbU6* αGFP AgoshR 1c F	tattATTGCATCACCTTCACCCTCTCCAGGGGTGAAGGTGATGCAACTTTT
P59	*PbU6* αGFP AgoshR 1c R	gcaaAAAAGTTGCATCACCTTCACCCCTGGAGAGGGTGAAGGTGATGCAAT
P60	*PbU6* αGFP AgoshR 2c F	tattACTAGTTGAACGCTTCCATCTTCAGTGGAAGCGTTCAACTAGCTTTT
P61	*PbU6* αGFP AgoshR 2c R	gcaaAAAAGCTAGTTGAACGCTTCCACTGAAGATGGAAGCGTTCAACTAGT
P62	*PbU6* αGFP AgoshR 3c F	tattAACAAGAATTGGGACAACTCCAGTGGTTGTCCCAATTCTTGTCTTTT
P63	*PbU6* αGFP AgoshR 3c R	gcaaAAAAGACAAGAATTGGGACAACCACTGGAGTTGTCCCAATTCTTGTT
P64	*PbU6* αGFP AgoshR 4c F	tattAACTCAAGAAGGACCATGTGGTCTGCATGGTCCTTCTTGAGTCTTTT
P65	*PbU6* αGFP AgoshR 4c R	gcaaAAAAGACTCAAGAAGGACCATGCAGACCACATGGTCCTTCTTGAGTT
P66	*PbU6* AgoshR scr F	tattAGACTCTCGTGTCCATAATCTTCAGTTATGGACACGAGAGTCCTTTT
P67	*PbU6* AgoshR scr R	gcaaAAAAGGACTCTCGTGTCCATAACTGAAGATTATGGACACGAGAGTCT
P68	*PbU6* αPPLP2 AgoshR 1 F	tattATCTAGTAGCGCATTCCTTCTTCAGAGGAATGCGCTACTAGACTTTT
P69	*PbU6* αPPLP2 AgoshR 1 R	gcaaAAAAGTCTAGTAGCGCATTCCTCTGAAGAAGGAATGCGCTACTAGAT
P70	*PbU6* αPPLP2 AgoshR 2 F	tattATAGAAGGAGTACTTACCTCTTCAGGGTAAGTACTCCTTCTACTTTT

ID	Name	Sequence (5' → 3')
P71	*PbU6* αPPLP2 AgoshR 2 R	gcaaAAAAGTAGAAGGAGTACTTACCCTGAAGAG GTAAGTACTCCTTCTAT
P72	*PbU6* αPPLP2 AgoshR 3 F	tattAATCTAGGTATCCATCATTCTTCAGATGATGG ATACCTAGATCTTTTT
P73	*PbU6* αPPLP2 AgoshR 3 R	gcaaAAAAGATCTAGGTATCCATCATCTGAAGAAT GATGGATACCTAGATT
P74	*PbU6* αPPLP2 AgoshR 4 F	tattACTATTCCAAGGGAGTGTTCTTCAGACACTCC CTTGGAATAGCTTTTT
P75	*PbU6* αPPLP2 AgoshR 4 R	gcaaAAAAGCTATTCCAAGGGAGTGTCTGAAGAA CACTCCCTTGGAATAGT
P76	*PbU6* αExp1 AgoshR 1 F	tattAATTACTGGTTCTGCTGGTCTTCAGCCAGCA GAACCAGTAATCTTTT
P77	*PbU6* αExp1 AgoshR 1 R	gcaaAAAAGATTACTGGTTCTGCTGGCTGAAGAC CAGCAGAACCAGTAATT
P78	*PbU6* αExp1 AgoshR 2 F	tattATCTTTGAGCATAGCTTCTCTTCAGGAAGCTA TGCTCAAAGACTTTT
P79	*PbU6* αExp1 AgoshR 2 R	gcaaAAAAGTCTTTGAGCATAGCTTCCTGAAGAGA AGCTATGCTCAAAGAT
P80	*PbU6* αExp1 AgoshR 3 F	tattATTGTTGAAGATTTGGCATCTTCAGTGCCAAA TCTTCAACAACTTTT
P81	*PbU6* αExp1 AgoshR 3 R	gcaaAAAAGTTGTTGAAGATTTGGCACTGAAGAT GCCAAATCTTCAACAAT
P82	*PbU6* αMSP1 AgoshR 1 F	tattATTTGTTGCAATAATGGCTCTTCAGGCCATTA TTGCAACAAACTTTT
P83	*PbU6* αMSP1 AgoshR 1 R	gcaaAAAAGTTTGTTGCAATAATGGCCTGAAGAG CCATTATTGCAACAAAT
P84	*PbU6* αMSP1 AgoshR 2 F	tattAGATTGTGATGAGGCTTGTCTTCAGCAAGCC TCATCACAATCCTTTT
P85	*PbU6* αMSP1 AgoshR 2 R	gcaaAAAAGGATTGTGATGAGGCTTGCTGAAGAC AAGCCTCATCACAATCT
P86	*PbU6* αMSP1 AgoshR 3 F	tattATATTCTTCTGATTGACCTCTTCAGGGTCAAT CAGAAGAATACTTTT
P87	*PbU6* αMSP1 AgoshR 3 R	gcaaAAAAGTATTCTTCTGATTGACCCTGAAGAGG TCAATCAGAAGAATAT
P88	SIL6 3' Integration F	CCACCCCGTGTGAATATG
P89	SIL6 3' WT R	GCACATTTGTGTATTACATATCAC

ID	Name	Sequence (5' → 3')
P90	SIL6 5' WT F	AATACTGCAACAATTGTGTTTG
P91	SIL6 5' Integration R	ACAATTCCGCAATTTGTTGTAC
P92	3'*PbDHFS-FPGS* for negative selection	ATATACGTGAAAAAGCATCATTAC
P93	GFPmut3 qRT-PCR F	GGAGAGGGTGAAGGTGATGC
P94	GFPmut3 qRT-PCR R	TGACAAGTGTTGGCCATGGA
P95	mCherry qRT-PCR F	GCTCCAAGGCCTACGTGAAG
P96	mCherry qRT-PCR R	CCGTCCTCGAAGTTCATCAC
P97	PPLP2 qRT-PCR F	GCAAGTAGTAGAACAAAATGAAGC
P98	PPLP2 qRT-PCR R	TAGCAGATGATCTACCTGTTCC
P99	GamHK qRT-PCR F	GCCAGAATCATTATGTTTTACTATAATGG
P100	GamHK qRT-PCR R	CTTAATATATAATCCATAAATTGGTGC
P101	*BamH*I-*Sac*I stuffer F	gatcAGTCGAAGCTTACGTGagct
P102	*BamH*I-*Sac*I stuffer R	CACGTAAGCTTCGACT

Plasmids

All plasmids used in this work are listed in TABLE 19. The ID of each plasmid refers to its internal number in the plasmid library of the Grimm laboratory.

Table 19: **Plasmids used in this work**

ID	Plasmid name	Description	Source
#1546	pBAT-SIL6	Vector to integrate expression cassettes into *P. berghei*	Kooij *et al.*, 2015[279]
#1547	pBAT-SIL6-MCS	A modified vector of #1546, lacking the mCherry-tag and with a multiple cloning site instead of the GFP	This work

ID	Plasmid name	Description	Source
#1548	pBAT-SIL6-Ago2	Vector to integrate the 5'*HSP70*-Ago2-expression cassette into *P. berghei*	This work
#1873	pBAT-SIL6-5'*LISP2*-Ago2	Vector to integrate the 5'*LISP2*-Ago2-expression cassette into *P. berghei*	This work
#1870	pBAT-SIL6-mCherry-*PbU6*	Vector to episomally express AgoshRNAs in *P. berghei* along with an mCherry as fluorescence marker	This work
#1871	pBAT-SIL6-*PbU6*int (V1)	First version to integrate a *PbU6*-AgoshRNA cassette into *Pb*Ago2	This work
#1872	pBAT-SIL6-*PbU6*int(V2)	Optimized vector to integrate a *Pb*U6-AgoshRNA into *Pb*Ago2.	This work
#1552	pBS-sds-mCherry-*U6*-empty	Vector to express an sh- or AgoshRNA *in vitro* along with an mCherry fluorescence marker	Dominik Niopek
#1339	pBS-sds-*CMV*-mCherry	Control vector expressing only mCherry	Silke Uhrig
#66	pBS-sds-*CMV*-GFP	CMV-GFP expression vector in an AAV context	Nina Schuermann
#1551	pBS-sds-*CMV*-GFPmut3	Vector to express the GFP encoded by *Pb*GFPcon *in vitro*	This work
#1424	#1552-αRen-shRNA1	Based on #1552, encoding for a non-targeting shRNA	This work
#1873	#1552-*U6*-αGFP-shRNA1a	Based on #1552, encoding for the αGFP-shRNA 1a	This work
#1875	#1552-*U6*-αGFP-shRNA2a	Based on #1552, encoding for the αGFP-shRNA 2a	This work
#1876	#1552-*U6*-αGFP-shRNA3a	Based on #1552, encoding for the αGFP-shRNA 3a	This work
#1877	#1552-*U6*-αGFP-shRNAscr	Based on #1552, encoding for the αGFP-shRNAscr	This work
#1878	#1552-*U6*-αGFP-AgoshR1a	Based on #1552, encoding for the αGFP-AgoshRNA 1a	This work

ID	Plasmid name	Description	Source
#1879	#1552-*U6*-αGFP-AgoshR2a	Based on #1552, encoding for the αGFP-AgoshRNA 2a	This work
#1880	#1552-*U6*-αGFP-AgoshR3a	Based on #1552, encoding for the αGFP-AgoshRNA 3a	This work
#1881	#1552-*U6*-αGFP-AgoshR4a	Based on #1552, encoding for the αGFP-AgoshRNA 4a	This work
#1882	#1552-*U6*-αGFP-AgoshR1b	Based on #1552, encoding for the αGFP-AgoshRNA 1b	This work
#1883	#1552-*U6*-αGFP-AgoshR2b	Based on #1552, encoding for the αGFP-AgoshRNA 2b	This work
#1884	#1552-*U6*-αGFP-AgoshR3b	Based on #1552, encoding for the αGFP-AgoshRNA 3b	This work
#1885	#1552-*U6*-αGFP-AgoshR4b	Based on #1552, encoding for the αGFP-AgoshRNA 4b	This work
#1886	#1552-*U6*-αGFP-AgoshR1c	Based on #1552, encoding for the αGFP-AgoshRNA 1c	This work
#1887	#1552-*U6*-αGFP-AgoshR2c	Based on #1552, encoding for the αGFP-AgoshRNA 2c	This work
#1888	#1552-*U6*-αGFP-AgoshR3c	Based on #1552, encoding for the αGFP-AgoshRNA 3c	This work
#1889	#1552-*U6*-αGFP-AgoshR4c	Based on #1552, encoding for the αGFP-AgoshRNA 4c	This work
#1890	#1552-*U6*-αGFP-AgoshRscr	Based on #1552, encoding for the AgoshRNAscr	This work
#1891	pBAT-SIL6-mCherry-*PbU6*-αGFP-AgoshR1c	Based on #1870, encoding for the αGFP-AgoshRNA 1c	This work
#1892	pBAT-SIL6-mCherry-*PbU6*-αGFP-AgoshR2c	Based on #1870, encoding for the αGFP-AgoshRNA 2c	This work
#1893	pBAT-SIL6-mCherry-*PbU6*-αGFP-AgoshR3c	Based on #1870, encoding for the αGFP-AgoshRNA 3c	This work
#1894	pBAT-SIL6-mCherry-*PbU6*-αGFP-AgoshR4c	Based on #1870, encoding for the αGFP-AgoshRNA 4c	This work

ID	Plasmid name	Description	Source
#1895	pBAT-SIL6-mCherry-*PbU6*-AgoshRscr	Based on #1870, encoding for the AgoshRNAscr	This work
#1896	pBAT-SIL6-*PbU6*int(V1)-AgoshRscr	Based on #1871, encoding for the AgoshRNAscr	This work
#1897	pBAT-SIL6-*PbU6*int(V1)-αGFP-AgoshR2c	Based on #1871, encoding for the αGFP-AgoshRNA 2c	This work
#1898	pBAT-SIL6-mCherry-*PbU6*-αPPLP2-AgoshR1	Based on #1870, encoding for the αPPLP2-AgoshRNA 1	This work
#1899	pBAT-SIL6-mCherry-*PbU6*-α PPLP2-AgoshR2	Based on #1870, encoding for the α PPLP2-AgoshRNA 2	This work
#1900	pBAT-SIL6-mCherry-*PbU6*-α PPLP2-AgoshR3	Based on #1870, encoding for the α PPLP2-AgoshRNA 3	This work
#1901	pBAT-SIL6-mCherry-*PbU6*-α PPLP2-AgoshR4	Based on #1870, encoding for the α PPLP2-AgoshRNA 4	This work
#1902	pBAT-SIL6-mCherry-*PbU6*-αExp1-AgoshR1	Based on #1870, encoding for the αExp1-AgoshRNA 1	This work
#1903	pBAT-SIL6-mCherry-*PbU6*-αExp1-AgoshR2	Based on #1870, encoding for the αExp1-AgoshRNA 2	This work
#1904	pBAT-SIL6-mCherry-*PbU6*-αExp1-AgoshR3	Based on #1870, encoding for the αExp1-AgoshRNA 3	This work
#1905	pBAT-SIL6-*PbU6*int(V2)-AgoshRscr	Based on #1872, encoding for the AgoshRNAscr	This work
#1906	pBAT-SIL6-*PbU6*int(V2)-αMSP1-AgoshR1	Based on #1872, encoding for the αMSP1-AgoshRNA 1	This work
#1907	pBAT-SIL6-*PbU6*int(V2)-αMSP1-AgoshR2	Based on #1872, encoding for the αMSP1-AgoshRNA 2	This work
#1908	pBAT-SIL6-*PbU6*int(V2)-αMSP1-AgoshR3	Based on #1872, encoding for the αMSP1-AgoshRNA 3	This work

5.1.7 SOFTWARE

Software that is either associated with laboratory equipment used in this work or has been used to further process data is listed in Table 20.

TABLE 20: **Software**

Name	Description	Source/Reference
Flowing Software 2.5	To analyze flow cytometric data	http://www.uskonaskel.fi/flowingsoftware/
AxioVision 4.8.2 SP3	For taking images at the fluorescence microscope	Carl Zeiss (Oberkochen, Germany)
Serial Cloner 2.6.1	For *in silico* cloning and primer design	http://serialbasics.free.fr/Serial_Cloner.html
GraphPad Prism 5	For statistical analysis of data and graph design	GraphPad Software Inc.,
StepOne™ Software v2.3	For evaluating qRT-PCR data	Applied Biosystems/ Thermo Fisher Scientific (Waltham, CA, USA)
Fiji	For image analysis	https://fiji.sc/ Schindelin *et al.*, 2012[341]
Quantity One 1-D Analysis 4.6.9	Gel Doc XR-associated software	Bio-Rad (Hercules, CA, USA)
MXP	Cytomics FC500MPL analyzer-associated software	Beckman Coulter (Brea, MA, USA)
ChemoStar Imager	Software associated with the Western blot imaging system	INTAS Science Imaging Instruments (Göttingen, Germany)

5.2 METHODS

"An experiment is a question which science poses to nature, and a measurement is the recording of nature's answer."[342]

~ Max Planck (1858 – 1947)

5.2.1 CLONING PROCEDURES

The following part details the cloning strategy used for each plasmid (listed in TABLE 19) and which oligonucleotides were used (listed in TABLE 18). The ID number of each plasmid is indicated in brackets behind the name.

To express GFP in HEK293T or MEF cells, the GFPmut3 encoded by the strain *Pb*GFPcon[343] was amplified using primers P1 and P2 and cloned in the *Xho*I/*Nhe*I-digested vector pBS-sds-CMV-GFP (#66), yielding pBS-sds-CMV-GFPmut3 (#1551).

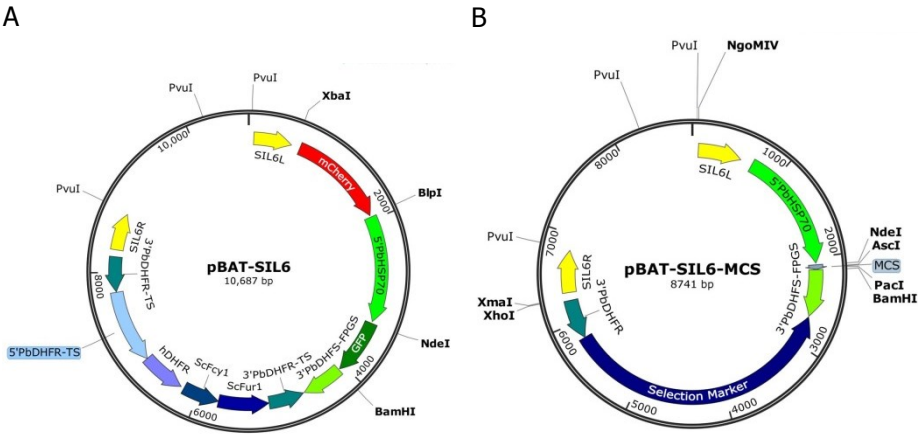

FIGURE 49: **Plasmid maps of (A) pBAT-SIL6 and (B) pBAT-SIL6-MCS.** Indicated are all restriction sites that are used in subsequent cloning steps as well as the *Pvu*I site, which is used to linearize the plasmid before transfection into *P. berghei*. The selection marker, comprising the 5'*PbDHFR-TS*, the h*DHFR*, the *ScFcy*1/*ScFur*1 and the 3'*PbDHFR-TS* regions (depicted in (A)), is in (B) as well as in all subsequent plasmid maps depicted as a single feature.

All vectors designed to express genes in *Plasmodium* are based on a modified version of the previously published vector pBAT-SIL6[279] (#1546) (Figure 49 A). To reduce vector size and facilitate cloning, I removed the mCherry open reading frame by *Xba*I/*Blp*I digest and ligation to the annealed oligonucleotides P3 und P4. Digestion with *BamH*I/*Nde*I removed the GFP open reading frame from this vector, allowing the insertion of the annealed oligonucleotides P5/P6 downstream of the *HSP70* promoter, which introduced a cloning site consisting of *Pac*I and *Asc*I. The resulting vector, pBAT-SIL6-MCS (#1547), is a versatile vector that can be used to easily express extra copies of genes in *P. berghei* (Figure 49 B).

To integrate an Ago2-expression cassette under the control of the *HSP70* promoter (5'*HSP70*) into *P. berghei*, I cloned the vector pBAT-SIL6-Ago2 (#1548) (Figure 50 A). For this, I PCR-amplified a previously published, codon-optimized version of the human Ago2[344] using primers P7/P8, and inserted the fragment via standard restriction digest with *Nde*I/*BamH*I into pBAT-SIL6-MCS. Correct cloning was confirmed by sequencing Ago2 using the primers P19/P20. To drive Ago2-expression not by the 5'*HSP70*, but by the *LISP2* promoter (5'*LISP*), Vera Mitesser excised the *HSP*70 promoter from pBAT-SIL6-Ago2 by *SpeI*/*SwaI* digestion and inserted a previously published ~1 kB long region upstream of the *LISP2* gene[307] (PbANKA_10_v3:190,309..191,296; amplified from genomic DNA with the primers P9/P10) via Gibson Assembly. This resulting vector, which sequence was confirmed by sequencing the promoter using primer P21, was called pBAT-SIL6-5'*LISP2*-Ago2 (#1873) (Figure 50 B).

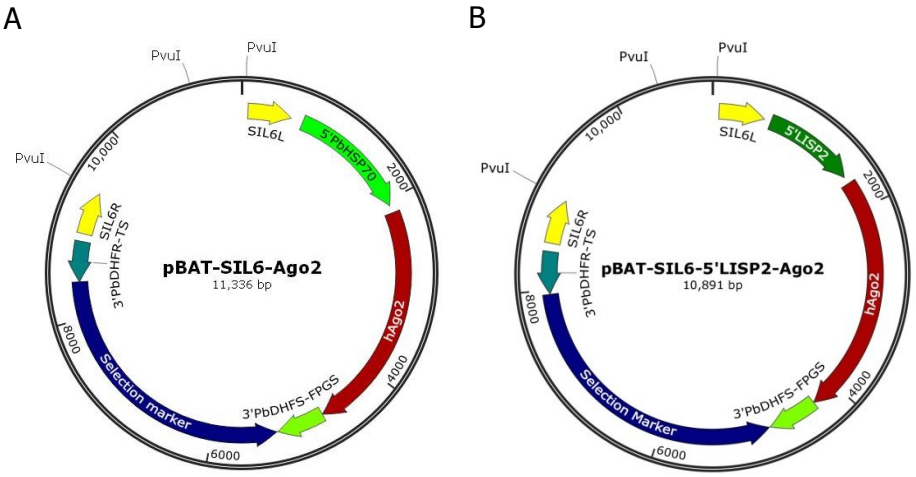

FIGURE 50: **Plasmid maps of (A) pBAT-SIL6-Ago2 and (B) pBAT-SIL6-5'*LISP2*-Ago2.** Indicated is the *Pvu*I site, which is used to linearize the plasmid before transfection into *P. berghei*.

For expression of AgoshRNAs in *Plasmodium*, I amplified a ~500 bp long region upstream of the *PbU6* promoter using the primers P11/P12 and ligated it into the *Xho*I/*Xma*I-digested vector pBAT-SIL6-MCS. The correct sequence of the 5'*PbU6* was confirmed by sequencing with primer P22. I then cloned the vector pBAT-SIL6-mCherry-*Pb*U6 (#1870) by integrating an mCherry gene (amplified with the primers P13/P14) via Gibson assembly into the *Swa*I/*BamH*I-digested pBAT-SIL6-MCS vector (Figure 51 A). Sequencing with P19/P20 verified the correct integration of mCherry.

The initial vector to integrate AgoshRNAs, pBAT-SIL6-*PbU6*int(V1) (#1871) was cloned by removing the left homology arm of SIL6 and the *HSP70* promoter from pBAT-SIL6-MCS-*Pb*U6 with *NgoMV*I/*BamH*I and inserting the annealed oligonucleotides P15/P16 (Figure 51 B). Since this construct design was inefficient to integrate AgoshRNAs due to an internal homologous region, I further improved the construct by replacing the *PbDHFR-TS* duplicate with a duplicate of the *3'PbDHFS-FPGS* region. To this end, I PCR-amplified the 3'*PbDHFS-FPGS* with primers P17/18, digested the PCR product with *Xho*I/*Bcl*I

and ligated it into the equally digested backbone. Subsequently, I removed the first 3'*PbDHFS-FPGS* via *BamHI/SacI* digest and ligation of the backbone to the annealed oligonucleotides P101/102, resulting in pBAT-SIL6-*PbU6*int V2 (#1872) (Figure 51 C).

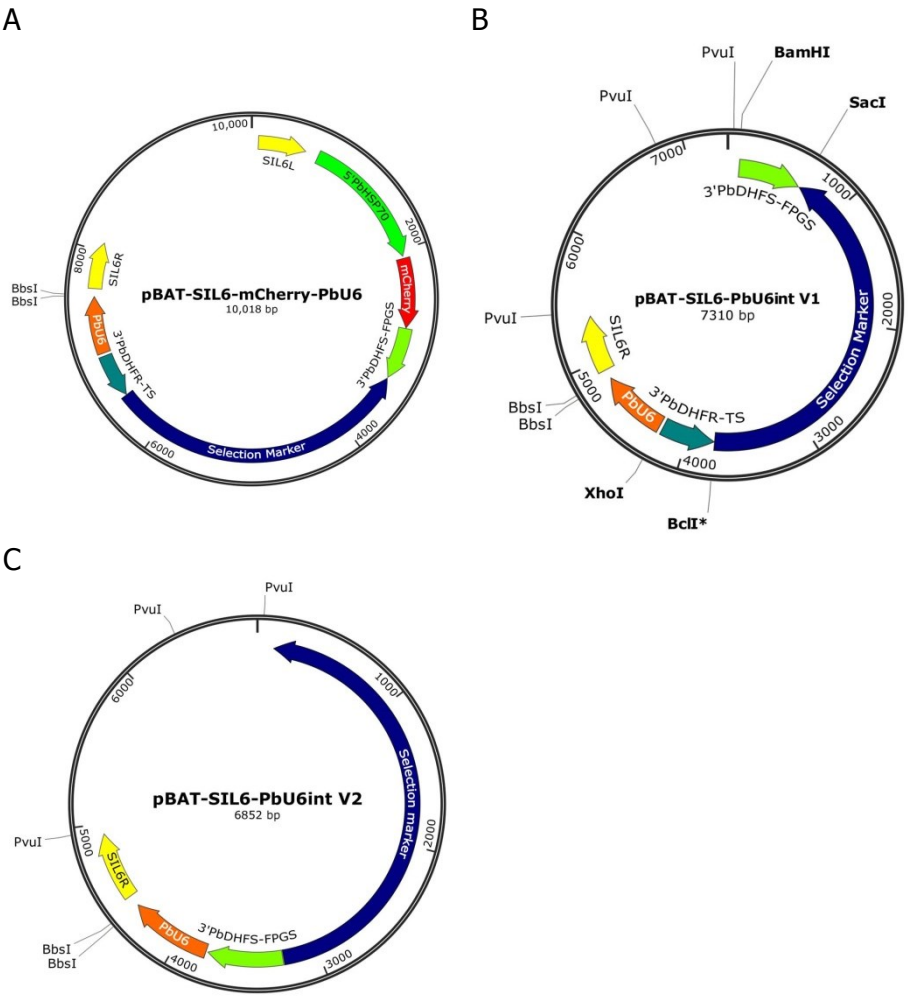

FIGURE 51: **Plasmid maps of AgoshRNA expression plasmids.** Indicated are all restriction sites that are used in subsequent cloning steps as well as the *Pvu*I site, which is used to linearize the plasmid before transfection into *P. berghei* (not applicable for (A), which is transfected circular).

AgoshRNAs were inserted into pBAT-SIL6-mCherry-*Pb*U6 or pBAT-SIL6-*PbU6*int V1 and V2 by *Bbs*I-digest and ligation to annealed oligonucleotides, as further described in the next Section. The sequence of the AgoshRNA was verified in each plasmid by sequencing with P23.

Design of AgoshRNAs

"AgoshRNA target sequences were identified using the siRNA wizard (http://www.invivogen.com/sirnawizard/design.php), searching for 19 nt target sequences that start with an A and end with a T. The antiparallel sequence (antisense) of this sequence then precedes a 5 bp long loop sequence that can consist either of the target sequence or of CTTCA, followed by the

sense sequence. To create an initial A-C and terminal G-U mismatch, the first and the last nucleotide of the sense sequence was substituted for a G and a C, respectively. The reverse oligonucleotide is formed of the reverse complement sequence. Initial and terminal overhangs were created to match the respective overhangs of the BbsI-digested target vector. For cloning behind the *Pb*U6 promoter, additional four Ts were added to the AgoshRNA to serve as a termination signal." (Hentzschel *et al*., 2017, manuscript in preparation).

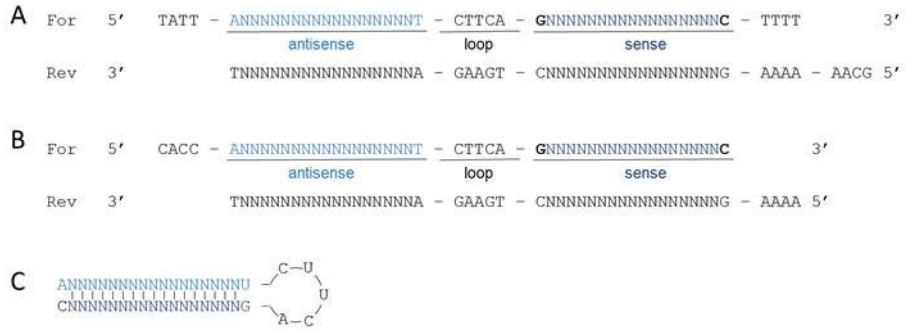

FIGURE 52: "**Design and structure of AgoshRNAs**. Depicted is the design of forward and reverse oligonucleotide for cloning of AgoshRNAs into a target vector. The sense strand equal to the mRNA target sequence is depicted in dark blue, the complementary antisense strand in light blue. The first and last nucleotide of the sense strand is swapped for a G and a C, respectively, to facilitate recognition and processing by Ago2. (A) Overhangs for cloning behind the *Pb*U6 promoter in pBAT-SIL6-*PbU6* or pBAT-SIL6-mCherry-*PbU6*. (B) Overhangs for cloning behind the *MmU6* promoter of pBS-sds-*CMV*-mCherry-*U6*. (C) The secondary structure of the transcribed AgoshRNA." (Hentzschel *et al.*, 2017, manuscript in preparation)

The design of the AgoshRNA is depicted in Figure 52. Sequences of all AgoshRNA-target sequences are listed in Table 21, which also includes the ID of the oligonucleotides that were designed for that particular RNA. The sequence of the oligonucleotides can be found in TABLE 18. "For *in vitro* screens, AgoshRNAs were cloned as annealed oligonucleotides into the *Bbs*I-digested pBS-sds-CMV-mCherry-*U6* kindly provided by Kathleen Boerner (University Hospital Heidelberg, Centre for Infectious Diseases, Virology). For expression in *Plasmodium*, AgoshRNAs were cloned in the *Bbs*I-digested pBAT-SIL6-mCherry-*PbU6* or pBAT-SIL6-*PbU6*int vector." (Hentzschel *et al*., 2017, manuscript in preparation).

TABLE 21: **Sequence of all AgoshRNAs**

AgoshRNA	Sequence (5' → 3')	Oligo-nucleotides	Plasmid
AgoshRscr	GTTATGGACACGAGAGTCC	P56/P57	#1889
		P66/P67	#1894
			#1895
			#1905
αGFP-AgoshR1a	GACGGGAACTACAAGACAC	P24/P25	#1878
αGFP-AgoshR2a	GAATGGAATCAAAGTTAAC	P26/P27	#1879
αGFP-AgoshR3a	GAAGATGGAAGCGTTCAAC	P28/P29	#1880
αGFP-AgoshR4a	AGGGTGAAGGTGATGCAAC	P30/P31	#1881
αGFP-AgoshR1b	AGGGTGAAGGTGATGCAAC	P40/P41	#1882
αGFP-AgoshR2b	ATGGAAGCGTTCAACTAGC	P42/P43	#1883
αGFP-AgoshR3b	AGTTGTCCCAATTCTTGTT	P44/P45	#1884
αGFP-AgoshR4b	ACATGGTCCTTCTTGAGTT	P46/P47	#1885
αGFP-AgoshR1c	AGGGTGAAGGTGATGCAAC	P48/P49	#1886
		P58/P59	#1891
αGFP-AgoshR2c	ATGGAAGCGTTCAACTAGC	P50/P51	#1887
		P60/P61	#1892
			#1897
αGFP-AgoshR3c	AGTTGTCCCAATTCTTGTT	P52/P53	#1888
		P62/P63	#1893
αGFP-AgoshR4c	ACATGGTCCTTCTTGAGTT	P54/P55	#1889
		P64/P65	#1894
αPPLP2-AgoshR1	AAGGAATGCGCTACTAGAT	P68/P69	#1898
αPPLP2-AgoshR2	AGGTAAGTACTCCTTCTAT	P70/P71	#1899
αPPLP2-AgoshR3	AATGATGGATACCTAGATT	P72/P73	#1900
αPPLP2-AgoshR4	AACACTCCCTTGGAATAGT	P74/P75	#1901
αExp1-AgoshR1	ACCAGCAGAACCAGTAATT	P76/P77	#1902
αExp1-AgoshR2	AGAAGCTATGCTCAAAGAT	P78/P79	#1903
αExp1-AgoshR3	ATGCCAAATCTTCAACAAT	P80/P81	#1904
αMSP1-AgoshR1	AGCCATTATTGCAACAAAT	P88/P89	#1909
αMSP1-AgoshR2	ACAAGCCTCATCACAATCT	P90/P91	#1910
αMSP1-AgoshR3	GGGTCAATCAGAAGAATAT	P92/P93	#1911

5.2.2 MICROBIOLOGY

Production and transformation of chemo-competent *E. coli*

One milliliter of an overnight culture of DH5α *E. coli* was used to inoculate 200 ml SOB medium and bacteria were grown at 37 °C, 180 rpm. When they reached an optical density of 0.5 at 600 nm, bacteria were cooled down on ice to 4 °C and pelleted for 15 min at 1800x g, 4 °C. Subsequent steps were all performed at 4 °C. The pellet was resuspended in 40 ml TFB I and incubated for 10 min on ice before a second centrifugation for 12 min at 1800x g and 4 °C. The pelleted cells were then resuspended in another 10 ml TFB II buffer and again incubated for 10 min on ice. Cells were then aliquoted à 50 µl, shock-frozen in liquid N_2 and stored at -80 °C.

For transformation, 50 µl freshly thawed chemo-competent *E. coli* were mixed with 5-10 µl ligation reaction and incubated for 30 min on ice before exposing them to a heat shock for 45 s at 42 °C. After another 2 min on ice, cells were plated on LB-amp plates and incubated overnight at 37 °C.

Production and transformation of electrocompetent *E. coli*

For the preparation of electrocompetent *E. coli*, 30 ml LB medium were inoculated with Mega X DH10B bacteria and cultured overnight at 37 °C. Four cultures of 400 ml LB media were inoculated with 5 ml pre-culture and incubated at 37 °C until the culture reached an optical density of 0.5-0.55 at 600 nm. Bacteria were then incubated on ice for 15 to 20 min before centrifugation for 15 min at 4 °C, 4424x g. The pellet was resuspended in a total volume of 60 ml ice-cold ddH_2O, and bacteria were transferred to four pre-cooked dialysis tubings (Typ 20/32 inch, wall thickness 0.02 mm) and dialyzed overnight against 8 l H_2O at 4 °C. Subsequently, bacteria were pelleted again for 15 min at 4 °C, 4424x g, and resuspended in sufficient 10 % glycerin to reach a final optical density of 1 at 600 nm. Cells were aliquoted, shock frozen in liquid N_2 and stored at -80 °C until electroporation.

For transformation, 2 µl of ligation mix were added to 30 µl electro-competent bacteria that were freshly thawed on ice. The mix was transferred to a 1 mm cuvette and electroporated in a Gene Pulser Xcell® electroporation system machine using the following settings: 1800 V, 25 µF and 200 W. After electroporation, bacteria were resuspended in 1 ml SOC medium and recovered for 1 h at 37 °C, shaking. Cells were pelleted by 2.5 min centrifugation at 2300x g; the pellet was resuspended in 100 µl SOC and then plated on LB-amp plates.

5.2.3 MOLECULAR BIOLOGY

Plasmid DNA preparations

Depending on the amount of plasmid needed, DNA was prepared in small, medium or large scale. For small-scale DNA preparation, 3 ml of ampicillin-containing LB-medium (50 µg/ml final concentration) were inoculated with *E. coli* carrying the desired plasmid and incubated at 37 °C for 8 h at 220 rpm or overnight at 180 rpm. Part of the culture (2 ml) was pelleted for 2.5 min at full speed, and the pellet was resuspended in 300 µl P1 resuspension buffer. Cells were lysed by addition of 300 µl P2 lysis buffer and incubation for 3 min at room temperature. Lysis was stopped by addition of 300 µl P3 neutralization buffer prior to centrifugation for 10 min at full speed. The supernatant (800 µl) was added to 600 µl isopropanol and then spun for 15 min at full speed. The DNA pellet was washed once with 70 % ethanol (5 min at full speed) and then air-dried before resuspension in 30 – 50 µl DNA.

For medium or large scale plasmid preparations, 40 – 80 ml or 200 ml LB-Amp medium, respectively, were inoculated with a single colony or 50 – 200 µl liquid culture of *E. coli* and incubated overnight at 37 °C and 180 rpm. Medium plasmid preparations were performed using the PureYield™ Plasmid Midiprep Kit (Promega) according to manufacturer's instruction. DNA was eluted in 500 – 800 µl ddH_2O. Large-scale plasmid preparations were performed using the NucleoBond® Xtra Maxi kit (Machery-Nagel) according to manufacturer's instruction, and the DNA pellet was resuspended in 1 – 2 ml ddH_2O. DNA concentrations were determined spectro-photometrically.

Polymerase chain reaction (PCR)

DNA fragments for cloning or diagnostic purposes were amplified via PCR. For all cloning reactions, PCRs were performed in 50 µl reactions using the Phusion Hot Start (HS) II polymerase (Thermo Fisher Scientific) according to manufacturer's instructions using approximately 10-100 ng template DNA. Final concentrations for each reaction were 1x HF buffer, 200 µM dNTPs, 1 µM forward and reverse primer, 3 % DMSO and 1 U Phusion polymerase. If no specific amplification was observed, the HF buffer was substituted by the GC buffer. Diagnostic PCRs were performed in 10 µl reactions with 0.5 to 2 µl gDNA as a template, using either the Phusion HS II polymerase as described above, but with GC buffer instead of HF buffer, or the OneTaq® 2x master mix (NEB). For the latter, the gDNA template was added to 1x master mix supplemented with 10 µM forward and reverse primer. A list of primer combinations used for diagnostic PCR and the polymerase used for each reaction can be found in Table 22. Subsequently, DNA was amplified using the cycling conditions listed in Table 23.

For the integration of AgoshRNAs, the "negative selection" PCR served as diagnostic PCR for the parental locus

*Pb*Ago2 *was genotyped with P97,* Pb$_{LISP2}$*Ago2 was genotyped with P21*

TABLE 22: **Primers and polymerases for diagnostic PCR**

Diagnostic PCR	Primer combination	Polymerase
Wild type locus	P95/P96	Taq
5' Integration	P96/P97 or P21*	Taq
3' Integration	P94/P95	Phusion HS II
Negative Selection	P98/P95	Phusion HS II

TABLE 23: **Cycling conditions of PCRs**

Polymerase		Phusion HS II				Taq	
Application		Non-*Plasmodium*		*Plasmodium*		Diagnostic PCR	
		T	**time**	**T**	**time**	**T**	**time**
Initial denaturation		98 °C	10 min	98 °C	10 min	95 °C	2 min
35 x	Denaturation	98 °C	10 s	98 °C	10 s	95 °C	15 s
	Annealing	60 °C	10 s	55 °C	10 s	55 °C	15 s
	Extension	72 °C	15 s/kb	68 °C	30 s/kb	60 °C	45 s/kb
Final extension		72 °C	10 min	68 °C	10 min	60 °C	10 min

Enzymatic digests of DNA

Restriction enzymes and corresponding buffers, except *Bbs*I (Fermentas), were purchased from NEB. For preparative digests, 3-10 µg plasmid DNA or 30 µl of purified PCR product and for analytical digests, 0.5-1 µg plasmid DNA were digested with 2-10 U restriction enzymes in buffers recommended by the manufacturer. Reactions were usually incubated for 2-4 h or overnight at 37 °C unless the enzyme required a different reaction temperature.

DNA agarose gel electrophoresis

DNA fragments were separated on agarose gels consisting of 1 % agarose (w/v) in TAE buffer and approximately 1 µl/ml ethidium bromide. DNA was mixed with 6x loading dye and loaded next to a standard marker for size determination. Electrophoresis was performed in TAE buffer at 80 – 150 V for approximately 20 to 30 min, depending on the separation required. DNA fragments in the gel were visualized by UV illumination. If necessary, DNA fragments were excised and purified using the QIAquick gel extraction kit (QIAGEN) according to manufacturer's instruction and eluted in 30 to 50 µl ddH_2O.

DNA clean-up

If the purification of DNA did not require a separation of differently sized fragments, *e. g*. in the case of linearized plasmids, or if DNA needed to be further concentrated in a smaller volume, the DNA sample was purified and concentrated over a column. For this, the DNA Clean& Concentrator-5 kit (Zymo Research) was used according to manufacturer's instructions.

Oligonucleotide annealing

For cloning inserts shorter than 100 nt in length, such as sh- or AgoshRNAs, complementary forward and reverse oligonucleotides were designed in such a way that the overhangs of the annealed dsDNA match the overhangs of the digested backbone. An annealing reaction consisted of forward and reverse oligonucleotide (5 µM final concentration) and 1x NEB buffer 2 in 50 µl ddH_2O. The reaction was heated to 95 °C for 5 min and then slowly cooled down to room temperature over the course of 2-3 h. Annealed oligonucleotides were diluted 1:200 in ddH_2O before ligation (see below).

Gibson Assembly

Large vectors were preferably assembled by Gibson assembly[345]. Inserts for the vectors were PCR-amplified (see p. 113) using primers that create a homology arm of about 20 to 40 nucleotides to the neighboring gene. The PCR products were gel-purified (see p. 114), followed by a digest with 1 µl *Dpn*I to remove remaining plasmid (30-60 min at 37 °C). The backbone was digested as required for the cloning strategy and also gel-purified. To improve purity and concentration, PCR fragments and backbone were additionally column-purified (see p. 114) and eluted in 10-15 µl H_2O before assembly. Vector and insert were mixed in a 1:3 molar ratio, in a total volume of 5 µl, before addition of 5 µl Gibson Assembly Master Mix (NEB). The reaction was incubated for 1-2 h at 40 °C. Subsequently, 1 µl of a 1:3 dilution was electroporated into *E. coli* as described on p. 112.

Ligation of DNA fragments

DNA fragments were ligated using the T4 DNA ligase. A reaction consisted typically of 100 – 300 ng total DNA in a molar ratio of 1:3 to 1:5 (backbone to insert), or of 100 ng digested plasmid and 1 µl of annealed oligonucleotides. Ligations were performed in 10 µl total volume containing 1 µl ligase and 1x supplied ligase buffer and incubated for either 0.5 to 2 h at room temperature or overnight at 16 °C. Subsequently, 1 µl (electroporation) or 5 – 10 µl (heat shock transformation) were used to transform *E. coli* (see also pp. 112, 112).

Ethanol precipitation

To increase the quality of DNA preparations or for transfections, DNA was purified by ethanol precipitation. To this end, NaAc (pH 5.3) was added to the DNA to a final concentration of 300 mM, and then DNA was precipitated by addition of 2.5 volumes 100 % ethanol. The DNA was incubated for 1 h at -80 °C or overnight at -20 °C and then pelleted by centrifugation for 15 min at 4 °C, full speed. The DNA pellet was washed with 500 µl 70 % ethanol (5 min at 4 °C, full speed). The DNA was then resuspended in varying amounts of ddH_2O, depending on the further application.

Preparation of genomic DNA

For diagnostic PCR, genomic DNA was isolated from mixed blood stage parasites using the Qiagen DNA Blood & Tissue kit according to manufacturer's instructions. DNA was eluted in 75 µl AE buffer supplied with the kit.

RNA extraction

HEK293T cells (seeded in 24-well format) or parasite samples were resuspended in 700 µl Qiazol. After addition of 140 µl chloroform, phases were separated by 15 min centrifugation at 4 °C, full speed. The upper, clear phase was transferred to a new tube, and 1.5 volumes ethanol were added. RNA was purified using the miRNeasy kit (QIAGEN) according to manufacturer's instructions. The protocol included an on-column DNase digest to remove remnants of DNA. RNA was eluted in 30 – 100 µl of nuclease-free ddH_2O.

cDNA synthesis

cDNA was synthesized from RNA using the Tetro cDNA synthesis kit (Bioline) as described in the supplied protocol but in a final volume of 10 µl. One reaction consisted of 6 µl RNA, 2 µl buffer, 0.5 µl random primer, 0.5 µl dNTPs, 0.5 µl RNase inhibitor and 0.5 µl reverse transcriptase. Within one experiment, equal RNA amounts of all samples were used, ranging from 100 ng to 2.4 µg RNA per reaction depending on the concentration of RNA available. If possible, cDNAs were prepared in parallel. A single –RT sample was prepared per experiment without RNase inhibitor and reverse transcriptase as a negative control, comprising equal amounts of all RNA samples. Reactions were incubated for 5 min at 25 °C, followed by 45 min at 42 °C and 5 min at 85 °C. cDNA was diluted 1:5 to 1:100 before quantitative reverse-transcription PCR (qRT-PCR), depending on the target assessed.

Quantitative reverse-transcription PCR (qRT-PCR)

Quantitative RT-PCR was performed on a StepOnePlus Real-Time PCR System (Applied Biosystems) using the Power SYBR® Green PCR Master Mix (Applied Biosystems). A single reaction consisted of 1.25 µl cDNA, 6.25 µl RT-Mix, 1.25 µl primer (10 µM of each forward and reverse primer) and 3.75 µl H_2O. All primer sequences for qRT-PCR are listed in TABLE 18 (P93 – P100). The PCR cycles for mammalian and for *Plasmodium* cycles are listed in Table 24. All reactions were followed by a standard melting curve to assess the formation of any by-products or primer dimers. The C_T values were determined by using the auto threshold feature of the software StepOne™ Software v2.3.

TABLE 24: **qRT-PCR cycling conditions**

	Target	Non-*Plasmodium*		*Plasmodium*	
		T	**time**	**T**	**time**
Initial denaturation		95 °C	10 min	95 °C	10 min
40 x	Denaturation	95 °C	15 s	95 °C	15 s
	Annealing	60 °C	15 s	55 °C	15 s
	Extension	72 °C	15 s	72 °C	15 s

The relative mRNA expression was calculated using the Pfaffl method, which adjusts for the different primer efficiencies[346]. The efficiency of the primer pairs was determined using a serial dilution of cDNA and plotting the CT value against the log(DNA dilution). From the slope m of the linear regression of this plot, the efficiency E is calculated as follows:

$$E = 10^{-\frac{1}{m}}$$

The mRNA expression of a GOI in a sample was calculated relative to its expression in an untreated control. First, the expression of both GOI and reference gene (ref) in the sample were normalized to their respective expression in an untreated control by calculating the ΔC_T.

$$\Delta C_T(GOI) = C_T(control) - C_T(sample)$$

Then, the expression of the GOI was normalized to the expression of the reference gene (ref), thereby adjusting for RNA input.

$$Relative\ mRNA\ expression = \frac{(E_{GOI})^{\Delta C_T(GOI)}}{(E_{ref})^{\Delta C_T(ref)}}$$

5.2.4 PROTEIN BIOCHEMISTRY

Preparation and quantification of protein samples

Schizont-enriched parasite protein samples (see p. 122) were incubated for 1 h on ice and vortexed every ten minutes. Parasite debris was removed by 2 min centrifugation at 4 °C and full speed. The protein concentration in the supernatant was measured using the Qbit® protein assay kit (Thermo Fisher Scientific) as described in the supplied protocol.

Sodium dodecyl sulfate polyacrylamide gel electrophoresis (SDS-PAGE) and Western blotting

Protein samples were denatured by adding required amounts of 2x or 6x SDS sample buffer and 5 min incubation at 95 °C. For the analysis of small proteins, *e. g.* GFP, 10 % SDS-gels, for the analysis of larger proteins, such as Ago2, 6 % SDS-gels were used for SDS-PAGE. The composition of these gels is found in Table 25. If the protein concentration of the sample was quantified before, 100 µg protein, else 15 µl sample were loaded on each lane. As a marker, 3 µl PageRuler™ Plus prestained protein ladder were loaded next to the samples. Gels were run in 1x TGS at 90 – 120 V for approximately 2 h until the loading dye ran out.

TABLE 25: **Composition of SDS-PAGE gels**

Components	Stacking gel	Resolving gel 6%	Resolving gel 10%
H_20	1.46 ml	2.9 ml	2.4 ml
40% acryl-bisacrylamide	0.25 ml	0.75 ml	1.25 ml
0.5M Tris (pH 6.8)	0.25 ml	-	-
1.5M Tris (pH 8.8)	-	1.25 ml	1.25 ml
10% SDS	20 µl	50 µl	50 µl
10% APS	20 µl	50 µl	50 µl
TEMED	2 µl	4 µl	2 µl

For semi-dry blotting, a stack consisting of four filter papers, a nitrocellulose membrane, the gel and another four filter papers was soaked in transfer buffer and placed in the electrophoretic transfer cell. The proteins were transferred onto the membrane by applying 150 mA for 1 h at 4 °C. Successful blotting was assessed by staining the membrane for 3 min in Ponceau S solution.

TABLE 26: **Dilutions and incubation settings for WB antibodies**

Antibody	Dilution	Incubation time
mouse-anti-GFP	1:300	2 h at RT
rat-anti-Ago2	1:300	Overnight at 4 °C
mouse-anti-HSP70	1:300	2 h at RT or overnight at 4 °C
mouse-anti-EXP1	1:1000	Overnight at 4 °C
HRP-anti-mouse HRP-anti-rat	1:10,000	1 h at RT

The membrane was washed with 1xTBS-T until the staining disappeared and blocked in 5 % milk/TBS-T (w/v) (blocking buffer) for 1 – 3 h at room temperature, shaking. Blots were then incubated with primary antibody diluted in blocking buffer, washed three times for 5 min in 1xTBS-T and incubated with secondary, HRP-conjugated antibody also diluted in blocking buffer. Dilutions

and incubation conditions of the individual antibodies can be found in Table 26. After another three times washing in 1x TBS-T, bands were revealed with ECL solutions by adding about 1 ml of a 1:1 mixture of the reagents on the blot and incubation for 3 min at room temperature. Blots were developed either at the ECL imager with the camera (ChemoCam, INTAS) or using a film developing machine (X-OMAT 2000 processor, KODAK).

5.2.5 CELL BIOLOGY

Standard maintenance of cell lines

Cell lines (HEK293T, Huh7, wt MEF, and Dicer$^{-/-}$ MEF) were cultured under standard conditions at 37 °C, 5 % CO_2, in DMEM complete. Huh7 cells were additionally supplemented with 1 % MEM-non-essential amino acids. Cells were split two- to three times a week, depending on growth and viability. For this, cells were washed once with PBS, detached by incubating for 3 min at 37 °C with 0.025 % trypsin (1 ml for a T175 flask) and resuspended in 10 ml pre-warmed DMEM complete. Between 1/5 and 1/20 of the final volume was used to inoculate a new flask. In order to seed a defined amount, cells were quantified by mixing 10 µl of cell suspension with 10 µl of trypan blue and counting in an automated cell counter. TABLE 27 lists the amount of cells seeded per well for different cell types and different formats.

Table 27: **Seeding density of different cell types**

		Cells per well		
Format	**Volume of medium**	HEK293T	WT or Dicer$^{-/-}$ MEF	Huh7
96-well	100 µl	$3.3*10^4$	$1*10^4$	-
24-well	0.5 ml	$1.4*10^5$	-	-
6-well	2 ml	$5*10^5$	-	-
8-well LabTek	0.25 ml	-	-	$4*10^4$

Transfection with lipofectamine 2000

For flow cytometric analysis, HEK293T cells were seeded in 96-well format one day before lipofectamine 2000-mediated transfection. For this, 200 ng total DNA (equal parts of co-transfected plasmids) were mixed with 25 µl DMEM without supplements. In parallel, a Lipofectamine mix consisting of 0.5 µl Lipofectamine in 25 µl DMEM was prepared and incubated for 5 min at room temperature. The DNA- and Lipofectamine mix were combined and incubated for 30 min at RT before adding the total 50 µl to the cells. For qRT-PCR, transfections were performed in a 24-well format, using the same protocol, but 500 ng DNA and 1 µl Lipofectamine. Cells were usually analyzed two days post transfection.

Flow cytometry

In preparation for flow cytometry analysis, cells seeded in a 96-well format were washed once with PBS, then detached with 30 µl 0.025 % Trypsin/EDTA per well and 7 min incubation at 37°C. Cells were resuspended thoroughly after addition of 170 µl 1 % BSA/PBS per well. Flow-cytometric analysis was performed on a Cytomics FC500MPL analyzer (Beckman Coulter), gating for living cells (Forward scatter $(FSC)^{high}$/Side scatter $(SSC)^{high}$ population) and using non-transduced or non-transfected cells as a negative control to set up the flow cytometer. The mCherry- and the GFP-signal were compensated using single-transfected/transduced cells. The mCherry-positive events were gated, and median GFP fluorescence of this population was calculated using the software Flowing Software.

5.2.6 VIROLOGY

Crude lysate production of AAV vectors

To produce crude lysates of AAVs, HEK293T cells were seeded in a 6-well format ($5*10^5$ cells per well) and transfected one day later using polyethyleneimine (PEI)-based transfection. Per well, 2.6 µg DNA consisting of equal parts of Adeno-helper plasmid[347], a plasmid encoding the capsid AAV-DJ[277] and the AAV-genome were mixed with 49 µl H_2O and 49 µl NaCl (300 mM). A separate mix consisted of 22 µl PEI solution, 49 µl NaCl (300 mM), and 27 µl H_2O. The DNA- and the PEI-mix were mixed, vortexed and incubated for 10 min at room temperature, before adding the mixture dropwise to the cells. Cells were incubated for three days at 37 °C and 5% CO_2.

Crude lysates were harvested by removing media from the cells and washing the wells once with 500 µl PBS. Cells were resuspended in 1 ml PBS and pelleted by 10 min centrifugation at 1500x g. The pellet was resuspended in 500 µl PBS and cells were lysed through five freeze-thaw cycles (alternating 2 min in liquid N_2 and 5 min in a 37 °C-water bath). Cells were sonicated for 1 min, and cell debris was removed by pelleting for 10 min at full speed. The supernatant containing the AAV was then transferred to a fresh tube and stored at -80 °C until transduction.

Transduction of cells

Wild type (wt) MEF cells and $Dicer^{-/-}$ MEF cells were seeded in a 96-well format ($1*10^5$ cells/well) one day prior to transduction. Cells were transduced by adding 5 µl crude lysate supernatant (see above) of each AAV. Cells were analyzed four days after transduction by flow cytometry.

5.2.7 PARASITOLOGY

Maintenance of mice

"All animal experiments were performed according to European regulations concerning FELASA category B and GV-SOLAS standard guidelines. Animal experiments were approved by German authorities (Regierungspräsidium Karlsruhe, Germany), § 8 Abs. 1 Tierschutzgesetz (TierSchG) under the license G-260/12 and were performed according to National and European regulations." (Hentzschel *et al.*, 2017, manuscript in preparation) Female inbred C57BL/6J or outbred NMRI mice were purchased from Janvier at the age of 6 to 8 weeks. Mice were kept under specified pathogen-free (SPF) conditions at a constant room temperature of 22 °C, 50 - 60 % humidity, and a 12/12 h light/dark cycle within the animal facility of the Heidelberg University (Interfakultäre Biodedizinische Forschungseinrichtung). Animals were fed with standard dry pellet food.

Maintenance of *P. berghei* blood stages

Mice were inoculated with *P. berghei* by either i.p. injection of cryopreserved parasites (see below) or i.v. or i.p. administration of parasite-infected blood, depending on the parasitemia of the donor blood and the parasite growth required. Parasitemia of the infected mice was monitored as described below. Blood containing parasites was collected either from the tail vein or by bleeding anesthetized mice through puncture of the inferior *vena cava*, depending on the amount of blood needed, using heparinized syringes.

Determination of parasitemia

Parasites in the blood of infected mice were detected by smearing a drop of tail blood onto a glass slide, fixing it for approximately 5 s in methanol and staining the dried slide in 10 % Giemsa/H_2O. Slides were microscopically examined, using the 100x objective with immersion oil. For a rough estimation of the parasitemia, the number of infected erythrocytes (#iRBCs) was counted in 10 to 20 fields of view (FOV). For a precise determination of parasitemia, *e. g.* for assessment of parasite growth or limited dilutions, sufficient FOV were examined to observe at least 30 parasites (at most 50 FOV). In all cases, the number of erythrocytes (#RBCs) was determined in every tenth FOV. The parasitemia is thus calculated as follows:

$$Parasitemia\ (in\ \%) = \frac{\#iRBCs}{\#RBCs * 10} * 100\%$$

Cryopreservation of *P. berghei*

For long-term storage of parasites, 100 µl of freshly isolated blood with at least 1 % parasitemia was mixed with 200 µl freezing solution and immediately stored in liquid N_2.

Purification of blood-stage parasites

If purified blood-stage parasites were needed, *e. g.* for genotyping, leucocytes were removed from freshly isolated parasite-infected blood by size-exclusion over self-made cellulose columns. To prepare the columns, the plunger was removed from a 5 ml syringe, and the syringe was filled with a small amount of cotton (~ 3 mm), about 4 cm of CF-11 cellulose powder and on top ~ 0.5 cm glass beads. Columns were equibrilated with 5 ml PBS before loading the blood. Leucocyte-depleted blood was eluted in 15 ml PBS, pelleted by 8 min centrifugation at 400x g and erythrocytes were lysed in 0.2 % Saponin/PBS (w/v). Parasites were pelleted by a second centrifugation (8 min, 1400x g) and washed once more with 1 ml PBS. Parasites were resuspended in 200 µl PBS for gDNA isolation or in 30 – 50 µl RIPA buffer for Western blotting.

Preparation of gametocyte-enriched parasites

In order to increase gametocytaemia in infected mice, NMRI mice were pretreated with phenylhydrazine (2 µg in 200 µl PBS, i.p.) to stimulate reticulocytosis[294]. Two days later, mice were i.v. infected with $2*10^6$ iRBC. Exflagellation assays as well as collecting blood for RNA extraction was performed four days later. Gametocyte-enriched parasites were purified from whole blood as described above and resuspended in 700 µl Qiazol for subsequent RNA extraction.

Preparation of schizont-enriched parasites

Schizont-enriched parasite samples were prepared as described previously[303]. In brief, *Plasmodium*-infected mice were bled via the inferior *vena cava* using a heparinized needle. Blood cells were washed once with 10 ml pre-warmed transfection medium by centrifugation for 8 min, 400x g. The pellet was resuspended in 15 ml pre-warmed transfection medium, transferred to a 25 cm^2 cell-culture flask and parasites were cultured for 16 to 18 h at 37 °C and 5 % CO_2, 5% O_2. The next day, the culture was examined for the presence of schizonts via Giemsa-stained smear. If positive, parasites were transferred to a tube, underlaid with 12 ml of 55 % Nycodenz/PBS (v/v), and separated from uninfected red blood cells via centrifugation for 25 min at 180x g, without brake. Infected RBCs were collected from the intermediate phase forming at the top of the Nycodenz layer using a Pasteur pipette and washed in a total volume of 35 ml transfection medium (8 min, 400x g). The pellet containing schizont-enriched parasites and leukocytes was then resuspended depending on the purpose: In 30-60 µl RIPA buffer for protein extraction or in 1 ml transfection medium for transfection (for the latter, the schizont pellet was divided up according to the number of transfections required).

Transfection of *P. berghei*

P. berghei parasites were transfected following a previously published protocol[303]. Per transfection, 10 µg linearized or circular DNA (for stable integration or episomal expression, respectively) was ethanol-precipitated as described on p. 115 and resuspended in 10 µl PBS. The DNA was then mixed with 100 µl Nucleofector solution and stored on ice until transfection. Schizont-enriched samples (prepared as described above) were resuspended in 1 ml transfection medium per transfection, split to individual tubes (1 tube per transfection) and pelleted for 20 sec at full speed. The schizont pellet was resuspended in the DNA-Nucleofector Mix and transferred to an electroporation cuvette. The sample was electroporated on an Amaxa gene pulser, with the program U033. After addition of 50 µl transfection medium, the transfected schizonts were i.v. injected into one NMRI mouse. One day after transfection, the drinking water of mice was supplemented with 7 mg/L pyrimethamine, pH 3-5. Giemsa-stained blood smears of the mice were monitored every second day starting day 7 post-transfection for the appearance of parasites. When parasitemia reached over 1-2 %, mice were bled, and parasites were genotyped.

Generation of clonal transgenic *P. berghei* lines by limiting dilution

If genotyping revealed the correct integration of a construct in a subpopulation of the transfected parasites, single clones of these transgenic parasites were obtained by limiting dilution. For this, the blood of a donor mouse (with a parasitemia between 0.1 and 1 %) was diluted in RPMI medium in a serial dilution comprising six 1:10 dilutions (resulting in a final $1{:}10^6$ dilution). Assuming an RBC density in the undiluted blood of $7 * 10^6$ RBCs/µl, the concentration of iRBCs in the final $1{:}10^6$ dilution can be calculated from the parasitemia P%. The volume that statistically contains a single iRBC is then determined as follows:

$$V(1\ iRBC) = \frac{1}{7 * 10^6 \frac{RBC}{\mu l} * 10^{-6} * \frac{P\%}{100}} = \frac{1\ \mu l}{7 * \frac{P\%}{100}}$$

The number of mice injected for the limiting dilution depended on the abundance of the transgenic parasites in as estimated from the genotyping.

Four to twenty mice were i.v. injected with statistically one iRBC in a final volume of 100 µl. Approximately half of the mice became parasite-positive around 7 days post-injection, and parasites were genotyped.

Recycling of the selection marker in transgenic parasites

If required, the resistance marker was subsequently recycled from a single clone by administering 5-FC (1 µg/ml) to the drinking water of mice infected with a parasitemia of 1 %[348]. Parasitemia then dropped below the detection limit and resurged about 5 to 7 days later. Upon reaching a parasitemia over 1 %, mice were bled, and parasites were genotyped. A single parasite clone that recycled the resistance marker was obtained by another limiting dilution.

Visualization and quantification of exflagellation

"To increase gametocytaemia, mice were pretreated with phenylhydrazine (2 µg per mouse in 200 µl PBS, intraperitoneally (i.p.) injected)[294]. Two days later, mice were infected i.p. with AgoshRNA-transfected *Pb*Ago2. Four to five days after *Plasmodium* infection, a drop of blood was collected from tail veins, mixed with 2 µl of xanthurenic acid (50 µM), covered with a coverslip and incubated for 12 min at room temperature. Exflagellations were observed under a 40x microscope and scored for 2.5 min according to the presence of free flagella (normal) or one or two thick superflagella (abnormal). This procedure was repeated until at least 100 exflagellations per *Pb*Ago2 + AgoshRNA line could be observed. To quantify exflagellation rates, PHZ-pretreated mice were infected intravenously with $2x10^6$ iRBC, and at least three exflagellation assays per mouse were performed 4 days post infection. Fields of view were counted additionally to determine exflagellation per field of view. Exflagellation rates were always normalized to the exflagellation rate of *Pb*Ago2 + AgoshRscr determined in parallel." (Hentzschel *et al.*, 2017, manuscript in preparation).

Breeding of *Anopheles stephensi* mosquitoes

Anopheles stephensi mosquitoes were reared at 28°C and 80% humidity under a 14 h/10 h light/dark cycle and fed on 10% sucrose/PABA solution. Adult mosquitoes were fed on parasite-infected mice as described below and maintained at 21°C and 80% humidity

Transmission of *P. berghei* to mosquitoes and back

Prior to the characterization of a new *P. berghei* line, parasites were first passaged once through the mosquito to avoid that long blood-stage passage selects for parasites that are unable to transmit. To infect mosquitoes with *P. berghei*, two NRMI mice were intravenously injected with $1*10^6$ iRBC. Four days later, mice were anesthetized by i.p, injection of 80 – 120 µl Ketamine/Xylazine (K/X) and mosquitoes were allowed to feed on the mice for 15 to 20 min. The feeding was repeated on the next day. From day 17 post-feeding, *P. berghei* sporozoites are found in salivary glands of mosquitoes, and the parasites can be transmitted back to the mammalian host. To infect mice via the natural route ("bite-back infection"), C57BL/6J mice were anesthetized by i.p. injection of 80 µl K/X per mouse, and placed on top of a *P. berghei*-infected mosquito cage. The mosquitoes were allowed to feed on the mice for about 10 to 15 min. Mice were monitored for the appearance of parasites by Giemsa-stained blood smears and usually bled 5 to 6 days post-infection to collect parasites and prepare cryostabilates.

Isolation of midgut oocysts

The infectivity of a mosquito cage was estimated by isolating the midguts of 10 – 20 mosquitoes on day 10 to 14 post-infection. Dissection was done in 3 % RPMI/BSA (w/v) under a stereomicroscope using needles. The number of green-fluorescent oocysts per midgut was estimated by examining the midguts under a fluorescent microscope. Midguts were classified with the following categories: 0; 1-10; 11-30; 31-100 and >100 oocysts/midgut.

Isolation and purification of salivary gland sporozoites

To isolate sporozoites, salivary glands of female mosquitoes were dissected 18 days after the blood meal. Salivary glands were collected in 3 % BSA/RPMI (w/v) and smashed using a pestle. Debris was removed by a first centrifugation for 3 min at 100x g, 4 °C, and the supernatant was carefully collected. After addition of about 30-100 µl 3 % BSA/RPMI (w/v) to the pellet, it was smashed a second time, and the centrifugation was repeated. The supernatant of the first and the second centrifugation were pooled, and an aliquot was diluted 1:10 to count the sporozoite numbers in a Neubaur counting chamber. Sporozoites were then used for *in vitro* or *in vivo* experiments as described below or pelleted by 10 min centrifugation at full speed, 4 °C and resuspended in 30 µl RIPA buffer for Western blotting.

For determining the sporozoite-induced blood stage growth, 10^4 sporozoites were diluted to a total volume of 100 µl in RPMI medium and intravenously administered to C57BL/6J mice. Mice were monitored from day 3 to day 14 post-infection via Giemsa-stained blood smears

In vitro culture of liver stages and immunofluorescence

For monitoring liver stage development *in vitro*, Huh7 cells were seeded in an 8-well labtek slide as described on p. 119. The next day, the medium was removed and 10^4 freshly isolated sporozoites in 100 µl RPMI were added to each well. Sporozoites were allowed to invade for 1.5 h at 37 °C and then removed by washing the cells once with 500 µl PBS per well. After addition of 250 µl medium per well, cells were incubated for 48 h at 37 °C, 5% CO_2.

TABLE 28: **Dilutions and incubation settings for IF antibodies**

Antibody	Dilution
rabbit-anti-GFP	1:125
Mouse-anti-HSP70	1:100
Mouse-anti-FLAG	1:125
Rat-anti-EXP1	1:33
Alexa-488-anti-mouse Alexa-546-anti-rat	1:300

Liver stages were fixed by replacing the medium with 400 µl/well ice-cold methanol and 10 min incubation at RT. After washing twice with 400 µl/well 1 % FCS/PBS (v/v), unspecific binding partners were blocked with 400 µl/well 10 % FCS/PBS (v/v) (30 min at 37 °C or overnight at 4 °C). The blocking solution was then replaced by 100 µl/well primary antibody, which was incubated for at least 45 min at 37 °C. Cells were again washed twice with 400 µl/well 1 % FCS/PBS (v/v) and then incubated with 100 µl secondary antibody for at least 45 min at 37 °C. The dilutions of the primary and secondary antibodies used are listed in Table 28. Five minutes prior the end of the incubation time, Hoechst was added to a final dilution of 1:10,000. Cells were washed a final time three times with 400 µl/well 1 % FCS/PBS (v/v), then mounted with 10 % glycerol/PBS (v/v) and sealed with nail polish.

5.2.8 MICROSCOPY AND IMAGE PROCESSING

All microscopy to quantify GFP fluorescence or to image liver stages for size measurements has been done on the Axiovert 200M widefield fluorescence microscope (Zeiss). Within one experiment, settings were kept constant to allow comparison between samples (Table 29). All images, except for HEK293T cells (10x objective), were taken with the 63x objective and a 1.0 optovar. Some representative images of liver stages were taken with a 1.6 optovar.

TABLE 29: **Exposure times (ms) and gain settings**

	Green	**Red**	**Blue**	**DIC**	**Gain**
HEK293T	80	500	-	-	1
Blood stages	200	100	1000	20	3
Oocysts	200	-	-	20	1
Sporozoites	200	-	-	20	3
Liver stages*	10-200	100	1000	20	1

*Settings adjusted depending on the quality of the staining

To quantify the GFP fluorescence of individual parasites, images were opened in FIJI and a single parasite was selected. Then, the following macro was run:

```
run("Duplicate...", "title=[12] duplicate");
setMinAndMax(0, 65536);
run("16-bit");
run("Duplicate...", "title=[background mask] duplicate");
run("Median...", "radius=5");
run("Auto Threshold", "method=Huang white");
run("Divide...", "value=255.000");
run("Duplicate...", "title=[sample mask] duplicate");
selectWindow("background mask");
run("Multiply...", "value=255.000");
run("Invert");
run("Divide...", "value=255.000");
imageCalculator("Multiply create", "12","sample mask");
run("Duplicate...", "title=[sample] duplicate");
imageCalculator("Multiply create", "12","background mask");
run("Duplicate...", "title=[background] duplicate");
selectWindow("sample");
run("Measure");
run("Subtract...", "value=1");
run("Measure");
selectWindow("background");
run("Measure");
run("Subtract...", "value=1");
run("Measure");
selectWindow("Result of 12");
close();
selectWindow("Result of 12");
close();
selectWindow("background mask");
close();
selectWindow("background");
close();
selectWindow("sample mask");
close();
selectWindow("12");
close();
wait(1000)
selectWindow("sample");
close();
```

The macro separates the parasite from the background by thresholding and then determines the integrated fluorescence for each. It then subtracts 1 from the value of every pixel of both background and parasite and repeats the intensity measurement. Subtraction of the second from the first value thus yields the size of both the parasite and the background in pixels. Dividing the total intensity by the size in pixel then yields the average fluorescence per pixel for both background and parasite. The background intensity per pixel is subtracted from the parasite intensity per pixel to remove the background signal. Multiplying the background-corrected parasite intensity per pixel again

with the size of the parasite in pixel finally yields the integrated fluorescence intensity of the parasite.

For determining the liver stage size, a macro was used that first converts the first channel (green, usually Hsp70 signal) of the .zvi output file and saves it as a .tiff file. In a second step, it then thresholds the .tiff image and determines the size of individual particles (corresponding to an individual liver stage) by using the ImageJ command “Analyze Particles…”. The macro is depicted below.

```
directory = getDirectory("Choose input files");
fileList = getFileList(directory);
outputDirectory = getDirectory("Choose output directory");

run("Bio-Formats Macro Extensions");
setBatchMode(true);

for (i=0; i<fileList.length; i++) {
  file = directory + fileList[i];

    Ext.setId(file);
    Ext.getImageCount(imageCount);
    for (image=0; image<1; image++) {
      Ext.openImage("", image);
      Ext.getPixelsPhysicalSizeX(sizeX);
      outFile = outputDirectory + fileList[i] + "-" + image + ".tiff";
      saveFile(outFile);
      run("Set Scale...", "distance=1 known=sizeX unit=µm");
      save(outFile);
      close();
    }
    Ext.close();
}

fileList = getFileList(outputDirectory);

for (i=0; i<fileList.length; i++) {
  tifffile = outputDirectory + fileList[i];
  open(tifffile);
       run("Auto Threshold", "method=Huang white");
       run("Invert");
       run(
"Analyze Particles...",
"size=10-Infinity show=Overlay display exclude summarize"
);
       close();
}

showStatus("Finished.");
setBatchMode(false);

function saveFile(outFile) {
   run("Bio-Formats Exporter", "save=[" + outFile + "] compression=Uncompressed");
}
```

5.2.9 RNA-SEQ

Sample preparation

To prepare samples for RNA-Seq, mice were bled at a parasitemia of around 1-2 % and leucocytes were removed from the blood by column filtration as described on p. 122. Over-night cultures were prepared as on p. 122. To ensure highest-possible synchrony of the cultures, the incubation was always started at 1.30 pm and samples were harvested 18 h later (7.30 am). Blood from the culture was pelleted for 8 min at 1500 rpm, and the blood was resuspended in 3 ml RLT buffer supplemented with 1% β-Mercaptoethanol.

RNA-Seq library preparation

The preparation of the RNA library and RNA-Seq has been done by Sabine Fraschka, Radboud University, Nijmwegen, The Netherlands. The analysis of the data was done by Sabine Fraschka and Richard Bartfái, Radboud University, Nijmwegen, The Netherlands.

"Total RNA was extracted using the RNeasy Mini Kit (Qiagen, #74106; including on-column DNase treatment and RNA clean-up) and PolyA-selected using the Oligotex mRNA Mini Kit (Qiagen, #70022) according to manufacturer's instructions. PolyA-selected RNA was checked for genomic DNA contamination via qPCR and additionally treated twice with TURBO DNase (Ambion, #AM2238) to eliminate remaining genomic DNA. 2 µg of PolyA-selected total RNA equivalent were fragmented by alkaline hydrolysis (5x fragmentation buffer: 200 mM Tris acetate pH 8.2, 500 mM potassium acetate, 150 mM magnesium acetate) for 2 min at 85 °C in 250 µl volume as described [previously][349], precipitated and further processed for strand-specific RNA-seq as described [previously][350]. In short, first strand cDNA synthesis was performed using AT-corrected Random N9 primers and in presence of 0.2 µg Actinomycin D to prevent unwanted DNA-dependent second strand cDNA synthesis, and during second strand synthesis dTTPs were replaced with dUTPs. For each sequencing library, 5 ng of double stranded cDNA were end repaired, extended with 3' A-overhangs, ligated to barcoded NextFlex adapters (Bio Scientific, #514122) and treated with USER enzyme (NEB, #M5505L) to induce dUTP-dependent second strand-specific degradation. Subsequently, libraries were amplified using KAPA HiFi HotStart ready mix (KAPA Biosystems, #KM2602), NEXTflex primer mix (Bio Scientific, #514122) and the following PCR program: 98 °C for 2 min; 4 cycles of 98 °C for 20 sec, 62 °C for 3 min; 62 °C for 5 min. Amplified libraries were gel size-selected for 300 – 400 bp using 2% E-Gel Size Select agarose gels (Invitrogen, #G6610-02) and amplified for additional 8 cycles as described above. Adapter dimer depletion and DNA clean-up were performed using Agencourt AMPure XP beads (Beckman Coulter, #A63880) in a 1:1 library beads ratio." (Hentzschel *et al*., 2017, manuscript in preparation)

High throughput sequencing and data analysis

"Strand-specific RNA-seq libraries were sequenced on the Illumina NextSeq 500 system to obtain 75bp single-end reads (TruSeq SR Cluster Kit v2). 75bp reads were mapped against the annotated *P. berghei* ANKA transcriptome from PlasmoDB version 26 and the GFP coding sequence encoded by the *Pb*GFPcon parasite line using BWA samse (version 0.7.12-r1039). Single-end RNA reads were filtered to mapping quality ≥15 (samtools version 1.2) and only uniquely mapped reads (between 5.3 and 8.1 million reads) were used for further analysis. To assess RNA abundance of each gene, only reads aligned to the sense strand (FLAG16) were taken into account. Tags were counted for all transcripts (excluding mitchochondrial RNA, apicoplast RNA and RNAs without PolyA tail such as rRNAs and tRNAs) and offset by +1 to avoid division by zero while calculating fold change in expression. Transcript counts were normalized to the amount of reads per kb per million mapped reads (RPKM). Correlations between datasets were calculated and plotted with R studio (R version 3.2.2, standard packages)." (Hentzschel *et al*., 2017, manuscript in preparation)

5.2.10 STATISTICAL ANALYSIS

"Statistics are no substitute for judgment"

~ Henry Clay (1777 – 1852)

All statistical analysis was done using the software GraphPad Prism 5.0. Experiments were usually performed in biological duplicates or triplicates on separate occasions, with three technical replicates each. Where appropriate, data was compared to a control using a standard t-test (if the experiment included only two groups) or a one-way ANOVA (if the experiments included three or more groups). The statistical analysis used for each data analysis is indicated in the respective figure legend.

Bibliography

6

" If I have seen further, it is by standing on the shoulders of giants."[351]

~ Isaak Newton (1642-1726)

1. Laveran, A. *Paludism*. (New Sydenham Society, 1893). doi:10.5962/bhl.title.106948

2. Reiter, P. From Shakespeare to Defoe: Malaria in England in the Little Ice Age. *Emerging Infectious Diseases* **6,** 1–11 (2000).

3. World Health Organization. WHO | World Malaria Report 2015. *WHO* (2016).

4. World Health Organization. *Guidelines for the treatment of malaria*. (2015).

5. RTS, S. C. T. P. Efficacy and safety of RTS,S/AS01 malaria vaccine with or without a booster dose in infants and children in Africa: final results of a phase 3, individually randomised, controlled trial. *Lancet* **386,** 31–45 (2015).

6. Dondorp, A. M. *et al.* Artemisinin resistance in Plasmodium falciparum malaria. *N. Engl. J. Med.* **361,** 455–67 (2009).

7. Ashley, E. A. *et al.* Spread of Artemisinin Resistance in Plasmodium falciparum Malaria. *N. Engl. J. Med.* **371,** 411–423 (2014).

8. Ariey, F. *et al.* A molecular marker of artemisinin-resistant Plasmodium falciparum malaria. *Nature* **505,** 50–55 (2013).

9. Olotu, A. *et al.* Seven-Year Efficacy of RTS,S/AS01 Malaria Vaccine among Young African Children. *N. Engl. J. Med.* **374,** 2519–2529 (2016).

10. Etymologia: Anopheles. *Emerg. Infect. Dis.* **18,** 1511–1511 (2012).

11. Craig, A. G. *et al.* The role of animal models for research on severe malaria. *PLoS Pathog.* **8,** e1002401 (2012).

12. Wykes, M. N. & Good, M. F. What have we learnt from mouse models for the study of malaria? *Eur. J. Immunol.* **39,** 2004–2007 (2009).

13. Amino, R. *et al.* Quantitative imaging of Plasmodium transmission from mosquito to mammal. *Nat. Med.* **12,** 220–224 (2006).

14. Coppi, A. *et al.* Heparan Sulfate Proteoglycans Provide a Signal to Plasmodium Sporozoites to Stop Migrating and Productively Invade Host Cells. *Cell Host Microbe* **2,** 316–327 (2007).

15. Tavares, J. *et al.* Role of host cell traversal by the malaria sporozoite during liver infection. *J. Exp. Med.* **210,** 905–15 (2013).

16. Baer, K. *et al.* Kupffer cells are obligatory for Plasmodium yoelii sporozoite infection of the liver. *Cell. Microbiol.* **9,** 397–412 (2007).

17. Frevert, U. *et al.* Intravital Observation of Plasmodium berghei Sporozoite Infection of the Liver. *PLoS Biol.* **3,** e192 (2005).

18. Mota, M. M. *et al.* Migration of Plasmodium sporozoites through cells before infection. *Science (80-.).* **291,** 141–4 (2001).

19. Sá e Cunha, C. *et al.* Plasmodium berghei EXP-1 interacts with host Apolipoprotein H during Plasmodium liver-stage development. *Proc. Natl. Acad. Sci.* 201606419 (2017). doi:10.1073/pnas.1606419114

20. Itoe, M. A. *et al.* Host cell phosphatidylcholine is a key mediator of malaria parasite survival during liver stage infection. *Cell Host Microbe* **16,** 778–786 (2014).

21. Graewe, S., Stanway, R. R., Rennenberg, A. & Heussler, V. T. Chronicle of a death foretold: Plasmodium liver stage parasites decide on the fate of the host cell. *FEMS Microbiol. Rev.* **36,** 111–130 (2012).

22. Kaushansky, A. & Kappe, S. H. Selection and refinement: the malaria parasite's infection and exploitation of host hepatocytes. *Curr. Opin. Microbiol.* **26,** 71–78 (2015).

23. Lang, K. S. *et al.* Immunoprivileged status of the liver is controlled by Toll-like receptor 3 signaling. *J. Clin. Invest.* **116,** 2456–2463 (2006).

24. Liehl, P. *et al.* Host-cell sensors for Plasmodium activate innate immunity against liver-stage infection. *Nat. Med.* **20,** 47–53 (2014).

25. Nussenzweig, R. S., Vanderberg, J., Most, H. & Orton, C. Protective immunity produced by the injection of x-irradiated sporozoites of plasmodium berghei. *Nature* **216,** 160–162 (1967).

26. Seder, R. A. *et al.* Protection against malaria by intravenous immunization with a nonreplicating sporozoite vaccine. *Science* **341,** 1359–65 (2013).

27. Mueller, A.-K., Labaied, M., Kappe, S. H. I. & Matuschewski, K. Genetically modified Plasmodium parasites as a protective experimental malaria vaccine. *Nature* **433,** 164–7 (2005).

28. Mordmüller, B. *et al.* Sterile protection against human malaria by chemoattenuated PfSPZ vaccine. *Nature* **58,** 7250–7 (2014).

29. Bijker, E. M. *et al.* Novel approaches to whole sporozoite vaccination against malaria. *Vaccine* **33,** 7462–7468 (2015).

30. Sturm, A. *et al.* Manipulation of host hepatocytes by the malaria parasite for delivery into liver sinusoids. *Science* **313,** 1287–90 (2006).

31. Graewe, S. *et al.* Hostile takeover by plasmodium: Reorganization of parasite and host cell membranes during liver stage egress. *PLoS Pathog.* **7,** e1002224 (2011).

32. Tarun, A. S. *et al.* Quantitative isolation and in vivo imaging of malaria parasite liver stages. *Int. J. Parasitol.* **36,** 1283–1293 (2006).

33. Baer, K., Klotz, C., Kappe, S. H. I., Schnieder, T. & Frevert, U. Release of hepatic Plasmodium yoelii merozoites into the pulmonary microvasculature. *PLoS Pathog.* **3,** 1651–1668 (2007).

34. Koch, M. & Baum, J. The mechanics of malaria parasite invasion of the human erythrocyte - towards a reassessment of the host cell contribution. *Cell. Microbiol.* **18,** 303–450 (2016).

35. Gilson, P. R., Chisholm, S. A., Crabb, B. S. & de Koning-Ward, T. F. Host cell remodelling in malaria parasites: a new pool of potential drug targets. *Int. J. Parasitol.* **47,** 119–127 (2017).

36. de Koning-Ward, T. F. *et al.* A newly discovered protein export machine in malaria parasites. *Nature* **459,** 945–9 (2009).

37. Leech, J. H., Barnwell, J. W., Miller, L. H. & Howard, R. J. Identification of a strain-specific malarial antigen exposed on the surface of Plasmodium falciparum-infected erythrocytes. *J. Exp. Med.* **159,** 1567–75 (1984).

38. Baruch, D. I. *et al.* Cloning the P. falciparum gene encoding PfEMP1, a malarial variant antigen and adherence receptor on the surface of parasitized human erythrocytes. *Cell* **82,** 77–87 (1995).

39. Pasternak, N. D. & Dzikowski, R. PfEMP1: an antigen that plays a key role in the pathogenicity and immune evasion of the malaria parasite Plasmodium falciparum. *Int. J. Biochem. Cell Biol.* **41,** 1463–6 (2009).

40. Smith, J. D., Rowe, J. A., Higgins, M. K. & Lavstsen, T. Malaria's deadly grip: Cytoadhesion of Plasmodium falciparum-infected erythrocytes. *Cell. Microbiol.* **15,** 1976–1983 (2013).

41. Smith, J. D. *et al.* Switches in expression of plasmodium falciparum var genes correlate with changes in antigenic and cytoadherent phenotypes of infected erythrocytes. *Cell* **82,** 101–110 (1995).

42. Scherf, A., Lopez-Rubio, J. J. & Riviere, L. Antigenic variation in Plasmodium falciparum. *Annu. Rev. Microbiol.* **62,** 445–70 (2008).

43. Guizetti, J. & Scherf, A. Silence, activate, poise and switch! Mechanisms of antigenic variation in Plasmodium falciparum. *Cell. Microbiol.* **15,** 718–726 (2013).

44. Wah, S. T. *et al.* Molecular basis of human cerebral malaria development. *Trop. Med. Health* **44,** 1–7 (2016).

45. Yoeli, M. & Hargreaves, B. J. Brain capillary blockage produced by a virulent strain of rodent malaria. *Science* **184,** 572–573 (1974).

46. Mantel, P.-Y. *et al.* Malaria-Infected Erythrocyte-Derived Microvesicles Mediate Cellular Communication within the Parasite Population and with the Host Immune System. *Cell Host Microbe* **13,** 521–534 (2013).

47. Regev-Rudzki, N. *et al.* Cell-Cell Communication between Malaria-Infected Red Blood Cells via Exosome-like Vesicles. *Cell* **153,** 1120–1133 (2013).

48. Joice, R. *et al.* Plasmodium falciparum transmission stages accumulate in the human bone marrow. *Sci. Transl. Med.* **6,** 244re5 (2014).

49. Aguilar, R. *et al.* Molecular evidence for the localization of plasmodium falciparum immature gametocytes in bone marrow. *Blood* **123,** 959–966 (2014).

50. Billker, O. *et al.* Identification of xanthurenic acid as the putative inducer of malaria development in the mosquito. *Nature* **392,** 289–292 (1998).

51. Bennink, S., Kiesow, M. J. & Pradel, G. The development of malaria parasites in the mosquito midgut. *Cellular Microbiology* **18,** 905–918 (2016).

52. Aly, A. S. I., Vaughan, A. M. & Kappe, S. H. I. Malaria Parasite Development in the Mosquito and Infection of the Mammalian Host. *Annu. Rev. Microbiol.* **63,** 195–221 (2009).

53. Klug, D. & Frischknecht, F. Motility precedes egress of malaria parasites from oocysts. *Elife* **6,** 71–73 (2017).

54. Douglas, R. G., Amino, R., Sinnis, P. & Frischknecht, F. Active migration and passive transport of malaria parasites. *Trends in Parasitology* **31,** 357–362 (2015).

55. Gardner, M. J. *et al.* Genome sequence of the human malaria parasite Plasmodium falciparum. *Nature* **419,** 498–511 (2002).

56. de Koning-Ward, T. F., Gilson, P. R. & Crabb, B. S. Advances in molecular genetic systems in malaria. *Nat. Rev. Microbiol.* **13,** 373–387 (2015).

57. Shaw, P. J. & Aroonsri, A. Tools for attenuation of gene expression in malaria parasites. *Int. J. Parasitol.* (2017). doi:10.1016/j.ijpara.2016.11.006

58. Wu, Y., Sifri, C. D., Lei, H. H., Su, X. Z. & Wellems, T. E. Transfection of Plasmodium falciparum within human red blood cells. *Proc. Natl. Acad. Sci. U. S. A.* **92,** 973–7 (1995).

59. Wu, Y., Kirkman, L. A. & Wellems, T. E. Transformation of Plasmodium falciparum malaria parasites by homologous integration of plasmids that confer resistance to pyrimethamine. *Proc. Natl. Acad. Sci. U. S. A.* **93,** 1130–4 (1996).

60. van Dijk, M. R., Waters, a P. & Janse, C. J. Stable transfection of malaria parasite blood stages. *Science* **268,** 1358–1362 (1995).

61. Crabb, B. S. & Cowman, A. F. Characterization of promoters and stable transfection by homologous and nonhomologous recombination in Plasmodium falciparum. *Proc. Natl. Acad. Sci. U. S. A.* **93,** 7289–7294 (1996).

62. Ménard, R. & Janse, C. Gene targeting in malaria parasites. *Methods* **13,** 148–57 (1997).

63. Ménard, R. *et al.* Circumsporozoite protein is required for development of malaria sporozoites in mosquitoes. *Nature* **385,** 336–340 (1997).

64. Crabb, B. S. *et al.* Targeted Gene Disruption Shows That Knobs Enable Malaria-Infected Red Cells to Cytoadhere under Physiological Shear Stress. *Cell* **89,** 287–296 (1997).

65. Gomes, A. R. *et al.* A genome-scale vector resource enables high-throughput reverse genetic screening in a malaria parasite. *Cell Host Microbe* **17,** 404–413 (2015).

66. Schwach, F. *et al.* PlasmoGEM, a database supporting a community resource for large-scale experimental genetics in malaria parasites. *Nucleic Acids Res.* **43,** D1176–D1182 (2015).

67. Miller, J. C. *et al.* An improved zinc-finger nuclease architecture for highly specific genome editing. *Nat. Biotechnol.* **25,** 778–85 (2007).

68. Straimer, J. *et al.* Site-specific genome editing in Plasmodium falciparum using engineered zinc-finger nucleases. *Nat. Methods* **9,** 993–8 (2012).

69. Lee, A. H., Symington, L. S. & Fidock, D. A. DNA Repair Mechanisms and Their Biological Roles in the Malaria Parasite Plasmodium falciparum. *Microbiol. Mol. Biol. Rev.* **78,** 469–486 (2014).

70. Moraes Barros, R. R. *et al.* Editing the Plasmodium vivax Genome, Using Zinc-Finger Nucleases. *J. Infect. Dis.* **211,** 125–129 (2015).

71. Singer, M. *et al.* Zinc finger nuclease-based double-strand breaks attenuate malaria parasites and reveal rare microhomology-mediated end joining. *Genome Biol* **16,** 249 (2015).

72. Ghorbal, M. *et al.* Genome editing in the human malaria parasite Plasmodium falciparum using the CRISPR-Cas9 system. *Nat. Biotechnol.* (2014). doi:10.1038/nbt.2925

73. Wagner, J. C., Platt, R. J., Goldfless, S. J., Zhang, F. & Niles, J. C. Efficient CRISPR-Cas9–mediated genome editing in Plasmodium falciparum. *Nat. Methods* **11,** 915–918 (2014).

74. Wang, H., La Russa, M. & Qi, L. S. CRISPR/Cas9 in Genome Editing and Beyond. *Annu. Rev. Biochem.* **85,** 227–264 (2016).

75. Sidik, S. M. *et al.* A Genome-wide CRISPR Screen in Toxoplasma Identifies Essential Apicomplexan Genes. *Cell* **166,** 1423–1435.e12 (2016).

76. Zhang, C. *et al.* Efficient Editing of Malaria Parasite Genome Using the CRISPR/Cas9 System. *MBio* **5,** (2014).

77. McLeod, M., Craft, S. & Broach, J. R. Identification of the crossover site during FLP-mediated recombination in the Saccharomyces cerevisiae plasmid 2 microns circle. *Mol. Cell. Biol.* **6,** 3357–67 (1986).

78. Hoess, R. H., Ziese, M. & Sternberg, N. P1 site-specific recombination: nucleotide sequence of the recombining sites. *Proc. Natl. Acad. Sci. U. S. A.* **79,** 3398–3402 (1982).

79. O'Neill, M. T., Phuong, T., Healer, J., Richard, D. & Cowman, A. F. Gene deletion from Plasmodium falciparum using FLP and Cre recombinases: Implications for applied site-specific recombination. *Int. J. Parasitol.* **41,** 117–123 (2011).

80. Jullien, N. Regulation of Cre recombinase by ligand-induced complementation of inactive fragments. *Nucleic Acids Res.* **31,** 131e–131 (2003).

81. Andenmatten, N. *et al.* Conditional genome engineering in Toxoplasma gondii uncovers alternative invasion mechanisms. *Nat. Methods* **10,** 125–7 (2013).

82. Yap, A. *et al.* Conditional expression of apical membrane antigen 1 in Plasmodium falciparum shows it is required for erythrocyte invasion by merozoites. *Cell. Microbiol.* **16,** 642–656 (2014).

83. Jones, M. L. *et al.* A versatile strategy for rapid conditional genome engineering using loxP sites in a small synthetic intron in Plasmodium falciparum. *Sci. Rep.* **6,** 21800 (2016).

84. Gordon, E. B. *et al.* Inhibiting the mammalian target of rapamycin blocks the development of experimental cerebral malaria. *MBio* **6,** e00725 (2015).

85. Combe, A. *et al.* Clonal Conditional Mutagenesis in Malaria Parasites. *Cell Host Microbe* **5,** 386–396 (2009).

86. Bargieri, D. Y. *et al.* Apical membrane antigen 1 mediates apicomplexan parasite attachment but is dispensable for host cell invasion. *Nat. Commun.* **4,** (2013).

87. Lacroix, C. *et al.* FLP/FRT-mediated conditional mutagenesis in pre-erythrocytic stages of Plasmodium berghei. *Nat. Protoc.* **6,** 1412–1428 (2011).

88. Laurentino, E. C. *et al.* Experimentally controlled downregulation of the histone chaperone FACT in Plasmodium berghei reveals that it is critical to male gamete fertility. *Cell. Microbiol.* **13,** 1956–1974 (2011).

89. Le Roch, K. G. Discovery of Gene Function by Expression Profiling of the Malaria Parasite Life Cycle. *Science (80-.).* **301,** 1503–1508 (2003).

90. Kooij, T. W., Janse, C. J. & Waters, A. P. Plasmodium post-genomics: better the bug you know? *Nat Rev Microbiol* **4,** 344–357 (2006).

91. Meissner, M. *et al.* Tetracycline analogue-regulated transgene expression in Plasmodium falciparum blood stages using Toxoplasma gondii transactivators. *Proc. Natl. Acad. Sci. U. S. A.* **102,** 2980–5 (2005).

92. Pino, P. *et al.* A Tetracycline-Repressible Transactivator System to Study Essential Genes in Malaria Parasites. *Cell Host Microbe* **12,** 824–834 (2012).

93. Balaji, S., Madan Babu, M., Iyer, L. M. & Aravind, L. Discovery of the principal specific transcription factors of Apicomplexa and their implication for the evolution of the AP2-integrase DNA binding domains. *Nucleic Acids Res.* **33,** 3994–4006 (2005).

94. Ghosh, S. *et al.* The Plasmodium rhoptry associated protein complex is important for parasitophorous vacuole membrane structure and intraerythrocytic parasite growth. *Cell. Microbiol.* (2017). doi:10.1111/cmi.12733

95. Baum, J. *et al.* Molecular genetics and comparative genomics reveal RNAi is not functional in malaria parasites. *Nucleic Acids Res.* **37,** 3788–98 (2009).

96. Wang, G. & Xu, X. S. Peptide nucleic acid (PNA) binding-mediated gene regulation. *Cell Res.* **14,** 111–116 (2004).

97. Dahan-Pasternak, N. *et al.* PfSec13 is an unusual chromatin-associated nucleoporin of Plasmodium falciparum that is essential for parasite proliferation in human erythrocytes. *J. Cell Sci.* **126,** 3055–69 (2013).

98. Kolevzon, N., Nasereddin, A., Naik, S., Yavin, E. & Dzikowski, R. Use of peptide nucleic acids to manipulate gene expression in the malaria parasite Plasmodium falciparum. *PLoS One* **9,** e86802 (2014).

99. Garg, A. *et al.* Targeting protein translation, RNA splicing, and degradation by morpholino-based conjugates in Plasmodium falciparum. *Proc. Natl. Acad. Sci.* **112,** 201515864 (2015).

100. Piccinelli, P., Rosenblad, M. A. & Samuelsson, T. Identification and analysis of ribonuclease P and MRP RNA in a broad range of eukaryotes. *Nucleic Acids Res.* **33,** 4485–4495 (2005).

101. Augagneur, Y., Wesolowski, D., Tae, H. S., Altman, S. & Ben Mamoun, C. Gene selective mRNA cleavage inhibits the development of Plasmodium falciparum. *Proc. Natl. Acad. Sci.* **109,** 6235–6240 (2012).

102. Winkler, W. C., Nahvi, A., Roth, A., Collins, J. A. & Breaker, R. R. Control of gene expression by a natural metabolite-responsive ribozyme. *Nature* **428,** 281–286 (2004).

103. Prommana, P. *et al.* Inducible Knockdown of Plasmodium Gene Expression Using the glmS Ribozyme. *PLoS One* **8,** e73783 (2013).

104. Aroonsri, A. *et al.* Identifying antimalarial compounds targeting dihydrofolate reductase-thymidylate synthase (DHFR-TS) by chemogenomic profiling. *Int. J. Parasitol.* **46,** 527–535 (2016).

105. Belmont, B. J. & Niles, J. C. Engineering a direct and inducible protein-RNA interaction to regulate RNA biology. *ACS Chem. Biol.* **5,** 851–861 (2010).

106. Goldfless, S. J., Wagner, J. C. & Niles, J. C. Versatile control of Plasmodium falciparum gene expression with an inducible protein-RNA interaction. *Nat. Commun.* **5,** 5329 (2014).

107. Ganesan, S. M., Falla, A., Goldfless, S. J., Nasamu, A. S. & Niles, J. C. Synthetic RNA-protein modules integrated with native translation mechanisms to control gene expression in malaria parasites. *Nat Commun* **7,** 1–10 (2016).

108. Mair, G. R. *et al.* Regulation of sexual development of Plasmodium by translational repression. *Science* **313,** 667–9 (2006).

109. Banaszynski, L. A., Chen, L. chun, Maynard-Smith, L. A., Ooi, A. G. L. & Wandless, T. J. A Rapid, Reversible, and Tunable Method to Regulate Protein Function in Living Cells Using Synthetic Small Molecules. *Cell* **126,** 995–1004 (2006).

110. Armstrong, C. M. & Goldberg, D. E. An FKBP destabilization domain modulates protein levels in Plasmodium falciparum. *Nat. Methods* **4,** 1007–1009 (2007).

111. Muralidharan, V., Oksman, A., Iwamoto, M., Wandless, T. J. & Goldberg, D. E. Asparagine repeat function in a Plasmodium falciparum protein assessed via a regulatable fluorescent affinity tag. *Proc. Natl. Acad. Sci. U. S. A.* **108,** 4411–6 (2011).

112. Jain, S. *et al.* The prokaryotic ClpQ protease plays a key role in growth and development of mitochondria in Plasmodium falciparum. *Cell. Microbiol.* **15,** 1660–1673 (2013).

113. Azevedo, M. F. *et al.* Inhibition of Plasmodium falciparum CDPK1 by conditional expression of its J-domain demonstrates a key role in schizont development. *Biochem. J.* **452,** 433–41 (2013).

114. de Azevedo, M. F. *et al.* Systematic analysis of FKBP inducible degradation domain tagging strategies for the human malaria parasite Plasmodium falciparum. *PLoS One* **7,** e40981 (2012).

115. Pei, Y. *et al.* Plasmodium yoelii inhibitor of cysteine proteases is exported to exomembrane structures and interacts with yoelipain-2 during asexual blood-stage development. *Cell. Microbiol.* **15,** 1508–1526 (2013).

116. Kreidenweiss, A., Hopkins, A. V & Mordmüller, B. 2A and the auxin-based degron system facilitate control of protein levels in Plasmodium falciparum. *PLoS One* **8,** e78661 (2013).

117. Philip, N. & Waters, A. P. Conditional Degradation of Plasmodium Calcineurin Reveals Functions in Parasite Colonization of both Host and Vector. *Cell Host Microbe* **18,** 122–131 (2015).

118. Nishimura, K., Fukagawa, T., Takisawa, H., Kakimoto, T. & Kanemaki, M. An auxin-based degron system for the rapid depletion of proteins in nonplant cells. *Nat. Methods* **53,** 1689–1699 (2009).

119. Saridaki, T., Sanchez, C. P., Pfahler, J. & Lanzer, M. A conditional export system provides new insights into protein export in Plasmodium falciparum-infected erythrocytes. *Cell. Microbiol.* **10,** 2483–2495 (2008).

120. Birnbaum, J. *et al.* A genetic system to study Plasmodium falciparum protein function. *Nat. Methods* (2017). doi:10.1038/nmeth.4223

121. Hughes, K. R. & Waters, A. P. Rapid inducible protein displacement in Plasmodium in vivo and in vitro using knocksideways technology. *Wellcome Open Res.* **2,** 18 (2017).

122. Lee, R. C., Feinbaum, R. L. & Ambros, V. The C. elegans heterochronic gene lin-4 encodes small RNAs with antisense complementarity to lin-14. *Cell* **75,** 843–854 (1993).

123. Friedman, R. C., Farh, K. K.-H., Burge, C. B. & Bartel, D. P. Most mammalian mRNAs are conserved targets of microRNAs. *Genome Res.* **19,** 92–105 (2009).

124. Rodriguez, A., Griffiths-Jones, S., Ashurst, J. L. & Bradley, A. Identification of mammalian microRNA host genes and transcription units. *Genome Res.* **14,** 1902–1910 (2004).

125. Kim, Y.-K. & Kim, V. N. Processing of intronic microRNAs. *EMBO J.* **26,** 775–83 (2007).

126. Ha, M. & Kim, V. N. Regulation of microRNA biogenesis. *Nat. Rev. Mol. Cell Biol.* **15,** 509–524 (2014).

127. Cai, X., Hagedorn, C. H. & Cullen, B. R. Human microRNAs are processed from capped, polyadenylated transcripts that can also function as mRNAs. *RNA* **10,** 1957–66 (2004).

128. Saini, H. K., Griffiths-Jones, S. & Enright, A. J. Genomic analysis of human microRNA transcripts. *Proc. Natl. Acad. Sci. U. S. A.* **104,** 17719–24 (2007).

129. Lee, Y. *et al.* The nuclear RNase III Drosha initiates microRNA processing. *Nature* **425,** 415–419 (2003).

130. Lee, Y., Jeon, K., Lee, J. T., Kim, S. & Kim, V. N. MicroRNA maturation: Stepwise processing and subcellular localization. *EMBO J.* **21,** 4663–4670 (2002).

131. Ballarino, M. *et al.* Coupled RNA processing and transcription of intergenic primary microRNAs. *Mol. Cell. Biol.* **29,** 5632–8 (2009).

132. Morlando, M. *et al.* Primary microRNA transcripts are processed co-transcriptionally. *Nat. Struct. Mol. Biol.* **15,** 902–9 (2008).

133. Han, J. *et al.* The Drosha-DGCR8 complex in primary microRNA processing. *Genes Dev.* **18,** 3016–3027 (2004).

134. Gregory, R. I. *et al.* The Microprocessor complex mediates the genesis of microRNAs. *Nature* **432,** 235–240 (2004).

135. Denli, A. M., Tops, B. B. J., Plasterk, R. H. a, Ketting, R. F. & Hannon, G. J. Processing of primary microRNAs by the Microprocessor complex. *Nature* **432,** 231–5 (2004).

136. Landthaler, M., Yalcin, A. & Tuschl, T. The human DiGeorge syndrome critical region gene 8 and its D. melanogaster homolog are required for miRNA biogenesis. *Curr. Biol.* **14,** 2162–2167 (2004).

137. Bohnsack, M. T., Czaplinski, K. & Gorlich, D. Exportin 5 is a RanGTP-dependent dsRNA-binding protein that mediates nuclear export of pre-miRNAs. *RNA* **10,** 185–91 (2004).

138. Lund, E., Güttinger, S., Calado, A., Dahlberg, J. E. & Kutay, U. Nuclear export of microRNA precursors. *Science (80-.).* **303,** 95–98 (2004).

139. Yi, R., Qin, Y., Macara, I. G. & Cullen, B. R. Exportin-5 mediates the nuclear export of pre-microRNAs and short hairpin RNAs. *Genes Dev.* **17,** 3011–6 (2003).

140. Patel, R. C. & Sen, G. C. PACT, a protein activator of the interferon-induced protein kinase, PKR. *EMBO J.* **17,** 4379–90 (1998).

141. Ketting, R. F. *et al.* Dicer functions in RNA interference and in synthesis of small RNA involved in developmental timing in C. elegans. *Genes Dev.* **15,** 2654–2659 (2001).

142. Grishok, A. *et al.* Genes and mechanisms related to RNA interference regulate expression of the small temporal RNAs that control C. elegans developmental timing. *Cell* **106,** 23–34 (2001).

143. Hutvagner, G. *et al.* A Cellular Function for the RNA-Interference Temporal RNA Small let-7 Enzyme Dicer in the Maturation of the . *Science (80-.).* **293,** 1–6 (2010).

144. Knight, S. W. & Bass, B. L. A role for the RNase III enzyme DCR-1 in RNA interference and germ line development in Caenorhabditis elegans. *Science (80-.).* **293,** 2269–2271 (2001).

145. Chendrimada, T. P. *et al.* TRBP recruits the Dicer complex to Ago2 for microRNA processing and gene silencing. *Nature* **436,** 740–4 (2005).

146. Haase, A. D. *et al.* TRBP, a regulator of cellular PKR and HIV-1 virus expression, interacts with Dicer and functions in RNA silencing. *EMBO Rep.* **6,** 961–7 (2005).

147. Lee, Y. *et al.* The role of PACT in the RNA silencing pathway. *EMBO J.* **25,** 522–32 (2006).

148. Lee, H. Y., Zhou, K., Smith, A. M., Noland, C. L. & Doudna, J. A. Differential roles of human Dicer-binding proteins TRBP and PACT in small RNA processing. *Nucleic Acids Res.* **41,** 6568–6576 (2013).

149. Hammond, S. M., Boettcher, S., Caudy, A. A., Kobayashi, R. & Hannon, G. J. Argonaute2, a Link Between Genetic and Biochemical Analyses of RNAi. *Science (80-.).* **293,** 1146–1150 (2001).

150. Mourelatos, Z. *et al.* miRNPs: A novel class of ribonucleoproteins containing numerous microRNAs. *Genes Dev.* **16,** 720–728 (2002).

151. Tabara, H. *et al.* The rde-1 gene, RNA interference, and transposon silencing in C. elegans. *Cell* **99,** 123–32 (1999).

152. Azuma-Mukai, A. *et al.* Characterization of endogenous human Argonautes and their miRNA partners in RNA silencing. *Proc. Natl. Acad. Sci. U. S. A.* **105,** 7964–9 (2008).

153. Meister, G. *et al.* Human Argonaute2 mediates RNA cleavage targeted by miRNAs and siRNAs. *Mol. Cell* **15,** 185–197 (2004).

154. Dueck, A., Ziegler, C., Eichner, A., Berezikov, E. & Meister, G. MicroRNAs associated with the different human Argonaute proteins. *Nucleic Acids Res.* **40,** 9850–9862 (2012).

155. Khvorova, A., Reynolds, A. & Jayasena, S. D. Functional siRNAs and miRNAs exhibit strand bias. *Cell* **115,** 209–216 (2003).

156. Schwarz, D. S. *et al.* Asymmetry in the assembly of the RNAi enzyme complex. *Cell* **115,** 199–208 (2003).

157. Matranga, C., Tomari, Y., Shin, C., Bartel, D. P. & Zamore, P. D. Passenger-strand cleavage facilitates assembly of siRNA into Ago2-containing RNAi enzyme complexes. *Cell* **123,** 607–620 (2005).

158. Shin, C. Cleavage of the star strand facilitates assembly of some microRNAs into Ago2-containing silencing complexes in mammals. *Mol. Cells* **26,** 308–313 (2008).

159. Diederichs, S. & Haber, D. A. Dual Role for Argonautes in MicroRNA Processing and Posttranscriptional Regulation of MicroRNA Expression. *Cell* **131,** 1097–1108 (2007).

160. Leuschner, P. J. F., Ameres, S. L., Kueng, S. & Martinez, J. *Cleavage of the siRNA passenger strand during RISC assembly in human cells*. *EMBO Rep* **7,** 314–320 (2006).

161. Rand, T. A., Petersen, S., Du, F. & Wang, X. Argonaute2 cleaves the anti-guide strand of siRNA during RISC activation. *Cell* **123,** 621–629 (2005).

162. Tomari, Y. *et al.* RISC assembly defects in the Drosophila RNAi mutant armitage. *Cell* **116,** 831–841 (2004).

163. Meister, G. *et al.* Identification of novel argonaute-associated proteins. *Curr. Biol.* **15,** 2149–2155 (2005).

164. Nykänen, A., Haley, B. & Zamore, P. D. ATP requirements and small interfering RNA structure in the RNA interference pathway. *Cell* **107,** 309–321 (2001).

165. Robb, G. B. & Rana, T. M. RNA Helicase A Interacts with RISC in Human Cells and Functions in RISC Loading. *Mol. Cell* **26,** 523–537 (2007).

166. Liu, X., Jin, D. Y., McManus, M. T. & Mourelatos, Z. Precursor MicroRNA-Programmed Silencing Complex Assembly Pathways in Mammals. *Mol. Cell* **46,** 507–517 (2012).

167. Kawamata, T., Seitz, H. & Tomari, Y. Structural determinants of miRNAs for RISC loading and slicer-independent unwinding. *Nat. Struct. Mol. Biol.* **16,** 953–960 (2009).

168. Yoda, M. *et al.* ATP-dependent human RISC assembly pathways. *Nat. Struct. Mol. Biol.* **17,** 17–23 (2010).

169. Yang, J.-S. *et al.* Widespread regulatory activity of vertebrate microRNA* species. *RNA* **17,** 312–326 (2011).

170. Leung, A. K. L. & Sharp, P. A. Quantifying argonaute proteins in and out of GW/P-bodies: Implications in microRNA activities. *Adv. Exp. Med. Biol.* **768,** 165–182 (2013).

171. Lai, E. C., Tam, B. & Rubin, G. M. Pervasive regulation of Drosophila Notch target genes by GY-box-, Brd-box-, and K-box-class microRNAs. *Genes Dev.* **19,** 1067–1080 (2005).

172. Lewis, B. P., Shih, I. H., Jones-Rhoades, M. W., Bartel, D. P. & Burge, C. B. Prediction of Mammalian MicroRNA Targets. *Cell* **115,** 787–798 (2003).

173. Jackson, A. L. *et al.* Expression profiling reveals off-target gene regulation by RNAi. *Nat. Biotechnol.* **21,** 635–637 (2003).

174. Bartel, D. P. MicroRNAs: target recognition and regulatory functions. *Cell* **136,** 215–33 (2009).

175. Pasquinelli, A. E. MicroRNAs and their targets: recognition, regulation and an emerging reciprocal relationship. *Nat. Rev. Genet.* **13,** 271–82 (2012).

176. Wilczynska, A. & Bushell, M. The complexity of miRNA-mediated repression. *Cell Death Differ.* **22,** 22–33 (2014).

177. Liu, J. *et al.* Argonaute2 is the catalytic engine of mammalian RNAi. *Science* **305,** 1437–41 (2004).

178. Doench, J. G., Petersen, C. P. & Sharp, P. A. siRNAs can function as miRNAs. *Genes Dev.* **17,** 438–42 (2003).

179. Pillai, R. S. *et al. Inhibition of translational initiation by Let-7 MicroRNA in human cells*. *Science* **309,** 1573–1576 (2005).

180. Thermann, R. & Hentze, M. W. Drosophila miR2 induces pseudo-polysomes and inhibits translation initiation. *Nature* **447,** 875–8 (2007).

181. Bhattacharyya, S. N., Habermacher, R., Martine, U., Closs, E. I. & Filipowicz, W. Relief of microRNA-Mediated Translational Repression in Human Cells Subjected to Stress. *Cell* **125,** 1111–1124 (2006).

182. Iwasaki, S., Kawamata, T. & Tomari, Y. Drosophila Argonaute1 and Argonaute2 Employ Distinct Mechanisms for Translational Repression. *Mol. Cell* **34,** 58–67 (2009).

183. Humphreys, D. T., Westman, B. J., Martin, D. I. K. & Preiss, T. MicroRNAs control translation initiation by inhibiting eukaryotic initiation factor 4E/cap and poly(A) tail function. *Proc. Natl. Acad. Sci. U. S. A.* **102,** 16961–6 (2005).

184. Wakiyama, M., Takimoto, K., Ohara, O. & Yokoyama, S. Let-7 microRNA-mediated mRNA deadenylation and translational repression in a mammalian cell-free system. *Genes Dev.* **21,** 1857–1862 (2007).

185. Kong, Y. W. *et al.* The mechanism of micro-RNA-mediated translation repression is determined by the promoter of the target gene. *Proc. Natl. Acad. Sci. U. S. A.* **105,** 8866–8871 (2008).

186. Mathonnet, G. *et al.* MicroRNA inhibition of translation initiation in vitro by targeting the cap-binding complex eIF4F. *Science* **317,** 1764–1767 (2007).

187. Eulalio, A., Huntzinger, E. & Izaurralde, E. GW182 interaction with Argonaute is essential for miRNA-mediated translational repression and mRNA decay. *Nat. Struct. Mol. Biol.* **15,** 346–353 (2008).

188. Eulalio, A., Helms, S., Fritzsch, C., Fauser, M. & Izaurralde, E. A C-terminal silencing domain in GW182 is essential for miRNA function. *RNA* **15,** 1067–77 (2009).

189. Till, S. *et al.* A conserved motif in Argonaute-interacting proteins mediates functional interactions through the Argonaute PIWI domain. *Nat. Struct. Mol. Biol.* **14,** 897–903 (2007).

190. Fabian, M. R. *et al.* miRNA-mediated deadenylation is orchestrated by GW182 through two conserved motifs that interact with CCR4–NOT. *Nat. Struct. Mol. Biol.* **19,** 1211–1217 (2012).

191. Braun, J. E., Huntzinger, E., Fauser, M. & Izaurralde, E. GW182 proteins directly recruit cytoplasmic deadenylase complexes to miRNA targets. *Mol. Cell* **44,** 120–133 (2011).

192. Chekulaeva, M. *et al.* miRNA repression involves GW182-mediated recruitment of CCR4–NOT through conserved W-containing motifs. *Nat. Struct. Mol. Biol.* **18,** 1218–1226 (2011).

193. Chu, C. Y. & Rana, T. M. Translation repression in human cells by MicroRNA-induced gene silencing requires RCK/p54. *PLoS Biol.* **4,** 1122–1136 (2006).

194. Mathys, H. *et al.* Structural and Biochemical Insights to the Role of the CCR4-NOT Complex and DDX6 ATPase in MicroRNA Repression. *Mol. Cell* **54,** 751–765 (2014).

195. Chen, Y. *et al.* A DDX6-CNOT1 Complex and W-Binding Pockets in CNOT9 Reveal Direct Links between miRNA Target Recognition and Silencing. *Mol. Cell* **54,** 737–750 (2014).

196. Rouya, C. *et al.* Human DDX6 effects miRNA-mediated gene silencing via direct binding to CNOT1. *RNA* **20,** 1398–409 (2014).

197. Eulalio, A., Behm-Ansmant, I., Schweizer, D. & Izaurralde, E. P-Body Formation Is a Consequence, Not the Cause, of RNA-Mediated Gene Silencing . *Mol. Cell. Biol.* **27,** 3970–3981 (2007).

198. Behm-Ansmant, I. *et al.* mRNA degradation by miRNAs and GW182 requires both CCR4:NOT deadenylase and DCP1:DCP2 decapping complexes. *Genes Dev.* **20,** 1885–1898 (2006).

199. Elbashir, S. M. *et al.* Duplexes of 21-nucleotide RNAs mediate RNA interference in cultured mammalian cells. *Nature* **411,** 494–8 (2001).

200. Paddison, P. J., Caudy, A. A., Bernstein, E., Hannon, G. J. & Conklin, D. S. Short hairpin RNAs (shRNAs) induce sequence-specific silencing in mammalian cells. *Genes Dev.* **16,** 948–58 (2002).

201. Alsford, S. *et al.* High-throughput phenotyping using parallel sequencing of RNA interference targets in the African trypanosome. *Genome Res.* **21,** 915–924 (2011).

202. Kamath, R. S. *et al.* Systematic functional analysis of the Caenorhabditis elegans genome using RNAi. *Nature* **421,** 231–237 (2003).

203. Boutros, M. *et al.* Genome-wide RNAi analysis of growth and viability in Drosophila cells. *Science (80-.).* **303,** 832–835 (2004).

204. Daugaard, I. & Hansen, T. B. Biogenesis and Function of Ago-Associated RNAs. *Trends Genet.* **33,** 208–219 (2017).

205. Miyoshi, K., Miyoshi, T. & Siomi, H. Many ways to generate microRNA-like small RNAs: Non-canonical pathways for microRNA production. *Molecular Genetics and Genomics* **284,** 95–103 (2010).

206. Burroughs, A. M. *et al.* Deep-sequencing of human Argonaute-associated small RNAs provides insight into miRNA sorting and reveals Argonaute association with RNA fragments of diverse origin. *RNA Biol.* **8,** 158–77 (2011).

207. Cole, C. *et al.* Filtering of deep sequencing data reveals the existence of abundant Dicer-dependent small RNAs derived from tRNAs. *Rna* **15,** 2147–2160 (2009).

208. Haussecker, D. *et al.* Human tRNA-derived small RNAs in the global regulation of RNA silencing. *RNA (New York, NY)* **16,** 673–695 (2010).

209. Hasler, D. & Meister, G. From tRNA to miRNA: RNA-folding contributes to correct entry into noncoding RNA pathways. *FEBS Letters* 2354–2363 (2016). doi:10.1002/1873-3468.12294

210. Ender, C. *et al.* A Human snoRNA with MicroRNA-Like Functions. *Mol. Cell* **32,** 519–528 (2008).

211. Taft, R. J. *et al.* Small RNAs derived from snoRNAs. *RNA* **15,** 1233–40 (2009).

212. Brameier, M., Herwig, A., Reinhardt, R., Walter, L. & Gruber, J. Human box C/D snoRNAs with miRNA like functions: Expanding the range of regulatory RNAs. *Nucleic Acids Res.* **39,** 675–686 (2011).

213. Watanabe, T. *et al.* Endogenous siRNAs from naturally formed dsRNAs regulate transcripts in mouse oocytes. *Nature* **453,** 539–543 (2008).

214. Okamura, K. & Lai, E. C. Endogenous small interfering RNAs in animals. *Nat. Rev. Mol. Cell Biol.* **9,** 673–8 (2008).

215. Tam, O. H. *et al.* Pseudogene-derived small interfering RNAs regulate gene expression in mouse oocytes. *Nature* **453,** 534–538 (2008).

216. Xie, M. *et al.* Mammalian 5???-capped microRNA precursors that generate a single microRNA. *Cell* **155,** 1568–1580 (2013).

217. Berezikov, E., Chung, W. J., Willis, J., Cuppen, E. & Lai, E. C. Mammalian Mirtron Genes. *Mol. Cell* **28,** 328–336 (2007).

218. Okamura, K., Hagen, J. W., Duan, H., Tyler, D. M. & Lai, E. C. The Mirtron Pathway Generates microRNA-Class Regulatory RNAs in Drosophila. *Cell* **130,** 89–100 (2007).

219. Ruby, J. G., Jan, C. H. & Bartel, D. P. Intronic microRNA precursors that bypass Drosha processing. *Nature* **448,** 83–6 (2007).

220. Westholm, J. O. & Lai, E. C. Mirtrons: MicroRNA biogenesis via splicing. *Biochimie* **93,** 1897–1904 (2011).

221. Hansen, T. B. *et al.* Argonaute-associated short introns are a novel class of gene regulators. *Nat Commun* **7,** 1–10 (2016).

222. Nelson, P. T. *et al.* A novel monoclonal antibody against human Argonaute proteins reveals unexpected characteristics of miRNAs in human blood cells. *RNA* **13,** 1787–92 (2007).

223. Rasmussen, K. D. *et al.* The miR-144/451 locus is required for erythroid homeostasis. *J. Exp. Med.* **207,** 1351–8 (2010).

224. Pase, L. *et al.* miR-451 regulates zebrafish erythroid maturation in vivo via its target gata2. *Blood* **113,** 1794–1804 (2009).

225. Patrick, D. M. *et al.* Defective erythroid differentiation in miR-451 mutant mice mediated by 14-3-3?? *Genes Dev.* **24,** 1614–1619 (2010).

226. Yu, D. *et al.* miR-451 protects against erythroid oxidant stress by repressing 14-3-3?? *Genes Dev.* **24,** 1620–1633 (2010).

227. Dore, L. C. *et al.* A GATA-1-regulated microRNA locus essential for erythropoiesis. *Proc. Natl. Acad. Sci. U. S. A.* **105,** 3333–8 (2008).

228. Cheloufi, S., Dos Santos, C. O., Chong, M. M. & Hannon, G. J. A dicer-independent miRNA biogenesis pathway that requires Ago catalysis. *Nature* **465,** 584–589 (2010).

229. Cifuentes, D. *et al.* A novel miRNA processing pathway independent of Dicer requires Argonaute2 catalytic activity. *Science* **328,** 1694–8 (2010).

230. Yang, J. S. & Lai, E. C. Dicer-independent, Ago2-mediated microRNA biogenesis in vertebrates. *Cell Cycle* **9,** 4455–4460 (2010).

231. Yoda, M. *et al.* Poly(A)-specific ribonuclease mediates 3'-end trimming of argonaute2-cleaved precursor microrna. *Cell Rep.* **5,** 715–726 (2013).

232. Liu, Y. P., Schopman, N. C. T. & Berkhout, B. Dicer-independent processing of short hairpin RNAs. *Nucleic Acids Res.* **41,** 3723–33 (2013).

233. Ma, H., Zhang, J. & Wu, H. Designing Ago2-specific siRNA/shRNA to Avoid Competition with Endogenous miRNAs. *Mol. Ther. Nucleic Acids* **3,** e176 (2014).

234. Herrera-Carrillo, E., Harwig, A., Liu, Y. P. & Berkhout, B. Probing the shRNA characteristics that hinder Dicer recognition and consequently allow Ago-mediated processing and AgoshRNA activity. *RNA* **20,** 1410–1408 (2014).

235. Liu, Y. P. *et al.* Mechanistic insights on the Dicer-independent AGO2-mediated processing of AgoshRNAs. *RNA Biol.* **12,** 92–100 (2015).

236. Liu, Y. P., Karg, M., Herrera-Carrillo, E. & Berkhout, B. Towards Antiviral shRNAs Based on the AgoshRNA Design. *PLoS One* **10,** e0128618 (2015).

237. Herrera-Carrillo, E., Gao, Z., Harwig, A., Heemskerk, M. T. & Berkhout, B. The influence of the 5′-terminal nucleotide on AgoshRNA activity and biogenesis: importance of the polymerase III transcription initiation site. *Nucleic Acids Res.* gkw1203 (2016). doi:10.1093/nar/gkw1203

238. Harwig, A., Herrera-Carrillo, E., Jongejan, A., van Kampen, A. H. & Berkhout, B. Deep Sequence Analysis of AgoshRNA Processing Reveals 3' A Addition and Trimming. *Mol. Ther. - Nucleic Acids* **4,** e247 (2015).

239. Grimm, D. *et al.* Fatality in mice due to oversaturation of cellular microRNA/short hairpin RNA pathways. *Nature* **441,** 537–41 (2006).

240. Coley, W. *et al.* Absence of DICER in monocytes and its regulation by HIV-1. *J. Biol. Chem.* **285,** 31930–31943 (2010).

241. Rathjen, T., Nicol, C., McConkey, G. & Dalmay, T. Analysis of short RNAs in the malaria parasite and its red blood cell host. *FEBS Lett.* **580,** 5185–5188 (2006).

242. Xue, X., Zhang, Q., Huang, Y., Feng, L. & Pan, W. No miRNA were found in Plasmodium and the ones identified in erythrocytes could not be correlated with infection. *Malar. J.* **7,** 47 (2008).

243. Mantel, P.-Y. *et al.* Infected erythrocyte-derived extracellular vesicles alter vascular function via regulatory Ago2-miRNA complexes in malaria. *Nat. Commun.* **7,** 12727 (2016).

244. Chen, S. Y., Wang, Y., Telen, M. J. & Chi, J. T. The genomic analysis of erythrocyte microRNA expression in sickle cell diseases. *PLoS One* **3,** (2008).

245. LaMonte, G. *et al.* Translocation of sickle cell erythrocyte MicroRNAs into Plasmodium falciparum inhibits parasite translation and contributes to malaria resistance. *Cell Host Microbe* **12,** 187–199 (2012).

246. Friedman, M. J. Erythrocytic mechanism of sickle cell resistance to malaria. *Proc. Natl. Acad. Sci. U. S. A.* **75,** 1994–7 (1978).

247. Delić, D., Dkhil, M., Al-Quraishy, S. & Wunderlich, F. Hepatic miRNA expression reprogrammed by Plasmodium chabaudi malaria. *Parasitol. Res.* **108,** 1111–1121 (2011).

248. Hentzschel, F. *et al.* AAV8-mediated in vivo overexpression of miR-155 enhances the protective capacity of genetically-attenuated malarial parasites. *Mol. Ther.* **22,** 2130–2141 (2014).

249. El-Assaad, F. *et al.* Differential microRNA expression in experimental cerebral and noncerebral malaria. *Infect. Immun.* **79,** 2379–84 (2011).

250. Barker, K. R. *et al.* miR-155 Modifies Inflammation, Endothelial Activation and Blood-Brain Barrier Dysfunction in Cerebral Malaria. *Mol. Med.* **23,** 24–33 (2017).

251. Ngô, H., Tschudi, C., Gull, K. & Ullu, E. Double-stranded RNA induces mRNA degradation in Trypanosoma brucei. *Proc. Natl. Acad. Sci. U. S. A.* **95,** 14687–14692 (1998).

252. Patrick, K. L. *et al.* Distinct and overlapping roles for two Dicer-like proteins in the RNA interference pathways of the ancient eukaryote Trypanosoma brucei. *Proc. Natl. Acad. Sci. U. S. A.* **106,** 17933–8 (2009).

253. Shi, H., Tschudi, C. & Ullu, E. An unusual Dicer-like1 protein fuels the RNA interference pathway in Trypanosoma brucei. *Rna* **12,** 2063–2072 (2006).

254. Durand-Dubief, M. & Bastin, P. TbAGOI, an Argonaute protein required for RNA interference, is involved in mitosis and chromosome segragation in Trypanosoma brucei. *BMC Biol.* **1,** (2003).

255. Shi, H., Djikeng, A., Tschudi, C. & Ullu, E. Argonaute protein in the early divergent eukaryote Trypanosoma brucei: control of small interfering RNA accumulation and retroposon transcript abundance. *Mol. Cell. Biol.* **24,** 420–7 (2004).

256. Mony, B. M. *et al.* Genome-wide dissection of the quorum sensing signalling pathway in Trypanosoma brucei. *Nature* **505,** 681–685 (2014).

257. Lye, L.-F. *et al.* Retention and Loss of RNA Interference Pathways in Trypanosomatid Protozoans. *PLoS Pathog.* **6,** e1001161 (2010).

258. Darocha, W. D., Otsu, K., Teixeira, S. M. R. & Donelson, J. E. Tests of cytoplasmic RNA interference (RNAi) and construction of a tetracycline-inducible T7 promoter system in Trypanosoma cruzi. *Mol. Biochem. Parasitol.* **133,** 175–186 (2004).

259. Robinson, K. A. & Beverley, S. M. Improvements in transfection efficiency and tests of RNA interference (RNAi) approaches in the protozoan parasite Leishmania. *Mol. Biochem. Parasitol.* **128,** 217–228 (2003).

260. Braun, L. *et al.* A Complex Small RNA Repertoire Is Generated by a Plant/Fungal-Like Machinery and Effected by a Metazoan-Like Argonaute in the Single-Cell Human Parasite Toxoplasma gondii. *PLoS Pathog.* **6,** e1000920 (2010).

261. Riyahi, A. Al, Al-Anouti, F., Al-Rayes, M. & Ananvoranich, S. Single argonaute protein from Toxoplasma gondii is involved in the double-stranded RNA induced gene silencing. *Int. J. Parasitol.* **36,** 1003–1014 (2006).

262. Crater, A. K., Manni, E. & Ananvoranich, S. Utilization of inherent miRNAs in functional analyses of Toxoplasma gondii genes. *J. Microbiol. Methods* **108,** 92–102 (2015).

263. Al-Anouti, F. & Ananvoranich, S. Comparative analysis of antisense RNA, double-stranded RNA, and delta ribozyme-mediated gene regulation in Toxoplasma gondii. *Antisense Nucleic Acid Drug Dev.* **12,** 275–81 (2002).

264. Yu, L. *et al.* Toxoplasma gondii: siRNA can mediate the suppression of adenosine kinase expression. *Exp. Parasitol.* **118,** 96–102 (2008).

265. Kolev, N. G., Tschudi, C. & Ullu, E. RNA interference in protozoan parasites: achievements and challenges. *Eukaryot. Cell* **10,** 1156–63 (2011).

266. McRobert, L. & McConkey, G. A. RNA interference (RNAi) inhibits growth of Plasmodium falciparum. *Mol. Biochem. Parasitol.* **119,** 273–278 (2002).

267. Malhotra, P. *et al.* Double-stranded RNA-mediated gene silencing of cysteine proteases (falcipain-1 and -2) of Plasmodium falciparum. *Mol. Microbiol.* **45,** 1245–1254 (2002).

268. Eksi, S., Czesny, B., Greenbaum, D. C., Bogyo, M. & Williamson, K. C. Targeted disruption of Plasmodium falciparum cysteine protease, falcipain 1, reduces oocyst production, not erythrocytic stage growth. *Mol. Microbiol.* **53,** 243–250 (2004).

269. Sijwali, P. S. *et al.* Plasmodium falciparum cysteine protease falcipain-1 is not essential in erythrocytic stage malaria parasites. *Proc. Natl. Acad. Sci.* **101,** 8721–8726 (2004).

270. Sijwali, P. S., Koo, J., Singh, N. & Rosenthal, P. J. Gene disruptions demonstrate independent roles for the four falcipain cysteine proteases of Plasmodium falciparum. *Mol. Biochem. Parasitol.* **150,** 96–106 (2006).

271. Mohmmed, A., Dasaradhi, P. V. N., Bhatnagar, R. K., Chauhan, V. S. & Malhotra, P. In vivo gene silencing in Plasmodium berghei--a mouse malaria model. *Biochem. Biophys. Res. Commun.* **309,** 506–11 (2003).

272. Schwentke, A. *et al.* In vitro and in vivo silencing of plasmodial dhs and eIf-5a genes in a putative, non-canonical RNAi-related pathway. *BMC Microbiol.* **12,** 107 (2012).

273. Feynman, R. P. Cargo Cult Science. (1974).

274. Franke-Fayard, B. *et al.* A Plasmodium berghei reference line that constitutively expresses GFP at a high level throughout the complete life cycle. *Mol. Biochem. Parasitol.* **137,** 23–33 (2004).

275. Ma, H. *et al.* Pol III Promoters to Express Small RNAs: Delineation of Transcription Initiation. *Mol. Ther. Nucleic Acids* **3,** e161 (2014).

276. Herrera-Carrillo, E., Harwig, A. & Berkhout, B. Toward optimization of AgoshRNA molecules that use a non-canonical RNAi pathway: variations in the top and bottom base pairs. *RNA Biol.* **12,** 447–456 (2015).

277. Grimm, D. *et al.* In vitro and in vivo gene therapy vector evolution via multispecies interbreeding and retargeting of adeno-associated viruses. *J. Virol.* **82,** 5887–911 (2008).

278. Glasmacher, E. *et al.* Roquin binds inducible costimulator mRNA and effectors of mRNA decay to induce microRNA-independent post-transcriptional repression. *Nat. Immunol.* **11,** 725–733 (2010).

279. Kooij, T. W. A. A., Rauch, M. M. & Matuschewski, K. Expansion of experimental genetics approaches for Plasmodium berghei with versatile transfection vectors. *Mol. Biochem. Parasitol.* **185,** 19–26 (2012).

280. Hliscs, M., Nahar, C., Frischknecht, F., Matuschewski, K. & Frischknecht, F. Expression Profiling of Plasmodium berghei HSP70 Genes for Generation of Bright Red Fluorescent Parasites. *PLoS One* **8,** e72771 (2013).

281. Meister, G. Argonaute proteins: functional insights and emerging roles. *Nat. Rev. Genet.* **14,** 447–459 (2013).

282. Vembar, S. S., Scherf, A. & Siegel, T. N. Noncoding RNAs as emerging regulators of Plasmodium falciparum virulence gene expression. *Curr. Opin. Microbiol.* **20,** 153–61 (2014).

283. Engwerda, C., Belnoue, E., Gruner, A. C. & Renia, L. Experimental models of cerebral malaria. *Curr Top Microbiol Immunol* **297,** 103–143 (2005).

284. Iwanaga, S. *et al.* Functional identification of the Plasmodium centromere and generation of a Plasmodium artificial chromosome. *Cell Host Microbe* **7,** 245–255 (2010).

285. van Dijk, M. R. *et al.* Replication, expression and segregation of plasmid-borne DNA in genetically transformed malaria parasites. *Mol. Biochem. Parasitol.* **86,** 155–162 (1997).

286. Dieci, G., Conti, A., Pagano, A. & Carnevali, D. Identification of RNA polymerase III-transcribed genes in eukaryotic genomes. *Biochimica et Biophysica Acta - Gene Regulatory Mechanisms* **1829,** 296–305 (2013).

287. Bawankar, P., Shaw, P. J., Sardana, R., Babar, P. H. & Patankar, S. 5' and 3' end modifications of spliceosomal RNAs in Plasmodium falciparum. *Mol. Biol. Rep.* **37,** 2125–33 (2010).

288. Sidik, S. M., Hackett, C. G., Tran, F., Westwood, N. J. & Lourido, S. Efficient Genome Engineering of Toxoplasma gondii Using CRISPR/Cas9. *PLoS One* **9,** e100450 (2014).

289. Shen, B., Brown, K. M., Lee, T. D. & Sibley, L. D. Efficient Gene Disruption in Diverse Strains of Toxoplasma gondii Using CRISPR / CAS9. *MBio* **5,** e01114-14 (2014).

290. Lee, M. C. & Fidock, D. A. CRISPR-mediated genome editing of Plasmodium falciparum malaria parasites. *Genome Med.* **6,** 63 (2014).

291. Deligianni, E. *et al.* A perforin-like protein mediates disruption of the erythrocyte membrane during egress of Plasmodium berghei male gametocytes. *Cell. Microbiol.* **15,** 1438–1455 (2013).

292. Wirth, C. C. *et al.* Perforin-like protein PPLP2 permeabilizes the red blood cell membrane during egress of Plasmodium falciparum gametocytes. *Cell. Microbiol.* **16,** 709–33 (2014).

293. Drew, D. R. & Reece, S. E. Development of reverse-transcription PCR techniques to analyse the density and sex ratio of gametocytes in genetically diverse Plasmodium chabaudi infections. *Mol. Biochem. Parasitol.* **156,** 199–209 (2007).

294. Beetsma, A. L., van de Wiel, T. J., Sauerwein, R. W. & Eling, W. M. Plasmodium berghei ANKA: purification of large numbers of infectious gametocytes. *Exp. Parasitol.* **88,** 69–72 (1998).

295. O'Donnell, R. A. *et al.* An alteration in concatameric structure is associated with efficient segregation of plasmids in transfected Plasmodium falciparum parasites. *Nucleic Acids Res.* **29,** 716–24 (2001).

296. Tucker, K. *et al.* in *Current Topics in Malaria* (ed. Rodriguez-Morales, A. J.) (InTech, 2016). doi:10.5772/65592

297. Hall, R. *et al.* Antigens of the erythrocytes stages of the human malaria parasite Plasmodium falciparum detected by monoclonal antibodies. *Mol. Biochem. Parasitol.* **7,** 247–265 (1983).

298. Simmons, D., Woollett, G., Bergin-Cartwright, M., Kay, D. & Scaife, J. A malaria protein exported into a new compartment within the host erythrocyte. *EMBO J.* **6,** 485–491 (1987).

299. Sanchez, G. I., Rogers, W. O., Mellouk, S. & Hoffman, S. L. Plasmodium falciparum: Exported Protein-1, a Blood-Stage Antigen, Is Expressed in Liver Stage Parasites. *Exp. Parasitol.* **79,** 59–62 (1994).

300. Lisewski, A. M. *et al.* Supergenomic network compression and the discovery of exp1 as a glutathione transferase inhibited by artesunate. *Cell* **158,** 916–928 (2014).

301. Fu, Y. *et al.* High-frequency off-target mutagenesis induced by CRISPR-Cas nucleases in human cells. *Nat. Biotechnol.* **31,** 822–826 (2013).

302. Bozdech, Z. *et al.* The Transcriptome of the Intraerythrocytic Developmental Cycle of Plasmodium falciparum. *PLoS Biol.* **1,** e5 (2003).

303. Janse, C. J., Ramesar, J. & Waters, A. P. High-efficiency transfection and drug selection of genetically transformed blood stages of the rodent malaria parasite Plasmodium berghei. *Nat. Protoc.* **1,** 346–356 (2006).

304. Modrzynska, K. *et al.* A Knockout Screen of ApiAP2 Genes Reveals Networks of Interacting Transcriptional Regulators Controlling the Plasmodium Life Cycle. *Cell Host Microbe* **21,** 11–22 (2017).

305. Mair, G. R. *et al.* Universal Features of Post-Transcriptional Gene Regulation Are Critical for Plasmodium Zygote Development. *PLoS Pathog.* **6,** e1000767 (2010).

306. Khan, S. M. *et al.* Proteome analysis of separated male and female gametocytes reveals novel sex-specific Plasmodium biology. *Cell* **121,** 675–687 (2005).

307. Helm, S. *et al.* Identification and Characterization of a Liver Stage-Specific Promoter Region of the Malaria Parasite Plasmodium. *PLoS One* **5,** e13653 (2010).

308. Das, S. *et al.* Processing of Plasmodium falciparum Merozoite Surface Protein MSP1 Activates a Spectrin-Binding Function Enabling Parasite Egress from RBCs. *Cell Host Microbe* **18,** 433–444 (2015).

309. De Niz, M. *et al.* In vivo and in vitro characterization of a Plasmodium liver stage-specific promoter. *PLoS One* **10,** e0123473 (2015).

310. De Niz, M. *et al.* In Vivo and In Vitro Characterization of a Plasmodium Liver Stage-Specific Promoter. *PLoS One* **10,** e0123473 (2015).

311. Sapolsky, R. Belief and Biology. *Freeth. Today* **20,** (2003).

312. Pollack, Y., Katzen, A. L., Spira, D. T. & Golenser, J. The genome of Plasmodium falciparum. I: DNA base composition. *Nucleic Acids Res.* **10,** 539–46 (1982).

313. Otto, T. D. *et al.* A comprehensive evaluation of rodent malaria parasite genomes and gene expression. *BMC Biol.* **12,** 86 (2014).

314. Hu, X. *et al.* Relative gene-silencing efficiencies of small interfering RNAs targeting sense and antisense transcripts from the same genetic locus. *Nucleic Acids Res.* **32,** 4609–17 (2004).

315. Hong, S. W., Jiang, Y., Kim, S., Li, C. J. & Lee, D. Target gene abundance contributes to the efficiency of siRNA-mediated gene silencing. *Nucleic Acid Ther.* **24,** 192–8 (2014).

316. Dornseifer, S. *et al.* RNAi revised--target mRNA-dependent enhancement of gene silencing. *Nucleic Acids Res.* **43,** 10623–32 (2015).

317. Larsson, E., Sander, C. & Marks, D. mRNA turnover rate limits siRNA and microRNA efficacy. *Mol. Syst. Biol.* **6,** 433 (2010).

318. Fellmann, C. & Lowe, S. W. Stable RNA interference rules for silencing. *Nat. Cell Biol.* **16,** 10–8 (2014).

319. Suarez, C. *et al.* The Malarial Serine Protease SUB1 Plays an Essential Role in Parasite Liver Stage Development. *PLoS Pathog.* **9,** e1003811 (2013).

320. Börner, K. *et al.* Robust RNAi enhancement via human Argonaute-2 overexpression from plasmids, viral vectors and cell lines. *Nucleic Acids Res.* **41,** e199 (2013).

321. Silva, P. A. G. C. *et al.* Translational Control of UIS4 Protein of the Host-Parasite Interface Is Mediated by the RNA Binding Protein Puf2 in Plasmodium berghei Sporozoites. *PLoS One* **11,** e0147940 (2016).

322. Silvie, O., Briquet, S., Müller, K., Manzoni, G. & Matuschewski, K. Post-transcriptional silencing of *UIS4* in *P lasmodium berghei* sporozoites is important for host switch. *Mol. Microbiol.* **91,** 1200–1213 (2014).

323. Tomas, A. M. *et al.* P25 and P28 proteins of the malaria ookinete surface have multiple and partially redundant functions. *EMBO J.* **20,** 3975–3983 (2001).

324. Pujol, F. M. *et al.* HIV-1 Vpu Antagonizes CD317/Tetherin by Adaptor Protein-1-Mediated Exclusion from Virus Assembly Sites. *J. Virol.* **90,** 6709–23 (2016).

325. Mohr, S. E., Smith, J. A., Shamu, C. E., Neumüller, R. A. & Perrimon, N. RNAi screening comes of age: improved techniques and complementary approaches. *Nat. Rev. Mol. Cell Biol.* **15,** 591–600 (2014).

326. Deitsch, K., Driskill, C. & Wellems, T. Transformation of malaria parasites by the spontaneous uptake and expression of DNA from human erythrocytes. *Nucleic Acids Res.* **29,** 850–853 (2001).

327. Lamonte, G. *et al.* Translocation of sickle cell erythrocyte MicroRNAs into Plasmodium falciparum inhibits parasite translation and contributes to malaria resistance. *Cell Host Microbe* **12,** 187–199 (2012).

328. Martins, Y. C. *et al.* Endothelin-1 Treatment Induces an Experimental Cerebral Malaria–Like Syndrome in C57BL/6 Mice Infected with Plasmodium berghei NK65. *Am. J. Pathol.* **186,** 2957–2969 (2016).

329. Amani, V. *et al.* Cloned lines of Plasmodium berghei ANKA differ in their abilities to induce experimental cerebral malaria. *Infect. Immun.* **66,** 4093–9 (1998).

330. Ozgur, S. & Stoecklin, G. Role of Rck-Pat1b binding in assembly of processing-bodies. *RNA Biol.* **10,** 528–539 (2013).

331. Suk, K. *et al.* Reconstitution of human RNA interference in budding yeast. *Nucleic Acids Res.* **39,** e43 (2011).

332. Bunnik, E. M. *et al.* The mRNA-bound proteome of the human malaria parasite Plasmodium falciparum. *Genome Biol.* **17,** 147 (2016).

333. Musiyenko, A., Majumdar, T., Andrews, J., Adams, B. & Barik, S. PRMT1 methylates the single Argonaute of Toxoplasma gondii and is important for the recruitment of Tudor nuclease for target RNA cleavage by antisense guide RNA. *Cell. Microbiol.* **14,** 882–901 (2012).

334. Qi, L. S. *et al.* Repurposing CRISPR as an RNA-guided platform for sequence-specific control of gene expression. *Cell* **152,** 1173–1183 (2013).

335. Gilbert, L. A. *et al.* CRISPR-mediated modular RNA-guided regulation of transcription in eukaryotes. *Cell* **154,** 442–451 (2013).

336. Larson, M. H. *et al.* CRISPR interference (CRISPRi) for sequence-specific control of gene expression. *Nat. Protoc.* **8,** 2180–96 (2013).

337. Perez-Pinera, P. *et al.* RNA-guided gene activation by CRISPR-Cas9-based transcription factors. *Nat. Methods* **10,** 973–6 (2013).

338. Maeder, M. L. *et al.* CRISPR RNA-guided activation of endogenous human genes. *Nat. Methods* **10,** 977–9 (2013).

339. Chen, B. *et al.* Dynamic imaging of genomic loci in living human cells by an optimized CRISPR/Cas system. *Cell* **155,** 1479–91 (2013).

340. Tsuji, M., Mattei, D., Nussenzweig, R. S., Eichinger, D. & Zavala, F. Demonstration of heat-shock protein 70 in the sporozoite stage of malaria parasites. *Parasitol. Res.* **80,** 16–21 (1994).

341. Schindelin, J. *et al.* Fiji: an open-source platform for biological-image analysis. *Nat. Methods* **9,** 676–682 (2012).

342. Planck, M. The Meaning and Limits of Exact Science. *Science (80-.).* **110,** (1949).

343. de Koning-Ward, T. F., Thomas, A. W., Waters, A. P. & Janse, C. J. Stable expression of green fluorescent protein in blood and mosquito stages of Plasmodium berghei. *Mol. Biochem. Parasitol.* **97,** 247–252 (1998).

344. Schürmann, N., Trabuco, L. G., Bender, C., Russell, R. B. & Grimm, D. Molecular dissection of human Argonaute proteins by DNA shuffling. *Nat. Struct. Mol. Biol.* **20,** 818–826 (2013).

345. Gibson, D. G. *et al.* Enzymatic assembly of DNA molecules up to several hundred kilobases. *Nat. Methods* **6,** 343–5 (2009).

346. Pfaffl, M. W. A new mathematical model for relative quantification in real-time RT-PCR. *Nucleic Acids Res.* **29,** e45 (2001).

347. Grimm, D. Production methods for gene transfer vectors based on adeno-associated virus serotypes. *Methods* **28,** 146–157 (2002).

348. Orr, R. Y., Philip, N. & Waters, A. P. Improved negative selection protocol for Plasmodium berghei in the rodent malarial model. *Malar. J.* **11,** 103 (2012).

349. Hoeijmakers, W., Bártfai, R. & Stunnenberg, H. Transcriptome analysis using RNA-Seq. *Malar. Methods Mol. Biol.* **923,** 221–239 (2013).

350. Kensche, P. R. *et al.* The nucleosome landscape of Plasmodium falciparum reveals chromatin architecture and dynamics of regulatory sequences. *Nucleic Acids Res.* **44,** 2110–2124 (2015).

351. Newton, I. Letter from Sir Isaac Newton to Robert Hooke. *Historical Society of Pennsylvania* (1675).

Acknowledgements

My PhD thesis would not have been possible without the support of many different people. First, I would like to thank my PIs, Dr. Ann-Kristin Mueller and Dr. Dirk Grimm, for the opportunity to work on this fascinating project, their joint supervision and their supportive and helpful advice. It was great to be able to combine the expertise of two different labs from different fields in one project. I am also thankful for all the opportunities they gave me during the time of my PhD, for the conferences I could travel to, for sending me off to the Biology of Parasitism Summer school (greatest idea ever), and for setting up all collaborations I needed for my work.

I am also for the expert guidance I received from the other members of my thesis advisory committee: Prof. Dr. Michael Lanzer, who is also my primary examiner, and Prof. Dr. Freddy Frischknecht. Both have been very helpful during the meetings and provided lots of good input into the progress of the work. They gave me valuable suggestions, not only scientifically, but also for my future career opportunities in the academic world. Last but not least, I appreciate having with Dr. Julien Bethúne another expert on RNAi in my defense committee.

Few projects can be done alone, and thus I am thankful for the collaboration with Dr. Richard Bartfái and Sabine Fraschka from Radboud University, The Netherlands, who performed the RNA-Seq analysis of *Pb*Ago2. The data they gathered provided a valuable new insight into my parasite line and I would not have been able to get this without their help. In addition, I want to thank Dr. Jude Przyborski and his student Matthias Diehl at the Philips University in Marburg, Germany, for their support with the *P. falciparum* work. Even though it was not successful, it was great to gain insight into working with this parasite. I also would like to thank Dr. Ben Berkhout and Elena Herrera Carrillo for their advice regarding the design of AgoshRNAs.

I was very fortunate that I had the opportunity to supervise three great students to help my project. Daria (Krzikalla) did a great job in her Master thesis to optimize the AgoshRNA design, and helped to generate the first *Pb*Ago2 line. Annika (Binder) supported me during her rotation with analyzing the first GFP knockdown I ever observed. Vera (Mitesser) finally imaged the lines *Pb*Ago2.scr and *Pb*Ago2.αGFP2c in mosquito- and liver stages and, most importantly, generated the line Pb_{LISP2}Ago2 during her Master thesis. All of them were smart, hardworking, and enjoyable students, and made the success of my project a lot easier.

I was lucky enough to be able to work in two labs. All of the members of the Grimm lab and the Mueller lab were very supportive, helpful, and friendly, and I thank all of them for being fun to work with. In the Mueller lab, I would like to especially acknowledge Kirsten (Heiss), who never refused when I asked for a favor, which helped me a lot to manage experiments in two labs in parallel. In the Grimm lab, I have to thank Anne (Herrmann), who helped me with experiments and discussions, cheered me up when experiments did not work as expected and constantly supplied chocolate. I also want to express my thanks to Ellen (Wiedtke) for keeping the lab running and for always providing me with cells when I needed some. This list wouldn't be complete without some of the old members of the Grimm lab, Stefanie (Grosse), Elena (Senis Herrero) and Nina (Schürmann), who helped me to get started, to find all reagents, protocols and equipments in the lab, to deal with this crazy thing called PhD and who danced with me to Barbed Wire. Without their advice I would have made much more mistakes than I already did. Thanks also to Flo (rian Schmidt) for tons of scientific discussions and sharing the passion for science. Without him I would have never figured out Gibson cloning for *Plasmodium*. It is really awesome that, even though all of you moved on to a new adventure in your life, we are still in touch and maintain the friendship!

I have to thank Mirko Singer from the Frischknecht group for the ImageJ macro he provided me, and his patience when I repeatedly asked him countless questions about microscopy. I also have to thank Christian Sommerauer, who bravely enough took care of the bulk of the mosquito breeding work. I am also grateful to Moya, who was probably the most excited person ever to proof-read my thesis, even though we barely knew each other.

Doing a PhD is stressful, and I could not have done it without my friends and family. Franziska and Miriam, my oldest friends, were patient with me when I again was late or spontaneously had to cancel our weekends because of sudden lab work, were always ready for a phone call (although we should have phone calls much more often), and even if we meet less often than we should, it always feels like we have never been apart. Kathrin – who started my PhD with me and became an awesome flatmate and friend – was always there for a "Feierabend-Bier", listened to my endless complaints when experiments failed and celebrated every successful result with me. I also want to thank Fabi, for his love and care through all the ups and downs of my PhD, for his patience when I was once again stressed and annoyed, and for staying with me for almost 6 years now. Let's tackle the next 6 years (and the next, and the next…)! Finally, I have to thank my parents for all the support I had during my studies and for being there for me whenever I needed them. Papa, von dir habe ich gelernt, frickelige kleine Dinge mit großem Perfektionismus zu tun, und dass man NIE etwas wegwirft. Mama, du hast mir systematisches, strukturiertes und zielorientiertes Arbeiten beigebracht, aber genauso, das Leben außerhalb der Arbeit zu genießen. Genau das sind die Eigenschaften, die man braucht, um einen PhD erfolgreich zu meistern. Ohne euch hätte ich es nicht geschafft!